Liver-targeted therapies in Zellweger spectrum disorders

TANGUY DEMARET

Cover figure:
Human skin fibroblasts collected from a Zellweger spectrum disorder patient and transduced with a third generation lentivirus to express an enhanced green fluorescent protein fused to a peroxisomal targeting signal 1 (eGFP-PTS1, in green). The eGFP-PTS1 is diffusely present in the cytosol due to the peroxisomal biogenesis disorder. Nuclei were stained with diamidino-2-phenylindole dihydrochloride (DAPI, in blue). The 70-kDa peroxisomal membrane protein (PMP70, in red) was immuno-labeled and highlighted peroxisomal ghosts. Cells were imaged on a Cell Observer Spinning Disk confocal microscope (Zeiss) using a Plan Apochromat 100 ×/1.4 Oil DICII objective.

Composition of the jury

President	Prof. Isabelle Leclercq, UCLouvain
Promotor	Prof. Etienne Sokal, UCLouvain
Secretary	Prof. Nisha Limaye, UCLouvain
Members	Patrick Van Der Smissen, UCLouvain
	Prof. Marie-Françoise Vincent, UCLouvain
External members	Prof. Ronald Wanders, Amsterdam UMC
	Prof. Myriam Baes, KULeuven

Aux esprits passionnés

Guérir parfois,

Soulager souvent,

Écouter toujours.

LOUIS PASTEUR

This work was supported by the Fonds de la Recherche Scientifique (FRS-FNRS):

Formation à la Recherche dans l'Industrie et dans l'Agriculture (FRIA)

Je remercie les Professeur·e·s Vincent Blondel, recteur de l'UCLouvain, Frédéric Houssiau, vice-recteur du Secteur des Sciences de la Santé, Françoise Smets, doyenne de la Faculté de Médecine et Médecine Dentaire, Jean-Luc Balligand, président de l'Institut de Recherche Expérimentale et Clinique, et Jean-Louis Vanoverschelde, directeur médical des Cliniques universitaires Saint-Luc, de m'avoir offert l'opportunité de mener à bien ce projet de recherche académique au sein de l'UCLouvain, en collaboration avec les Cliniques universitaires Saint-Luc.

Je remercie le Fonds de la Recherche Scientifique (FRS-FNRS) pour son soutien financier à la réalisation de cette thèse ainsi que la Belgian Week of Gastroenterology et Astellas. Merci également à la Fondation Saint-Luc et aux Fonds Spéciaux de Recherche (UCLouvain) d'avoir cru au projet dès les premiers instants.

Je remercie tout particulièrement le Professeur Étienne Sokal, mon promoteur, de m'avoir ouvert les portes de son laboratoire de thérapie cellulaire. Par son accueil aux staffs cliniques, il m'a permis d'accéder au monde merveilleux de la transplantation hépatique pédiatrique. En outre, grâce à ses contacts, il m'a permis de me former aux maladies héréditaires du métabolisme dans les meilleures conditions, y compris en stage à l'Hôpital Necker-Enfants malades à Paris. Cela a été un réel honneur de partager l'expérience de son service de greffe lors de congrès internationaux et de réunions d'associations de patients. Pour tout cela et plus encore, je lui suis éternellement reconnaissant.

Je remercie la Professeure Isabelle Leclercq, présidente du comité d'accompagnement de thèse, de m'avoir fait bénéficier de son expertise en hépatologie (mention spéciale à son œil aguerri pour détecter les mitoses et les gros hépatocytes) et de m'avoir ouvert son laboratoire pour la réalisation de dosages et l'utilisation d'anticorps. Merci aussi à elle pour ses questions toujours pointues et pertinentes.

Je remercie les membres du comité d'accompagnement pour leur soutien : Professeure Nisha Limaye pour ses précieux conseils en biologie moléculaire, Monsieur Patrick Van Der Smissen pour son expertise en microscopie, Professeure Marie-Françoise Vincent pour m'avoir permis d'accéder à son laboratoire de biologie clinique et Professeur Jean-Christophe Jonas, membre extérieur, pour ses suggestions pertinentes quant au métabolisme glucidique.

Je remercie Madame Catherine Lombard pour sa bienveillance et sa rigueur qui ont permis de mettre en place les bases de mon travail. Merci aussi, Catherine, pour tes nombreuses relectures attentives de nos demandes de financement et de notre chapitre de livre.

Dear Professor Myriam Baes and Professor Ronald Wanders. We met at the scientific conference organized by the Global Foundation for Peroxisomal Disorders in Washington, DC. Professor Baes, when I asked you for tips to rescue the inheritance of the *Pex1* mouse model, you suggested the backcrossing of the allele to a different mouse strain and, by this, you unlocked the *in vivo* part of my thesis.

Professor Wanders, you coached me when I had to sum up the liver workshop at the scientific conference and you invited me in Amsterdam to present our liver transplantation experience. Finally, you both agreed to be external members of the jury of my PhD. I'm indebted to you for your great input into this thesis.
I take this opportunity to thank Ms Melissa Bryce Gamble for having created and for managing the Global Foundation for Peroxisomal Disorders. She deserves many thanks for the support that her association gives to the affected families. Melissa, you also gave me the chance to meet numerous great peroxisomal researchers from all over the world and I thank you very much for that.

À l'hôpital, j'ai reçu l'aide de la Professeure Françoise Smets que je remercie pour sa disponibilité, ainsi que ses précieux et nombreux conseils quant à la prise en charge des patients atteints de pathologies digestives. Je remercie également le Professeur Xavier Stéphenne pour sa bienveillance dans les moments difficiles, ainsi que pour ses compétences en hépatologie pédiatrique. À la Professeure Isabelle Scheers, j'adresse mes chaleureux remerciements pour son soutien sans faille, ses conseils éclairés et éclairants et ses attentions précieuses tout au long de ma thèse. Merci également au Professeur Philippe Lysy pour ses multiples suggestions pertinentes et son soutien de longue date.

Je profite de ce moment pour remercier Madame Ilse van Elewijck pour sa bienveillance et son professionnalisme dans la gestion des consultations de gastro-entérologie pédiatrique. Ça a été un réel plaisir pour moi de travailler avec toi, Ilse.

Sans Monsieur Mustapha Najimi, cette thèse n'aurait pas été semblable. Merci d'avoir challengé ma démarche scientifique à de nombreuses reprises et de m'avoir permis de renforcer mes *soft skills*.

Lors de mon travail quotidien au laboratoire, j'ai pu compter sur les expertises de Joachim Ravau et Jonathan Evraerts, que je que tiens à remercier de m'avoir formé aux différentes techniques nécessaires à la réalisation de cette thèse. Merci plus spécifiquement à Joachim pour les nombreux génotypages et à Jonathan pour le soin qu'il a apporté à mes souris.

Un remerciement particulier va à la Docteure Louise Coppin, chère ex-doctorante et collègue, qui m'a donné les trucs et ficelles nécessaire à la réalisation d'un doctorat. Louise, merci d'avoir répondu patiemment à mes (nombreuses) questions quant à ta recherche. Merci aussi à Giulia Jannone pour les nombreux thés (et ensuite, tisanes) que nous avons partagés ensemble et d'avoir écouté mon (trop fréquent) désarroi de doctorant. Je n'oublie pas Caroline Daems et Pierre-Edouard Dollet qui ont partagé leur bureau avec moi et à qui je dois, pour l'une, le succès du clonage de plasmide et, pour l'autre, le succès de la culture cellulaire. Merci à vous deux, ainsi qu'à Sophie Welsch, Paola Gallo et Milena Rozzi pour la bonne humeur qui a régné dans notre bureau.

Je remercie également Valéry Payen, ami et ex-collègue, avec qui j'ai pu discuter de nombreuses problématiques d'un niveau scientifique variable. Valéry, une partie

du mérite du succès du clonage lentiviral te revient également ! Ce fut un réel plaisir de passer ces deux années en ta compagnie.

Cette thèse m'a également donné l'occasion de rencontrer Adil El Taghdouini. Adil, quelle joie ce fut de discuter avec toi de la recherche scientifique en général et de ses applications industrielles en particulier. Merci beaucoup de m'y avoir éveillé.
Je tiens également à remercier les membres, passés et présents, du laboratoire PEDI : Camillo Sargiacomo, Charlotte Vanhoorne, Elisa Corritore, Floriane André, Hoda El Kehdy, Julie Vandewalle, Nawal Jazouli, Nawfal Chibani, Niki Sarika et Olivier Pollé – en espérant n'oublier personne =). I would like to give a special thank to Sharat Varma who teached me how to collect data and write my first paper published in an international journal. Thank you also for our running sessions and the associated talks. See you in India !

J'ai reçu de nombreux conseils et astuces, quant à l'élevage et la gestion d'une colonie de souris, de la part de Magali Crutzen et du Professeur Jean-Paul Dehoux, que je remercie tous deux très sincèrement.

Martin Roumain et Guillaume Courtoy sont deux précieux co-auteurs. Je les remercie pour leurs compétences techniques et leurs relectures pointues, associées à leurs suggestions pertinentes. Je remercie également le Professeur Giulio Muccioli pour ses excellentes propositions relatives à notre article, tant au point de vue biochimique que rédactionnel. Merci aussi à Caroline Bouzin pour sa gentillesse et sa serviabilité, pour ses très nombreux conseils relatifs à l'immunofluorescence,

pour ses algorithmes Visiopharm et surtout de m'avoir dépanné de nombreuses fois avec le ($#!%`£) scanner de lames.

Je tiens à remercier très chaleureusement Michele De Beukelaer pour les innombrables coupes et colorations qu'elle a réalisées pour cette thèse, ainsi qu'Aurélie Daumerie pour les multiples tentatives d'immunomarquage CK19. Merci également à Marc de Bournonville pour l'usage de l'enrobeur en paraffine et d'avoir toléré mes (trop) nombreux oublis de blocs sur la plaque froide. Je suis également redevable au Docteur Nicolas van Baren de m'avoir donné accès et formé, dans l'urgence, à l'utilisation du scanner à fluorescence.

Je remercie Jérôme Ambroise qui m'a grandement aidé à analyser et déchiffrer les données du RNA-seq. Merci beaucoup d'avoir pris le temps de m'expliquer les bases de la biostatistique.

Je remercie Sandrine Marie de m'avoir donné accès au laboratoire de biochimie analytique afin d'y réaliser de multiples dosages. Merci d'avoir répondu patiemment à mes questions techniques. Je tiens à adresser un remerciement particulier à Philippine Debeyne, Jennifer Destrée, Abderrahman Tamah et Maxime Vanbever qui ont réalisé certaines analyses sur mes échantillons.

Un remerciement spécial va à Yvette Cnops pour le prêt des cages métaboliques qui m'ont permis de récolter l'urine de mes souris. Ce remerciement va également à Sébastien Druart qui m'a, en outre, permis d'utiliser le matériel de biologie clinique

du laboratoire NEFR, ainsi que le spectrophotomètre en plaque qui m'a fait économiser de nombreux pipetages.

Merci à Janne Tys qui m'a transmis ses compétences pour isoler les fibroblastes embryonnaires de souris, ce qui a permis la publication de mon premier article de recherche fondamentale. Je lui en suis extrêmement reconnaissant.

I also thank Hedwig Stepman and Anniek Van Landschoot for the great collaboration we had to quantifiy erythrocyte plasmalogen content.
I would like to thank Professor Bwee Thien Poll-The for the discussions we had in the different meetings where we met. I remember particularly this *verre de vin blanc* we had in the sunny spring of Paris at the ELA meeting. Thank you also for coming in Brussels to meet the first liver transplanted ZSD patient in the world. I thank also Doctors Femke Klouwer and Kevin Berendse for sharing their scientific experience about peroxisomal disorders.

J'adresse mes remerciements à mes collègues du laboratoire GAEN, particulièrement Justine Gillard, qui m'a formé au dosage des lipides, et Maxime Nachit, qui m'a partagé ses conseils de rédaction de figures et de graphes. Descendre vous voir et recevoir vos réponses à mes problèmes analytiques a été une grande source d'épanouissement pour moi et je vous en remercie.

The plasmids I used during my PhD were a gift from Jay Brenman, Didier Trono et Bob Weinberg, I thank them for their contributions. I acknowledge all the researchers

around the world who work for the spread of open science, including Jean-Philippe Fauconnier.

Je tiens à adresser mes plus sincères et chaleureux remerciements à mes parents et à ma sœur Roxane qui me soutiennent depuis tant d'années dans la recherche du bonheur. À Madouille, mon épouse, j'adresse toute ma reconnaissance et mon amour.

Table of Contents

LIST OF ABBREVIATIONS **5**

SUMMARY **9**

CHAPTER 1. INTRODUCTION **13**

PEROXISOMES 14
PEROXISOMAL FUNCTIONS 14
Etherphospholipid biosynthesis *14*
Bile acid biosynthesis *15*
Peroxisomal fatty acid alpha-oxidation *17*
Peroxisomal beta-oxidation *17*
Glyoxylate metabolism *18*
Other functions *18*
Interaction with other organelles *19*
PEROXISOME BIOGENESIS 19
Peroxisomal membrane formation and protein import *19*
Peroxisomal matrix protein import *20*
Peroxisome proliferation *21*
Peroxisome motility *22*
ZELLWEGER SPECTRUM DISORDERS 22
History *22*
Clinical description *23*
Laboratory diagnosis *24*
Standard of care *26*
Emerging therapies *27*
HEPATOCYTE TRANSPLANTATION 28
Clinical application *29*
Material source *32*
Hepatocyte isolation *32*
Quality control *33*
Dose and route of administration *33*
Engraftment evaluation and enhancement *34*
Immunosuppression *35*
How to overcome hepatocyte transplantation barriers *36*
OBJECTIVES 36
SIGNIFICANCE 38
ACKNOWLEDGMENTS 39
REFERENCES 39

CHAPTER 2. ACCURATE AND LIVE PEROXISOME BIOGENESIS EVALUATION ACHIEVED BY LENTIVIRAL EXPRESSION OF A GREEN FLUORESCENT PROTEIN FUSED TO A PEROXISOME TARGETING SIGNAL 1 **47**

ABSTRACT 48
INTRODUCTION 49
MATERIALS AND METHODS 51

Cell isolation and culture *51*
Peroxisome targeting signal cloning *52*
Lentivirus production *54*
Immunofluorescence *55*
Image analysis *56*
Time-lapse analysis *58*
Figure drawing and statistical analysis *58*
RESULTS 59
PTS1 was functionally cloned in eGFP lentiviral vector allowing stable eGFP-PTS1 expression *59*
Decreased catalase+PMP70 colocalization confirmed PBD in ZSD cells *60*
eGFP-PTS1+PMP70 colocalization was efficient to evaluate PB *63*
eGFP-PTS1 signal alone allowed PB evaluation and peroxisome morphometry in living cells *65*
DISCUSSION 67
CONCLUSIONS 70
ACKNOWLEDGMENTS 70
APPENDIX 71
Peroxisomes and nuclei detection macro for ImageJ *71*
REFERENCES 71

CHAPTER 3. LONGITUDINAL STUDY OF *PEX1*-G844D NMRI MOUSE MODEL: A ROBUST PRE-CLINICAL MODEL FOR MILD ZELLWEGER SPECTRUM DISORDER 75

ABSTRACT 76
INTRODUCTION 77
MATERIALS AND METHODS 79
Mice care and breeding *79*
Pex1-G844D NMRI mice generation and genotyping *79*
Blood, urine, and organs collection *80*
Histological analyses *81*
RNA-seq *84*
MEF collection and characterization *86*
Biochemical analyses *87*
General statistical analysis and artwork *92*
RESULTS 92
Pex1-G844D backcrossing in NMRI background eased the breeding and restored autosomal recessive Mendelian inheritance pattern *92*
ZSD mice presented growth retardation and relative hepatomegaly associated to progressive hepatocyte hypertrophy *95*
Pathological liver analysis revealed reduced peroxisome number, bile duct proliferation, and discrete collagen deposition in ZSD mice *99*
ZSD mice exhibited severe liver glycogen metabolism impairment leading to poor fasting resistance *101*
ZSD mice liver expression profile unraveled modulations in multiple pathways among which glucose metabolism was switched to glucose consumption .. *103*
ZSD MEF biochemical and immuno-labelling analysis highlighted PBD *106*
ZSD mice presented multiple biochemical alterations resulting from PBD .. *107*

DISCUSSION 114
CONCLUSION 117
ACKNOWLEDGMENTS 117
REFERENCES 118

CHAPTER 4. HIGH DOSE *VERSUS* LOW DOSE SYNGENEIC HEPATOCYTE TRANSPLANTATION IN PEX1-G844D NMRI MOUSE MODEL IS SAFE BUT DOES NOT ACHIEVE LONG TERM ENGRAFTMENT 123

ABSTRACT 124
INTRODUCTION 125
MATERIAL AND METHODS 126
Mice care, breeding, and genotyping 126
Hepatocyte transplantation 126
Clinical evaluation and glycemia 128
Blood and liver collection 128
Peroxisomal markers quantification 128
Histological analyses 128
Microchimerism evaluation 129
General statistical analysis and artwork 129
RESULTS 130
HT was well tolerated in ZSD mice 130
Growth and normalized daily energy intake were not affected by HT 132
HT did not modify plasma nor liver peroxisomal marker anomalies 132
Fasting glycemia in ZSD mice was improved after high dose HT but this was not correlated to liver glycogen content 133
HT did not reverse relative hepatomegaly in ZSD mice 133
Male liver microchimerism was detected in female ZSD mice after 24 h and was lost during follow-up 133
DISCUSSION 134
CONCLUSION 137
ACKNOWLEDGMENTS 137
REFERENCES 137

CHAPTER 5. LIVING-DONOR LIVER TRANSPLANTATION FOR MILD ZELLWEGER SPECTRUM DISORDER: UP TO 17 YEARS FOLLOW-UP 141

ABSTRACT 142
INTRODUCTION 143
PATIENTS DESCRIPTION 143
BIOCHEMICAL RESPONSE AFTER LT IN MILD ZSD 146
SENSORINEURAL RESPONSE AFTER LT IN MILD ZSD 148
GROWTH AND DEVELOPMENT RESPONSE AFTER LT IN MILD ZSD 150
ALLOGRAFT FUNCTION 151
DISCUSSION 151
CONCLUSION 155
REFERENCES 156

CHAPTER 6. GENERAL DISCUSSION AND CONCLUSIONS 159

General discussion and implications 160
Perspectives 162
LT or gene therapy for ZSD ? 163
Conclusions 165
Acknowledgments 165
References 165

CHAPTER 7. COLLABORATIONS AND AWARDS 169

Congress abstracts 170
Liver transplantation does not impact the renal function outcome in Alagille syndrome (European Association for the Study of the Liver – International Liver Congress, Amsterdam, 2017) 170
Clinical features and natural history of 1154 Alagille syndrome patients: results from the International Multicenter GALA Study Group (European Association for the Study of the Liver – International Liver Congress, London, 2020) 172
Characterization of the NOTCH2-associated Alagille syndrome phenotype: Results from the international multicenter GALA study group (World Congress of Pediatric Gastroenterology, Hepatology and Nutrition, Copenhagen, 2020) 175
Guidelines 178
Minimal information for studies of extracellular vesicles 2018 (MISEV2018): a position statement of the International Society for Extracellular Vesicles and update of the MISEV2014 guidelines (Journal of Extracellular Vesicles, 8(1), 2019) 178
Original articles 179
Intracranial Hypertension and Papilledema in a Large Cohort of Pediatric Patients with Alagille syndrome (Journal of Pediatric Gastroenterology and Nutrition, 2020) 179
Awards, grants and invited lectures 181
2016 181
2017 181
2018 181
2019 181
2020 181

List of abbreviations

7-OHC	7-hydroxycholesterol
7α-OHCnone	7α-hydroxy-4-cholesten-3-one
AAA	ATPases associated with diverse cellular activities
AAV	Adeno-associated vector
ACLF	Acute on chronic liver failure
ADHLSC	Adult-derived human liver stem/progenitor cells
AGPS	Alkylglycerone phosphate synthase
AGT	Alanine-glyoxylate aminotransferase
AMACR	α-methylacyl-Coa racemase
ATMP	Advanced therapy medicinal product
BA	Bile acid
BAAT	Bile acyl-CoA: amino acid N-acyltransferase
BCFA	Branched-chain fatty acid
BERA	Brainstem-evoked response audiometry
bp	Base-pair
BSEP	Bile salt export pump
C26LPC	$C_{26:0}$lysophosphatidylcholine
Cas9	CRISPR-associated protein 9
CN1	Crigler-Najjar syndrome type 1
CPT1	Carnitine palmitoytransferase 1
CRISPR	Clustered regularly interspaced short palindromic repeats
DAPI	Diamidino-2-phenylindole dihydrochloride
ddPCR	Droplet digital polymerase chain reaction
DHA	Docosahexaenoic acid
DHAP	Dihydroxyacetone phosphate
DHAPAT	Dihydroxyacetonephosphate acyltransferase
DHCA	Dihydroxycholestanoic acid
DLP1	Dynamin-like protein 1
DMA	Dimethyl acetal
DQ	Developmental quotient
eGFP	Enhanced green fluorescent protein
eGFP-PTS1	eGFP fused with a peroxisome targeting signal 1
eGFP-PTS1-LV	eGFP-PTS1 lentivirus
eGFP+	eGFP-positive

EMA	European Medicines Agency
ER	Endoplasmic reticulum
ESC	Embryonic stem cells
FACS	Fluorescence activated cell sorting
FBS	Fetal bovin serum
FDA	Food and Drug Administration
FDR	False discovery rate
FIS1	Fission mitochondrial 1
G6Pase	Glucose-6-phosphatase
gDNA	Genomic DNA
gGT	Gamma-glutamyltransferases
GMP	Good Manufacturing Practice
GNPAT	Glyceronephosphate-O-acyltransferase
GPT	Glutamate-pyruvate transaminase
H&E	Hematoxylin and eosin
HNF4α	Hepatocyte nuclear factor 4 alpha
HSC	Hepatic stellate cells
HT	Hepatocyte transplantation
IEM	Inborn errors of metabolism
IF	Immunofluorescence
IL	Interleukin
INL	Irradiation of the native liver
iPSC	Induced pluripotent stem cells
KO	Knockout
LCT	Liver cell therapy
LDH	Lactate dehydrogenase
LML	Left medial lobe
LT	Liver transplantation
MEF	Mouse embryonic fibroblast
MFF	Mitochondrial fission factor
MOC	Manders' overlap coefficient
mPTS	Membrane peroxisome targeting signal
MS	Mass spectrometer
MSC	Mesenchymal stromal cells
NAC	N-acetylcysteine
NADH	Nicotinamide adenine dinucleotide

NGS	Normal goat serum
NMRI	Naval Medical Research Institute
ON	Overnight
ORO	Oil red O
PAS	Periodic-acid Schiff
PB	Peroxisome biogenesis
PBD	Peroxisome biogenesis disorder
PBS	Phosphate-buffered saline
PCC	Pearson's correlation coefficient
PCR	Polymerase chain reaction
PEX	Peroxin
PH	Partial hepatectomy
PMP	Peroxisomal membrane protein
PMP70	70-kDa peroxisomal membrane protein
POD	Post-operative day
PPARα	Peroxisome proliferator-activated receptor alpha
PTS	Peroxisome targeting signal
PVO	Portal vein occlusion
qPCR	Quantitative polymerase chain reaction
RBC	Red blood cell
RNA-seq	RNA sequencing
ROS	Reactive oxygen species
RT	Room temperature
SD	Standard deviation
SKL	Serine-lysine-leucine
SR	Sirius red
SRY	Sex determining region Y
TBE	Trypan blue exclusion test
TBS	Tris-buffered saline
THCA	Trihydroxycholestanoic acid
UCD	Urea cycle disorders
VLCFA	Very long-chain fatty acids
WGA	Wheat germ agglutinin
WT	Wild-type
X-ALD	X-linked adrenoleukodystrophy
ZSD	Zellweger spectrum disorder

Summary

Our clinical center has pioneered the organ and cell transplantation approaches to treat Zellweger spectrum disorders (ZSD). The present work aimed to develop innovative tools to evaluate peroxisome biogenesis (PB) *in vitro* and in a pre-clinical model, in order to assess the potential benefit of hepatocyte transplantation in ZSD. ZSD are inborn errors of metabolism (IEM) caused by genetic alterations in *PEX* genes leading to peroxisome biogenesis disorder (PBD)[1]. The phenotype is broad and extends between neonatal death by liver failure, in severe ZSD, to developmental delay and/or deafness and/or blindness, in milder forms of the disease[2] (**Chapter 1**). Diagnosis is supported by peroxisomal marker quantification in blood and urine, and is further confirmed by sequencing the 13 *PEX* genes associated with ZSD[3]. Supportive care is standard since no curative treatment have been validated in clinical practice[4]. Drug screening on ZSD patient skin fibroblasts uncovered several compounds able to restore PB *in vitro*[5, 6]. Some of these molecules are currently under clinical trials (NCT01838941, NCT03856866). In addition, we and other reported favorable bio-clinical short-term outcomes after hepatocyte transplantation (HT) or liver transplantation (LT) in mild ZSD patients[7-9]. Methods to evaluate PBD *in vitro* are time-consuming and exhibit low sensitivity on cells from mild ZSD patients[10]. In **Chapter 2**, we developed a stable expression system for an enhanced green fluorescent protein fused with a peroxisome targeting signal 1 (eGFP-PTS1). eGFP-PTS1 is a fluorescent peroxisomal reporter used to evaluate PB. The transduction efficiency ranged from 45% to 85% and eGFP-PTS1 expression was maintained more than 8 passages. The eGFP-PTS1 signal was then

digitally analyzed and validated to evaluate PB in human skin fibroblasts and mouse embryonic fibroblasts isolated from our optimized mild ZSD mouse model (see Chapter 3). Live cell imaging of transduced cells allowed peroxisome motility measurement. In the future, this tool could be used to screen for molecules able to restore PB *in vitro*[5].

Available ZSD mouse models are fragile and difficult to breed. It makes them unsuitable to evaluate rigorously HT as a therapeutic approach in ZSD. *Pex1* p.G844D (equivalent to the human *PEX1* p.G843D mutation associated with a mild ZSD phenotype) is an hypomorphic allele which has been developped in a C57BL/6 mouse background to create a mild ZSD mouse model[11, 12]. We backcrossed the murine allele in an NMRI mouse strain, known for delivering large litters and for its robustness. In **Chapter 3**, we report the longitudinal evaluation of this new mild ZSD mouse model. Hepatomegaly and liver glycogen metabolism impairment are further deciphered. Our mouse model exhibited classical peroxisomal marker alterations including the urine organic acid profile. We used this model to evaluate HT impact on disease markers (see Chapter 4).

LT is indicated in the management of several IEM[13, 14]. Yet, organ shortage limits LT availability, especially for IEM patients who do usually not exhibit classical LT indication criteria (e.g. decompensated cirrhosis). HT has been developed to overcome some of the LT limitations. Our clinical transplant program initially treated one mils ZSD patient using HT and showed positive biochemical outcomes, 18 months post-HT, highlighted by the marked reduction of some peroxisomal metabolites (i.e., the C_{27} bile acids intermediates and the very long-chain fatty acids)[7]. To confirm the benefit of HT in mild ZSD, we evaluated two doses of

syngeneic HT in our ZSD mouse model. In **Chapter 4**, we relate that HT was feasible and safe in our mouse model. Unfortunately, none of the HT protocols could achieve persistent liver engraftment more than 24 h. In accordance with that, no impact on peroxisomal markers could be detected.

We and a Japanese pediatric liver transplant team reported biochemical and clinical improvement up to 2 years after living-donor LT in two mild ZSD patients[8, 9]. Long-term clinical outcomes post-LT for ZSD are lacking. In **Chapter 5**, the biochemical and clinical results 17 years post-LT for the first mild ZSD patient are described along with two others mild ZSD patients who benefited from living-donor LT.

In **Chapter 6**, a general discussion and perspectives are presented along with a comparison between LT and a potential gene therapy for ZSD.

In **Chapter 7**, publications from international collaborations are reported.

References

1. Waterham, H.R. and M.S. Ebberink, Genetics and molecular basis of human peroxisome biogenesis disorders. Biochim Biophys Acta, 2012. 1822(9): p. 1430-41.
2. Klouwer, F.C., K. Berendse, S. Ferdinandusse, R.J. Wanders, M. Engelen, and B.T. Poll-The, Zellweger spectrum disorders: clinical overview and management approach. Orphanet J Rare Dis, 2015. 10: p. 151.
3. Wanders, R.J., F.C. Klouwer, S. Ferdinandusse, H.R. Waterham, and B.T. Poll-The, Clinical and Laboratory Diagnosis of Peroxisomal Disorders. Methods Mol Biol, 2017. 1595: p. 329-342.
4. Braverman, N.E., G.V. Raymond, W.B. Rizzo, A.B. Moser, M.E. Wilkinson, E.M. Stone, S.J. Steinberg, M.F. Wangler, E.T. Rush, J.G. Hacia, and M. Bose, Peroxisome biogenesis disorders in the Zellweger spectrum: An overview of current diagnosis, clinical manifestations, and treatment guidelines. Mol Genet Metab, 2016. 117(3): p. 313-21.
5. MacLean, G.E., C. Argyriou, E. Di Pietro, X. Sun, S. Birjandian, P. Saberian, J.G. Hacia, and N.E. Braverman, Zellweger spectrum disorder patient-derived fibroblasts with the PEX1-Gly843Asp allele recover peroxisome functions in response to flavonoids. J Cell Biochem, 2019. 120(3): p. 3243-3258.
6. Law, K.B., D. Bronte-Tinkew, E. Di Pietro, A. Snowden, R.O. Jones, A. Moser, J.H. Brumell, N. Braverman, and P.K. Kim, The peroxisomal AAA ATPase complex prevents pexophagy and development of peroxisome biogenesis disorders. Autophagy, 2017. 13(5): p. 868-884.
7. Sokal, E.M., F. Smets, A. Bourgois, L. Van Maldergem, J.P. Buts, R. Reding, J. Bernard Otte, V. Evrard, D. Latinne, M.F. Vincent, A. Moser, and H.E. Soriano, Hepatocyte transplantation in a 4-year-old girl with peroxisomal biogenesis disease: technique, safety, and metabolic follow-up. Transplantation, 2003. 76(4): p. 735-8.

8. Van Maldergem, L., A.B. Moser, M.F. Vincent, D. Roland, R. Reding, J.B. Otte, R.J. Wanders, and E. Sokal, Orthotopic liver transplantation from a living-related donor in an infant with a peroxisome biogenesis defect of the infantile Refsum disease type. J Inherit Metab Dis, 2005. 28(4): p. 593-600.
9. Matsunami, M., N. Shimozawa, A. Fukuda, T. Kumagai, M. Kubota, P.F. Chong, and M. Kasahara, Living-Donor Liver Transplantation From a Heterozygous Parent for Infantile Refsum Disease. Pediatrics, 2016. 137(6).
10. Gootjes, J., F. Schmohl, P.A. Mooijer, C. Dekker, H. Mandel, M. Topcu, M. Huemer, M. Von Schutz, T. Marquardt, J.A. Smeitink, H.R. Waterham, and R.J. Wanders, Identification of the molecular defect in patients with peroxisomal mosaicism using a novel method involving culturing of cells at 40 degrees C: implications for other inborn errors of metabolism. Hum Mutat, 2004. 24(2): p. 130-9.
11. Hiebler, S., T. Masuda, J.G. Hacia, A.B. Moser, P.L. Faust, A. Liu, N. Chowdhury, N. Huang, A. Lauer, J. Bennett, P.A. Watkins, D.J. Zack, N.E. Braverman, G.V. Raymond, and S.J. Steinberg, The Pex1-G844D mouse: a model for mild human Zellweger spectrum disorder. Mol Genet Metab, 2014. 111(4): p. 522-32.
12. Berendse, K., M. Boek, M. Gijbels, N.N. Van der Wel, F.C. Klouwer, M.A. van den Bergh-Weerman, A.B. Shinde, R. Ofman, B.T. Poll-The, S.M. Houten, M. Baes, R.J.A. Wanders, and H.R. Waterham, Liver disease predominates in a mouse model for mild human Zellweger spectrum disorder. Biochim Biophys Acta Mol Basis Dis, 2019.
13. Darwish, A.A., P. McKiernan, and C. Chardot, Paediatric liver transplantation for metabolic disorders. Part 1: Liver-based metabolic disorders without liver lesions. Clin Res Hepatol Gastroenterol, 2011. 35(3): p. 194-203.
14. Darwish, A.A., P. McKiernan, and C. Chardot, Paediatric liver transplantation for metabolic disorders. Part 2: Metabolic disorders with liver lesions. Clin Res Hepatol Gastroenterol, 2011. 35(4): p. 271-80.

Chapter 1.
Introduction

Peroxisomes

In 1954, Rhodin described “microbodies” as single membrane organelles in mouse kidney cells[1]. A few years later, De Duve and coworkers characterized some of their properties and introduced the name “peroxisome”[2]. Peroxisomes are virtually present in all eukaryotic cells. Their diameter ranges between 0.1 µm and 0.9 µm, depending on the organ in which they are analyzed[3]. Cultured mammalian cell peroxisomes have a half-life of 2 days[4]. More than 50 different peroxisomal enzyme activities are described[5]. Peroxisomal functions relevant for this thesis are pinned down below.

Peroxisomal functions

Etherphospholipid biosynthesis

Etherphospholipids are composed of a fatty alcohol and a polyunsaturated fatty acid at the *sn*-1 and *sn*-2 positions on the glycerol backbone, respectively[6]. Depending on the modification (or not) of the ether bond, plasmanyl-phospholipids (unmodified ether bond) and plasmenyl-phospholipids (or plasmalogens, modified vinyl ether bond) are defined. Plasmalogens constitute the majority of etherphospholipids and exhibit specific tissue and subcellular membrane distribution[7]. Plasmalogens are known reactive oxygen species (ROS) scavengers[8].

Etherphospholipids biosynthesis begins inside peroxisomes. Dihydroxyacetone phosphate (DHAP), a glycolysis intermediate, is first acylated at the *sn*-1 position by glyceronephosphate-O-acyltransferase (GNPAT, also known as dihydroxyacetonephosphate acyltransferase (DHAPAT)) and then the acyl group is exchanged for an alkyl group by alkylglycerone phosphate synthase (AGPS, also

known as alkyldihydroxyacetonephosphate synthase). GNPAT and AGPS are located on the luminal side of the peroxisome membrane. The next etherphospholipids biosynthesis steps take place in the endoplasmic reticulum (ER)[6].

Bile acid biosynthesis

The liver is responsible for bile acids (BA) biosynthesis from cholesterol, through several reactions that occur in different subcellular compartments including peroxisomes (**Figure 1**). Cholesterol is first converted into oxysterols (7-hydroxycholesterol (7-OHC) then 7α-hydroxy-4-cholesten-3-one (7α-OHCnone)) through the classical or the alternative pathway. 7α-OHCnone is further modified into C_{27} BA intermediates (di- and trihydroxycholestanoic acids (DHCA and THCA))[9]. After, C_{27} BA intermediates are activated by the BA coenzyme A (CoA) ligase, they enter peroxisomes to undergo racemization by α-methylacyl-CoA racemase (AMACR) and then peroxisomal beta-oxidation (see below). After that, BA are conjugated to glycine or taurine by bile acyl-CoA: amino acid N-acyltransferase (BAAT) [10]. Finally, BA leave peroxisomes and are transported into the bile.

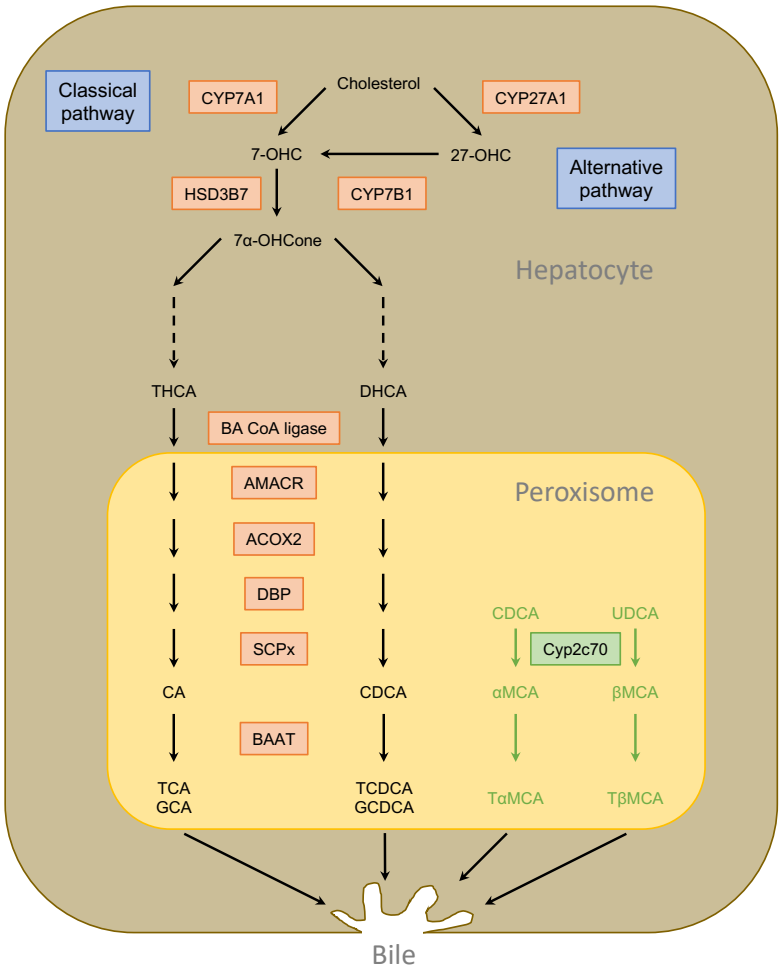

Figure 1 – Bile acid (BA) biosynthesis overview. First, cholesterol is converted into 7-hydroxycholesterol (7-OHC) by the cholesterol 7α-hydroxylase (CYP7A1), or by the sterol 27-hydroxylase (CYP27A1) followed by the oxysterol 7α-hydroxylase (CYP7B1), via the classical and the alternative pathways, respectively. The 7-OHC is further metabolized to 7α-hydroxy-4-cholesten-3-one (7α-OHCnone) by the 3β-hydroxy-Δ^5-C_{27} steroid oxidoreductase (HSD3B7). Next, 7α-OHCnone undergoes ring structure modification to form di- and trihydroxycholestanoic acids (DHCA and THCA) which are then activated by the BA coenzyme A (CoA) ligase. Activated C_{27} BA intermediates enter peroxisomes, the 25(*R*) isomers are changed into 25(*S*) isomers by the α-methylacyl-CoA racemase (AMACR), and then peroxisomal beta-oxidation peroxisomal takes place via the branched-chain acyl-CoA oxidase (ACOX2), the D-bifunctional protein (DBP) and the peroxisomal thiolase 2 (also known as sterol carrier protein-chi, SCPx) to form cholic and chenodeoxycholic acids (CA and CDCA). CA and CDCA are finally conjugated to glycine (except in mice) or taurine by the BA CoA:amino acid N-acyltransferase (BAAT). In mice only (shown in green), CDCA and ursodeoxycholic acid (UDCA) are converted by Cyp2c70 to α- and β-muricholic acids (αMCA and βMCA), respectively[11]. They are next conjugated with taurine. 27-OHC: 27-hydroxycholesterol.

Peroxisomal fatty acid alpha-oxidation

Phytanic acid is a branched-chain fatty acid (BCFA) originating solely from diet (meat and dairy products)[12]. Its degradation begins by peroxisomal alpha-oxidation leading to pristanic acid which is further metabolized by peroxisomal beta-oxidation (see below).

Peroxisomal beta-oxidation

In physiological condition, peroxisomes are responsible for very long-chain fatty acids (VLCFA: C_{22}, C_{24}, C_{26}) beta-oxidation. These VLCFA cannot enter mitochondria because they are no substrates for carnitine palmitoytransferase 1 (CPT1) which performs the first step of mitochondrial fatty acids entry[13]. Peroxisomal beta-oxidation is also required to degrade pristanic acid, a BCFA derived from diet or from phytanic acid after its alpha-oxidation.

C_{27} BA intermediates, DHCA and THCA, undergo one cycle of peroxisomal beta-oxidation before conjugation by BAAT and their release into the bile flow[10].

Docosahexaenoic acid (DHA) is one of the most abundant omega-3 fatty acids in the brain and retina. DHA biosynthesis is achieved by beta-oxidation of its direct precursor tetracosahexaenoic acid.

In addition, long-chain dicarboxylic acids, some xenobiotics, certain prostaglandins and leukotrienes and vitamins E and K are also substrates for peroxisomal beta-oxidation[7].

Metabolites produced by peroxisomal beta-oxidation (acetyl-CoA, nicotinamide adenine dinucleotide (NADH), etc.) need to be transferred to mitochondria for further degradation and energy production. H_2O_2 is an exception and is degraded inside peroxisomes mainly by catalase (see below)[13].

Glyoxylate metabolism

Glyoxylate is a highly reactive compound resulting from hydroxyproline and glycolate metabolisms. In the cytosol, glyoxylate is transformed into oxalate by lactate dehydrogenase (LDH). Oxalate is eliminated in urine and tend to precipitate into tissue-damaging calcium oxalate.

In order to limit oxalate production and further precipitation, glyoxylate has to be metabolized. Inside liver and kidney peroxisomes, alanine-glyoxylate aminotransferase (AGT) converts glyoxylate into glycine and prevents glyoxylate (and thus oxalate) accumulation[14].

Other functions

Peroxisomes contain enzymes generating H_2O_2 as by-product. H_2O_2 is eliminated via several enzymes among which catalase is well-known[15].

In addition to these essential metabolic pathways, peroxisomes are also accountable for pipecolic acid degradation. Pipecolic acid comes from lysin metabolism and is oxidized inside liver peroxisomes by pipecolate oxidase.

A series of reports, published mainly by one group of researchers, claim that cholesterol biosynthesis begins in peroxisomes and finishes in the ER[16-19]. The supporting data are mainly derived from *in vitro* and *in vivo* models that are far from physiological conditions, and from human samples which were in bad condition and/or incorrectly preserved. Based on the published cholesterol synthesis data gathered under physiological conditions, there is little evidence for a major peroxisomal involvement in cholesterol synthesis[7].

Interaction with other organelles

Peroxisomes have membrane contact sites with several organelles of which the ER and mitochondria are the most abundant[20]. The link between peroxisomes and specific subcellular compartments is further delineated by the fact that *de novo* peroxisome synthesis begins by ER budding to form pre-peroxisome[5]. Moreover, peroxisomes and mitochondria share common mechanism for fission as depicted by abnormally elongated peroxisomes and mitochondria present in fibroblasts isolated from a patient presenting dynamin-like protein 1 (DLP1) deficiency[21].

Peroxisome biogenesis

Peroxisomes are single membrane organelles present in eukaryotic cells[20]. Peroxisome biogenesis (PB) is mainly fulfilled by PEX proteins, or peroxins, encoded by *PEX* genes[5]. In human beings, 14 peroxins have been identified[22]. PB begins by peroxisomal membrane formation and peroxisomal membrane protein (PMP) import allowing further peroxisomal matrix protein import. In reaction to various stimuli, peroxisomes proliferate by growth and division mechanism or *de novo* synthesis. These two models have been co-existing for decades and probably operate within the same cell[20].

Peroxisomal membrane formation and protein import

PMP are mainly brought to their final destination by a direct pathway involving PEX19 and the recognition of a membrane peroxisome targeting signal (mPTS). After cytosolic mPTS recognition by PEX19, the cargo (PEX19•PMP) docks on PEX3 and PEX16, present at the peroxisome surface. The PMP is then inserted into peroxisome membrane. Beside this PEX19-dependent pathway, a second, indirect,

and PEX19-independent pathway, allows PMP targeting via the ER and pre-peroxisome budding[20].

Peroxisomal matrix protein import

Peroxisomal matrix proteins are synthetized by free ribosomes in the cytosol and possess peroxisome targeting signal (PTS)[23]. The most common, PTS1, is present at the C-termini of peroxisomal matrix proteins and frequently ends by serine-lysine-leucine (SKL) sequence. PTS2 is located at the N-termini of peroxisomal matrix proteins. In mammals, only three peroxisomal matrix proteins are known to possess PTS2: the straight-chain thiolase (beta-oxidation), the phytanoyl-CoA 2 hydroxylase (alpha-oxidation) and the AGPS (plasmalogen biosynthesis)[7]. PTS1 and PTS2 are recognized by soluble receptors, PEX5S/PEX5L and PEX7, respectively (**Figure 2**). PEX5S and PEX5L are produced by alternative splicing of PEX5 pre-mRNA. PEX5L is specifically required for PEX7•PTS2-protein interaction stabilization[24].

After cargo binding, PEX5S•PTS1-protein or PEX5L•PEX7•PTS2-protein docks on peroxisomal docking complex formed by two PMP: PEX14 and PEX13[5]. Matrix proteins are then imported to peroxisome lumen and receptors are released from peroxisome membrane for another round of importation, or degradation, depending on the action of three peroxins: PEX2, PEX10 and PEX12. They form a complex that mono- or polyubiquitinates PEX5, promoting its recycling or its degradation by the proteasome, respectively. PEX1 and PEX6 compose an ATPases Associated with diverse cellular Activities (AAA)-complex anchored to peroxisome membrane via PEX26. Finally, the AAA-complex releases PEX5 from the peroxisome membrane and, this way, prevents peroxisome autophagy (i.e., pexophagy)[25].

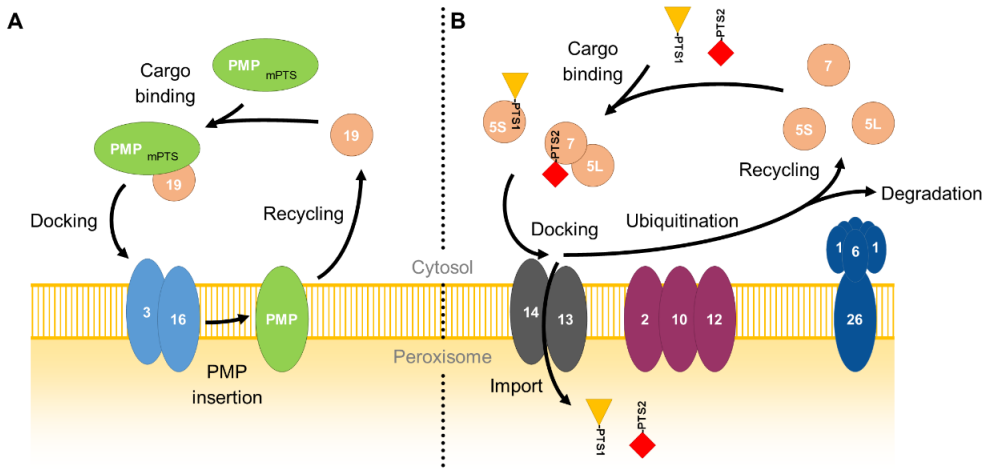

Figure 2 - Mammal peroxisome biogenesis overview including **A** peroxisomal membrane protein (PMP) import, and **B** peroxisomal matrix protein import achieved by PEX proteins. mPTS: membrane peroxisome targeting signal, PTS: peroxisome targeting signal (modified from[5, 20]).

Peroxisome proliferation

Growth and fission, and *de novo* synthesis are two peroxisome proliferation models co-existing to regulate peroxisome number in response to various intrinsic and extrinsic stimuli[20]. PEX11 proteins regulate both pathways and exist in three isoforms encoded by *PEX11α*, *PEX11β* and *PEX11γ* genes (in human beings). PEX11α regulates peroxisome number.

PEX11β plays an important role in the elongation and constriction of pre-existing peroxisomes, the first two steps of the growth and fission pathway. The last step is achieved by DLP1, fission mitochondrial 1 (FIS1) and mitochondrial fission factor (MFF), among others proteins[5].

PEX11γ acts on the *de novo* pathway by promoting the import of the peroxisomal matrix proteins into pre-peroxisomes derived from the ER.

Peroxisome motility

In human cells, peroxisomes are associated with microtubule cytoskeleton via PEX14[26]. Dyneins and kinesins are the motor proteins responsible for peroxisome movements on microtubules with an average velocity ranging from 0.1 to 1 µm/s[27, 28]. Only a small fraction (10-15%) of all peroxisomes move along microtubules.

Peroxisome motility is closely linked to peroxisome proliferation via both *de novo* and growth and fission pathways[20, 28]. Peroxisome motility is also required for equal peroxisome distribution between mother and daughter cells during mitosis[27]. Moreover, peroxisome uniform dispersion throughout the cytosol ensures homogeneous protection from the toxic substrates that peroxisomes catabolize[28]. Peroxisome displacement on microtubules is also required for pexophagy[29].

Zellweger spectrum disorders

History

Bowen and colleagues described two infants exhibiting severe hypotonia, uncontrollable seizures, renal cysts, biological hepatitis, and failure to thrive in 1964. The term “cerebro-hepato-renal syndrome” was coined a few years later[30-32]. Nine years after the first clinical description, Goldfischer *et al.* highlighted the absence of peroxisome in hepatocytes and renal tubular epithelial cells from 2 patients affected by Zellweger syndrome (severe Zellweger spectrum disorders (ZSD))[33].

During the 1980s, milder clinical phenotypes were identified : neonatal adrenoleukodystrophy (intermediate ZSD)[34] and infantile Refsum disease (mild ZSD)[35-37]. Their names were given based on similarities with known disorders. Infantile Refsum disease was associated with ultrastructural and biochemical

anomalies similar to Zellweger syndrome, but suggesting residual peroxisomal function[35, 36].

In the last half of the 1990s, mutations in *PEX* genes were shown to be responsible for ZSD, based on sequence similarity studies with PB genes from yeasts[38-40].

Nowadays, ultra-mild phenotypes are reported in association with *PEX* mutations. Heimler syndrome which associates some ZSD features (sensorineural and dental anomalies) but no mental retardation is one of these ultra-mild phenotypes[41].

Clinical description

ZSD affect around 1/50-100.000 births with various presentations[42, 43]. ZSD exhibit a high inter- and intra-familial phenotypic variability partly explained by the genotype[44, 45]. The phenotypic spectrum extends from neonatal death to mild adult presentations.

Severe ZSD patients present, shortly after birth, with profound hypotonia leading to feeding problems and failure to thrive, intractable seizures, neuronal migration defects, facial dysmorphism (high forehead and large anterior fontanel, among others) associated with hepatocellular insufficiency and renal cortical cysts[32]. Most patients do not achieve developmental milestones and die during the first year of life[46].

Intermediate ZSD patients present, during the first or second year of life, developmental delay associated with hypotonia. Developmental regression is noted in some patients and leads to the initial disease description as neonatal adrenoleukodystrophy by comparison with the X-linked form of the disease[34]. Dysmorphic features are less pronounced than in the neonatal presentation. Liver disease is usually mild and comprises hepatomegaly, cholestasis and portal

hypertension. The progressive leukodystrophy and liver disease mainly determine the life expectancy which is limited to the first decade in most patients[47].

In adolescent and adult mild ZSD patients, sensorineural hearing deficit or ocular abnormalities (retinitis pigmentosa, cataract, glaucoma, etc.) are the main symptoms[48]. Developmental delay is common, but the range of severity is wide as it is for the limitation of independent living skills[47]. Patients also display other neurological anomalies like cerebellar ataxia, peripheral neuropathy and slowly progressive leukoencephalopathy[49]. Primary adrenal insufficiency is affecting up to one third of the patients, but it is probably underdiagnosed[50-52].

Dental anomalies[53], hearing loss and ocular problems are present all along the spectrum of the disease[54]. Hyperoxaluria is common and one third of these patients exhibit renal involvement (urolithiasis, nephrocalcinosis, etc.) [55].

A severity scoring system was developed and validated to evaluate the severity of the ZSD phenotype[56]. Interestingly, multiple peroxisomal biochemical markers were correlated to the score.

Laboratory diagnosis

ZSD diagnosis is first suggested by evident clinical findings in severely affected patients (see above). Patients exhibiting milder phenotypes are more difficult to diagnose on a clinical basis. Quantification of several peroxisomal markers are thus required to evoke the diagnosis before its confirmation by genetic analysis. If genetic studies are inconclusive, patient's skin fibroblast analysis can ascertain the diagnosis[57].

Fasting plasma VLCFA analysis combined with phytanic and pristanic acid quantifications is the preferred analysis to diagnose ZSD[46]. False positive VLCFA

results may occur in case of ketogenic or peanut-rich diets and hemolyzed samples[47]. During the neonatal period, false negative plasma phytanic acid results are frequent because phytanic acid solely derives from dietary sources and it may take several months to accumulate[58]. Recently, $C_{26:0}$lysophosphatidylcholine (C26LPC) measured on dried blood spots have been reported as a very sensitive ZSD marker[59].

Since this marker has been implemented in some part of the United States for the newborn screening of X-linked adrenoleukodystrophy (X-ALD), a related peroxisomal disorder[60], early ZSD diagnosis is possible. In the same blood sample, erythrocyte plasmalogen levels should be measured, keeping in mind their lower sensitivity than VLCFA, especially in mildly affected and/or older patients[61].

Other plasma peroxisomal metabolites can help the clinician to diagnose ZSD. Among them are pipecolic acid resulting from a block in lysine catabolism and C_{27} BA intermediates (DHCA and THCA) derived from incomplete BA biosynthesis. Furthermore, the urine organic acid profile, which is often performed during broad metabolic workup, can underline a relatively specific pattern including the presence of an odd-numbered dicarboxylic aciduria[62, 63].

All these biochemical studies can be marginally abnormal or even completely normal in mild ZSD especially in patients reaching adulthood[46, 64].

Based on biochemical clues pointing to ZSD, next generation sequencing is the preferred method to look for bi-allelic pathogenic variant in one of the 13 *PEX* genes associated with ZSD. Genetic diagnosis allows counselling and genotype-phenotype correlation (i.e., the *PEX1* p.G843D is associated with a mild ZSD phenotype)[45]. If the suspicion is high and the genetic study is inconclusive, collecting patient's skin

punch to culture skin fibroblasts is required. Cell analysis is also needed to confirm the pathogenicity of the genetic variants detected when they are unknown[43].

Patient skin fibroblast analysis is able to uncover peroxisome biogenesis disorder (PBD) by immunofluorescence labelling of peroxisomal matrix enzymes (e.g., catalase), *in vitro* expression of fluorescent peroxisomal reporters[57], peroxisomal enzyme activity measurement[65], immunoblot analysis, or peroxisomal marker quantification (e.g., VLCFA). Cell culture at 40 °C is sometimes required to sensitize the techniques in case of hypomorphic *PEX* alleles[66]. Moreover, skin fibroblast collection allows PEX mRNA quantification and sequencing in case of variants affecting mRNA stability or splicing, respectively.

Standard of care

To date, no curative therapeutic approach exists for ZSD patients. Thus, the interventions are supportive and based on symptoms or screening results (e.g., asymptomatic adrenal insufficiency)[47].

All ZSD patients should be screened for hyperoxaluria, primary adrenal insufficiency (through a Synacthen® test), epilepsy, fat-soluble vitamins deficiency, high levels of phytanic acid, insufficient caloric intake, hearing or visual impairment and enamel hypoplasia. Based on the results, ZSD patients could benefit from citrate prescriptions and high fluid intakes, cortisone supplements, anti-epileptic drugs, vitamins supplements (especially vitamin K[67]), low phytanic acid diet, gastrostomy, hearing aids or cochlear implant, cataract removal or glasses and dentist referral, respectively[43, 47].

Cholic acid has a negative feedback effect on bile acid synthesis and thus, on abnormal C_{27} BA intermediates in ZSD patients[68]. In an open-label pretest-posttest

design study, cholic acid failed to improve liver elasticity, fat-soluble vitamin levels or body weight. Moreover, cholic acid resulted in elevation of plasma transaminases and bilirubin in ZSD patients with advanced liver disease[68, 69]. Nonetheless, the Food and Drug Administration, but not the European Medicines Agency, approved cholic acid as a safe treatment for ZSD patients in the United States. Approval was based on small case report studies analyzed with questionable statistical methods, to say the least[70, 71].

Emerging therapies

Mild ZSD patient skin fibroblasts exhibit residual PB *in vitro* that can be partially rescued by compounds, probably acting as chaperone, like arginine[72], betaine[73] or acacetin diacetate[74]. Moreover, 65% of cases of ZSD might potentially be linked to pexophagy anomalies[75]. Autophagy inhibitors like hydroxychloroquine were shown to partially rescue PB in mild ZSD patient skin fibroblasts[25]. For ZSD patients carrying disease-causing nonsense mutations, nonsense suppression therapies might be an option as demonstrated *in vitro* with aminoglycoside G418 (geneticin)[76]. Clinical trials are ongoing to evaluate some of these molecules in ZSD patients (ClinicalTrials.gov NCT01838941, NCT03856866).

Beside these molecular therapeutic approaches, cell and organ transplantation could deliver a large number of functional peroxisomes to ZSD patients. Living-donor liver transplantation (LT) was performed on a 6-month-old ZSD patient. Clinical and biochemical improvement were reported 2 years post-LT[77]. More than 10 years later, a Japanese team published similar results in a 2-year-old ZSD patient[78]. In this thesis, we report the long-term follow-up 17 years post-LT in the first ZSD patient and 2 additional cases of living-donor liver transplantation for mild ZSD (Chapter

6)[79]. The first pediatric hepatocyte transplantation (HT) in Europe was carried out in Brussels on a mild ZSD patient. Encouraging biochemical results (plasma C_{26} and DHCA levels decrease) were reported up to 18 months post-HT in this 4-year-old ZSD patient[80]. Bone marrow transplantation was performed on a ZSD patient but no chimerism could be achieved and the patient eventually died of the disease (Pr Troy Lund, personal communication).

In the future, gene augmentation therapy could provide cellular correction of the PBD for ZSD patients. *Pex1* gene was functionally delivered through an adeno-associated virus serotype 8 vector to retina cells in a ZSD mouse model. Six months post-subretinal injection, electroretinogram responses were improved[81, 82]. Currently, *PEX1* retinal gene therapy is under clinical development (Catherine Argyriou, personal communication).

Hepatocyte transplantation

Liver transplantation (LT) is a lifesaving procedure in children with numerous liver diseases. Yet, it requires scarce fresh organs, a highly experienced team to manage the surgical procedure, the complications and the follow-up, and a lifelong immunosuppression for the recipient[83]. Living-donor organs and split livers gave us the proof of concept that a partial organ is sufficient to restore liver metabolic functions[84]. Hepatocyte transplantation (HT), where hepatocytes rather than organs are transplanted in the patient, was first evaluated in acute liver failure to support liver function while awaiting spontaneous recovery or as a bridge to transplantation. Recently, HT has been proposed as a treatment in itself to overcome LT barriers

with an off-the-shelf, easily injectable and reversible procedure. In addition, it has the advantage of not inducing a strong immunogenic response[85].

Clinical application

Hepatocyte transplantation (HT) has been translated to human medicine in the 1990s in order to overcome the limitations of LT (lack of donors, heavy surgical operation, cost, lifelong immunosuppression). In 1994, Habibullah *et al.* reported on intraperitoneal fetal hepatocytes administration in 7 patients with acute liver failure; one child was included in the study and survived the acute decompensation[86]. The next year, Grossman *et al.* published the first intraportal injection of autologous hepatocytes transduced with LDL-receptor in 5 patients (3 children) with familial hypercholesterolemia; a decrease of LDL cholesterol was measured in 3 of them[87]. The autologous procedure was developed to avoid the immunosuppression and the allogenic variable[88]. Finally, in 1997, an intraportal heterologous hepatocyte infusion in a 5-year-old male diagnosed with ornithine transcarbamylase (OTC) deficiency was reported. His ammonia and glutamine levels returned to normal value at discharge. Unfortunately, the child died 43 days post-HT of liver biopsy complications. Since the first report in 1994, HT has been evaluated 58 children for indications ranging from biliary atresia[89] or acute liver failure (**Table 1**) to liver-based IEM (**Table 2**) with variable clinical success. At least 52% of them (30/58) received LT after HT. Currently HT is seen as a bridge to transplant especially for patients with liver-based IEM who usually face a long waiting time before LT[90].

Table 1. Clinical hepatocyte transplantation in pediatric acute liver failure.

Etiology	Age	Effect/Outcome	Reference
Drug induced	16 years	Ammonia reduction, death 2 days post-HT	91
	12 years	Ammonia reduction, death 7 days post-HT	
	10 years	Ammonia reduction, death 7 days post-HT	
	6 months	Ammonia reduction, life support withdrawing and death 7 days post-HT	92
	13 years	Death 4 days post-HT	93
	14 years	Ammonia reduction and improved encephalopathy/LT 1 day post-HT	88
Idiopathic	8 years	Intraperitoneal injection of fetal hepatocytes/full recovery	86
		Ammonia reduction and improved encephalopathy in both:	91
	3 years	Full recovery and immunosuppression weaned	
	5 years	Successful bridge to LT 4 days post-HT	
	3.5 months	No clear benefit/LT 1 day post-HT	94
Viral induced	4 years	Ammonia reduction and improved encephalopathy/intracranial hypertension in day 2	88
	3 weeks	Ammonia reduction/death 11 days post-HT	95

HT: hepatocyte transplantation, LT: liver transplantation.

Table 2. Clinical hepatocyte transplantation in pediatric liver-based inborn errors of metabolism.

Etiology	Age	Effect/Outcome	Reference
CN1	10 years	50% reduction in bilirubin, reduction in phototherapy/LT 4 years post-HT	96
	8 years	40% reduction in bilirubin/LT 20 months post-HT	97
	9 years	30% reduction in bilirubin, 35% reduction in phototherapy/LT 5 months post-HT	98
	1.5 years	> 50% reduction in bilirubin, reduction in phototherapy/LT 8 months post-HT	99
	3 years	30% reduction in bilirubin/LT 18 months post-HT	
	3.5 years	Lowered serum bilirubin/outcome unknown	100
	8 years	35% reduction in bilirubin, 50% reduction in phototherapy/LT 11 months post-HT	101
	9 years	20% reduction in bilirubin/LT 6 months post-HT	102
	1 year	25% reduction in bilirubin/LT 4 months post-HT	
	2 years	50% reduction in bilirubin/outcome unknown	103
	11 years	20% reduction in bilirubin/LT waiting list	95
	7 months	50% reduction in bilirubin and in phototherapy, psychomotor improvement/bilirubin stable at 1 year follow-up	104
	13 years	50% reduction in bilirubin, presence of bile glucuronides in bile/LT 19 months post-HT	105
	11 years	50% reduction in bilirubin, presence of bile glucuronides in bile/LT 31 months post-HT	
A1ATD	18 weeks	LT 2 days post-HT/cirrhosis on explant	93
FH		*Ex vivo* gene therapy with autologous cells.	87
	12 years	No benefit	
	7 years	6% reduction in total cholesterol and LDL cholesterol	
	11 years	19% reduction in total cholesterol and LDL cholesterol	
Factor VII deficiency	3 months	70% reduction in rFVII requirement/LT 7 months post-HT	106
	35 months	70% reduction in rFVII requirement/LT 8 months post-HT	
	4 months	Reduction in rFVII requirement/outcome unknown	100
PFIC2	32 months	No benefit (cirrhosis established)/LT 5 months post-HT	99
	16 months	No benefit (cirrhosis established)/LT 14 months post-HT	

Table 2. Clinical hepatocyte transplantation in pediatric liver-based inborn errors of metabolism.

Etiology	Age	Effect/Outcome	Reference
PKU	6 years	Reduction in Phe levels and improved dietary tolerance up to 3 months post-HT (cells from "domino" GSD1b liver)/PAH activity on liver biopsy at 11 months post-HT	107
Tyrosinemia type 1	59 days	Improved coagulopathy and bilirubin/LT 45-days post-HT (cirrhosis on explant)	104
GSD1a	6 years	Reduction in hypoglycemic episodes and cholesterol and triglycerides levels/no hypoglycemic admission at 1 year follow-up	104
GSD1b	18 years	Improved blood glucose, decreased epistaxis/normal G6Pase activity on liver biopsy at 8 months post-HT	108
Mild ZSD	4 years	40% reduction in pipecolic acid for 18 months, decreased cholestasis and abnormal bile acid, and psychomotor improvement/outcome unknown	80
PH1	15 months	Reduction un plasma oxalate/liver-kidney transplant 13 months post-HT	109
UCD			
OTCD	5 years	Ammonia reduction and protein tolerance/septic death 43 days post-HT	110
	5 years	Ammonia reduction, normal glutamine/death 45 days post-HT	111
	10 hours	Ammonia reduction and protein tolerance/LT 6 months post-HT	112
	1 day	Ammonia reduction, increased urea, and protein tolerance/auxiliary partial LT 7 months post-HT and neurologically normal	113
	14 months	Ammonia reduction, increased urea, and psychomotor improvement/LT 6 months post-HT	90
	1 day	Ammonia reduction, increased urea, and protein tolerance/auxiliary partial LT 7 months post-HT	114
	6 h	Ammonia reduction, increased urea, normal urine orotic acid/death 4 months post-HT	115
	9 days	Ammonia reduction, protein tolerance, normal urine orotic acid/LT waitlist 6 months post-HT	
	12 years	Ammonia reduction, increased urea, normal glutamine/septic death 30 days post-HT	104
	11 days	Ammonia reduction/neurologically normal 3 months post-HT	116
	7 months	No effect/LT 4 months post-HT	117
ASLD	3.5 years	Ammonia reduction, and psychomotor improvement/LT 18 months post-HT	97, 118
CPS1D	2.5 months	Ammonia reduction and increased urea/LT 15 months post-HT	95, 115
	4 months	No effect/LT 3.5 months post-HT	117
ASSD	25 months	Ammonia reduced and increased urea/outcome unknown	Lee *et al*, unpublished
	3 years	Ammonia reduction, increased urea, and protein tolerance/outcome unknown	115

CN1: Crigler-Najjar syndrome type 1, LT: liver transplantation, HT: hepatocyte transplantation, A1ATD: alpha-1 antitrypsin deficiency, FH: familial hypercholesterolemia, LDL: low density lipoprotein, PFIC2: progressive familial intrahepatic cholestasis type 2, PKU: phenylketonuria, PAH: phenylalanine hydroxylase, GSD1a: glycogen storage disease type 1a, G6Pase: glucose-6-phosphatase, GSD1b: glycogen storage disease type 1b, ZSD: Zellweger spectrum disorder, PH1: primary hyperoxaluria type 1, UCD: urea cycle defects, OTCD: ornithine transcarbamylase deficiency, ASLD: argininosuccinate lyase deficiency, CPS1D: carbamoyl phosphate synthase I deficiency, ASSD: citrullinemia type 1 (modified from[119-123]).

Material source

The first HT procedure was performed with fetal hepatocytes, generating some ethical considerations[86]. One team used a magnetic activated cell sorting to purify hepatic progenitor cells from fetal hepatocyte based on the CD326 expression[103].

Today, the main source of cells for HT is livers unsuitable for LT such as reduction remnants or unused split livers, damaged livers or livers from young donors. Steatotic livers are also of less quality for hepatocytes[123]. Hepatocytes seem to well tolerate ischemia in comparison to cholangiocytes. Yet, their viability has been shown to be inversely correlated to ischemia time[100]. Hepatocytes can also be isolated from segment IV with or without the caudate lobe during split-liver procedure[113] or from non-heart-beating donors[100]. As for domino liver transplantation, hepatocytes collected from an explanted liver affected by a specific IEM are suitable for HT in another IEM[107, 124]. A 6-year-old child with tetrabiopterin nonresponsive phenylketonuria received hepatocytes isolated from the native live of a patient transplanted for glycogen storage disease type 1b. Phenylalanine levels returned to normal and its half-life decreased significantly after the procedure[107]. To date, no difference in clinical outcome has been reported based on the hepatocytes' origin.

Hepatocyte isolation

A two-step collagenase digestion procedure was developed by Seglen to obtain hepatocytes from rat liver[125]. The procedure was adapted to human liver by Strom and has remained the standard protocol to isolate human hepatocytes since then[126]. Briefly, the liver is perfused with a buffered solution containing a calcium-chelating agent to loosen the desmosomal junctions. Then, the collagenase is infused into the

liver via the cannulated hepatic veins[121]. After isolation, hepatocytes are usually cryopreserved to be available off-the-shelf. Unfortunately, this affects their viability after thawing[127]. The whole hepatocyte isolation process has to be done under a laminar flow in a clean room with regular bacterial & fungus checking. Moreover, because HT falls under advanced therapy medicinal product (ATMP) laws, the US Food and Drug Administration (FDA) and the European Medicines Agency (EMA) require to comply with the guidelines for Good Manufacturing Practice (GMP)[123].

Quality control

Hepatocytes must be tested for bacterial contamination and Mycoplasma. A Trypan blue exclusion test (TBE) is usually performed to quantify the viability of the cells before and after the infusion and after thawing in case of cryopreserved cells[128]. A viability superior to 60% is required to use the cells for clinical application. In order to evaluate cell engraftment potential, hepatocytes are plated on collagen-coated dishes during 24 h and then adherent cells are counted and reported to the seeded cells number. Recently, a team developed an assay comprising 11 endpoints to quantify the metabolic capacity of the isolated hepatocytes, but their clinical relevance has yet to be demonstrated[129].

Dose and route of administration

A 70-kg adult liver is estimated to contain 2.8×10^{11} hepatocytes, or 4×10^{9} cells per kg of body weight[130]. HT is aimed to replace 2-5% of the patient liver mass to restore substantial metabolic liver function, which is equivalent to $8\text{-}20 \times 10^{7}$ cells/kg. This number of cells is usually infused in multiple infusions to avoid the risk of portal

thrombosis linked of the procoagulant activity of the hepatocytes[131]. In patients with liver-based IEM, HT can be repeated in case of loss of effect over time[104].

The first and only report of HT delivered through an intraperitoneal infusion was for acute liver failure, as this route allows severely ill patients to benefit from HT[86]. Intrasplenic arterial infusions have also been evaluated in patients with altered liver architecture and coagulation trouble[110]. Intraportal infusions are the most common way used to deliver cells to the recipient. During the infusion, the portal pressure and vital signs must be regularly followed[95]. Indium-111 labeled hepatocytes were intraportaly infused in a 5-year-old child with OTC deficiency and showed that cells are preferentially retained in the recipient liver[111].

Engraftment evaluation and enhancement

Hepatocyte engraftment quantification has been performed on liver biopsies (with the sampling phenomenon limit, meaning the quantification is based on a small fraction of the whole organ which limits its extrapolation[118]) and more accurately on explanted livers from patients undergoing LT after HT[109]. In donor-recipient sex-mismatch, engraftment can be extrapolated from the sex determining region Y (SRY) gene quantification by quantitative polymerase chain reaction (qPCR)[92, 132]; yet this technique is limited by the signal coming from dead cells, cell debris and apoptotic cells. The enzyme activity quantification on liver sample is a clinically more relevant marker of engraftment in liver-based IEM[96]. In these diseases, the decrease of an accumulating compound (i. e. ammonia in urea cycle disorders (UCD)[110]) or the appearance of a product following HT (i.e., urea in UCD[118] or conjugated bilirubin in Crigler-Najjar syndrome type 1 (CN1)[96]) are routinely measured to evaluate the effect of HT.

Partial hepatectomy (PH) is regularly performed in living-donor liver harvesting or liver tumor resection. This induces a strong stimulus for hepatocyte replication. PH has been used in HT to stimulate infused hepatocytes to proliferate but in the absence of a growth advantage, the proliferation should be the same for the donor and the recipient cells[87]. Preoperative portal vein occlusion (PVO) is also a common surgical procedure to induce hepatic regeneration before PH for tumor resection for example[123]. To our knowledge, this technique has never been applied in HT. Taken together, PH and PVO would make HT a heavier procedure and the risk-benefit ratio would need to be carefully evaluated.

Irradiation of the native liver (INL) has been developed to induce a strong mitogenic signal in the liver parenchyma with a proliferative advantage of the (non-irradiated) infused hepatocytes without the potential risks of PH. Recently, Soltys *et al.* reported HT in 2 pediatric patients (4 months & 7 months) with UCD preconditioned with radiation therapy to the right lobe of the liver (5 Gy and 7.5 Gy, respectively)[117]. HT had no effect on the metabolic control and both patients underwent LT a few months after HT. The explanted livers were not screened for infused cells and showed no sign of radiation-induced damage. Yet, liver irradiation is not without side effects; namely, it was shown, in 6 adult patients treated with high dose radiation (12-54 Gy) for biliopancreatic carcinoma, to activate stellates cells with risk of liver fibrosis in the long term[133].

Immunosuppression

Immunosuppression regimens following HT have been largely inspired by LT protocols: an induction based on basiliximab at day 0 and day 4 and a maintenance therapy with tacrolimus to reach blood levels of 6-8 ng/mL[80]. Some add, as induction

regimen, an intravenous bolus of methylprednisolone followed by prednisolone daily tapered over the first 6 months post-HT[105]. Recently, a patient received anti-lymphocyte antibody as a way to target immune rejection of the infused hepatocytes and loss of effect[117]. In an attempt to avoid immune rejection of the infused hepatocytes, Grossman *et al.* used autologous transduced hepatocytes to treat patients with familial hypercholesterolemia without much clinical success[87].

How to overcome hepatocyte transplantation barriers

Since the first report of HT nearly 25 years ago, much effort has focused on how to translate HT into a validated clinical option. Hepatocytes are fragile cells with low proliferative capacities in vitro, and their engraftment is low even with intense preconditioning methods such as radiation therapy associated with strong immunosuppression regimen (anti-lymphocyte antibody). The field of liver cell therapy is now looking for a new type of cell which can overcome the disadvantages of a fully differentiated primary cell. Mesenchymal stromal cells (MSC) or, as recently renamed, medicinal signaling cells seem to hold promise for clinical application in a near future[134].

Objectives

ZSD are a group of diseases associated with high morbidity and mortality. Both are mainly driven by central nervous system and liver involvement of the disease[47]. To date, supportive approaches have been the standard of care for ZSD patients[43]. ZSD therapeutic approaches are currently developed by the evaluation of molecules that are able to rescue PBD *in vitro.* These *in vitro* assays are time-consuming, cumbersome, and/or expensive [72-74]. Beside these *in vitro* approaches, ZSD mouse

models are used to evaluate the therapeutic effect of molecules acting on specific tissues or to confirm the therapeutic potential of hit compounds previously discovered *in vitro* [135]. The ZSD mouse models currently available are limited by poor survival rate and/or breeding limitations[136, 137]. In research settings, we and others have published encouraging biochemical and clinical results after the delivery of functional peroxisomes by HT or LT in ZSD patients[77, 78, 80]. This was further supported by the discovery that brain development depends on intact liver peroxisomal function in a ZSD mouse model[138].

First, we hypothesize that by optimizing and refining *in vitro* PBD evaluation we could more easily detect even mild PBD phenotypes. Secondly, we postulate that developing a robust *in vivo* ZSD mouse model would allow us to ascertain HT as a therapeutic approach in ZSD. Thirdly, we guess that reporting the long-term outcome of LT in mild ZSD patients would interest other pediatric LT centers in order to broaden their LT indications to this incurable disease.

Transient transfection of an enhanced green fluorescent protein fused with a PTS1 (eGFP-PTS1) in skin fibroblasts from ZSD patients underlines the PBD by the cytosolic eGFP-PTS1 distribution. The absence of peroxisomal import of the eGFP-PTS1 explains this pattern in ZSD cells compared to punctiform (peroxisomal) eGFP-PTS1 distribution in control cells[57]. This technique has several drawbacks such as cell toxicity, transientness and a low efficiency, especially on primary cells such as human skin fibroblasts[139-142]. We aim to develop a stable eGFP-PTS1 expression system associated with a digital image analysis that is able to discriminate control and ZSD cells including mild PBD.

ZSD mouse models available for preclinical studies are fragile and/or difficult to breed[136, 137, 143]. Clinical results obtained after HT or LT in ZSD patients need to be evaluated with a robust ZSD mouse model to ascertain the outcome in a highly controlled environment[77, 78, 80]. We aim to improve the breeding features and the robustness of a mouse model carrying the hypomorphic *Pex1* p.G844D mutation by mouse strain modification as already performed in a *Pex2* knockout mouse model[144]. Then, we aspire to evaluate HT in this new mouse model.

Short-term encouraging outcomes of LT in mild ZSD are reported from two patients worldwide[77, 78]. We aim to collect and report clinical and biochemical long-term outcomes after having performed three living-donor LT for mild ZSD. This could reinforce the interest for liver-targeted therapies in ZSD.

Significance

Early ZSD diagnosis is rendered feasible, in the United States, by the progressive implementation of the newborn screening for X-ALD, a related peroxisomal disorder[60]. By C26LPC quantification on Guthrie card, both diseases can be diagnosed but, contrary to X-ALD, no preventive treatment is available for ZSD patients[59]. With an estimated incidence of 1/50-100 000 births[42, 43], it means that, in the United States, 75 to 150 ZSD neonates will be diagnosed each year. As a consequence, the affected families will avoid the long and distressing quest for a diagnosis, but they will face the stressful absence of curative treatment for their affected child[145, 146]. Thus, refining a method for *in vitro* screening of molecules able to rescue PBD and optimizing a mouse model for their further *in vivo* evaluation is highly relevant for both the scientific community and the affected families. Moreover,

reporting long-term outcomes after LT for mild ZSD is awaited by the same communities[47].

Acknowledgments

I thank Emilie Van Leemput for language editing.

References

1. Rhodin, J., Correlation of ultrastructural organization and function in normal and experimentally changed proximal convoluted tubule cells of the mouse kidney. [Ph.D. thesis], 1954.
2. De Duve, C. and P. Baudhuin, Peroxisomes (microbodies and related particles). Physiol Rev, 1966. 46(2): p. 323-57.
3. Schonenberger, M.J. and W.J. Kovacs, Isolation of Peroxisomes from Mouse Brain Using a Continuous Nycodenz Gradient: A Comparison to the Isolation of Liver and Kidney Peroxisomes. Methods Mol Biol, 2017. 1595: p. 13-26.
4. Huybrechts, S.J., P.P. Van Veldhoven, C. Brees, G.P. Mannaerts, G.V. Los, and M. Fransen, Peroxisome dynamics in cultured mammalian cells. Traffic, 2009. 10(11): p. 1722-33.
5. Waterham, H.R., S. Ferdinandusse, and R.J. Wanders, Human disorders of peroxisome metabolism and biogenesis. Biochim Biophys Acta, 2016. 1863(5): p. 922-33.
6. Braverman, N.E. and A.B. Moser, Functions of plasmalogen lipids in health and disease. Biochim Biophys Acta, 2012. 1822(9): p. 1442-52.
7. Wanders, R.J. and H.R. Waterham, Biochemistry of mammalian peroxisomes revisited. Annu Rev Biochem, 2006. 75: p. 295-332.
8. Wallner, S. and G. Schmitz, Plasmalogens the neglected regulatory and scavenging lipid species. Chem Phys Lipids, 2011. 164(6): p. 573-89.
9. Russell, D.W., The enzymes, regulation, and genetics of bile acid synthesis. Annu Rev Biochem, 2003. 72: p. 137-74.
10. Ferdinandusse, S., S. Denis, P.L. Faust, and R.J. Wanders, Bile acids: the role of peroxisomes. J Lipid Res, 2009. 50(11): p. 2139-47.
11. Takahashi, S., T. Fukami, Y. Masuo, C.N. Brocker, C. Xie, K.W. Krausz, C.R. Wolf, C.J. Henderson, and F.J. Gonzalez, Cyp2c70 is responsible for the species difference in bile acid metabolism between mice and humans. J Lipid Res, 2016. 57(12): p. 2130-2137.
12. Wanders, R.J., J. Komen, and S. Ferdinandusse, Phytanic acid metabolism in health and disease. Biochim Biophys Acta, 2011. 1811(9): p. 498-507.
13. Wanders, R.J., Metabolic functions of peroxisomes in health and disease. Biochimie, 2014. 98: p. 36-44.
14. Salido, E., A.L. Pey, R. Rodriguez, and V. Lorenzo, Primary hyperoxalurias: disorders of glyoxylate detoxification. Biochim Biophys Acta, 2012. 1822(9): p. 1453-64.
15. De Duve, C., H. Beaufay, P. Jacques, Y. Rahman-Li, O.Z. Sellinger, R. Wattiaux, and S. De Coninck, Intracellular localization of catalase and of some oxidases in rat liver. Biochim Biophys Acta, 1960. 40: p. 186-7.
16. Kovacs, W.J. and S. Krisans, Cholesterol biosynthesis and regulation: role of peroxisomes. Adv Exp Med Biol, 2003. 544: p. 315-27.
17. Kovacs, W.J., J.E. Shackelford, K.N. Tape, M.J. Richards, P.L. Faust, S.J. Fliesler, and S.K. Krisans, Disturbed cholesterol homeostasis in a peroxisome-deficient PEX2 knockout mouse model. Mol Cell Biol, 2004. 24(1): p. 1-13.
18. Kovacs, W.J., K.N. Tape, J.E. Shackelford, T.M. Wikander, M.J. Richards, S.J. Fliesler, S.K. Krisans, and P.L. Faust, Peroxisome deficiency causes a complex phenotype because of hepatic SREBP/Insig dysregulation associated with endoplasmic reticulum stress. J Biol Chem, 2009. 284(11): p. 7232-45.
19. Faust, P.L. and W.J. Kovacs, Cholesterol biosynthesis and ER stress in peroxisome deficiency. Biochimie, 2014. 98: p. 75-85.

20. Farre, J.C., S.S. Mahalingam, M. Proietto, and S. Subramani, Peroxisome biogenesis, membrane contact sites, and quality control. EMBO Rep, 2019. 20(1).
21. Waterham, H.R., J. Koster, C.W. van Roermund, P.A. Mooyer, R.J. Wanders, and J.V. Leonard, A lethal defect of mitochondrial and peroxisomal fission. N Engl J Med, 2007. 356(17): p. 1736-41.
22. Kalel, V.C. and R. Erdmann, Unraveling of the Structure and Function of Peroxisomal Protein Import Machineries. Subcell Biochem, 2018. 89: p. 299-321.
23. Dias, A.F., T. Francisco, T.A. Rodrigues, C.P. Grou, and J.E. Azevedo, The first minutes in the life of a peroxisomal matrix protein. Biochim Biophys Acta, 2016. 1863(5): p. 814-20.
24. Kunze, M., N. Malkani, S. Maurer-Stroh, C. Wiesinger, J.A. Schmid, and J. Berger, Mechanistic insights into PTS2-mediated peroxisomal protein import: the co-receptor PEX5L drastically increases the interaction strength between the cargo protein and the receptor PEX7. J Biol Chem, 2015. 290(8): p. 4928-40.
25. Law, K.B., D. Bronte-Tinkew, E. Di Pietro, A. Snowden, R.O. Jones, A. Moser, J.H. Brumell, N. Braverman, and P.K. Kim, The peroxisomal AAA ATPase complex prevents pexophagy and development of peroxisome biogenesis disorders. Autophagy, 2017. 13(5): p. 868-884.
26. Bharti, P., W. Schliebs, T. Schievelbusch, A. Neuhaus, C. David, K. Kock, C. Herrmann, H.E. Meyer, S. Wiese, B. Warscheid, C. Theiss, and R. Erdmann, PEX14 is required for microtubule-based peroxisome motility in human cells. J Cell Sci, 2011. 124(Pt 10): p. 1759-68.
27. Schrader, M., M. Thiemann, and H.D. Fahimi, Peroxisomal motility and interaction with microtubules. Microsc Res Tech, 2003. 61(2): p. 171-8.
28. Neuhaus, A., C. Eggeling, R. Erdmann, and W. Schliebs, Why do peroxisomes associate with the cytoskeleton? Biochim Biophys Acta, 2016. 1863(5): p. 1019-26.
29. Smith, J.J. and J.D. Aitchison, Peroxisomes take shape. Nat Rev Mol Cell Biol, 2013. 14(12): p. 803-17.
30. Bowen, P., C.S. Lee, H. Zellweger, and R. Lindenberg, A FAMILIAL SYNDROME OF MULTIPLE CONGENITAL DEFECTS. Bull Johns Hopkins Hosp, 1964. 114: p. 402-14.
31. Zellweger, H., P. Maertens, D. Superneau, and W. Wertelecki, History of the cerebrohepatorenal syndrome of Zellweger and other peroxisomal disorders. South Med J, 1988. 81(3): p. 357-64.
32. Passarge, E. and A.J. McAdams, Cerebro-hepato-renal syndrome. A newly recognized hereditary disorder of multiple congenital defects, including sudanophilic leukodystrophy, cirrhosis of the liver, and polycystic kidneys. J Pediatr, 1967. 71(5): p. 691-702.
33. Goldfischer, S., C.L. Moore, A.B. Johnson, A.J. Spiro, M.P. Valsamis, H.K. Wisniewski, R.H. Ritch, W.T. Norton, I. Rapin, and L.M. Gartner, Peroxisomal and mitochondrial defects in the cerebro-hepato-renal syndrome. Science, 1973. 182(4107): p. 62-4.
34. Benke, P.J., P.F. Reyes, and J.C. Parker, Jr., New form of adrenoleukodystrophy. Hum Genet, 1981. 58(2): p. 204-8.
35. Scotto, J.M., M. Hadchouel, M. Odievre, M.H. Laudat, J.M. Saudubray, O. Dulac, I. Beucler, and P. Beaune, Infantile phytanic acid storage disease, a possible variant of Refsum's disease: three cases, including ultrastructural studies of the liver. J Inherit Metab Dis, 1982. 5(2): p. 83-90.
36. Poulos, A., P. Sharp, and M. Whiting, Infantile Refsum's disease (phytanic acid storage disease): a variant of Zellweger's syndrome? Clin Genet, 1984. 26(6): p. 579-86.
37. Roels, F., A. Cornelis, B.T. Poll-The, P. Aubourg, H. Ogier, J. Scotto, and J.M. Saudubray, Hepatic peroxisomes are deficient in infantile refsum disease: a cytochemical study of 4 cases. Am J Med Genet, 1986. 25(2): p. 257-71.
38. Ebberink, M.S., P.A. Mooijer, J. Gootjes, J. Koster, R.J. Wanders, and H.R. Waterham, Genetic classification and mutational spectrum of more than 600 patients with a Zellweger syndrome spectrum disorder. Hum Mutat, 2011. 32(1): p. 59-69.
39. Portsteffen, H., A. Beyer, E. Becker, C. Epplen, A. Pawlak, W.H. Kunau, and G. Dodt, Human PEX1 is mutated in complementation group 1 of the peroxisome biogenesis disorders. Nat Genet, 1997. 17(4): p. 449-52.
40. Dodt, G., N. Braverman, C. Wong, A. Moser, H.W. Moser, P. Watkins, D. Valle, and S.J. Gould, Mutations in the PTS1 receptor gene, PXR1, define complementation group 2 of the peroxisome biogenesis disorders. Nat Genet, 1995. 9(2): p. 115-25.
41. Ratbi, I., K.D. Falkenberg, M. Sommen, N. Al-Sheqaih, S. Guaoua, G. Vandeweyer, J.E. Urquhart, K.E. Chandler, S.G. Williams, N.A. Roberts, M. El Alloussi, G.C. Black, S. Ferdinandusse, H. Ramdi, A. Heimler, A. Fryer, S.A. Lynch, N. Cooper, K.R. Ong, C.E. Smith, C.F. Inglehearn, A.J. Mighell, C. Elcock, J.A. Poulter, M. Tischkowitz, S.J. Davies, A. Sefiani,

A.A. Mironov, W.G. Newman, H.R. Waterham, and G. Van Camp, Heimler Syndrome Is Caused by Hypomorphic Mutations in the Peroxisome-Biogenesis Genes PEX1 and PEX6. Am J Hum Genet, 2015. 97(4): p. 535-45.
42. Vasiljevic, E., Z. Ye, D.M. Pavelec, B.F. Darst, C.D. Engelman, and M.W. Baker, Carrier frequency estimation of Zellweger spectrum disorder using ExAC database and bioinformatics tools. Genet Med, 2019. 21(9): p. 1969-1976.
43. Braverman, N.E., G.V. Raymond, W.B. Rizzo, A.B. Moser, M.E. Wilkinson, E.M. Stone, S.J. Steinberg, M.F. Wangler, E.T. Rush, J.G. Hacia, and M. Bose, Peroxisome biogenesis disorders in the Zellweger spectrum: An overview of current diagnosis, clinical manifestations, and treatment guidelines. Mol Genet Metab, 2016. 117(3): p. 313-21.
44. Simons, J. and M. Nowaczyk, Phenotypic Variability in Fraternal Twins with PEX1 Mutations: Zellweger Syndrome with Discordant Clinical Phenotype. MJM, 2013. S5(001): p. 1-3.
45. Poll-The, B.T., J. Gootjes, M. Duran, J.B. De Klerk, L.J. Wenniger-Prick, R.J. Admiraal, H.R. Waterham, R.J. Wanders, and P.G. Barth, Peroxisome biogenesis disorders with prolonged survival: phenotypic expression in a cohort of 31 patients. Am J Med Genet A, 2004. 126a(4): p. 333-8.
46. Wanders, R.J., F.C. Klouwer, S. Ferdinandusse, H.R. Waterham, and B.T. Poll-The, Clinical and Laboratory Diagnosis of Peroxisomal Disorders. Methods Mol Biol, 2017. 1595: p. 329-342.
47. Klouwer, F.C., K. Berendse, S. Ferdinandusse, R.J. Wanders, M. Engelen, and B.T. Poll-The, Zellweger spectrum disorders: clinical overview and management approach. Orphanet J Rare Dis, 2015. 10: p. 151.
48. Poll-The, B.T., J.M. Saudubray, H.A. Ogier, M. Odievre, J.M. Scotto, L. Monnens, L.C. Govaerts, F. Roels, A. Cornelis, R.B. Schutgens, and et al., Infantile Refsum disease: an inherited peroxisomal disorder. Comparison with Zellweger syndrome and neonatal adrenoleukodystrophy. Eur J Pediatr, 1987. 146(5): p. 477-83.
49. Klouwer, F.C., I.C. Huffnagel, S. Ferdinandusse, H.R. Waterham, R.J. Wanders, M. Engelen, and B.T. Poll-The, Clinical and Biochemical Pitfalls in the Diagnosis of Peroxisomal Disorders. Neuropediatrics, 2016. 47(4): p. 205-20.
50. Berendse, K., M. Engelen, G.E. Linthorst, A.S. van Trotsenburg, and B.T. Poll-The, High prevalence of primary adrenal insufficiency in Zellweger spectrum disorders. Orphanet J Rare Dis, 2014. 9: p. 133.
51. Govaerts, L., L. Monnens, T. Melis, and F. Trijbels, Disturbed adrenocortical function in cerebro-hepato-renal syndrome of Zellweger. Eur J Pediatr, 1984. 143(1): p. 10-2.
52. Govaerts, L., W.G. Sippell, and L. Monnens, Further analysis of the disturbed adrenocortical function in the cerebro-hepato-renal syndrome of Zellweger. J Inherit Metab Dis, 1989. 12(4): p. 423-8.
53. Tran, D., W. Greenhill, and S. Wilson, Infantile refsum disease with enamel defects: a case report. Pediatr Dent, 2011. 33(3): p. 266-70.
54. Sa, M.J., J.C. Rocha, M.F. Almeida, C. Carmona, E. Martins, V. Miranda, M. Coutinho, R. Ferreira, S. Pacheco, F. Laranjeira, I. Ribeiro, A.M. Fortuna, and L. Lacerda, Infantile Refsum Disease: Influence of Dietary Treatment on Plasma Phytanic Acid Levels. JIMD Rep, 2016. 26: p. 53-60.
55. van Woerden, C.S., J.W. Groothoff, F.A. Wijburg, M. Duran, R.J. Wanders, P.G. Barth, and B.T. Poll-The, High incidence of hyperoxaluria in generalized peroxisomal disorders. Mol Genet Metab, 2006. 88(4): p. 346-50.
56. Klouwer, F.C.C., A. Meester-Delver, F.M. Vaz, H.R. Waterham, R.C.M. Hennekam, and B.T. Poll-The, Development and validation of a severity scoring system for Zellweger spectrum disorders. Clin Genet, 2017.
57. Waterham, H.R. and M.S. Ebberink, Genetics and molecular basis of human peroxisome biogenesis disorders. Biochim Biophys Acta, 2012. 1822(9): p. 1430-41.
58. Aubourg, P. and R. Wanders, Peroxisomal disorders. Handb Clin Neurol, 2013. 113: p. 1593-609.
59. Klouwer, F.C.C., S. Ferdinandusse, H. van Lenthe, W. Kulik, R.J.A. Wanders, B.T. Poll-The, H.R. Waterham, and F.M. Vaz, Evaluation of C26:0-lysophosphatidylcholine and C26:0-carnitine as diagnostic markers for Zellweger spectrum disorders. J Inherit Metab Dis, 2017. 40(6): p. 875-881.
60. Wiens, K., S.A. Berry, H. Choi, A. Gaviglio, A. Gupta, A. Hietala, D. Kenney-Jung, T. Lund, W. Miller, E.I. Pierpont, G. Raymond, H. Winslow, H.A. Zierhut, and P.J. Orchard, A report on state-

wide implementation of newborn screening for X-linked Adrenoleukodystrophy. Am J Med Genet A, 2019. 179(7): p. 1205-1213.
61. Wanders, R.J., Y.R. Purvis, H.S. Heymans, J.A. Bakkeren, G.G. Parmentier, J. van Eldere, H. Eyssen, H. van den Bosch, J.M. Tager, and R.B. Schutgens, Age-related differences in plasmalogen content of erythrocytes from patients with the cerebro-hepato-renal (Zellweger) syndrome: implications for postnatal detection of the disease. J Inherit Metab Dis, 1986. 9(4): p. 335-42.
62. Korman, S.H., H. Mandel, and A. Gutman, Characteristic urine organic acid profile in peroxisomal biogenesis disorders. J Inherit Metab Dis, 2000. 23(4): p. 425-8.
63. Rocchiccioli, F., P. Aubourg, and P.F. Bougneres, Medium- and long-chain dicarboxylic aciduria in patients with Zellweger syndrome and neonatal adrenoleukodystrophy. Pediatr Res, 1986. 20(1): p. 62-6.
64. Berendse, K., M. Engelen, S. Ferdinandusse, C.B. Majoie, H.R. Waterham, F.M. Vaz, J.H. Koelman, P.G. Barth, R.J. Wanders, and B.T. Poll-The, Zellweger spectrum disorders: clinical manifestations in patients surviving into adulthood. J Inherit Metab Dis, 2016. 39(1): p. 93-106.
65. Wanders, R.J., S. Denis, J.P. Ruiter, R.B. Schutgens, C.W. van Roermund, and B.S. Jacobs, Measurement of peroxisomal fatty acid beta-oxidation in cultured human skin fibroblasts. J Inherit Metab Dis, 1995. 18 Suppl 1: p. 113-24.
66. Gootjes, J., F. Schmohl, P.A. Mooijer, C. Dekker, H. Mandel, M. Topcu, M. Huemer, M. Von Schutz, T. Marquardt, J.A. Smeitink, H.R. Waterham, and R.J. Wanders, Identification of the molecular defect in patients with peroxisomal mosaicism using a novel method involving culturing of cells at 40 degrees C: implications for other inborn errors of metabolism. Hum Mutat, 2004. 24(2): p. 130-9.
67. Zeynelabidin, S., F.C.C. Klouwer, J.C.M. Meijers, M.H. Suijker, M. Engelen, B.T. Poll-The, and C.H. van Ommen, Coagulopathy in Zellweger spectrum disorders: a role for vitamin K. J Inherit Metab Dis, 2018. 41(2): p. 249-255.
68. Berendse, K., F.C. Klouwer, B.G. Koot, E.M. Kemper, S. Ferdinandusse, K.V. Koelfat, M. Lenicek, F.G. Schaap, H.R. Waterham, F.M. Vaz, M. Engelen, P.L. Jansen, R.J. Wanders, and B.T. Poll-The, Cholic acid therapy in Zellweger spectrum disorders. J Inherit Metab Dis, 2016.
69. Klouwer, F.C.C., B.G.P. Koot, K. Berendse, E.M. Kemper, S. Ferdinandusse, K.V.K. Koelfat, M. Lenicek, F.M. Vaz, M. Engelen, P.L.M. Jansen, R.J.A. Wanders, H.R. Waterham, F.G. Schaap, and B.T. Poll-The, The cholic acid extension study in Zellweger spectrum disorders: results and implications for therapy. J Inherit Metab Dis, 2018.
70. Heubi, J.E., K.E. Bove, and K.D.R. Setchell, Oral Cholic Acid Is Efficacious and Well Tolerated in Patients With Bile Acid Synthesis and Zellweger Spectrum Disorders. J Pediatr Gastroenterol Nutr, 2017. 65(3): p. 321-326.
71. Klouwer, F.C.C., N.E. Braverman, H.J. Verkade, K. Berendse, H.R. Waterham, R.J.A. Wanders, B.T. Poll-The, and B.G.P. Koot, Oral Cholic Acid in Zellweger Spectrum Disorders: A Word of Caution. J Pediatr Gastroenterol Nutr, 2018. 66(2): p. e57.
72. Berendse, K., M.S. Ebberink, L. Ijlst, B.T. Poll-The, R.J. Wanders, and H.R. Waterham, Arginine improves peroxisome functioning in cells from patients with a mild peroxisome biogenesis disorder. Orphanet J Rare Dis, 2013. 8: p. 138.
73. MacLean, G.E., C. Argyriou, E. Di Pietro, X. Sun, S. Birjandian, P. Saberian, J.G. Hacia, and N.E. Braverman, Zellweger spectrum disorder patient-derived fibroblasts with the PEX1-Gly843Asp allele recover peroxisome functions in response to flavonoids. J Cell Biochem, 2019. 120(3): p. 3243-3258.
74. Zhang, R., L. Chen, S. Jiralerspong, A. Snowden, S. Steinberg, and N. Braverman, Recovery of PEX1-Gly843Asp peroxisome dysfunction by small-molecule compounds. Proc Natl Acad Sci U S A, 2010. 107(12): p. 5569-74.
75. Nazarko, T.Y., Pexophagy is responsible for 65% of cases of peroxisome biogenesis disorders. Autophagy, 2017. 13(5): p. 991-994.
76. Dranchak, P.K., E. Di Pietro, A. Snowden, N. Oesch, N.E. Braverman, S.J. Steinberg, and J.G. Hacia, Nonsense suppressor therapies rescue peroxisome lipid metabolism and assembly in cells from patients with specific PEX gene mutations. J Cell Biochem, 2011. 112(5): p. 1250-8.
77. Van Maldergem, L., A.B. Moser, M.F. Vincent, D. Roland, R. Reding, J.B. Otte, R.J. Wanders, and E. Sokal, Orthotopic liver transplantation from a living-related donor in an infant with a peroxisome biogenesis defect of the infantile Refsum disease type. J Inherit Metab Dis, 2005. 28(4): p. 593-600.

78. Matsunami, M., N. Shimozawa, A. Fukuda, T. Kumagai, M. Kubota, P.F. Chong, and M. Kasahara, Living-Donor Liver Transplantation From a Heterozygous Parent for Infantile Refsum Disease. Pediatrics, 2016. 137(6).
79. Demaret, T., S. Varma, X. Stephenne, F. Smets, I. Scheers, R. Wanders, L. Van Maldergem, R. Reding, and E. Sokal, Living-donor liver transplantation for mild Zellweger spectrum disorder: Up to 17 years follow-up. Pediatr Transplant, 2018. 22(3): p. e13112.
80. Sokal, E.M., F. Smets, A. Bourgois, L. Van Maldergem, J.P. Buts, R. Reding, J. Bernard Otte, V. Evrard, D. Latinne, M.F. Vincent, A. Moser, and H.E. Soriano, Hepatocyte transplantation in a 4-year-old girl with peroxisomal biogenesis disease: technique, safety, and metabolic follow-up. Transplantation, 2003. 76(4): p. 735-8.
81. Argyriou, C., J. Song, A. Polosa, B. Cecyre, D. McDougald, J.F. Bouchard, P. Lachapelle, J. Bennett, J.G. Hacia, and N. Braverman, rAAV mediated PEX1 gene augmentation improves visual function in a mouse model for Zellweger spectrum disorder, in The Global Foundation for Peroxisomal Disorders - Scientific Conference. 2017: Washington, D.C. p. 13-14.
82. Argyriou, C., J.Y. Song, A. Polosa, B. Cecyre, J.-F. Bouchard, P. Lachapelle, J. Bennett, and N. Braverman, AB037. rAAV mediated PEX1 gene augmentation improves visual function in a mouse model for Zellweger spectrum disorder. Annals of Eye Science, 2018. 3(3): p. AB037.
83. Gurevich, M., V. Guy-Viterbo, M. Janssen, X. Stephenne, F. Smets, E. Sokal, C. Lefebvre, J.L. Balligand, T. Pirotte, F. Veyckemans, P. Clapuyt, R. Menten, D. Dumitriu, E. Danse, L. Annet, S.C. Clety, T. Detaille, D. Latinne, C. Sempoux, P.F. Laterre, C. de Magnee, J. Lerut, and R. Reding, Living Donor Liver Transplantation in Children: Surgical and Immunological Results in 250 Recipients at Universite Catholique de Louvain. Ann Surg, 2015. 262(6): p. 1141-9.
84. Otte, J.B., J. de Ville de Goyet, R. Reding, L. Van Obbergh, F. Veyckemans, M.A. Carlier, M. De Kock, S. Clement de Clety, P. Clapuyt, E. Sokal, J. Lerut, I. Delbeke, V. Dierick, M. Janssen, R. Rosati, and F. Libert, Pediatric liver transplantation: from the full-size liver graft to reduced, split, and living related liver transplantation. Pediatr Surg Int, 1998. 13(5-6): p. 308-18.
85. Smets, F., M. Najimi, and E.M. Sokal, Cell transplantation in the treatment of liver diseases. Pediatr Transplant, 2008. 12(1): p. 6-13.
86. Habibullah, C.M., I.H. Syed, A. Qamar, and Z. Taher-Uz, Human fetal hepatocyte transplantation in patients with fulminant hepatic failure. Transplantation, 1994. 58(8): p. 951-2.
87. Grossman, M., D.J. Rader, D.W. Muller, D.M. Kolansky, K. Kozarsky, B.J. Clark, 3rd, E.A. Stein, P.J. Lupien, H.B. Brewer, Jr., S.E. Raper, and et al., A pilot study of ex vivo gene therapy for homozygous familial hypercholesterolaemia. Nat Med, 1995. 1(11): p. 1148-54.
88. Fisher, R.A. and S.C. Strom, Human hepatocyte transplantation: worldwide results. Transplantation, 2006. 82(4): p. 441-9.
89. Khan, A.A., N. Parveen, V.S. Mahaboob, A. Rajendraprasad, H.R. Ravindraprakash, J. Venkateswarlu, P. Rao, G. Pande, M.L. Narusu, M.N. Khaja, R. Pramila, A. Habeeb, and C.M. Habibullah, Management of hyperbilirubinemia in biliary atresia by hepatic progenitor cell transplantation through hepatic artery: a case report. Transplant Proc, 2008. 40(4): p. 1153-5.
90. Stephenne, X., M. Najimi, F. Smets, R. Reding, J. de Ville de Goyet, and E.M. Sokal, Cryopreserved liver cell transplantation controls ornithine transcarbamylase deficient patient while awaiting liver transplantation. Am J Transplant, 2005. 5(8): p. 2058-61.
91. Soriano, H.E., R.P. Wood, D.C. Kang, C.F. Ozaki, F.M. J., F.C. Bischoff, and B.S. Reid, Hepatocyte transplantation (HCT) in children with fulminant liver failure (FLF). Hepatology, 1997. 26(239A): p. 443.
92. Strom, S.C., R.A. Fisher, M.T. Thompson, A.J. Sanyal, P.E. Cole, J.M. Ham, and M.P. Posner, Hepatocyte transplantation as a bridge to orthotopic liver transplantation in terminal liver failure. Transplantation, 1997. 63(4): p. 559-69.
93. Strom, S.C., J.R. Chowdhury, and I.J. Fox, Hepatocyte transplantation for the treatment of human disease. Semin Liver Dis, 1999. 19(1): p. 39-48.
94. Sterling, R.K. and R.A. Fisher, Liver transplantation. Living donor, hepatocyte, and xenotransplantation. Clin Liver Dis, 2001. 5(2): p. 431-60, vii.
95. Meyburg, J., F. Hoerster, J. Schmidt, J. Poeschl, G.F. Hoffmann, and J.P. Schenk, Monitoring of intraportal liver cell application in children. Cell Transplant, 2010. 19(5): p. 629-38.
96. Fox, I.J., J.R. Chowdhury, S.S. Kaufman, T.C. Goertzen, N.R. Chowdhury, P.I. Warkentin, K. Dorko, B.V. Sauter, and S.C. Strom, Treatment of the Crigler-Najjar syndrome type I with hepatocyte transplantation. N Engl J Med, 1998. 338(20): p. 1422-6.

97. Darwish, A.A., E. Sokal, X. Stephenne, M. Najimi, J. de Ville de Goyet, and R. Reding, Permanent access to the portal system for cellular transplantation using an implantable port device. Liver Transpl, 2004. 10(9): p. 1213-5.
98. Ambrosino, G., S. Varotto, S.C. Strom, G. Guariso, E. Franchin, D. Miotto, L. Caenazzo, S. Basso, P. Carraro, M.L. Valente, D. D'Amico, L. Zancan, and L. D'Antiga, Isolated hepatocyte transplantation for Crigler-Najjar syndrome type 1. Cell Transplant, 2005. 14(2-3): p. 151-7.
99. Dhawan, A., R.R. Mitry, and R.D. Hughes, Hepatocyte transplantation for liver-based metabolic disorders. J Inherit Metab Dis, 2006. 29(2-3): p. 431-5.
100. Hughes, R.D., R.R. Mitry, A. Dhawan, S.C. Lehec, R. Girlanda, M. Rela, N.D. Heaton, and P. Muiesan, Isolation of hepatocytes from livers from non-heart-beating donors for cell transplantation. Liver Transpl, 2006. 12(5): p. 713-7.
101. Allen, K.J., N.A. Mifsud, R. Williamson, P. Bertolino, and W. Hardikar, Cell-mediated rejection results in allograft loss after liver cell transplantation. Liver Transpl, 2008. 14(5): p. 688-94.
102. Lysy, P.A., M. Najimi, X. Stephenne, A. Bourgois, F. Smets, and E.M. Sokal, Liver cell transplantation for Crigler-Najjar syndrome type I: update and perspectives. World J Gastroenterol, 2008. 14(22): p. 3464-70.
103. Khan, A.A., N. Parveen, V.S. Mahaboob, A. Rajendraprasad, H.R. Ravindraprakash, J. Venkateswarlu, P. Rao, G. Pande, M.L. Narusu, M.N. Khaja, R. Pramila, A. Habeeb, and C.M. Habibullah, Treatment of Crigler-Najjar Syndrome type 1 by hepatic progenitor cell transplantation: a simple procedure for management of hyperbilirubinemia. Transplant Proc, 2008. 40(4): p. 1148-50.
104. Ribes-Koninckx, C., E.P. Ibars, M.A. Calzado Agrasot, A. Bonora-Centelles, B.P. Miquel, J.J. Vila Carbo, E.D. Aliaga, J.M. Pallardo, M.J. Gomez-Lechon, and J.V. Castell, Clinical outcome of hepatocyte transplantation in four pediatric patients with inherited metabolic diseases. Cell Transplant, 2012. 21(10): p. 2267-82.
105. Jorns, C., G. Nowak, A. Nemeth, H. Zemack, L.M. Mork, H. Johansson, R. Gramignoli, M. Watanabe, A. Karadagi, M. Alheim, D. Hauzenberger, R. van Dijk, P.J. Bosma, F. Ebbesen, A. Szakos, B. Fischler, S. Strom, E. Ellis, and B.G. Ericzon, De Novo Donor-Specific HLA Antibody Formation in Two Patients With Crigler-Najjar Syndrome Type I Following Human Hepatocyte Transplantation With Partial Hepatectomy Preconditioning. Am J Transplant, 2016. 16(3): p. 1021-30.
106. Dhawan, A., R.R. Mitry, R.D. Hughes, S. Lehec, C. Terry, S. Bansal, R. Arya, J.J. Wade, A. Verma, N.D. Heaton, M. Rela, and G. Mieli-Vergani, Hepatocyte transplantation for inherited factor VII deficiency. Transplantation, 2004. 78(12): p. 1812-4.
107. Stephenne, X., F.G. Debray, F. Smets, N. Jazouli, G. Sana, T. Tondreau, R. Menten, P. Goffette, F. Boemer, R. Schoos, S.W. Gersting, M. Najimi, A.C. Muntau, P. Goyens, and E.M. Sokal, Hepatocyte transplantation using the domino concept in a child with tetrabiopterin nonresponsive phenylketonuria. Cell Transplant, 2012. 21(12): p. 2765-70.
108. Lee, K.W., J.H. Lee, S.W. Shin, S.J. Kim, J.W. Joh, D.H. Lee, J.W. Kim, H.Y. Park, S.Y. Lee, H.H. Lee, J.W. Park, S.Y. Kim, H.H. Yoon, D.H. Jung, Y.H. Choe, and S.K. Lee, Hepatocyte transplantation for glycogen storage disease type Ib. Cell Transplant, 2007. 16(6): p. 629-37.
109. Beck, B.B., S. Habbig, K. Dittrich, D. Stippel, I. Kaul, F. Koerber, H. Goebel, E.C. Salido, M. Kemper, J. Meyburg, and B. Hoppe, Liver cell transplantation in severe infantile oxalosis--a potential bridging procedure to orthotopic liver transplantation? Nephrol Dial Transplant, 2012. 27(7): p. 2984-9.
110. Strom, S.C., R.A. Fisher, W.S. Rubinstein, J.A. Barranger, R.B. Towbin, M. Charron, L. Mieles, L.A. Pisarov, K. Dorko, M.T. Thompson, and J. Reyes, Transplantation of human hepatocytes. Transplant Proc, 1997. 29(4): p. 2103-6.
111. Bohnen, N.I., M. Charron, J. Reyes, W. Rubinstein, S.C. Strom, D. Swanson, and R. Towbin, Use of indium-111-labeled hepatocytes to determine the biodistribution of transplanted hepatocytes through portal vein infusion. Clin Nucl Med, 2000. 25(6): p. 447-50.
112. Horslen, S.P., T.C. McCowan, T.C. Goertzen, P.I. Warkentin, H.B. Cai, S.C. Strom, and I.J. Fox, Isolated hepatocyte transplantation in an infant with a severe urea cycle disorder. Pediatrics, 2003. 111(6 Pt 1): p. 1262-7.
113. Mitry, R.R., A. Dhawan, R.D. Hughes, S. Bansal, S. Lehec, C. Terry, N.D. Heaton, J.B. Karani, G. Mieli-Vergani, and M. Rela, One liver, three recipients: segment IV from split-liver procedures as a source of hepatocytes for cell transplantation. Transplantation, 2004. 77(10): p. 1614-6.
114. Puppi, J., N. Tan, R.R. Mitry, R.D. Hughes, S. Lehec, G. Mieli-Vergani, J. Karani, M.P. Champion, N. Heaton, R. Mohamed, and A. Dhawan, Hepatocyte transplantation followed by

auxiliary liver transplantation--a novel treatment for ornithine transcarbamylase deficiency. Am J Transplant, 2008. 8(2): p. 452-7.
115. Meyburg, J., A.M. Das, F. Hoerster, M. Lindner, H. Kriegbaum, G. Engelmann, J. Schmidt, M. Ott, A. Pettenazzo, T. Luecke, H. Bertram, G.F. Hoffmann, and A. Burlina, One liver for four children: first clinical series of liver cell transplantation for severe neonatal urea cycle defects. Transplantation, 2009. 87(5): p. 636-41.
116. Enosawa, S., R. Horikawa, A. Yamamoto, S. Sakamoto, T. Shigeta, S. Nosaka, J. Fujimoto, A. Nakazawa, A. Tanoue, K. Nakamura, A. Umezawa, Y. Matsubara, A. Matsui, and M. Kasahara, Hepatocyte transplantation using a living donor reduced graft in a baby with ornithine transcarbamylase deficiency: a novel source of hepatocytes. Liver Transpl, 2014. 20(3): p. 391-3.
117. Soltys, K.A., K. Setoyama, E.N. Tafaleng, A. Soto Gutierrez, J. Fong, K. Fukumitsu, T. Nishikawa, M. Nagaya, R. Sada, K. Haberman, R. Gramignoli, K. Dorko, V. Tahan, A. Dreyzin, K. Baskin, J.J. Crowley, M.A. Quader, M. Deutsch, C. Ashokkumar, B.L. Shneider, R.H. Squires, S. Ranganathan, M. Reyes-Mugica, S.F. Dobrowolski, G. Mazariegos, R. Elango, D.B. Stolz, S.C. Strom, G. Vockley, J. Roy-Chowdhury, M. Cascalho, C. Guha, R. Sindhi, J.L. Platt, and I.J. Fox, Host conditioning and rejection monitoring in hepatocyte transplantation in humans. J Hepatol, 2017. 66(5): p. 987-1000.
118. Stephenne, X., M. Najimi, C. Sibille, M.C. Nassogne, F. Smets, and E.M. Sokal, Sustained engraftment and tissue enzyme activity after liver cell transplantation for argininosuccinate lyase deficiency. Gastroenterology, 2006. 130(4): p. 1317-23.
119. Puppi, J. and A. Dhawan, Human hepatocyte transplantation overview. Methods Mol Biol, 2009. 481: p. 1-16.
120. Khan, Z. and S.C. Strom, Hepatocyte Transplantation in Special Populations: Clinical Use in Children. Methods Mol Biol, 2017. 1506: p. 3-16.
121. Pareja, E., M.J. Gomez-Lechon, and L. Tolosa, Alternative Cell Sources to Adult Hepatocytes for Hepatic Cell Therapy. Methods Mol Biol, 2017. 1506: p. 17-42.
122. Hansel, M.C., R. Gramignoli, K.J. Skvorak, K. Dorko, F. Marongiu, W. Blake, J. Davila, and S.C. Strom, The history and use of human hepatocytes for the treatment of liver diseases: the first 100 patients. Curr Protoc Toxicol, 2014. 62: p. 14.12.1-23.
123. Gramignoli, R., M. Vosough, K. Kannisto, R.C. Srinivasan, and S.C. Strom, Clinical hepatocyte transplantation: practical limits and possible solutions. Eur Surg Res, 2015. 54(3-4): p. 162-77.
124. Gramignoli, R., V. Tahan, K. Dorko, K.J. Skvorak, M.C. Hansel, W. Zhao, R. Venkataramanan, E.C. Ellis, C. Jorns, B.G. Ericzon, S. Rosenborg, R. Kuiper, K.A. Soltys, G.V. Mazariegos, I.J. Fox, E.M. Wilson, M. Grompe, and S.C. Strom, New potential cell source for hepatocyte transplantation: discarded livers from metabolic disease liver transplants. Stem Cell Res, 2013. 11(1): p. 563-73.
125. Seglen, P.O., Preparation of isolated rat liver cells. Methods Cell Biol, 1976. 13: p. 29-83.
126. Strom, S.C., R.L. Jirtle, R.S. Jones, D.L. Novicki, M.R. Rosenberg, A. Novotny, G. Irons, J.R. McLain, and G. Michalopoulos, Isolation, culture, and transplantation of human hepatocytes. J Natl Cancer Inst, 1982. 68(5): p. 771-8.
127. Stephenne, X., M. Najimi, D.K. Ngoc, F. Smets, L. Hue, B. Guigas, and E.M. Sokal, Cryopreservation of human hepatocytes alters the mitochondrial respiratory chain complex 1. Cell Transplant, 2007. 16(4): p. 409-19.
128. Mitry, R.R., R.D. Hughes, M.M. Aw, C. Terry, G. Mieli-Vergani, R. Girlanda, P. Muiesan, M. Rela, N.D. Heaton, and A. Dhawan, Human hepatocyte isolation and relationship of cell viability to early graft function. Cell Transplant, 2003. 12(1): p. 69-74.
129. Gramignoli, R., V. Tahan, K. Dorko, R. Venkataramanan, I.J. Fox, E.C. Ellis, M. Vosough, and S.C. Strom, Rapid and sensitive assessment of human hepatocyte functions. Cell Transplant, 2014. 23(12): p. 1545-56.
130. Sussman, N.L. and J.H. Kelly, Artificial liver: a forthcoming attraction. Hepatology, 1993. 17(6): p. 1163-4.
131. Stephenne, X., O. Vosters, M. Najimi, C. Beuneu, K.N. Dung, W. Wijns, M. Goldman, and E.M. Sokal, Tissue factor-dependent procoagulant activity of isolated human hepatocytes: relevance to liver cell transplantation. Liver Transpl, 2007. 13(4): p. 599-606.
132. Wang, L.J., Y.M. Chen, D. George, F. Smets, E.M. Sokal, E.G. Bremer, and H.E. Soriano, Engraftment assessment in human and mouse liver tissue after sex-mismatched liver cell transplantation by real-time quantitative PCR for Y chromosome sequences. Liver Transpl, 2002. 8(9): p. 822-8.

133. Sempoux, C., Y. Horsmans, A. Geubel, J. Fraikin, B.E. Van Beers, J.F. Gigot, J. Lerut, and J. Rahier, Severe radiation-induced liver disease following localized radiation therapy for biliopancreatic carcinoma: activation of hepatic stellate cells as an early event. Hepatology, 1997. 26(1): p. 128-34.
134. Caplan, A.I., Mesenchymal Stem Cells: Time to Change the Name! Stem Cells Transl Med, 2017. 6(6): p. 1445-1451.
135. Keane, M.H., H. Overmars, T.M. Wikander, S. Ferdinandusse, M. Duran, R.J. Wanders, and P.L. Faust, Bile acid treatment alters hepatic disease and bile acid transport in peroxisome-deficient PEX2 Zellweger mice. Hepatology, 2007. 45(4): p. 982-97.
136. Berendse, K., M. Boek, M. Gijbels, N.N. Van der Wel, F.C. Klouwer, M.A. van den Bergh-Weerman, A.B. Shinde, R. Ofman, B.T. Poll-The, S.M. Houten, M. Baes, R.J.A. Wanders, and H.R. Waterham, Liver disease predominates in a mouse model for mild human Zellweger spectrum disorder. Biochim Biophys Acta Mol Basis Dis, 2019.
137. Hiebler, S., T. Masuda, J.G. Hacia, A.B. Moser, P.L. Faust, A. Liu, N. Chowdhury, N. Huang, A. Lauer, J. Bennett, P.A. Watkins, D.J. Zack, N.E. Braverman, G.V. Raymond, and S.J. Steinberg, The Pex1-G844D mouse: a model for mild human Zellweger spectrum disorder. Mol Genet Metab, 2014. 111(4): p. 522-32.
138. Janssen, A., P. Gressens, M. Grabenbauer, E. Baumgart, A. Schad, I. Vanhorebeek, A. Brouwers, P.E. Declercq, D. Fahimi, P. Evrard, L. Schoonjans, D. Collen, P. Carmeliet, G. Mannaerts, P. Van Veldhoven, and M. Baes, Neuronal migration depends on intact peroxisomal function in brain and in extraneuronal tissues. J Neurosci, 2003. 23(30): p. 9732-41.
139. Wiemer, E.A., T. Wenzel, T.J. Deerinck, M.H. Ellisman, and S. Subramani, Visualization of the peroxisomal compartment in living mammalian cells: dynamic behavior and association with microtubules. J Cell Biol, 1997. 136(1): p. 71-80.
140. Ivashchenko, O., P.P. Van Veldhoven, C. Brees, Y.S. Ho, S.R. Terlecky, and M. Fransen, Intraperoxisomal redox balance in mammalian cells: oxidative stress and interorganellar cross-talk. Mol Biol Cell, 2011. 22(9): p. 1440-51.
141. Schrader, T.A., M. Islinger, and M. Schrader, Detection and Immunolabeling of Peroxisomal Proteins. Methods Mol Biol, 2017. 1595: p. 113-130.
142. Koster, J. and H.R. Waterham, Transfection of Primary Human Skin Fibroblasts for Peroxisomal Studies. Methods Mol Biol, 2017. 1595: p. 63-67.
143. Baes, M., P. Gressens, E. Baumgart, P. Carmeliet, M. Casteels, M. Fransen, P. Evrard, D. Fahimi, P.E. Declercq, D. Collen, P.P. van Veldhoven, and G.P. Mannaerts, A mouse model for Zellweger syndrome. Nat Genet, 1997. 17(1): p. 49-57.
144. Faust, P.L., Abnormal cerebellar histogenesis in PEX2 Zellweger mice reflects multiple neuronal defects induced by peroxisome deficiency. J Comp Neurol, 2003. 461(3): p. 394-413.
145. Bose, M., M. Mahadevan, D.R. Schules, R.K. Coleman, K.M. Gawron, M.B. Gamble, J.B. Roullet, K.M. Gibson, and W.B. Rizzo, Emotional experience in parents of children with Zellweger spectrum disorders: A qualitative study. Mol Genet Metab Rep, 2019. 19: p. 100459.
146. Wanders, R.J.A., Peroxisomal disorders: Improved laboratory diagnosis, new defects and the complicated route to treatment. Mol Cell Probes, 2018. 40: p. 60-69.

Chapter 2.

Accurate and live peroxisome biogenesis evaluation achieved by lentiviral expression of a green fluorescent protein fused to a peroxisome targeting signal 1

Tanguy Demaret[1], Guillaume E Courtoy[2], Joachim Ravau[1], Patrick van der Smissen[3], Mustapha Najimi[1] and Etienne M Sokal[1]

[1] Laboratoire d'Hépatologie Pédiatrique et Thérapie Cellulaire, Unité PEDI, Institut de Recherche Expérimentale et Clinique (IREC), Université Catholique de Louvain (UCLouvain), 1200 Brussels, Belgium

[2] IREC Imaging Platform (2IP), Institut de Recherche Expérimentale et Clinique (IREC), Université Catholique de Louvain (UCLouvain), 1200 Brussels, Belgium

[3] PICT plateform, de Duve Institute, Université Catholique de Louvain (UCLouvain), 1200 Brussels, Belgium

Histochemistry and Cell Biology (2020)

Chapter 2

Abstract

Peroxisomes are ubiquitous organelles formed by peroxisome biogenesis (PB). During PB, peroxisomal matrix proteins harboring a peroxisome targeting signal (PTS) are imported inside peroxisomes by peroxins encoded by *PEX* genes. Genetic alterations in *PEX* genes lead to a spectrum of incurable diseases called Zellweger spectrum disorders (ZSD). *In vitro* drug screening is part of the quest for a cure in ZSD by restoring PB in ZSD cell models. *In vitro* PB evaluation is commonly achieved by immunofluorescent staining or transient peroxisome fluorescent reporter expression. Both techniques have several drawbacks (cost, time-consuming technique, etc.) which we overcame by developing a third-generation lentiviral transfer plasmid expressing an enhanced green fluorescent protein fused to PTS1 (eGFP-PTS1). By eGFP-PTS1 lentiviral transduction, we quantified PB and peroxisome motility in ZSD and control mouse and human fibroblasts. We confirmed the stable eGFP-PTS1 expression along cell passages. eGFP signal analysis distinguished ZSD from control eGFP-PTS1 transduced cells. Live eGFP-PTS1 transduced cells imaging quantified peroxisomes motility. In conclusion, we developed a lentiviral transfer plasmid allowing stable eGFP-PTS1 expression to study PB (deposited on Addgene: #133282). This tool meets the needs for *in vitro* PB evaluation and ZSD drug discovery.

Introduction

Peroxisomes are single membrane-bound ubiquitous organelles involved in numerous metabolic pathways including very long- and branched-chain fatty acids oxidation, and reactive oxygen species detoxification[1]. They are formed and maintained in a process called peroxisome biogenesis (PB) (reviewed in[2]). PB is governed by proteins called peroxins (PEX) through processes including peroxisome membrane assembly, peroxisomal matrix protein import, and peroxisome fission. Peroxisomal matrix protein import begins by the recognition of a peroxisome targeting signal (PTS) 1 or 2 (by PEX5 or PEX7, respectively) on matrix proteins newly synthetized in the cytosol (reviewed in[3, 4]); afterwards, the matrix proteins are translocated into the peroxisome lumen and finally, PEX5 and PEX7 are released in the cytosol for another round of import. Along with PB, peroxisome proliferation, peroxisome autophagy (i.e., pexophagy), and peroxisome motility take part in the peroxisome homeostasis in response to external stimuli (reviewed in[5]). Beside their complex biogenesis and regulation, peroxisomes are in close contact with other organelles like mitochondria and the endoplasmic reticulum (reviewed in[6]).

Genetic alterations in *PEX* genes lead to peroxisome biogenesis disorder (PBD) in cells and Zellweger spectrum disorders (ZSD) in patients (reviewed in[7]). ZSD is a continuum spectrum between severely affected patients (former Zellweger syndrome) which die of a progressive liver insufficiency during the first year of life, to mildly affected patients (former infantile Refsum disease) which suffer from leukodystrophy, failure to thrive, developmental delay, and hepatic dysfunction. These patients rarely survive after the third decade and the lack of independent living skills is the most handicapping[8]. To date, supportive management is considered the

standard of care, as no validated curative treatment has shown clinical benefits[9]. In the quest for a cure, liver and hepatocyte transplantation[10-13] have been used to deliver a large amount of functional peroxisomes to patients, with clinical and biological success. Beside this cellular approach, a molecular approach based on *in vitro* drug screening aims at restoring PB in cell models before starting clinical trials. Several compounds (arginine, betaine, hydroxychloroquine, etc.) are able to restore PB *in vitro*, mostly in cell carrying the *PEX1*-G843D hypomorphic mutation[14-18]. This molecular approach requires powerful tools to evaluate PB *in vitro*, especially in cell donors harboring peroxisomal mosaicism. Peroxisomal mosaicism refers to heterogeneous peroxisome labeling in cell population (see below) in which some cells harbor import-competent peroxisomes, while adjacent cells contain import-deficient peroxisomes (ghosts)[7]. Peroxisomal mosaicism was reported in fibroblasts and liver biopsies from mild ZSD patients[19, 20].

Immunofluorescence (IF) and transient peroxisomal fluorescent reporter transfection are two techniques of choice to evaluate PB *in vitro*. IF labeling of a peroxisomal membrane protein (e.g., the 70-kDa peroxisomal membrane protein (PMP70)) and a peroxisomal matrix protein (e.g., the catalase) allows import-competent peroxisomes identification by measuring colocalization between both markers[21]. Colocalization is lower in ZSD cells than in control, because the catalase is not properly imported inside peroxisomes (PMP70-positive particles). Plasmid transfection is a second approach used to transiently express a fluorescent protein fused to a PTS which drives the reporter to peroxisomes[22]. This technique demonstrates a diffuse cytosolic signal or a punctiform pattern in ZSD and control cells, respectively[23, 24]. IF and transient peroxisomal fluorescent reporter transfection

have several drawbacks such as the heaviness and the cost of the techniques. Moreover, the fixation required by IF precludes any dynamic study and the transfection technique is hampered by its cell toxicity, its transientness, and a low efficiency, especially on primary cells such as human fibroblasts[25].

To overcome all these limitations, we developed a third-generation lentiviral transfer plasmid expressing an enhanced green fluorescent protein (eGFP) fused to a PTS1 (eGFP-PTS1). By this approach, we obtained a highly efficient and stable eGFP-PTS1 expression both in mouse and human fibroblasts. eGFP automated signal analysis allowed to distinguish efficiently ZSD from control cell donors and to quantify peroxisome motility.

Materials and methods

Cell isolation and culture

Control and ZSD human fibroblasts were obtained by skin biopsy from a previously reported patient with *PEX1* deficiency, after written informed consent[10, 13]. Mouse fibroblasts from *Pex1*$^{wt/wt}$ and *Pex1*$^{G844D/G844D}$ embryos were collected from a mild ZSD mouse model as described previously[26, 27]. We selected the *Pex1*-G844D mouse model because the mutation is equivalent to the common *PEX1*-G843D hypomorphic human mutation. The *Pex1*-G844D mutation confers a high level of peroxisomal mosaicism in ZSD fibroblasts. It challenged our method to distinguish between control and ZSD cell donors[28]. Mice experiments were approved by the Ethical Committee for Animal Experimentation at the Health Science Sector, UCLouvain, Brussels, Belgium (2017/UCL/MD/006). Both cell types were cultured in Dulbecco's Modified Eagle Medium high glucose (DMEM, Gibco, 41965-039)

supplemented with 10% fetal bovine serum (FBS, Gibco, 10270-106) and 1% penicillin/streptomycin (P/S, Gibco, 15140-122), and cultured at 37 °C in a fully humidified atmosphere containing 5% CO_2. Cells were trypsinized (Trypsin-EDTA, Gibco, 25300-054) and seeded at a defined frequency and density (**Table 1**). Cell viability was always > 95% as measured by trypan blue 0.2% exclusion assay (HyClone, Thermo Fisher Scientific, SV30084.01).

Table 1. Characteristics of the fibroblasts analyzed and transduced.

Species	Age	Disease status	Plating density	Passage	Passages during the study
Mouse	E13.5[a]	Control	15.000 cells/cm^2	Twice a week	P4-P27
Mouse	E13.5 [a]	ZSD	15.000 cells/cm^2	Twice a week	P5-P42
Human	9 years	Control	5.000 cells/cm^2	At 80% confluency	P3-P17
Human	18 years	ZSD	5.000 cells/cm^2	At 80% confluency	P8-P22

[a] Mouse embryonic day. ZSD: Zellweger spectrum disorder.

Peroxisome targeting signal cloning

The eGFP fused to PTS1 from pEGFP-C1+SKL (Addgene #53450) was amplified by polymerase chain reaction (PCR) (GoTaq G2 Hot Start Polymerase, Promega, M740A) according to the manufacturer's instructions. Primer sequences were F-5′-GGCACCAAAATCAACGGGAC-3′ and R-5′-GGCGGTCGACGTTTCAGGTTCAGGGGGAGG-3′ (including a 5′ non-hybridizing SalI restriction site–underlined). The PCR product and pRRLSIN.cPPT.PGK-GFP.WPRE (Addgene #12252) were separately digested overnight (ON) at 37 °C with 10 U SalI (SalI, Thermo Fisher Scientific, #ER0641) and 10 U BsrGI (Bsp1407I, Thermo Fisher Scientific, #ER0931) in Tango 2X buffer (Tango Buffer 10X, Thermo Fisher Scientific, BY5) (**Figure 1A**). Restriction enzyme heat inactivation at 65 °C for 20 min was performed on the digested products. A small amount of the digested products was run on a 1% agarose gel (UltraPure Agarose, Invitrogen, 15510-027) containing intercalating agent diluted 1/20.000

(Midori Green Advance DNA Stain, Nippon Genetics, MG04) at 120 V during 45 min to confirm the successful digestion. Ligation was performed with a 1:3 vector:insert molar ratio according to the manufacturer's instructions (T4 DNA Ligase, New England, BioLabs, M0202S). Chemically competent E. coli were transformed with the ligation product (One Shot TOP10, Thermo Fisher Scientific, C404006) and plated onto LB agar plate containing ampicillin 100 µg/mL (Ampicillin sodium salt, Gibco, 11593027). Colonies were screened by PCR with the following primers F-5′-GTGTTCCGCATTCTGCAAG-3′ and R-5′-AGCAGCGTATCCACATAGCG-3′. Ladder (GeneRuler 1 kb Plus DNA Ladder, Thermo Fisher Scientific, SM1334) and PCR products were run on a 1% agarose gel showing a 925 or 1.067 bp product for the native and the modified vector, respectively (**Figure 1B**). Plasmid amplification and purification (PureYield Plasmid Maxiprep System, Promega, A2392) was performed on a colony containing the modified vector (pRRLSIN.cPPT.PGK-GFP-PTS1.WPRE). Next generation sequencing confirmed the expected plasmid sequence. The amplified plasmid passed the quality controls from a nonprofit plasmid repository and is available in open access (Addgene, #133282).

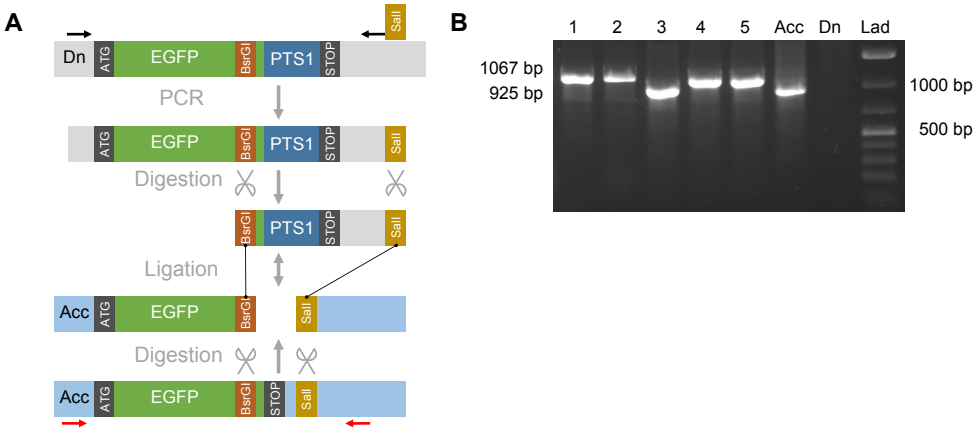

Figure 1 - **A** Cloning approach outline. The open reading frame of enhanced green fluorescent protein (EGFP) fused to the peroxisome targeting signal 1 (PTS1) was amplified from a donor plasmid (Dn). During amplification, a SalI restriction site was created thanks to a non-hybridizing 5′ end on the reverse primer (black arrow with box). The amplicon and the acceptor plasmid (Acc) were digested with BsrGI and SalI. Both digestion products were ligated, and the ligation product was transformed in chemocompetent bacteria. Red arrows below the acceptor plasmid represents the primers used to run screening PCR on bacterial colonies emerging after transformation. **B** Agarose gel of the colony screening PCR products. Products from colonies (1-5) and controls (Acc and Dn) were run on gel electrophoresis. Colonies 1, 2, 4, and 5 PCR produced a 1067 base pairs (bp) fragment showing genetic material insertion between primers compared to the 925 bp fragment of the Acc PCR. Dn PCR amplified no fragment as the PCR was designed for. Colony 3 PCR amplified a 925 bp fragment because of cloning failure.

Lentivirus production

HEK293FT cells (Invitrogen, R70007, cultivated according to the provider's instructions) at 70% confluency on CELLSTAR Cell Culture Flasks (Greiner Bio-One, 690 175) were transfected with PTS1 modified lentiviral transfer plasmid pRRLSIN.cPPT.PGK-GFP-PTS1.WPRE (Addgene, #133282), and pCMV-VSV-G, pMDLg/pRRE, pRSV-Rev (Addgene, #8454, #12251, #12253) third-generation lentiviral packaging system in a 4/1/1/1 molar ratio using Lipofectamine 2000 Transfection Reagent (Thermo Fisher Scientific, 11668-030) in Opti-MEM (Gibco, 31985-062) according to the manufacturer's instructions. After 6 h, transfection medium was replaced by growing medium without antibiotics. Every 24 h for 3 days, the eGFP-PTS1 lentivirus-containing supernatant (eGFP-PTS1-LV) was harvested,

centrifuged for 5 min at 2500 *g* to remove cell debris, and aliquoted and stored at - 80 °C.

Fibroblasts (n = 4) at 50-70% confluency were incubated 48 h with eGFP-PTS1-LV and hexadimethrine bromide at a final concentration of 6 µg/mL (Sigma-Aldrich, H9268, diluted in distilled water and filtered at 0.22 µm). Transduced cells were expanded, trypsinized and suspended at 10^7 cells /mL in 0.22 µm filtered phosphate buffered saline (PBS, Lonza, 15-512F), 2% FBS, 1 mM ethylenediaminetetraacetic acid tetrasodium salt hydrate (EDTA, Sigma-Aldrich, E5391-250G). Fluorescence activated cell sorting (FACS) on an FACSAriaIII (BD Biosciences) was used to collect eGFP-positive (eGFP+) fibroblasts (i.e., eGFP-PTS1 transduced cells). To avoid the sorting of cell doublets or cell aggregates, single cells were sequentially selected on forward scatter area (FSC-A)/forward scatter width (FSC-W) and side scatter area (SSC-A)/side scatter width (SSC-W) dot plots. The sorting was performed using an 85 µm nozzle at 45 psi, and a flow rate that allowed collecting 2000 events per second. The data acquisition and analysis were performed using the FACSDiva software (BD Biosciences). The sorting was performed to get at least 150,000 eGFP+ cells, and purity was verified a first time just after the sorting and a second time > 5 passages after sorting.

Immunofluorescence

Fibroblasts seeded on 12 mm round autoclaved glass coverslips no. 1 (VWR, 631-1577) in 24 well plates (Greiner Bio-One, 662 160) were fixed with 1 volume formaldehyde 4% (VWR, 11699408) on culture medium (formaldehyde final concentration of 2%) during 5 min at room temperature (RT) and then 10 min with the original solution (formaldehyde final concentration of 4%). Fixed cells were

washed three times with PBS and permeabilized with Triton-X100 0.5% (Sigma-Aldrich, X100-500ML) in PBS (Gibco, 18912-014) during 15 minutes at RT. Permeabilized cells were washed 3 times with PBS and a blocking step was achieved with 1 h incubation in normal goat serum 5% (NGS, Sigma-Aldrich, G9023-10ML) in PBS at RT. Cells were incubated ON at 4 °C with primary antibodies anti-catalase (Thermo Fisher Scientific, A21987, lot 1673440) and anti-PMP70 (Abcam, ab85550, lot GR99621-1) diluted in NGS 0.5% in PBS at 1/100 and 1/1000, respectively. Cells were washed three times with PBS and incubated with AlexaFluor 488 goat anti-mouse (Thermo Fischer Scientific, A11001) and AlexaFluor 594 goat anti-rabbit (Thermo Fischer Scientific, A11012) diluted in NGS 0.5% in PBS at 1/500 for 90 min at RT and protected from light. Control immunolabeling was performed with secondary antibodies alone. Immunolabeled cells were washed three times with PBS and nuclei were stained with diamidino-2-phenylindole dihydrochloride (DAPI, Sigma-Aldrich, D9542-1MG) diluted in distilled water at a final concentration of 0.2 µg/mL. Cells were washed three times with PBS, and they were mounted with fluorescence mounting medium (Dako, S3023) on Superfrost Plus slides (Thermo Fisher Scientific, J1800AMNT). Cells were imaged on a cell observer spinning disk confocal microscope (Zeiss) using a Plan Apochromat 100 ×/1.4 Oil DICII objective. eGFP-PTS1 transduced cells seeded on µ-Slide glass bottom (Ibidi, 80287) were imaged at 37 °C during all the acquisition with a picture taken every 10 s for 45 cycles.

Image analysis

Our strategy was to detect PBD with a relatively small number of cell pictures. Overlap and correlation of catalase or eGFP-PTS1 (green) with PMP70 (red) signals

were investigated by calculating Manders' overlap coefficient (MOC, measure of the fraction of overlapping pixels) and Pearson's correlation coefficient (PCC, measure of the covariance in the two signals) using Axiovision v. 4.8.2.0 (Zeiss). Using a fixed intensity threshold for each signal, we defined four zones on a scatter-plot. Zone 3 was the zone above the threshold for both signals. MOC and POC were calculated on zone 3 (**Figure 2**). Illustrative image profiles were obtained with ZEN 2.3 Blue Edition (Zeiss).

Peroxisomes automated quantification was performed with ImageJ 1.52p (National Institutes of Health). Native high-definition (.czi) images were imported using Bio-Formats 6.3. The green (eGFP) and the blue (DAPI) channels were sequentially analyzed with a macro (see Appendix). In the green channel, the mean intensity of total image was measured for each sample. In a second step, the peroxisomes were segmented into individual particles according to the green signal. The number, size (μm^2), and mean intensity of the individualized peroxisomes were calculated using the AnalyzeParticles tool. Finally, nuclei were counted using the same approach in the blue channel for normalization purposes.

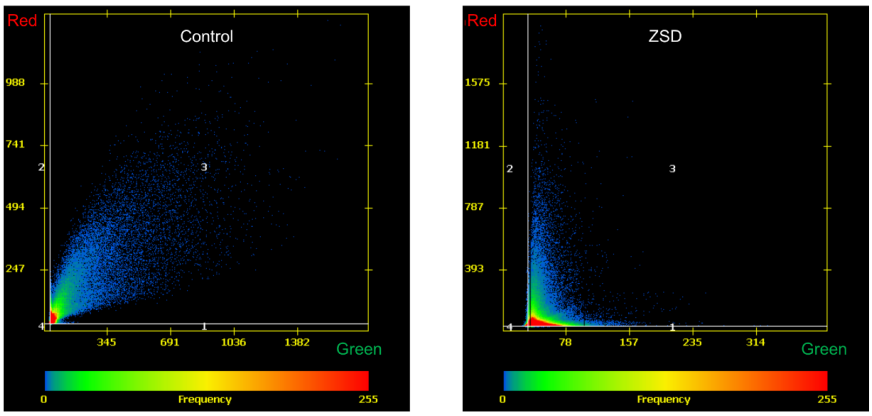

Figure 2 - Scatter plots of green and red signals for each pixel and related frequencies coded on a scale from blue (low frequency) to red (high frequency). Horizontal and vertical lines represent the thresholds used to define 4 zones. Manders' overlap and Pearson's correlation coefficients were calculated on zone 3. Control fibroblasts scatter plot (left panel) highlights a cloud of dots in the zone 3 diagonal meaning a correlation between green and red intensities. ZSD fibroblasts scatter plot show 2 clouds of dots (along green and red axes) meaning a low correlation between the two signals.

Time-lapse analysis

The image sequences (45 frames, one every 10 s) were opened in native high-definition format (.czi) with ImageJ 1.52p (National Institutes of Health). The signal was normalized by local contrast to ensure a homogeneous illumination throughout the sequence. The bright spots corresponding to the peroxisomes were then analyzed with the TrackMate plugin[29]. As a result, the maximal speed for each individual track (referred to as peroxisome track maximal velocity) was calculated and exported for statistical analysis.

Figure drawing and statistical analysis

Publisher (Office 365, Microsoft) was used to draw the figures. Two-tailed Mann-Whitney tests or Student's *t*-test with confidence intervals of 95% were performed using GraphPad Prism v.5.02 for Windows (GraphPad Software). *P*-values < 0.05 were considered significant.

Results

PTS1 was functionally cloned in eGFP lentiviral vector allowing stable eGFP-PTS1 expression

PTS1 was cloned in frame at the 3′ extremity of the eGFP in the third-generation lentiviral transfer plasmid (**Figure 1A**). A screening PCR designed to encompass the cloning site in the acceptor plasmid showed an increased fragment length in accordance with the cloned fragment (**Figure 1B**). HEK293FT cells transiently transfected with the original (pRRLSIN.cPPT.PGK-GFP.WPRE) or the PTS1 modified (pRRLSIN.cPPT.PGK-GFP-PTS1.WPRE) lentiviral transfer plasmids harbored a diffuse green signal (cytosolic location) or a punctiform green signal (peroxisomal location), respectively (**Figure 3A**). This highlighted the modified eGFP localization achieved by PTS1 cloning.

Fibroblasts (n = 4) were transduced with eGFP-PTS1-LV. FACS on the 4 cell populations measured a transduction efficiency ranging from 44.4% (cryopreserved lentiviruses) to 86.5% (freshly produced lentiviruses) (**Figure 3B**). After eGFP+ cell sorting, ~100% of the cells were eGFP+ and this was conserved in all donors after > 8 passages (**Figure 3C**). All the eGFP-PTS1 analysis described below were carried out on the 4 donors sorted populations.

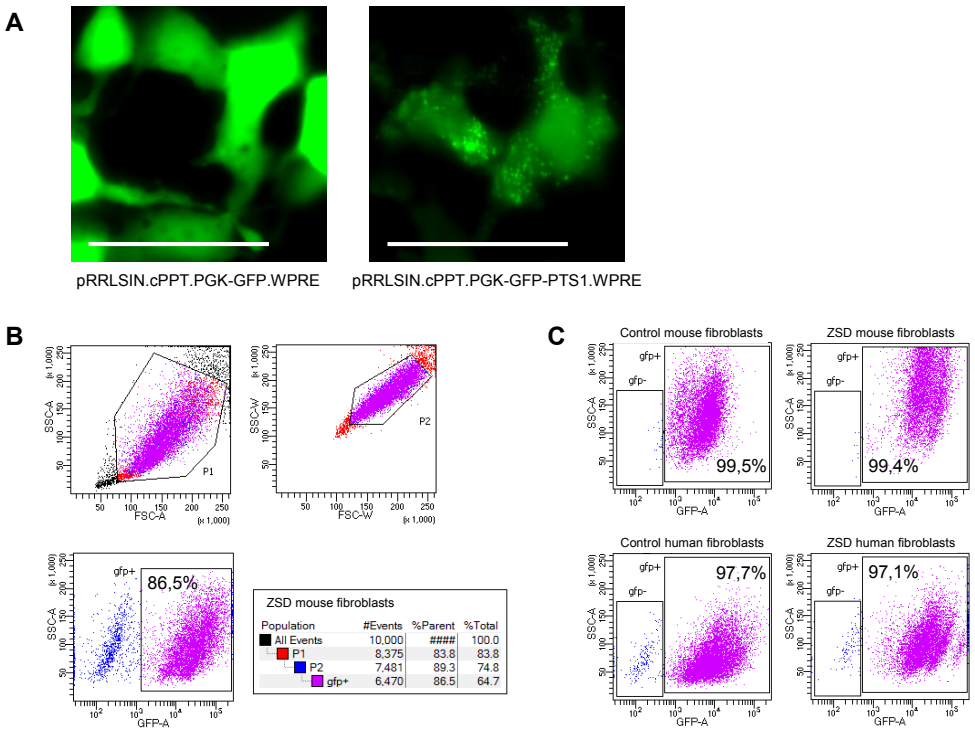

Figure 3 - **A** HEK293FT transfected with pRRLSIN.cPPT.PGK-GFP.WPRE (left panel) or pRRLSIN.cPPT.PGK-GFP-PTS1.WPRE (right panel). Note the change in enhanced green fluorescent protein (eGFP) localization achieved by peroxisome targeting signal 1 (PTS1) cloning. Scale bar: 50 µm. **B** Cell sorting strategy after pRRLSIN.cPPT.PGK-GFP-PTS1.WPRE transduction. Before sorting, 86.5% of the ZSD mouse fibroblasts were eGFP-positive. **C** Side scatter area (SSC-A)/eGFP area dot plots correspond to the 4 transduced donors > 8 passages after cell sorting. The analysis showed eGFP signal stability (> 97%).

Decreased catalase+PMP70 colocalization confirmed PBD in ZSD cells

Double IF targeting a peroxisomal matrix protein (catalase) and a peroxisomal membrane protein (PMP70) was performed to evaluate PB in cells, as published previously[30].

Catalase staining distribution was punctiform in control donors but lighter and more diffuse (in mouse fibroblasts) in the cytoplasm of ZSD cells, suggesting a lack of peroxisomal catalase import (i.e., PBD) (**Figure 4A1-4**). In ZSD mouse fibroblasts,

some cells displayed clear punctiform catalase staining next to cells with diffuse catalase staining (i.e., peroxisomal mosaicism) (**Figure 4A2**).

PMP70 staining evidenced a lower number of peroxisomes with enlarged size or irregular shape (peroxisomal ghosts) in ZSD donors than in controls (**Figure 4A5-8**, see inserts). Size and number of peroxisomal ghosts was previously reported to depend on the *PEX* mutation[21].

The low or absent catalase+PMP70 colocalization in ZSD donors confirmed the PBD. The distinct signal colocalizations in adjacent ZSD mouse fibroblasts brought firmly the peroxisomal mosaicism to light (**Figure 4A10**).

Profile lines were drawn on merged images to precisely visualize the catalase+PMP70 colocalization (**Figure 4A13-16**). The peroxisomal mosaicism in ZSD mouse fibroblasts was highlighted by the presence of colocalized green and red signal next to individual red or green peaks on the same profile line. MOC and PCC were calculated for catalase and PMP70 signals. MOC and PCC were higher in controls compared to ZSD donors (**Figure 4B,C**). Furthermore, among ZSD donors, MOC and PCC were particularly low in ZSD human fibroblasts, demonstrating the very low colocalization and underlying the absence of peroxisomal mosaicism in this donor.

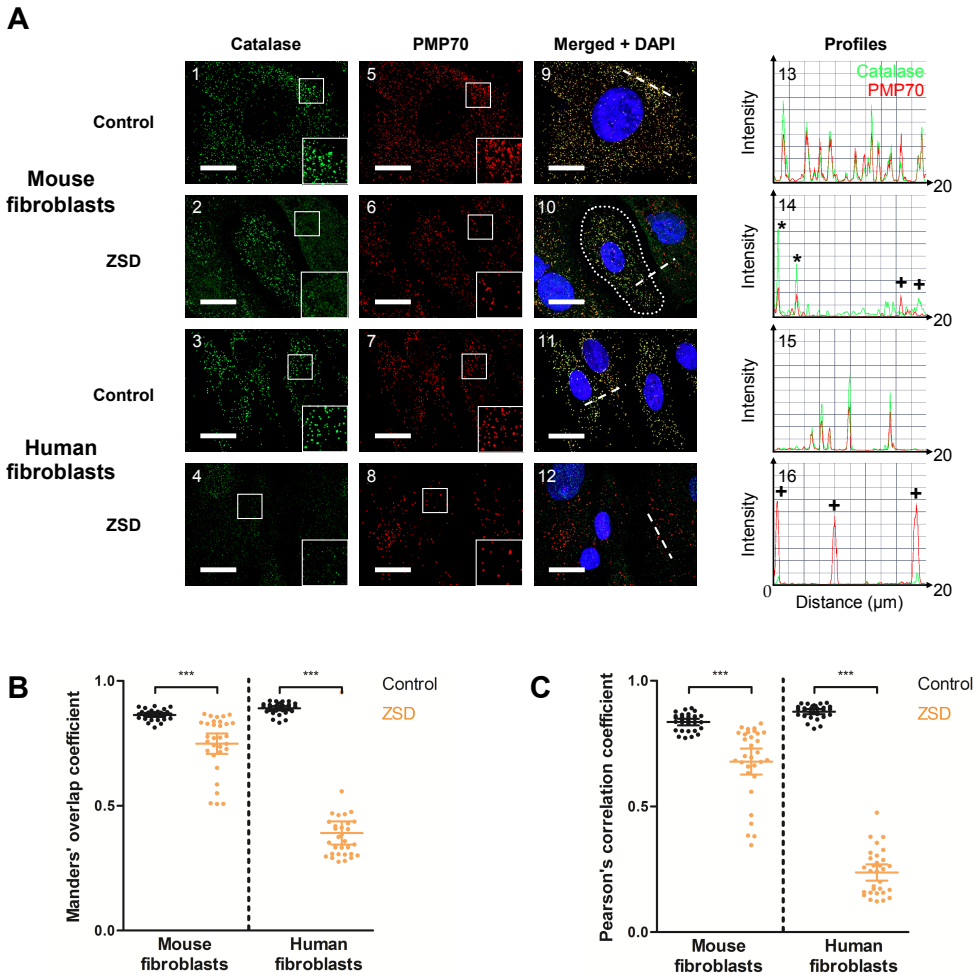

Figure 4 - **A** Catalase (green) and 70-kDa peroxisomal membrane protein (PMP70, red) immunofluorescence (IF) staining. Inserts show higher magnification of the boxed area. IF highlighted a lower colocalization of both signals in Zellweger spectrum disorder (ZSD) donors. Peroxisomal mosaicism (i.e., a mixed population of cells with and without functional peroxisome biogenesis) was detected in ZSD mouse fibroblasts as shown inside the dotted area (A10). Dotted lines localize the profile analysis (A13-16). In ZSD donors, profiles showed no localized correlation of intensities between both signals (marked with +), representing peroxisome biogenesis disorder. In ZSD mouse fibroblasts, some localized correlations of intensities were still present (marked with asterisk) representing residual peroxisome biogenesis among the peroxisome biogenesis disorder (i.e., peroxisomal mosaicism). Nuclei are stained with diamidino-2-phenylindole dihydrochloride (DAPI). Scale bar: 20 µm. Representative pictures of 30 micrographs by donor. **B** Manders' overlap coefficient (MOC) and **C** Pearson's correlation coefficient (PCC) graphs representing correlation of catalase and PMP70 signals among the four donors. MOC ranges from 0 to 1 and PCC ranges from – 1 to 1, with higher values indicating stronger correlation. Both coefficients concluded to a lower correlation (i.e., colocalization) in ZSD donors than in controls. Unpaired Student's *t*-test two-tailed, n = 30, mean ± 95% confidence interval, *** $p < 0.0001$.

eGFP-PTS1+PMP70 colocalization was efficient to evaluate PB

We measured eGFP-PTS1+PMP70 colocalization to evaluate PB. We confirmed that eGFP-PTS1+PMP70 colocalization was similar to catalase-PMP70 colocalization achieved by IF.

eGFP-PTS1 signal was punctiform in control fibroblasts and diffuse in ZSD fibroblasts cytoplasm (**Figure 5A1-4**). In eGFP-PTS1 transduced ZSD mouse fibroblasts, peroxisomal mosaicism was detected (**Figure 5A2**) similar to what catalase IF demonstrated (**Figure 4A2**).

Transduced cells were labeled by PMP70 IF. The low eGFP-PTS1+PMP70 colocalization in ZSD donors confirmed the PBD (**Figure 5A10,12**). Profile lines were drawn on merged images to visualize the eGFP-PTS1+PMP70 colocalization (**Figure 5A13-16**). The different eGFP-PTS1+PMP70 colocalization profiles in adjacent ZSD mouse fibroblasts confirmed peroxisomal mosaicism in this donor (**Figure 5A10**). Peroxisomal mosaicism was further highlighted by the presence of colocalized green and red signals next to individual red or green peaks on the same profile line (**Figure 5A14**).

MOC and PCC were calculated to quantify the correlation between eGFP-PTS1 and PMP70 signals. MOC and PCC were higher in control donors than in ZSD donors (**Figure 5B,C**). Among ZSD donors, MOC and PCC were strongly reduced in ZSD human fibroblasts, underlying the absence of peroxisomal mosaicism in this donor.

These results demonstrated that PMP70 colocalized with our eGFP-PTS1 fusion product, and that eGFP-PTS1+PMP70 signals was as sensitive as common IF protocol (catalase+PMP70) to evaluate PB *in vitro*.

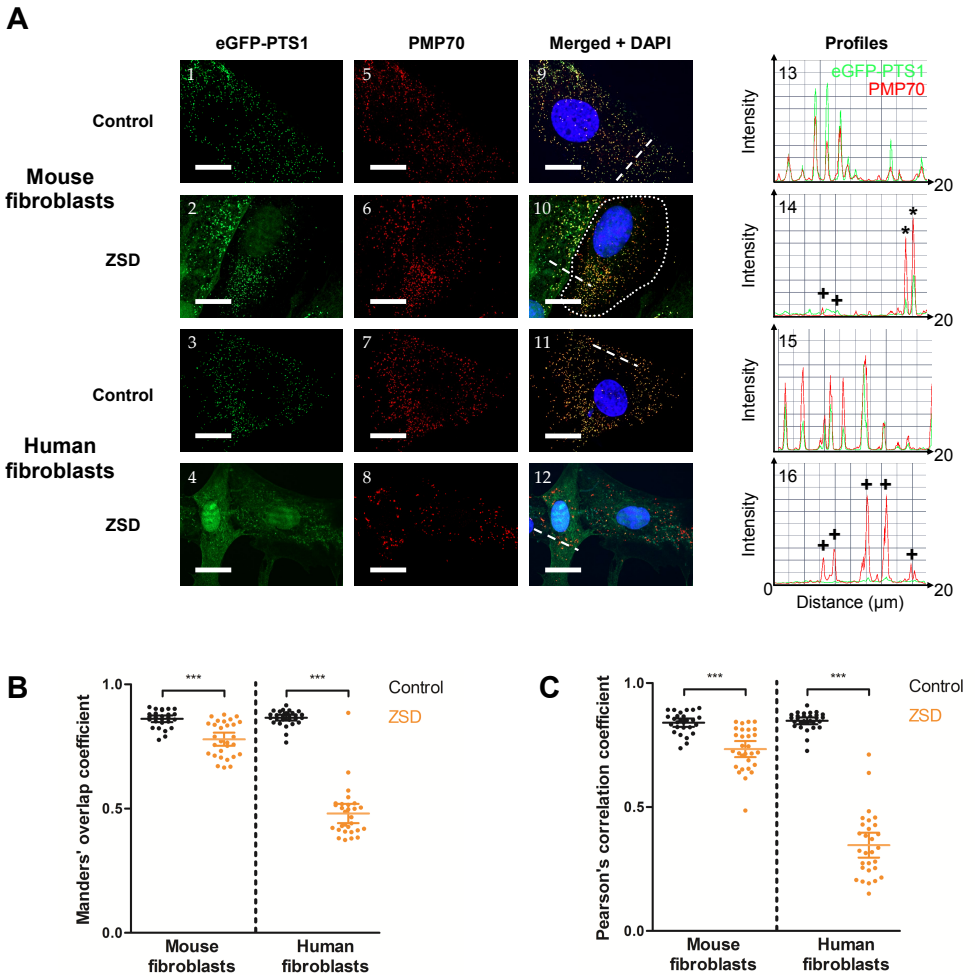

Figure 5 - **A** 70-kDa peroxisomal membrane protein (PMP70, red) immunofluorescent staining on cells transduced with an enhanced green fluorescent protein fused to a peroxisome targeting signal 1 (eGFP-PTS1). This method highlighted lower signal colocalization in Zellweger spectrum disorder (ZSD) donors. Peroxisomal mosaicism (i.e., a mixed population of cells with and without functional peroxisome biogenesis) was detected in ZSD mouse fibroblasts as shown inside the dotted area (A10). Dotted lines localize the profile analysis (A13-16). In ZSD donors, profiles showed the absence of localized correlation of intensities between both signals (marked with +), representing peroxisome biogenesis disorder. In ZSD mouse fibroblasts, some localized correlations of intensities were still present (marked with asterisk) representing residual peroxisome biogenesis among the peroxisome biogenesis disorder (i.e., peroxisomal mosaicism). Nuclei were stained with diamidino-2-phenylindole dihydrochloride (DAPI). Scale bar: 20 µm. Representative pictures of 30 micrographs by condition. **B** Manders' overlap coefficient (MOC) and **C** Pearson's correlation coefficient (PCC) graphs representing the colocalization of eGFP-PTS1 and PMP70 signals among the four donors. MOC ranges from 0 to 1 and PCC ranges from – 1 to 1, with higher values indicating stronger colocalization. Both coefficients highlighted lower colocalization in ZSD donors. Unpaired Student's *t*-test two-tailed, n = 30, mean ± 95% confidence interval, *** $p < 0.0001$.

eGFP-PTS1 signal alone allowed PB evaluation and peroxisome morphometry in living cells

eGFP signal from the four eGFP-PTS1 transduced donors was analyzed alone to evaluate PB without the need for cell transfection nor IF. Signal analysis was performed with ImageJ using the AnalyzeParticles tool (**Figure 6A**).

Among the four eGFP-PTS1 transduced donors, eGFP signal mean intensity (i.e., on the entire micrograph) was significantly higher in ZSD donors, indicative of a more diffuse eGFP signal in these donors (**Figure 6B**). Concerning eGFP+ particles, the mean intensity was higher in controls than in ZSD donors, suggesting more efficient eGFP-PTS1 peroxisomal import in control donors (**Figure 6B**).

In human fibroblasts, the eGFP+ particles number (normalized per cell number) and the average size (in μm^2) of these particles were significantly lower in ZSD than in control fibroblasts (**Figure 6B**). These results indicate that ZSD human fibroblasts contained less peroxisome matrices, of smaller size and with weaker eGFP signal than control cells.

Peroxisome motility was analyzed on photographs taken every 10 s from living cells transduced with eGFP-PTS1. The time-lapses were analyzed using automated tracking tool to quantify eGFP+ particles motility and peroxisome track maximal velocity (i.e., the maximal velocity recorded for each peroxisome) (**Figure 6C**). In ZSD human fibroblasts, the fastest particles were significantly slower than in controls as shown by the cumulative incidence of the peroxisome track maximal velocity (**Figure 6D**) and on the 25 fastest velocities recorded from the 4 donors (**Figure 6E**).

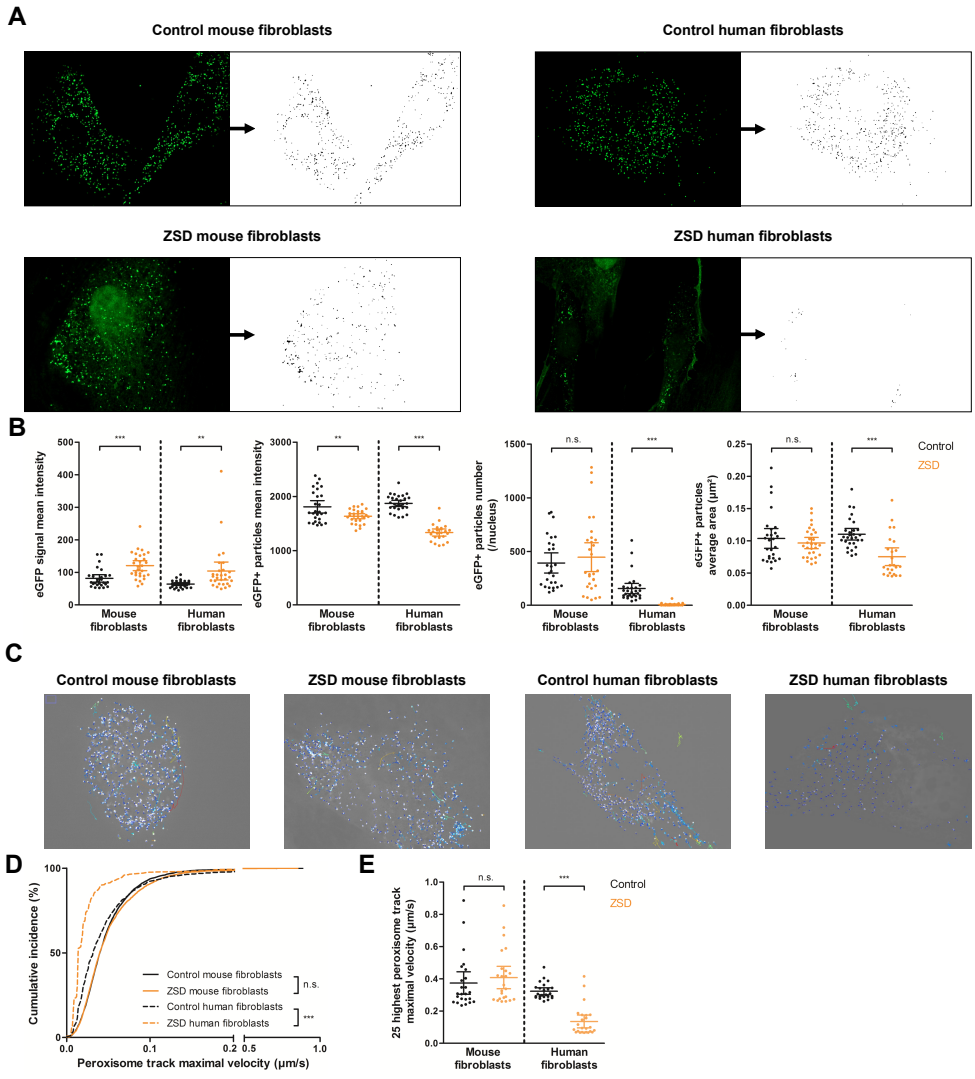

Figure 6 - **A** Masks created by "AnalyzeParticles" tool from ImageJ software to detect and measure the enhanced green fluorescent protein (eGFP) positive (eGFP+) particles in the 4 donors. **B** eGFP signal analysis from 4 cell donors transduced with eGFP-peroxisome targeting signal 1 (eGFP-PTS1) lentiviruses. eGFP signal mean intensity describes the eGFP average intensity value from the entire micrograph (left). eGFP+ particles mean intensity describes the eGFP average intensity value from the eGFP+ particles. eGFP signal mean intensity and eGFP+ particles mean intensity were respectively higher and lower in Zellweger spectrum disorder (ZSD) than in control fibroblasts. These results are explained by the fact that the eGFP-PTS1 remained diffuse in the cytosol of ZSD cells (higher eGFP signal mean intensity) because of the lack of peroxisomal import (lower eGFP+ particles mean intensity). eGFP+ particles number was normalized to nuclei for each picture. The eGFP+ particles average area describes the mean area of the eGFP+ particles (in µm²). These last two parameters were significantly decreased in ZSD human fibroblasts. n = 30/group. **C** eGFP+ particles tracking performed by TrackMate plugin for ImageJ on eGFP-PTS1 transduced cells from 4 donors to measure peroxisome motility. White dots are eGFP+ particles (peroxisomes) and colored lines represent the track of each peroxisome along

their displacement (blue to red lines reflect the slowest to the fastest particles). **D** Cumulative incidence of peroxisome track maximal velocity recorded for every eGFP+ particles in the 4 donors transduced with eGFP-PTS1. n > 400/group. **E** 25 highest peroxisome track maximal velocity recorded in the 4 donors transduced with eGFP-PTS1. n = 25/group. Unpaired Student's *t*-test two tailed, mean ± 95% confidence interval, n.s.: not significant, ** $p < 0.01$, *** $p < 0.001$.

Discussion

The aim of this study was to develop a new accessible method to evaluate PB *in vitro*. Our third-generation lentiviral vector allowed a persistent expression of eGFP-PTS1 fusion product and stable fluorescent signal along cell passages in control and ZSD mouse and human fibroblasts. First, eGFP-PTS1 pattern was similar to catalase, a peroxisomal matrix protein. Second, eGFP-PST1 colocalization with PMP70, a peroxisome membrane protein, was similar to catalase colocalization with PMP70, demonstrating correct technical sensitivity and no eGFP-PTS1 fusion product interaction with PB. Third, eGFP-PTS1 signal alone was sufficient to discriminate ZSD from control cells and allowed live cell imaging for peroxisome motility quantification.

eGFP-PTS1-LV allowed us to reach up to > 85% transduction efficiency on primary cells. After eGFP+ cell sorting, the signal remained > 97% for more than eight passages without any sign of signal loss. Our FACS approach collected cells with different eGFP-PTS1 expression levels among the same population (**Figure 3C**). This did not impede the precision of the different parameters measured afterwards. Yet, a more stringent cell sorting approach (i.e., a narrower positive cell gating) could potentially lead to reduced dispersion of the parameters measured.

Classical PB evaluation is achieved by transient transfection of a peroxisomal reporter plasmid with cationic lipid transfection agents such as Lipofectamine[31] or microporation[32]. Lipofectamine transfection efficiency is very low on primary cells

(< 1% in our experience on skin fibroblasts) and the compound exhibits cell toxicity. Microporation is more efficient than Lipofectamine on primary cells, but requires tricky optimization steps and expensive single-use cassettes[22]. Both techniques lead to transient protein expression and thus require transfection step before every experiment. Moreover, PTS1 protein import pathway is saturable[33]. Since transient transfection achieve high protein expression levels[34], PTS1 protein import pathway saturation by highly expressed eGFP-PTS1 thanks to transient transfection cannot be excluded. To our knowledge, the transfection or microporation effect on PB was never studied. After establishing transduced cells population, fibroblasts are ready for many experiments without potentially confounding factors.

Peroxisomes size and speed measured by eGFP-PTS1 particle analysis and tracking were comparable to previous publication based on eGFP-PTS1 transient transfection[35]. The cloning steps did not impede the correct eGFP-PTS1 localization. The lentiviral transduction did not modify the peroxisome matrix microscopic characteristics.

eGFP-PTS1 signal and catalase IF staining colocalized with PMP70 IF staining depending on the cell PB capacity. MOC and PCC used to quantify this colocalization as the reflect of PB in our study were previously used to study pexophagy by the colocalization of catalase or PMP70 with autophagy receptors[36, 37] and to decipher the link between peroxisomes and the endoplasmic reticulum[38]. MOC quantifies the overlap between two signals without evaluating the intensity of them, whereas PCC takes the intensity into account to give a correlation coefficient. In our study, both MOC and PCC gave similar results, because green and red signal overlapped and were also positively correlated in intensity. Using these two methods, we

demonstrate the colocalization of PMP70 with catalase and eGFP-PTS1 in peroxisomes of cells with functional PB and evidence the defective import in ZSD cells.

eGFP+ particles number, eGFP+ average area, and peroxisome track maximal velocity were statistically different between control and ZSD donors in human fibroblasts but not in mouse fibroblasts. This could be explained by peroxisomal mosaicism highlighted by eGFP-PTS1 signal in ZSD mouse fibroblasts (**Figure 5A10**) but not detected in ZSD human fibroblasts (**Figure 5A12**). ZSD mouse fibroblasts isolated from a similar mild ZSD mouse model were already shown to exhibit peroxisomal mosaicism[28]. Moreover, the PEX1-G844D protein expressed in ZSD mouse fibroblasts was shown to be expressed in normal quantity but with a lower functionality, meaning that the mutation has a reduced impact on the protein (i.e., affecting only functionality but not stability)[39]. In human fibroblasts, peroxisomal mosaicism was shown in cells from mildly affected ZSD patients[19, 20]. In our study, ZSD human fibroblasts were collected from a ZSD patient presenting already in the neonatal period with facial dysmorphism, feeding disturbance, cholestasis, and typical biochemical abnormalities[10]. In conclusion, our method is able to detect PBD in cells from classical ZSD donors, but our tool is also sensitive enough to decipher PBD in cells with milder phenotype.

To our knowledge, this is the first report, validation, and public availability (Addgene #133282) of a lentiviral transfer plasmid encoding a peroxisome targeted marker. The strengths of this method are its security, stable protein expression evaluated in two eukaryote species, easy setup, and PB sensitivity similar to catalase staining. The use of a single transduction (compared to recurrent transfections required by

Lipofectamine or microporation) and single signal (compared to catalase+PMP70 colocalization) make it suitable and convenient for high throughput screening. Some limitations are inherent to the technology used like handling in a biosafety level 2 environment and cell sorting requirement to get 100% cell positivity. Yet, these steps are to be performed only once for a given cell type. In the future, eGFP-PTS1 transduced ZSD cell donors with different *PEX* mutations could be exposed to chaperones to evaluate their effect on the PBD[18].

Conclusions

We developed an eGFP-PTS1 stable and highly potent third-generation lentiviral expression system in eukaryotic cells to study PB *in vitro* which allowed us to quantify and measure peroxisomes and their motility.

Acknowledgments

We acknowledge the patients for their implication in the study, Caroline Bouzin for the help with immunofluorescent staining, Caroline Daems for her great cloning tips, Valery Payen for the useful discussions about lentivirus production, and Julie Vandewalle for the proofreading. pEGFP-C1+SKL was a gift from Jay Brenman (Addgene plasmid #53450), pRRLSIN.cPPT.PGK-GFP.WPRE, pMDLg/pRRE, and pRSV-Rev were a gift from Didier Trono (Addgene plasmid #12252, #12251, and #12253), and pCMV-VSV-G was a gift from Bob Weinberg (Addgene plasmid #8454); we thank them for their contributions. We are thankful to the reviewers for their relevant remarks and suggestions.

Appendix

Peroxisomes and nuclei detection macro for ImageJ

```
run("Set Measurements...", "area mean modal centroid perimeter area_fraction limit redirect=None decimal=3");
run("Colors...", "foreground=white background=black selection=yellow");

//peroxisomes red C=2
setThreshold(1000, 65535);
setOption("BlackBackground", false);
run("Analyze Particles...", "size=0.03-3.00 circularity=0.10-1.00 show=Masks summarize");
waitForUser;
close(); close();

//peroxisomes green C=1
setThreshold(1000, 65535);
setOption("BlackBackground", false);
run("Analyze Particles...", "size=0.03-3.00 circularity=0.10-1.00 show=Masks summarize");
waitForUser;
close(); close();

//nuclei C=0
run("Mean...", "radius=70");
//run("Threshold...");
setAutoThreshold("Default dark");
setOption("BlackBackground", false);
run("Convert to Mask");
run("Watershed");
run("Analyze Particles...", "  circularity=0.20-1.00 show=Masks summarize");
waitForUser;
close(); close();
```

References

1. Wanders, R.J., Metabolic functions of peroxisomes in health and disease. Biochimie, 2014. 98: p. 36-44.
2. Fujiki, Y., Peroxisome biogenesis and human peroxisome-deficiency disorders. Proc Jpn Acad Ser B Phys Biol Sci, 2016. 92(10): p. 463-477.
3. Emmanouilidis, L., M. Gopalswamy, D.M. Passon, M. Wilmanns, and M. Sattler, Structural biology of the import pathways of peroxisomal matrix proteins. Biochim Biophys Acta, 2016. 1863(5): p. 804-13.
4. Dias, A.F., T. Francisco, T.A. Rodrigues, C.P. Grou, and J.E. Azevedo, The first minutes in the life of a peroxisomal matrix protein. Biochim Biophys Acta, 2016. 1863(5): p. 814-20.
5. Neuhaus, A., C. Eggeling, R. Erdmann, and W. Schliebs, Why do peroxisomes associate with the cytoskeleton? Biochim Biophys Acta, 2016. 1863(5): p. 1019-26.
6. Farre, J.C., S.S. Mahalingam, M. Proietto, and S. Subramani, Peroxisome biogenesis, membrane contact sites, and quality control. EMBO Rep, 2019. 20(1).
7. Argyriou, C., M.D. D'Agostino, and N. Braverman, Peroxisome biogenesis disorders. Transl Sci Rare Dis, 2016. 1(2): p. 111-144.
8. Berendse, K., M. Engelen, S. Ferdinandusse, C.B. Majoie, H.R. Waterham, F.M. Vaz, J.H. Koelman, P.G. Barth, R.J. Wanders, and B.T. Poll-The, Zellweger spectrum disorders: clinical manifestations in patients surviving into adulthood. J Inherit Metab Dis, 2016. 39(1): p. 93-106.
9. Klouwer, F.C., K. Berendse, S. Ferdinandusse, R.J. Wanders, M. Engelen, and B.T. Poll-The, Zellweger spectrum disorders: clinical overview and management approach. Orphanet J Rare Dis, 2015. 10: p. 151.

10. Demaret, T., S. Varma, X. Stephenne, F. Smets, I. Scheers, R. Wanders, L. Van Maldergem, R. Reding, and E. Sokal, Living-donor liver transplantation for mild Zellweger spectrum disorder: Up to 17 years follow-up. Pediatr Transplant, 2018. 22(3): p. e13112.
11. Matsunami, M., N. Shimozawa, A. Fukuda, T. Kumagai, M. Kubota, P.F. Chong, and M. Kasahara, Living-Donor Liver Transplantation From a Heterozygous Parent for Infantile Refsum Disease. Pediatrics, 2016. 137(6).
12. Van Maldergem, L., A.B. Moser, M.F. Vincent, D. Roland, R. Reding, J.B. Otte, R.J. Wanders, and E. Sokal, Orthotopic liver transplantation from a living-related donor in an infant with a peroxisome biogenesis defect of the infantile Refsum disease type. J Inherit Metab Dis, 2005. 28(4): p. 593-600.
13. Sokal, E.M., F. Smets, A. Bourgois, L. Van Maldergem, J.P. Buts, R. Reding, J. Bernard Otte, V. Evrard, D. Latinne, M.F. Vincent, A. Moser, and H.E. Soriano, Hepatocyte transplantation in a 4-year-old girl with peroxisomal biogenesis disease: technique, safety, and metabolic follow-up. Transplantation, 2003. 76(4): p. 735-8.
14. Law, K.B., D. Bronte-Tinkew, E. Di Pietro, A. Snowden, R.O. Jones, A. Moser, J.H. Brumell, N. Braverman, and P.K. Kim, The peroxisomal AAA ATPase complex prevents pexophagy and development of peroxisome biogenesis disorders. Autophagy, 2017. 13(5): p. 868-884.
15. Berendse, K., M.S. Ebberink, L. Ijlst, B.T. Poll-The, R.J. Wanders, and H.R. Waterham, Arginine improves peroxisome functioning in cells from patients with a mild peroxisome biogenesis disorder. Orphanet J Rare Dis, 2013. 8: p. 138.
16. Wei, H., S. Kemp, M.C. McGuinness, A.B. Moser, and K.D. Smith, Pharmacological induction of peroxisomes in peroxisome biogenesis disorders. Ann Neurol, 2000. 47(3): p. 286-96.
17. Zhang, R., L. Chen, S. Jiralerspong, A. Snowden, S. Steinberg, and N. Braverman, Recovery of PEX1-Gly843Asp peroxisome dysfunction by small-molecule compounds. Proc Natl Acad Sci U S A, 2010. 107(12): p. 5569-74.
18. MacLean, G.E., C. Argyriou, E. Di Pietro, X. Sun, S. Birjandian, P. Saberian, J.G. Hacia, and N.E. Braverman, Zellweger spectrum disorder patient-derived fibroblasts with the PEX1-Gly843Asp allele recover peroxisome functions in response to flavonoids. J Cell Biochem, 2019. 120(3): p. 3243-3258.
19. Mandel, H., M. Espeel, F. Roels, N. Sofer, A. Luder, T.C. Iancu, A. Aizin, M. Berant, R.J. Wanders, and R.B. Schutgens, A new type of peroxisomal disorder with variable expression in liver and fibroblasts. J Pediatr, 1994. 125(4): p. 549-55.
20. Giros, M., F. Roels, J. Prats, M. Ruiz, A. Ribes, M. Espeel, R.J. Wanders, R.B. Schutgens, and T. Pampols, Long survival in a case of peroxisomal biogenesis disorder with peroxisome mosaicism in the liver. Ann N Y Acad Sci, 1996. 804: p. 747-9.
21. Soliman, K., F. Gottfert, H. Rosewich, S. Thoms, and J. Gartner, Super-resolution imaging reveals the sub-diffraction phenotype of Zellweger Syndrome ghosts and wild-type peroxisomes. Sci Rep, 2018. 8(1): p. 7809.
22. Koster, J. and H.R. Waterham, Transfection of Primary Human Skin Fibroblasts for Peroxisomal Studies. Methods Mol Biol, 2017. 1595: p. 63-67.
23. Sexton, J.Z., Q. He, L.J. Forsberg, and J.E. Brenman, High content screening for non-classical peroxisome proliferators. Int J High Throughput Screen, 2010. 2010(1): p. 127-140.
24. Ebberink, M.S., P.A. Mooijer, J. Gootjes, J. Koster, R.J. Wanders, and H.R. Waterham, Genetic classification and mutational spectrum of more than 600 patients with a Zellweger syndrome spectrum disorder. Hum Mutat, 2011. 32(1): p. 59-69.
25. Schrader, T.A., M. Islinger, and M. Schrader, Detection and Immunolabeling of Peroxisomal Proteins. Methods Mol Biol, 2017. 1595: p. 113-130.
26. Tymms, M.J. and I. Kola, Gene Knockout Protocols. Methods in Molecular Biology. Vol. 158. 2001, Totowa, NJ: Humana Press Inc.
27. Hiebler, S., T. Masuda, J.G. Hacia, A.B. Moser, P.L. Faust, A. Liu, N. Chowdhury, N. Huang, A. Lauer, J. Bennett, P.A. Watkins, D.J. Zack, N.E. Braverman, G.V. Raymond, and S.J. Steinberg, The Pex1-G844D mouse: a model for mild human Zellweger spectrum disorder. Mol Genet Metab, 2014. 111(4): p. 522-32.
28. Berendse, K., M. Boek, M. Gijbels, N.N. Van der Wel, F.C. Klouwer, M.A. van den Bergh-Weerman, A.B. Shinde, R. Ofman, B.T. Poll-The, S.M. Houten, M. Baes, R.J.A. Wanders, and H.R. Waterham, Liver disease predominates in a mouse model for mild human Zellweger spectrum disorder. Biochim Biophys Acta Mol Basis Dis, 2019.
29. Tinevez, J.Y., N. Perry, J. Schindelin, G.M. Hoopes, G.D. Reynolds, E. Laplantine, S.Y. Bednarek, S.L. Shorte, and K.W. Eliceiri, TrackMate: An open and extensible platform for single-particle tracking. Methods, 2017. 115: p. 80-90.

30. Santos, M.J., T. Imanaka, H. Shio, G.M. Small, and P.B. Lazarow, Peroxisomal membrane ghosts in Zellweger syndrome--aberrant organelle assembly. Science, 1988. 239(4847): p. 1536-8.
31. Wiemer, E.A., T. Wenzel, T.J. Deerinck, M.H. Ellisman, and S. Subramani, Visualization of the peroxisomal compartment in living mammalian cells: dynamic behavior and association with microtubules. J Cell Biol, 1997. 136(1): p. 71-80.
32. Ivashchenko, O., P.P. Van Veldhoven, C. Brees, Y.S. Ho, S.R. Terlecky, and M. Fransen, Intraperoxisomal redox balance in mammalian cells: oxidative stress and interorganellar cross-talk. Mol Biol Cell, 2011. 22(9): p. 1440-51.
33. Brickner, D.G., J.J. Harada, and L.J. Olsen, Protein transport into higher plant peroxisomes. In vitro import assay provides evidence for receptor involvement. Plant Physiol, 1997. 113(4): p. 1213-21.
34. Hunter, M., P. Yuan, D. Vavilala, and M. Fox, Optimization of Protein Expression in Mammalian Cells. Curr Protoc Protein Sci, 2019. 95(1): p. e77.
35. Metz, J., I.G. Castro, and M. Schrader, Peroxisome Motility Measurement and Quantification Assay. Bio Protoc, 2017. 7(17).
36. Deosaran, E., K.B. Larsen, R. Hua, G. Sargent, Y. Wang, S. Kim, T. Lamark, M. Jauregui, K. Law, J. Lippincott-Schwartz, A. Brech, T. Johansen, and P.K. Kim, NBR1 acts as an autophagy receptor for peroxisomes. J Cell Sci, 2013. 126(Pt 4): p. 939-52.
37. Marcassa, E., A. Kallinos, J. Jardine, E.V. Rusilowicz-Jones, A. Martinez, S. Kuehl, M. Islinger, M.J. Clague, and S. Urbe, Dual role of USP30 in controlling basal pexophagy and mitophagy. EMBO Rep, 2018. 19(7).
38. Mast, F.D., A. Jamakhandi, R.A. Saleem, D.J. Dilworth, R.S. Rogers, R.A. Rachubinski, and J.D. Aitchison, Peroxins Pex30 and Pex29 Dynamically Associate with Reticulons to Regulate Peroxisome Biogenesis from the Endoplasmic Reticulum. J Biol Chem, 2016. 291(30): p. 15408-27.
39. Argyriou, C., A. Polosa, B. Cecyre, M. Hsieh, E. Di Pietro, W. Cui, J.F. Bouchard, P. Lachapelle, and N. Braverman, A longitudinal study of retinopathy in the PEX1-Gly844Asp mouse model for mild Zellweger Spectrum Disorder. Exp Eye Res, 2019: p. 107713.

Chapter 3.

Longitudinal study of *Pex1*-G844D NMRI mouse model: a robust pre-clinical model for mild Zellweger spectrum disorder

Tanguy Demaret[1], Martin Roumain[2], Jérôme Ambroise[3], Jonathan Evraerts[1], Joachim Ravau[1], Caroline Bouzin[4], Bertrand Bearzatto[3], Jean-Luc Gala[3], Hedwig Stepman[5], Sandrine Marie[6], Marie-Françoise Vincent[6], Giulio G. Muccioli[2], Mustapha Najimi[1], Etienne M Sokal[1]

[1] Laboratoire d'Hépatologie Pédiatrique et Thérapie Cellulaire, Unité PEDI, Institut de Recherche Expérimentale et Clinique (IREC), Université Catholique de Louvain (UCLouvain), 1200 Brussels, Belgium

[2] Bioanalysis and Pharmacology of Bioactive Lipids Research Group (BPBL), Louvain Drug Research Institute (LDRI), Université Catholique de Louvain (UCLouvain), 1200 Brussels, Belgium.

[3] Center for Applied Molecular Technologies (CTMA), Institut de Recherche Expérimentale et Clinique (IREC), Université Catholique de Louvain (UCLouvain), 1200 Brussels, Belgium.

[4] IREC Imaging Platform (2IP), Institut de Recherche Expérimentale et Clinique (IREC), Université Catholique de Louvain (UCLouvain), 1200 Brussels, Belgium

[5] Department of Laboratory Medicine, Ghent University Hospital, 9000 Ghent, Belgium.

[6] Department of Laboratory Medicine, Cliniques Universitaires Saint-Luc, Université Catholique de Louvain (UCLouvain), 1200 Brussels, Belgium

Biochimica et Biophysica Acta – Molecular Basis of Disease (2020)

Abstract

Zellweger spectrum disorders (ZSD) are inborn errors of metabolism caused by mutations in *PEX* genes that lead to peroxisomal biogenesis disorder (PBD). No validated treatment is able to modify the dismal progression of the disease. ZSD mouse models used to develop therapeutic approaches are limited by poor survival and breeding restrictions. To overcome these limitations, we backcrossed the hypomorphic *Pex1* p.G844D allele to NMRI background. NMRI mouse breeding restored an autosomal recessive Mendelian inheritance pattern with twice larger litters. Mice were longitudinally phenotyped up to 6 months of age to make this model suitable for therapeutic interventions. ZSD mice exhibited growth retardation and relative hepatomegaly associated to progressive hepatocyte hypertrophy. Biochemical studies associated with RNA sequencing deciphered ZSD liver glycogen metabolism alterations. Affected fibroblasts displayed classical PBD immunofluorescence pattern suitable for *in vitro* drug screening. Plasma and liver showed very long-chain fatty acids, specific oxysterols and C_{27} bile acids intermediates elevation in ZSD mice along with a specific urine organic acid profile. With ageing, C_{26} fatty acid and phytanic acid levels tended to normalize in ZSD mice, as described in patients reaching adulthood. In conclusion, our mouse model recapitulates a mild ZSD phenotype and is suitable for liver-targeted therapies evaluation.

Introduction

Zellweger spectrum disorders (ZSD) are autosomal recessive disorders affecting 1 in 90 000 births[1]. ZSD are caused by genetic alterations in *PEX* genes which lead to peroxisome biogenesis disorder (PBD)[2]. Severely affected patients present in the neonatal period with severe hypotonia, craniofacial dysmorphism, hepatic dysfunction and failure to thrive, and they will eventually die of liver insufficiency during their first year of life (former Zellweger syndrome)[3]. Reversible neonatal cholestasis is a milder form of the disease (former infantile Refsum disease) with part of the patients that survive into adulthood with, however, developmental delay, vision and/or hearing impairment and progressive leukodystrophy[4]. Since newborn screening implementation for X-linked adrenoleukodystrophy, a related peroxisomal disorder, neonatal diagnosis of ZSD is rendered possible, mostly in the United States, by $C_{26:0}$lysophosphatidylcholine (C26LPC) quantification on dried blood spot[5]. ZSD diagnosis is ascertained by biochemical studies on plasma, erythrocytes, patient's skin fibroblasts, and/or urine. Classically, plasma branched-chain fatty acids (BCFA) phytanic and pristanic acids, very long-chain fatty acids (VLCFA), C_{27} bile acids (BA) intermediates (di- and trihydroxycholestanoic acids) and pipecolic acid levels are elevated. Erythrocytes plasmalogen are synthetized within peroxisomes and their levels are decreased only in severe ZSD patients[6]. Analysis on patient's cells allow similar metabolites quantification along with enzymatic analysis and peroxisome immunofluorescence studies[7]. Some authors report a relatively specific urine organic acid profile in ZSD patients[8, 9]. Finally, next generation sequencing of all *PEX* genes related to ZSD confirms the diagnosis[10]. To date, standard of care is supportive since no intervention is validated in clinical

practice[11]. In a research setting, we performed the first pediatric hepatocyte transplantation in Europe in a 4-year-old girl affected by a mild ZSD and we achieved biochemical success[12]. After that, we reported bio-clinical benefits obtained by living-donor liver transplantation in 3 mild ZSD patients[13, 14].

Based on this experience in mild ZSD patients, pre-clinical studies are required to validate these liver-targeted therapies (i.e., hepatocyte and liver transplantation). ZSD mouse models are useful to study PBD pathophysiology and to evaluate therapeutic approaches[15]. Mouse models with generalized *Pex* gene deletion suffer from neonatal death impairing post-natal longitudinal studies and therapeutic intervention[16-18]. Conditional *Pex* gene knockout (KO) were developed to overcome these limitations. Hepatocyte *Pex5* deletion was carried out to study liver carbohydrate metabolism alterations caused by PBD, but this artificial condition does not clinically recapitulate liver glycogen alterations (i.e., ZSD mice resist to fast)[19]. *Pex1* p.G844D mouse model (hereafter called *Pex1*-G844D) was developed as a murine equivalent to the hypomorphic *PEX1* p.G843D human allele conferring a milder phenotype to ZSD patients[20]. *Pex1*-G844D allele was inserted in a pure C57BL/6N background and leads to a relatively severe ZSD phenotype with 20% survival at 1 month[21]. A second *Pex1*-G844D mouse model was created in a mixed 129/SvEv and C57BL/6N background[22]. This model exhibits a restricted survival rate of 59% at 1 month along with progressive retinal degeneration[23]. No robust longitudinal (> 15 days) biochemical study was carried out on ZSD mouse models, partly due to their restricted survival rate.

To set up a ZSD mouse model suitable for evaluation of liver-directed therapies, we backcrossed *Pex1*-G844D allele in Naval Medical Research Institute (NMRI)

background known for its robustness and for delivering large litters. NMRI mice homozygous for *Pex1*-G844D mutation reached 78% survival rate at 1 month while keeping a ZSD phenotype composed of growth retardation, hepatomegaly, chronic liver injury, cholestasis, and classical biochemical alterations associated with ZSD. We report for the first time in a ZSD mouse model that several disease markers tend to normalize with ageing, as reported for ZSD patients surviving into adulthood[4] and that urine organic acids profile is similar to that of ZSD patients[8]. Liver RNA sequencing (RNA-seq) highlighted multiple pathway modulations associated with ZSD. These data make NMRI ZSD mice a robust mouse model to evaluate liver-targeted therapies for ZSD.

Materials and Methods

Mice care and breeding

Mice were bred in a specific-pathogen-free environment in individually ventilated cages with 12h light/12h dark cycle. Mice had unrestricted access to food (Carfil, Mice Breeding diet) and water. No gel food was needed to wean pups at 4 weeks contrary to Hiebler *et al.*[22]. Mice and food were weighted once a week to evaluate growth and food consumption. All experiments were carried out in accordance with the EU Directive 2010/63/EU for animal experiments and approved by the Ethical Committee for Animal Experimentation at the Health Science Sector, UCLouvain, Brussels, Belgium (2017/UCL/MD/006).

Pex1-G844D NMRI mice generation and genotyping

Two males and 4 females C57BL/6N mice aged of 4 weeks and heterozygous for the *Pex1*-G844D allele were bought from The Jackson Laboratory (MMRRC stock

#37405)[22]. One ten-week-old female NMRI mouse from Charles River Laboratories (Sulzfeld, Deutschland) was used to backcross the *Pex1*-G844D allele for three generations. Litters genotyping was achieved by genomic DNA (gDNA) extraction from 1 mm tail snips following fast, cheap and straightforward HotSHOT DNA extraction protocol[24]. Polymerase chain reaction (PCR) (Promega, M7401) was run on gDNA following manufacturer's instructions, for 45 cycles, with the following forward 5'-TCCCTGCTCACTTCRGGAC-3' and reverse primer 5'-TAGGCAAGCTCTTTATCACC-3' (annealing temperature: 54 °C) in a PCR mix containing $MgCl_2$ and deoxynucleotides (Promega, U1511) at a final concentration of 1 mM and 0.2 mM, respectively. PCR products were run on a 1% agarose gel (UltraPure Agarose, Invitrogen, 15510-027) containing intercalating agent diluted 1/20.000 (Midori Green Advance DNA Stain, Nippon Genetics, MG04) at 120 V for 45 min. Wild-type (WT) and *Pex1*-G844D alleles yielded 230- and 407-base pair (bp) products, respectively (**Figure 1A**). NMRI *Pex1*-G844D cryopreserved embryos are available for collaboration.

Blood, urine, and organs collection

Mice were anesthetized by intraperitoneal injection (2 µL/g of body weight) with the following anesthetic solution: ketamine 100 mg/mL (Nimatek, Eurovet), xylazine 20 mg/mL (Rompun, Bayer), and NaCl 0.9% (Mini-Plasco NaCl 0.9%, B-Braun) in a volume ratio of 2/1/1 (final ketamine and xylazine concentration: 100 mg/kg and 10 mg/kg, respectively). Abdominal cavity was open by transverse laparotomy and blood was drawn from the inferior vena cava through 27G needle (Microlance 3, BD) in heparinized syringe (Portex Arterial Blood Sampling Syringe, Smiths Medical, 4041E). A drop of total blood was disposed on Guthrie card then total blood was

centrifuged 15 min at 1.500 *g* and 4 °C. Plasma was aliquoted and erythrocytes were washed twice in NaCl 0.9% and stored in butylated hydroxytoluene (Sigma, B1378) coated polypropylene microtubes. After blood collection, mice were killed by cervical dislocation and liver was collected, weighted and sampled following lobar segmentation[25]. Left lateral lobe was fixed in formaldehyde 4% (VWR, 11699408) overnight and embedded in paraffin or in Tissue-Tek O.C.T. (Sakura, 4583). Left medial lobe and right lateral lobe were weighted in lysing matrix tubes (Lysing Matrix D, MP Bio, 116913100), snap frozen in liquid nitrogen and stored at -80 °C. To collect urine samples, 2-month-old mice were individually placed in mouse metabolic cages (UNO, 100100007) for 24 h. Urine was centrifuged at 1500 *g* for 5 min at 4 °C and supernatant was snap frozen in liquid nitrogen and stored at -80 °C.

Histological analyses

H&E, PAS, SR, and ORO staining, imaging and quantification

Formalin-fixed paraffin-embedded left lateral liver lobes were cut into 5 µm sections and processed for hematoxylin and eosin (H&E), Periodic-acid Schiff (PAS) without and with prior saliva treatment and Sirius red (SR) staining. Slides were stained in one same batch to avoid inter-batches variations. Formalin-fixed sucrose impregnated Tissue-Tek O.C.T. embedded liver lobes were cut on a cryostat (Thermo Fisher Scientific Microm, HM 560) into 10 µm section and processed for Oil Red O (ORO) staining. Slides were digitalized at 20× using a slide scanner (Leica Biosystems, SCN400). Tissue was manually delineated and TissueIA (Leica Biosystems) “Measure Stained Area” algorithm was used to quantify PAS and SR stained area as a proxy for glycogen and collagen liver content, respectively. ORO stained area and characteristics were analyzed with Visiopharm (v2017.2) to

quantify total ORO-stained droplets surface, ORO-stained droplets number, and mean ORO-stained droplets area.

Glucose-6-phosphatase activity

Two-month-old mice left lateral liver lobes Tissue-Tek O.C.T. embedded in Tissue-Tek Cryomold (Sakura, 4557) were cut on a cryostat (Thermo Fisher Scientific Microm, HM 560) into 10 µm section and processed for glucose-6-phosphatase (G6Pase) activity staining as described elsewhere[26]. Briefly, slides were incubated in Tris acetate buffer (0.1 M, pH 6.5 or pH 4 for negative control) containing D-glucose-6-phosphate (2.1 mM) and lead nitrate (2.4 mM) at 37 °C for 3 min. Then, slides were immersed at room temperature (RT) for 5 seconds in 1% sulfur water (Sigma, A1952) to convert lead phosphate to lead sulfide precipitate. Slides were mounted with aqueous mounting medium (Dako, S3025) and digitalized at 20× using a slide scanner (Leica Biosystems, SCN400). Tissue was manually delineated with Visiopharm (v2017.2) and processed for G6Pase stained area quantification.

Fluorescent staining

Formalin-fixed paraffin-embedded left lateral liver lobes were cut into 5 µm section, deparaffinized and rehydrated.

Peroxisomal membrane protein

Slides were immersed in Target Retrieval Solution (Dako, S1699) for 30 min at 100 °C and rinsed three times in phosphate-buffered saline (PBS, Gibco, 18912-014). Non-specific immunostaining was prevented by 5% normal goat serum (NGS, Sigma, G9023) in PBS (v/v) incubation for 1h at RT. Slides were incubated with anti-70-kDa peroxisomal membrane protein (PMP70) antibody (Abcam, ab85550, lot GR99621-1, 1/1000) in 0.5% NGS overnight at 4 °C. Slides were rinsed three times

with PBS and incubated with Alexa Fluor 594 anti-rabbit antibody (Thermo Fischer Scientific, A11012, 1/500) in 0.5% NGS for 1h at RT. Slides were rinsed three times with PBS, nuclei were stained with 4′,6-diamidino-2-phenylindole (DAPI, Sigma, D9542) and slides were mounted with fluorescence mounting medium (Dako, S3023).

Hepatocytes and proliferative nuclei

Endogenous peroxidases were inhibited 20 min with 3% hydrogen peroxide in methanol. Sections were then subjected to antigen retrieval in 10 mM citrate buffer pH 5.7 and microwaved for 5 min at 900 W and 15 min at 90 W followed by aspecific antigen binding sites blocking in bovine serum albumin 5% + Tween20 0,1% in tris-buffered saline (TBS). Slides were incubated in anti-Ki67 primary antibody (CellSignaling, 12202, lot 5, 1/100) for 1h30 at RT. This was followed by an incubation with anti-rabbit antibody (Dako, K4003) for 40 min at RT. This reaction was visualized using Alexa Fluor 488-conjugated tyramide (Thermo Fisher Scientific, B40953, dilution 1/200). Hepatocyte nuclear factor 4 alpha (HNF4α) immunostaining was performed after a new citrate buffer incubation step, using anti-HNF4α antibody (Perseus Proteomics, PPH141500, lot A2, 1/200), anti-mouse antibody (Dako, K4001) and Alexa Fluor 647-conjugated tyramide (Thermo Fisher Scientific, B40958). After a washing step, nuclei were finally stained with Hoechst33342 (Sigma, 14533) and slides were mounted with fluorescent mounting medium.

Cell membranes

Slides were immersed in 10 mM citrate buffer pH 5.7, microwaved for 5 min at 900 W and 15 min at 90 W and then rinsed once in distilled water and once in Tween20 0.1% in TBS. To stain cell membranes, slides were incubated with wheat germ

agglutinin-rhodamine (WGA, Vector, RL-1022, lot ZF0717, 1/50) in PBS for 2h at RT. Slides were rinsed three times in Tween20 0.1% in TBS and nuclei were counterstained with Hoechst33342. After washing twice in Tween20 0.1% in TBS and once in distilled water, slides were mounted with fluorescence mounting medium.

Imaging and quantification

PMP70-stained slides were imaged on a Cell Observer Spinning Disk confocal microscope (Zeiss) using a Plan Apochromat 100×/1.4 Oil DICII objective.

HNF4α-Ki67-stained and WGA-stained slides were digitalized using a Pannoramic 250 FlashIII scanner (3DHistech) at 20× magnification. Scanned slides were then analyzed using Visiopharm (v2017.2). A 5.5 × 5.5 mm region of interest was delineated manually on each tissue sections at low magnification and large empty spaces (lumens of macro vessels) were automatically discarded. Cells were detected at high resolution (20×) with a cell shape-based or nuclear-based cell classification relying on the WGA or Hoechst staining, respectively. Following segmentation, post processing steps were applied to measure cell area or to separate HNF4α+/- and Ki67+/- cells. The same parameters were kept constant for all slides.

RNA-seq

Two-month-old mice right lateral liver lobes were placed into 2.0-ml Lysing Matrix D tubes (MP Bio, 116913100) and homogenized by mechanical grinding for 2 × 40 seconds at 6 m/s on the FastPrep system (MP Biomedicals). After guanidinium thiocyanate-phenol-chloroform extraction, RNA was further extracted

on column (RNeasy, QIAGEN, 74104) and treated with DNase (DNAse-set, QIAGEN, 79254) to reduce gDNA contamination. In total, RNA from 12 samples were quantified by Qubit RNA BR assay kit (Thermo Fisher Scientific, Q10211) on a Qubit 4 Fluorometer (Thermo Fisher Scientific). RNA integrity was evaluated on the Agilent 2100 Bioanalyzer using the RNA 6000 nano kit (Agilent, 5067-1511). All samples had RNA integrity number values ≥ 7.8. Libraries were prepared starting from 150 ng of total RNA using the KAPA RNA HyperPrep Kit with RiboErase (KAPA Biosystems, KK8560) following the manufacturer's recommendations (KR1351 – v1.16). Libraries were equimolarly pooled and sequenced on a single lane on an Illumina NovaSeq 6000 platform. All libraries were paired-end (2×100 bp reads) sequenced and a minimum of 25 million paired-end reads were generated per sample. All sequencing data were analyzed using the Automated Reproducible MOdular workflow for preprocessing and differential analysis of RNA-seq data (ARMOR) pipeline[27]. In this pipeline, reads underwent a quality check using FastQC[28]. Quantification and quality control results were summarized in a MultiQC report[29]. Reads were mapped using Salmon[30] to the transcriptome index which was built using all Ensembl cDNA sequences obtained in the Mus_musculus.GRCm38.cdna.all.fa file[31]. Then, estimated transcript abundances from Salmon were imported into R using the tximeta package[32], were expressed as log count per million, and analyzed with a principal component analysis. In parallel, estimated transcript abundances were analyzed for differential gene expression with edgeR in order to compute the modulation (i.e., the fold change): ZSD *versus* control mice liver[33]. Raw *p*-values were adjusted for multiple testing using Benjamini Hochberg method and a false discovery rate (FDR) < 0.05 was considered

significant. Over-representation analysis of gene ontologies were conducted from the resulting list of significantly modulated genes using the limma Bioconductor package. Reactome pathways for *Homo sapiens* glucose and glycogen metabolism (R-HSA-70326, R-HSA-70171, R-HSA-70263, R-HSA-8982491) were manually analyzed for mouse orthologs. If one gene had several isoforms, the non-liver isoforms were discarded. Cholangiocytes markers[34, 35], liver collagen genes[36], peroxisome proliferator-activated receptor alpha (PPARα) target genes[19, 21, 37] and hepatocytes proliferation genes[38] were collected from literature. Gene set enrichment of these pathways were shown as barcode plot in which genes were ranked according to the modulation (i.e., the $\log_2$ (fold change)) induced by the disease status. In addition, modulation of significantly modulated genes in *Pex5* mouse hepatocytes conditional KO mouse model reported by Peeters et al. were correlated to our data[19]. Raw and processed RNA-seq data were deposited and made publicly available on the Gene Expression Omnibus (GSE145524).

MEF collection and characterization

Mouse embryonic fibroblasts (MEF) were collected from WT and ZSD mouse embryos and cultured as described elsewhere[39]. Cells were collected between passage 4 and 10. Two million MEF by sample were collected in radioimmunoprecipitation assay buffer (150 mM sodium chloride (Sigma, 746398), 50 mM Tris-base pH 8 (Sigma, T6066), 1% v/v IGEPAL CA-630 (Sigma, I3021), 0.5% w/v sodium deoxycholate (Sigma, D6750), 0.1% w/v sodium dodecyl sulfate (Acros Organics, 226145000)) and stored at -80 °C before analysis. Cell protein content was quantified for normalization purposes (Pierce BCA Protein Assay Kit, Thermo Fisher Scientific, 23227). MEF were immuno-labelled for catalase, a

peroxisome lumen enzyme, and PMP70 to highlight PBD, as described previously[39]. MEF peroxisome biogenesis was further evaluated through lentiviral expression of a green fluorescent protein linked to peroxisome targeting signal 1 (eGFP-PTS1), as described elsewhere[39]. Nuclei were stained with DAPI and cells were imaged on a cell observer spinning disk confocal microscope (Zeiss) using a Plan Apochromat 100×/1.4 Oil DICII objective.

Biochemical analyses

Glycemia & fasting

Blood drop was collected from the tail vein and morning glycemia was measured using glucometer (FreeStyle Precision Neo, Abbott). To evaluate glycemic response to fast, mice were placed in a clean cage without food access for 6h after what glycemia was controlled.

Total lipids quantification

Total lipids were extracted in methanol-chloroform from about 100 mg liver lobe homogenized in distilled water (Baxter, AKF7114), and quantified as described here[40]. Briefly, standards (tripalmitin (Sigma, T5888) and triolein (Sigma, T7140), 30%/70% molar content in chloroform) and extracted lipids in chloroform were dried under nitrogen flow. Dried lipids were incubated with 95% sulfuric acid (VWR, 20690.327) at 95 °C for 10 min. Lipids-sulfuric acid aliquot was transferred in triplicate (10 µL each) in a 96-well plate (Greiner Bio-One, 655 180) and 300 µL of 2 g/L vanillin (Sigma, V2375) in 58 % aqueous phosphoric acid (VWR, 20626.361) solution were added and incubated, protected from light, for 1 h at RT. Absorbance was read at 520 nm on a microplate reader (Benchmark Plus ®, Bio-Rad). Lipid content was normalized to liver weight.

Protein quantification

Protein content of liver homogenates in distilled water was quantified using Pierce BCA Protein Assay Kit (Thermo Fisher Scientific, 23227) according to manufacturer's instructions. Protein content was normalized to liver weight.

Glycogen quantification

Liver glycogen content was measured following a protocol modified from[41, 42]. Briefly, left medial liver lobes were homogenized in lysing matrix tubes in distilled water. About 10 mg of liver were digested in acidic solution for 1 h at 100 °C. Digested solution was neutralized and glucose was quantified using a glucometer (FreeStyle Precision Neo, Abbott). A conversion factor of 0.9 was used to convert glucose to glycogen[43]. Glycogen was normalized to liver weight.

Urine organic acids quantification

Urine organic acids were oximized by incubation with hydroxylamine (Sigma, 255580) in basic solution at 60 °C for 30 min, followed by liquid-liquid ethyl acetate extraction and finally trimethylsilyl derivatization by incubation with *N*,*O*-Bis(trimethylsilyl)trifluoroacetamide:trimethylchlorosilane (BSTFA:TMCS 99:1, Supelco, 33155-U) at 80 °C for 30 min. Extracted derivatives were quantified using a gas chromatograph (Hewlett-Packard, 6890 Series) equipped with a CP-Sil 8CB capillary column (Agilent Technologies, CP8751) coupled to a mass spectrometer (MS) (Hewlett-Packard, 5973 Mass Selective Detector). Pentadecanoic acid was used as internal standard and quantification was normalized to urine creatinine.

Plasma clinical biology tests

Plasma alkaline phosphatases activity, gamma-glutamyltransferases (gGT) activity, glutamate-oxaloacetate transaminase activity, glutamate-pyruvate transaminase

(GPT) activity, total cholesterol, albumin and total bilirubin were quantified on plasma samples with a dry chemistry system (Fuji DRI-CHEM NX500, Fujifilm).

Erythrocyte plasmalogen quantification

Erythrocyte plasmalogens were derivatized in methanolic HCl 3M (Sigma, 33050 U) for 4h at 90 °C, extracted in hexane (Biosolve, 082906) and quantified using a gas chromatograph (Agilent Technologies, 6890N) equipped with a HP-5MS capillary column (Agilent Technologies, 19091S-433) and coupled to a MS (Agilent Technologies, 5973N). $C_{17:0}$ (Sigma, H3500) was used as internal standard, and $C_{16:0}$ and $C_{18:0}$ dimethyl acetals (DMA) (Avanti Polar Lipids, 852446 and 852448) and $C_{16:0}$ and $C_{18:0}$ (Sigma, P5585 and S4751) as calibration standards. Results are expressed as $C_{16:0}$ DMA/$C_{16:0}$ and $C_{18:0}$ DMA/$C_{18:0}$ ratios.

Pipecolic acid quantification

Pipecolic acid was quantified without derivatization by ultra-high performance liquid chromatography (1290 infinity LC, Agilent Technologies) equipped with Acquity UPLC HSS T3 column (Waters, 186003539) coupled to MS/MS (6460 Triple Quad Mass Spectrometer, Agilent Technologies, K6460). DL-2-piperidine-d_9-carboxylic acid (CDN isotopes, D5087) was used as internal standard. δ1-pipéridéine-6-carboxylate (synthetized as described elsewhere[44]) and pipecolic acid (Sigma, P2519) were used as calibration standards.

C26LPC quantification

Six millimeters diameter punches were cut from saturated area of dried blood spot. Punches were then immersed in glass vials containing $C_{17:0}$lysophosphatidylcholine as internal standard and chloroform (8 mL), methanol (4 mL), water (2 mL) and HCl (300 µL, 2 M). Samples were next centrifuged after mixing and sonicating, organic

phase was recovered and dried under a nitrogen steam. Organic residue was resuspended and pre-purified by solid phase extraction. C26LPC from the eluate was analyzed by HPLC-MS/MS using a Xevo TQ-S MS (Waters) coupled to an Acquity UPLC Class H (Waters). Analyte separation was performed using a Kinetex C18 HPLC column (5 µm, 150 × 4.6 mm, Phenomenex). Mobile phase was a gradient of methanol, acetonitrile and water containing ammonium acetate. MS analysis was performed using an electrospray ionization source in the positive mode. The multiple reaction monitoring mode was used to obtain one quantitative (Q) and one qualitative (q) transition per analyte. These transitions were 636.5 → 183.9 (Q) and 636.5 → 103.9 (q) for C26LPC and 510.4 → 183.9 (Q) and 510.4 → 103.9 (q) for its internal standard.

BCFA and VLCFA quantification

The BCFA phytanic and pristanic acids, and the VLCFA docosanoic acid (C_{22}), tetracosanoic acid (C_{24}) and hexacosanoic acid (C_{26}) were quantified following derivatization in 5% HCl (Merck, 1.00317.1000) in methanol (J.T.Baker, 9822) for 2h at 100 °C. Following extraction with heptane (Merck, 1.04365.1000), quantification was achieved using a gas chromatograph equipped with a CP-Sil 8CB capillary column (Agilent Technologies, CP8751) and coupled to a MS (TRACE 1310 Mainframe MS, Thermo Fisher Scientific, 14800402). Deuterated (Vrije Universiteit Medisch Centrum, 7639, 4784, 6398, 9808, 9818) and non-deuterated (Vrije Universiteit Medisch Centrum, 9029, 9058, Sigma, 216941, L6641 and H0388) phytanic and pristanic acids and C_{22}, C_{24} and C_{26} were used as internal standards and calibration standards, respectively.

Oxysterols and bile acids quantification

Oxysterols were analyzed using a validated HPLC-MS method[45]. Briefly, plasma samples (or liver homogenates) were placed in glass vials containing deuterated internal standards and dichloromethane (8 mL), methanol (4 mL, containing 10 µg of butylated hydroxytoluene) and water (2 mL, containing 20 ng ethylenediaminetetraacetic acid). Samples were next centrifuged after mixing and sonication, organic phase was recovered and dried under a nitrogen steam. Organic residue was resuspended and pre-purified by solid phase extraction. Cholesterol was removed from the samples. The eluate containing oxysterols was analyzed by HPLC-MS using an LTQ-Orbitrap XL MS (Thermo Fisher Scientific) coupled to an Accela HPLC system (Thermo Fisher Scientific). Chromatographic separation was performed using an Ascentis Express C-18 column (2.7 µm, 150 × 4.6 mm, Sigma), kept at 15 °C. Mobile phase was a gradient of methanol and water containing acetic acid. MS analysis was performed using an atmospheric pressure chemical ionization source in the positive mode. Calibration curves were prepared in the same conditions.

BA were analyzed using another validated method adapted from[46]. Samples (plasma or liver homogenates) were placed in acetone containing deuterated internal standards to allow for protein precipitation overnight. Samples were then centrifuged, supernatant recovered and evaporated to dryness. The resulting residue was resuspended and injected in the HPLC-MS system consisting of an LTQ-Orbitrap XL MS (Thermo Fisher Scientific) coupled to an Accela HPLC system (Thermo Fisher Scientific). Analyte separation was performed on an Ascentis Express C-18 column (2.7 µm, 150 × 4.6 mm) (Sigma-Aldrich). Mobile phase was a gradient of acetonitrile

and water containing formic acid. MS analysis was performed using an electrospray ionization source in the negative mode. Calibration curves were prepared in the same conditions. Bile acid species were grouped according to their family (**Table 1**). BA plasma-liver ratios were calculated and reported when different from 0 or ∞.

Table 1. Bile acid species detected according to their group

Total C_{27} bile acids	Total unconjugated C_{24} bile acids	Total conjugated C_{24} bile acids
Dihydroxycholestanoic acid	α-muricholic acid	Tauro-α-muricholic acid
Trihydroxycholestanoic acid	β-muricholic acid	Tauro-β-muricholic acid
	ω-muricholic acid	Tauro-ω-muricholic acid
	Cholic acid	Taurocholic acid
	Deoxycholic acid	Taurodeoxycholic acid
	Ursodeoxycholic acid	Tauroursodeoxycholic acid
		Taurochenodeoxycholic acid

The bile acids detected in plasma and liver were grouped to facilitate data presentation. Here are presented the 3 groups and the respective bile acid species detected in our study.

General statistical analysis and artwork

Log-rank test, two-tailed Mann-Whitney tests with confidence intervals of 95%, two-way ANOVA and Spearman's correlation were performed using GraphPad Prism v5.02 for Windows (GraphPad Software). *P*-values < 0.05 were considered significant. Chi-squared tests were performed with Statistical Package for the Social Sciences v24 (SPSS Statistics, I.B.M.) to assess sex ratios and genotypes imbalance. Publisher (Office 365, Microsoft) was used to draw the figures.

Results

Pex1-G844D backcrossing in NMRI background eased the breeding and restored autosomal recessive Mendelian inheritance pattern

Breeding of *Pex1*$^{G844D/+}$ C57BL/6N mice lead to 52 pups (among 12 litters, mean: 4.3 pups/litter), 7 pups (13.5%) were ZSD mice (*Pex1*$^{G844D/G844D}$) compared to 25% predicted by the Mendelian inheritance. None of the C57BL/6N homozygous pups survived more than 25 days (**Figure 1B**). To get larger litters and more robust pups, we backcrossed the *Pex1*-G844D allele in NMRI background for 3 generations.

Pex1$^{G844D/+}$ NMRI mice were bred and gave birth to 291 pups among 29 litters (mean: 10 pups/litter, *p*-value < 0.0001 *versus* C57BL/6N breeding). With this strain, we obtained an inheritance pattern that followed the Mendelian inheritance pattern for an autosomal recessive disorder: 77 *Pex1*$^{+/+}$ (26.5%), 146 *Pex1*$^{G844D/+}$ (50.2%) and 68 *Pex1*$^{G844D/G844D}$ (23.4%) (*p*-value > 0.05). This meant that all genotypes survived until birth. *Pex1*$^{+/+}$ and *Pex1*$^{G844D/+}$ exhibited a similar phenotype and were used as control for ZSD mice (*Pex1*$^{G844D/G844D}$). The male/female ratio was 1:1 in control mice and 1.16:1 in ZSD mice (*p*-value > 0.05), meaning that genotype did not alter the 1:1 expected sex ratio. Of note, female ZSD mice were sterile, male ZSD mice were fertile but they were not used for breeding. All the data reported hereafter were collected from our *Pex1*-G844D NMRI mice strain delivering large litters and robust ZSD pups.

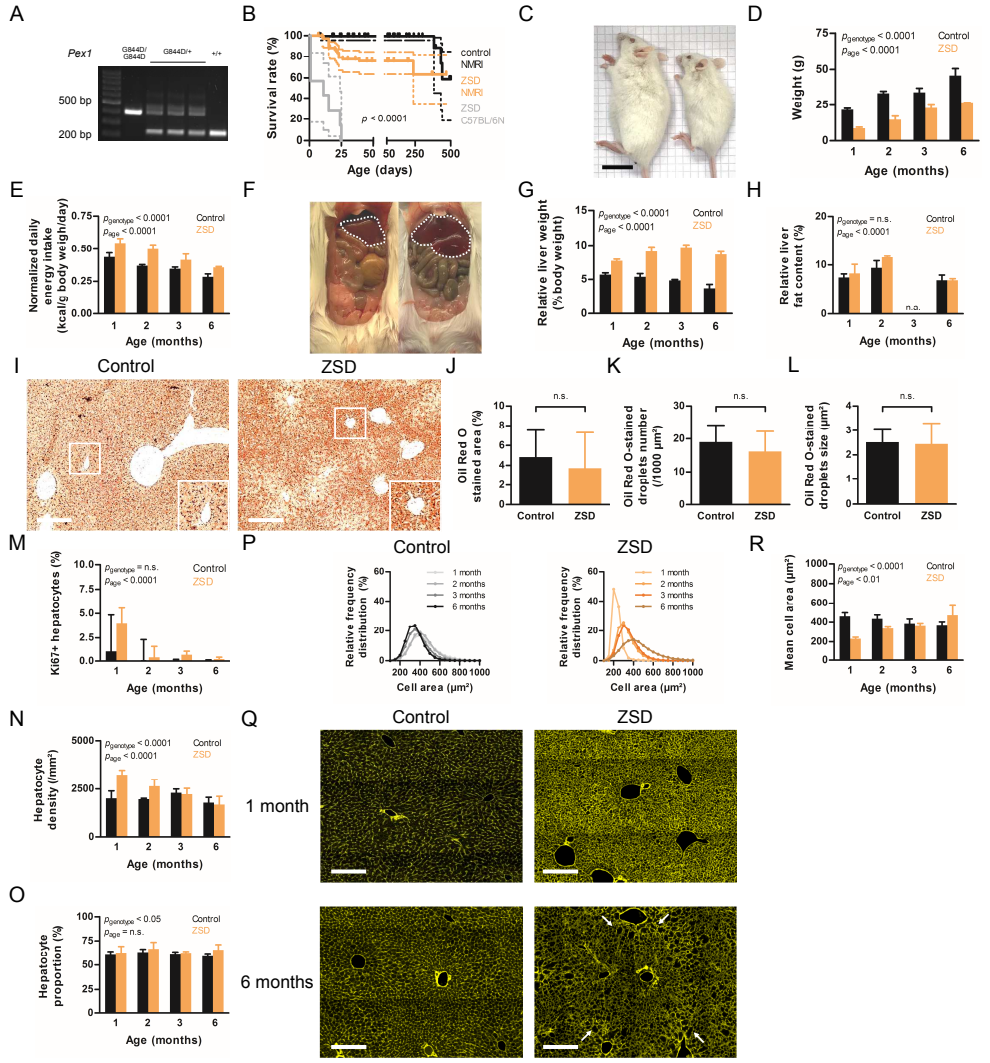

Figure 1 - Zellweger spectrum disorder (ZSD) mice exhibited reduced survival rate, growth retardation with higher energy intake, and relative hepatomegaly associated to progressive hepatocyte hypertrophy. **A** Genotyping gel from five 3-week-old pups. The product size difference is a consequence of 177 bp residual *Neo* cassette fragment in an intron near the *Pex1*-G844D allele[22]. **B** Survival curves from control mice (black curve, n = 223), ZSD mice in Naval Medical Research Institute (NMRI, orange curve, n = 68) and C57BL/6N (grey curve, n = 7) backgrounds. NMRI ZSD mice showed increased survival compared to C57BL/6N ZSD mice. All the data reported hereafter were collected from the NMRI background. Log-rank test, dashed lines represent 95% confidence interval. **C** Control (left) and ZSD (right) mouse at 2 months highlighted a significant growth retardation in ZSD mouse. Scale bar: 2 cm. **D** Mouse weight longitudinal study confirmed the significant growth retardation in ZSD mice with no catch up growth detectable. **E** Daily energy intake normalized for body weight disclosed a higher energy intake in ZSD mice. Thus, energy intake did not explain growth retardation detected in ZSD mice. **F** Control (left) and ZSD (right) mouse abdominal cavity at 3 months exposed an enlarged liver in ZSD mouse. **G** Mouse liver weight longitudinal analysis revealed a relative hepatomegaly which progressively increased in ZSD mice ($p_{interaction}$ < 0.0001). **H** Liver fat content quantification did not highlight any difference between ZSD and

control liver and thus ruled out liver lipid deposition as a cause to the relative hepatomegaly in ZSD mice. **I** Liver Oil Red O staining showed hepatocytes lipid droplets in both genotypes. Droplets deposition zonation favoring periportal space was perceptible in ZSD mice liver. Inserts show higher magnification of the boxed area. Scale bar: 200 µm. Liver Oil Red O **J** -stained area (%), **K** -stained droplets number (/1000 µm²) and **L** -stained droplets size (µm²) digital quantification did not detect difference between ZSD and control livers. Pigment precipitation (black dots) were excluded during digital quantification. Longitudinal study on liver slides stained for hepatocyte nuclear factor 4 alpha (hepatocyte marker) and Ki67 (proliferation marker) to measure **M** proportion of proliferative hepatocytes, **N** hepatocyte density (/mm²), **O** hepatocyte proportion relative to total liver cells. ZSD hepatocytes did not show any significant proliferation increase. Yet, compared to control, the ZSD hepatocyte density was higher at one month and slowly decreased to control levels afterwards. This suggested that hepatocyte proliferation took place before 1 month of age, followed by hepatocyte hypertrophy, in ZSD mice. **P** Longitudinal study of liver cell area relative distribution based on wheat germ agglutinin-rhodamine staining (WGA, cell membrane marker) highlighted a progressive trend to liver cell area increase in ZSD. **Q** WGA-stained liver slides depicted smaller hepatocytes in 1-month-old ZSD liver compared to control. At 6 months, ZSD liver slides presented enlarged cells with a zonation favoring the perivenular region (white arrows). Scale bar: 200 µm. **R** Longitudinal mean liver cell area quantification underlined a reduced ZSD liver cell area at 1 month of age followed by a progressive cell enlargement exceeding control liver cell area at 6 months. Two-way ANOVA and n = 6/timepoint/genotype (longitudinal) or Mann-Whitney test and n ≥ 5/group (2 groups), median ± interquartile range, n.a.: not available, n.s.: not significant.

ZSD mice presented growth retardation and relative hepatomegaly associated to progressive hepatocyte hypertrophy

ZSD mice presented a reduced survival rate compared to control mice (*p*-value < 0.0001, **Figure 1B**). The first month of life was a critical period during which 22% of ZSD mice died. After weaning, none except one ZSD mice died prematurely, however they exhibited severe growth retardation. This phenotype was already evident at day 3 and was maintained until death (**Figure 1C,D**). After weaning, daily energy intake normalized for body weight was higher in ZSD mice, and thus could not account for growth retardation (**Figure 1E**).

The presence of an enlarged liver was striking during ZSD mice dissection (**Figure 1F**), but no hydronephrosis was detected in contrast to the *Pex1*-G844D C57BL/6N strain reported by Berendse *et al.*[21]. ZSD mice exhibited progressive relative hepatomegaly as depicted by the increase in liver weight normalized for body weight (**Figure 1G**). In addition, absolute ZSD liver weight exceeded controls between 2 and 3 months of age (data not shown). Berendse *et al.* suggested that fat accumulation explains this hepatomegaly[21]. We performed both biochemical and

histological liver lipid quantification and we could not confirm liver fat accumulation in ZSD mice (**Figure 1H-L**). Beside lipids accumulation, sugar and proteins accumulation were ruled out by glycogen metabolism analysis (see below) and protein quantification (data not shown), respectively.

PBD increases BA and VLCFA levels leading to farnesoid X receptor and PPARα activation which upregulate proliferation markers *Foxm1* and *c-myc*, respectively[21, 38, 47]. Here we found that *Foxm1*, *c-myc*, *Pcna* and *Mki67* proliferation markers and PPARα target genes were upregulated in ZSD mouse liver (**Table 2**). To confirm these data, we quantified hepatocytes (HNF4α positive nuclei) and proliferation marker (Ki67 positive nuclei) on liver slides. Proliferative hepatocyte proportion was not different in ZSD livers compared to controls (**Figure 1M**). Unexpectedly, this method discovered a higher hepatocyte density that decreased over time in ZSD mice liver (**Figure 1N**). ZSD hepatocyte proportion (relative to all liver cells) remained constant during the whole study (**Figure 1O**). To further decipher hepatocyte density modification, we measured hepatocyte area and confirmed a progressive ZSD hepatocyte hypertrophy with age (**Figure 1P-R**). Based on these findings, we postulate that the progressive hepatomegaly presented by ZSD mice after 1 month of age is explained by hepatocyte hypertrophy and not hepatocyte proliferation.

Table 2. RNA sequencing analysis on 2-month-old control and ZSD mice liver.

Pathway	Symbol	Description	log_2 (fold change)	Fold change	*p*-value	FDR
Proliferation	Foxm1	Forkhead box M1	1.17	2.25	*	0.0434
	Mki67	Antigen identified by monoclonal antibody Ki 67	1.78	3.43	*	0.0323
	Myc	Myelocytomatosis oncogene	2.07	4.20	***	0.000845
	Pcna	Proliferating cell nuclear antigen	0.34	1.27	*	0.0408
Hypertrophy	Akt1	Thymoma viral proto-oncogene 1	0.23	1.17	*	0.0475

Table 2. RNA sequencing analysis on 2-month-old control and ZSD mice liver.

Pathway	Symbol	Description	log_2 (fold change)	Fold change	*p*-value	FDR
	Mtor	Mechanistic target of rapamycin kinase	0.60	1.51	**	0.00252
	Mrps6	Mitochondrial ribosomal protein S6	0.61	1.53	**	0.000907
	Eif4ebp1	Eukaryotic translation initiation factor 4E binding protein 1	0.36	1.29	*	0.0351
PPARα targets	Acot1	Acyl-CoA thioesterase 1	3.14	8.82	***	0.00000833
	Cd36	CD36 molecule = fatty acid translocase	4.35	20.39	***	0.000000722
	Cpt1a	Carnitine palmitoyltransferase 1a, liver	0.66	1.58	***	0.000496
	Cpt1b	Carnitine palmitoyltransferase 1b, muscle	2.41	5.31	***	0.00000316
	Cyp4a10	Cytochrome P450, family 4, subfamily a, polypeptide 10	4.59	24.08	***	0.000313
	Myc	Myelocytomatosis oncogene	2.07	4.20	***	0.000845
Synthesis	Afp	Alpha fetoprotein	6.23	75.06	***	7.93E-10
	Alb	Albumin	-0.82	0.57	***	0.00206
	Hmgcr	3-hydroxy-3-methylglutaryl-Coenzyme A reductase	1.91	3.76	***	0.00289
Collagen deposition	Col1a1	Collagen, type I, alpha 1	0.71	1.63	**	0.0124
	Col1a2	Collagen, type I, alpha 2	0.22	1.17	n.s.	> 0,05
	Col3a1	Collagen, type III, alpha 1	0.77	1.70	***	0.000748
	Col4a2	Collagen, type IV, alpha 2	1.47	2.77	***	0.000000198
	Acta2	Actin, alpha 2, smooth muscle, aorta	-0.27	0.83	n.s.	> 0,05
Glycogen metabolism	Slc2a2	Solute carrier family 2 (facilitated glucose transporter), member 2 = Glut2	-0.81	0.57	***	0.0000282
	Hk3	Hexokinase 3	-0.80	0.58	**	0.0178
	Gck	Glucokinase	-0.85	0.55	*	> 0,05
	Pgm1	Phosphoglucomutase 1	0.37	1.29	***	0.000349
	Ugp2	UDP-glucose pyrophosphorylase 2	0.04	1.03	n.s.	> 0,05
	Gyg	Glycogenin	1.73	3.32	***	0.000000201
	Gys2	Glycogen synthase 2	-1.01	0.50	***	0.00177
	Gsk3a	Glycogen synthase kinase 3 alpha	0.24	1.18	**	0.004
	Gbe1	Glucan (1,4-alpha-), branching enzyme 1	-0.27	0.83	**	0.0116
	Agl	Amylo-1,6-glucosidase, 4-alpha-glucanotransferase	-0.40	0.76	***	0.000115
	Pygl	Liver glycogen phosphorylase	-1.00	0.50	***	0.00000337
	G6pc	Glucose-6-phosphatase, catalytic	-2.46	0.18	***	0.000000398

Table 2. RNA sequencing analysis on 2-month-old control and ZSD mice liver.

Pathway	Symbol	Description	log_2 (fold change)	Fold change	*p*-value	FDR
	Slc37a4	Solute carrier family 37 (glucose-6-phosphate transporter), member 4 = G6pt	-1.21	0.43	***	0.00011
Glycolysis	Slc2a2	Solute carrier family 2 (facilitated glucose transporter), member 2 = Glut2	-0.81	0.57	***	0.0000282
	Hk3	Hexokinase 3	-0.80	0.58	**	0.0178
	Gck	Glucokinase	-0.85	0.55	*	> 0,05
	Gpi1	Glucose phosphate isomerase 1	0.51	1.42	***	0.00002
	Pfkl	Phosphofructokinase, liver, B-type	0.24	1.18	n.s.	> 0,05
	Pfkfb1	6-phosphofructo-2-kinase/fructose-2,6-biphosphatase 1	-0.86	0.55	***	0.0022
	Aldob	Aldolase B, fructose-bisphosphate	-0.09	0.94	n.s.	> 0,05
	Tpi1	Triosephosphate isomerase 1	-0.27	0.83	**	0.00518
	Gapdh	Glyceraldehyde-3-phosphate dehydrogenase	-0.07	0.95	n.s.	> 0,05
	Pgk1	Phosphoglycerate kinase 1	0.22	1.17	**	0.0089
	Pgam1	Phosphoglycerate mutase 1	0.06	1.05	n.s.	> 0,05
	Eno1	Enolase 1, alpha non-neuron	-0.19	0.88	n.s.	> 0,05
	Pklr	Pyruvate kinase liver and red blood cell	-1.02	0.49	***	0.00269
Gluconeogenesis	Pck1	Phosphoenolpyruvate carboxykinase 1, cytosolic	-1.19	0.44	**	0.00179
	Eno1	Enolase 1, alpha non-neuron	-0.19	0.88	n.s.	> 0,05
	Pgam1	Phosphoglycerate mutase 1	0.06	1.05	n.s.	> 0,05
	Pgk1	Phosphoglycerate kinase 1	0.22	1.17	**	0.0089
	Gapdh	Glyceraldehyde-3-phosphate dehydrogenase	-0.07	0.95	n.s.	> 0,05
	Tpi1	Triosephosphate isomerase 1	-0.27	0.83	**	0.00518
	Aldob	Aldolase B, fructose-bisphosphate	-0.09	0.94	n.s.	> 0,05
	Pfkfb1	6-phosphofructo-2-kinase/fructose-2,6-biphosphatase 1	-0.86	0.55	***	0.0022
	Fbp1	Fructose bisphosphatase 1	-0.08	0.94	n.s.	> 0,05
	Gpi1	Glucose phosphate isomerase 1	0.51	1.42	***	0.00002

Table 2. RNA sequencing analysis on 2-month-old control and ZSD mice liver.						
Pathway	**Symbol**	**Description**	**log_2 (fold change)**	**Fold change**	***p*-value**	**FDR**
	G6pc	Glucose-6-phosphatase, catalytic	-2.46	0.18	***	0.000000398
	Slc37a4	Solute carrier family 37 (glucose-6-phosphate transporter), member 4 = G6pt	-1.21	0.43	***	0.00011
	Slc2a2	Solute carrier family 2 (facilitated glucose transporter), member 2 = Glut2	-0.81	0.57	***	0.0000282
Modulation of genes related to hepatocytes proliferation and hypertrophy, to targets of PPARα, to liver collagen deposition and biochemically relevant in glycogen and glucose metabolism (ZSD *versus* control mice liver, n = 6/group). FDR: false discovery rate, PPARα: peroxisome proliferator-activated receptor alpha, ***: *p*-value < 0,001, **: *p*-value: < 0,01, *: *p*-value < 0,05, n.s.: not significant.						

Pathological liver analysis revealed reduced peroxisome number, bile duct proliferation, and discrete collagen deposition in ZSD mice

The liver of ZSD mice exhibited a strongly reduced PMP70-positive particle number, confirming PBD in this tissue (**Figure 2A**). When looking at the H&E-stained liver slides we found that the cytoplasm of control mice hepatocytes presented torn white spaces that were not present in ZSD mice hepatocytes, especially at young age (**Figure 2B**). The absence of these spaces suggested an impairment in liver glycogen metabolism in ZSD mice liver (see below). Moreover, in ZSD mice liver, H&E staining highlighted bile duct proliferation and progressive hepatocytes enlargement with age, especially in the centrilobular zone supporting the progressive hepatocyte hypertrophy detected earlier (**Figure 2B**). Bile plugs and hepatocellular bile pigments accumulation were detected in 6-month-old ZSD mice liver (**Figure 2B**). In line with bile duct proliferation, RNA-seq analysis showed cholangiocytes markers enrichment among the ZSD upregulated genes (**Figure 2C**). SR-stained area, a marker of collagen deposition, was slightly but significantly increased in ZSD mice liver along the longitudinal study (**Figure 2D, E**). Collagen genes (*Col1a1*, *Col1a2*, *Col3a1* and *Col4a2*) were significantly upregulated (1.2 to 2.8-fold) in ZSD

mice liver (**Table 2**) in line with increased SR staining. Together, histopathological studies of the liver highlighted clues to liver glycogen metabolism alteration (see below), mild collagen deposition, cholestasis and bile duct proliferation supported by RNA-seq analysis.

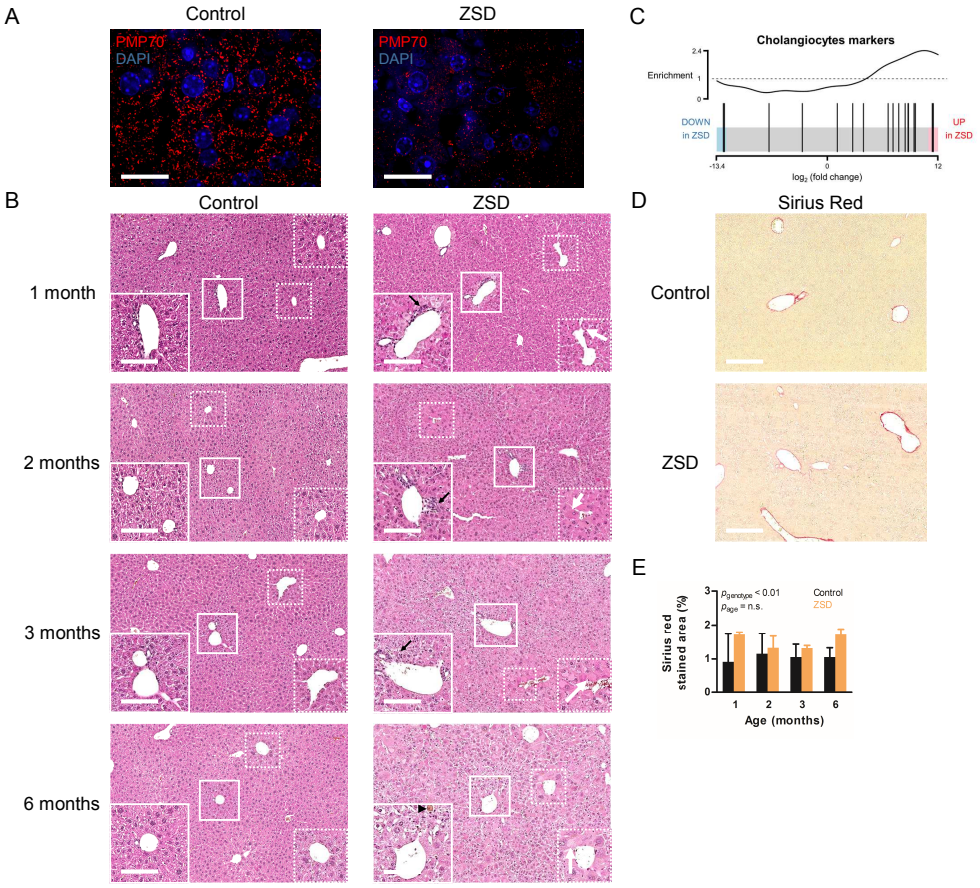

Figure 2 - Zellweger spectrum disorder (ZSD) mouse liver contained less peroxisomes, showed bile duct proliferation and discrete collagen deposition. **A** 2-month-old mouse liver immunolabelled for 70-kDa peroxisomal membrane protein (PMP70) and nuclei stained with diamidino-2-phenylindole dihydrochloride (DAPI). ZSD mouse hepatocytes contained less peroxisomes than control. Representative pictures of 2 livers/genotype. Scale bar: 20 µm. **B** Longitudinal study of H&E stained liver slides. Inserts show higher magnification of the periportal space (boxed area) or centrilobular zone (dashed boxed area). ZSD portal spaces showed bile duct proliferation (black arrow). ZSD mice hepatocytes enlarged progressively and contained pale eosinophilic material (white arrow) especially in the centrilobular zone. Bile plugs were seen in 6-month-old ZSD mouse liver (arrowhead). Representative pictures of 6 livers/timepoint/genotype. Scale bar: 200 µm. **C** Barcode plot illustrating cholangiocyte markers expression enrichment in 2-month-old mouse liver (n = 6/genotype). Comparison of ZSD *versus* control detected enrichment of cholangiocyte markers in ZSD mice liver upregulated genes in line with

the bile duct proliferation seen on ZSD mice liver H&E slides. **D** 6-month-old mice liver stained with Sirius red (SR) exhibited a slight increase in perivascular collagen deposition in ZSD samples. Representative pictures of 6 livers/genotype. Scale bar: 200 µm. **E** Longitudinal morphometry study of SR-stained liver slides unveiled a slight but significant increase in SR-stained area in ZSD livers. Two-way ANOVA, n = 6/timepoint/genotype, median ± interquartile range, n.s.: not significant.

ZSD mice exhibited severe liver glycogen metabolism impairment leading to poor fasting resistance

Liver glycogen metabolism alterations were reported previously in a liver-restricted PBD mouse model and in some ZSD patients[19, 48-50]. This, together with the ZSD hepatocytes' aspect, led us to evaluate whether liver glycogen metabolism was altered in our mouse model. PAS stained area was markedly reduced in ZSD mice liver, supporting an altered glycogen content (**Figure 3A,B**). The difference tended to disappear with age as detected by both PAS staining and biochemical glycogen quantification (**Figure 3B,C**). PAS stained area correlated significantly with glycogen content in ZSD mice liver (**Figure 3D**). Furthermore, PAS staining was amylase-sensitive supporting the presence of glycogen (**Figure 3F,G**). Our ZSD mice exhibited slightly decreased fed-glycemia and poor fasting resistance (**Figure 3E,K**). Both were not related to daily energy intake (**Figure 1E**). RNA-seq revealed glycogen metabolism genes enrichment in the downregulated ZSD liver genes (**Figure 3J**). Among those genes, *G6pc* was downregulated by 5.5-fold in ZSD mouse live (**Table 2**). *G6pc* encodes G6Pase which is responsible for the last step in liver glucose release pathway. To ascertain *G6pc* downregulation impact, we analyzed G6Pase activity on liver tissue and found that the G6Pase activity-stained area was significantly reduced in ZSD mice liver (**Figure 3H,I**). Thus, our ZSD mouse model exhibited liver glycogen metabolism alteration with clinical consequence (i.e., poor fasting resistance) which could be used as a robust readout in preclinical studies.

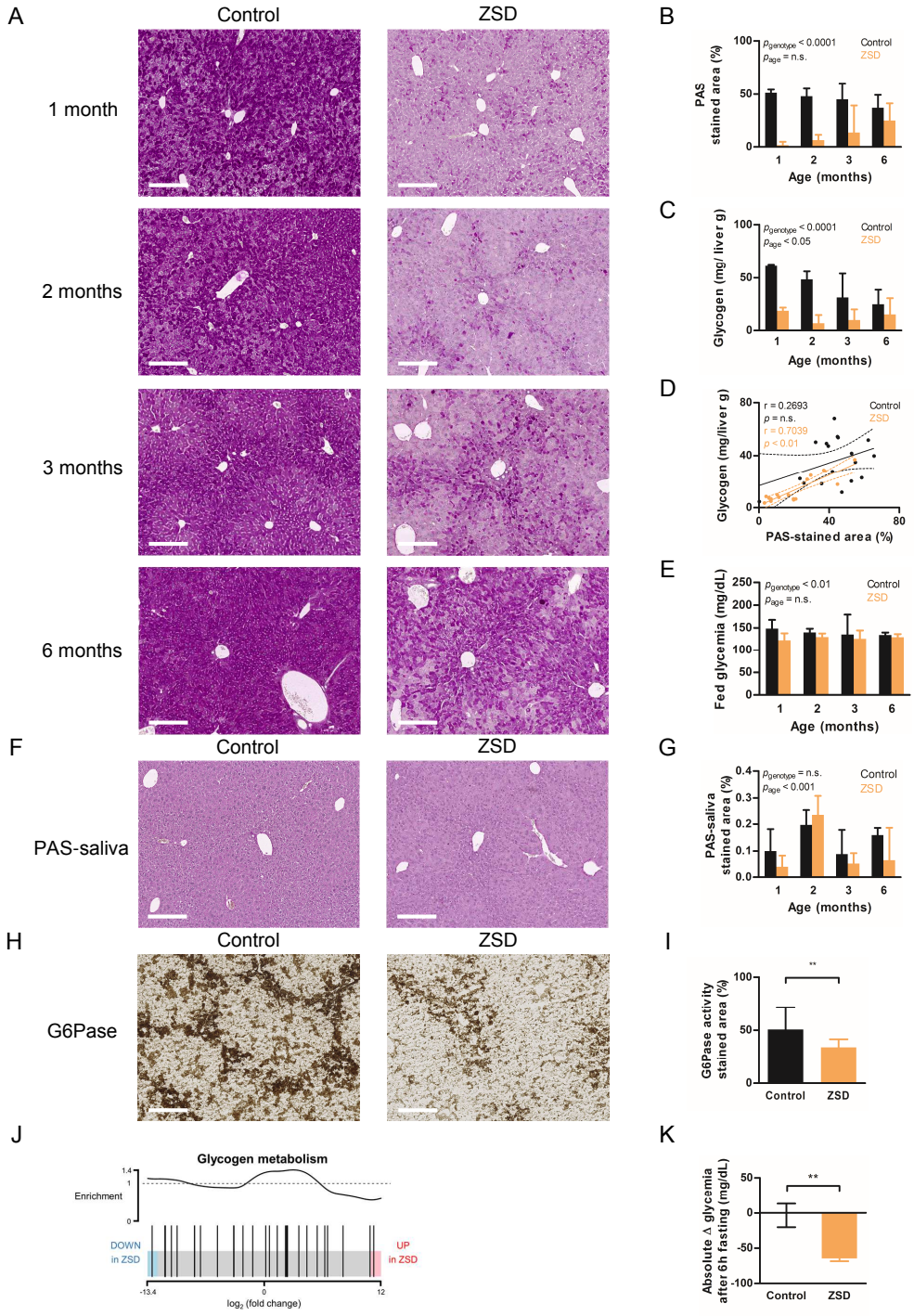
A
Control
ZSD
1 month
2 months
3 months
6 months
B
PAS stained area (%)
Age (months)
C
Glycogen (mg/ liver g)
Age (months)
D
Glycogen (mg/liver g)
PAS-stained area (%)
E
Fed glycemia (mg/dL)
Age (months)
F
PAS-saliva
G
PAS-saliva stained area (%)
Age (months)
H
G6Pase
I
G6Pase activity stained area (%)
Control
ZSD
J
Glycogen metabolism
Enrichment
DOWN in ZSD
UP in ZSD
log2 (fold change)
K
Absolute Δ glycemia after 6h fasting (mg/dL)

Figure 3 - Zellweger spectrum disorder (ZSD) mouse liver exhibited glycogen metabolism alterations leading to poor fasting resistance. **A** Longitudinal study of Periodic-acid Schiff (PAS) stained liver slides unveiled a severe lack of staining in ZSD mouse liver compared to control. The difference tended to decrease with age. **B** Longitudinal morphometry study of PAS-stained liver slides confirmed the lower PAS-stained area in ZSD. PAS staining in control mouse liver tended to decrease with age, opposite to what was detected in ZSD mice liver ($p_{interaction} < 0.01$). **C** Biochemical liver glycogen content quantification normalized for liver weight confirmed a decreased glycogen content in ZSD. An inverted trend with age was detected in controls compared to ZSD samples ($p_{interaction} = 0.016$). **D** Scatterplot showing the correlation between PAS-stained area and glycogen content in mouse liver. Both measures were tightly correlated in ZSD mice liver. **E** Mouse morning glycemia was lower in ZSD, especially in 1-month-old mice. **F** 2-month-old control and ZSD liver slides stained with PAS after saliva exposure lead to nearly complete PAS staining disappearance. It meant that PAS-stained area was amylase-sensitive sugar (i.e., glycogen). **G** Longitudinal morphometry study of mouse liver slides stained with PAS after saliva exposure detected no statistical difference between both genotypes. **H** 2-month-old control and ZSD liver unfixed slides stained for glucose-6-phosphatase activity (G6Pase) unveiled classical periportal space zonation with a dramatic activity decrease in ZSD liver. **I** G6Pase activity stained area quantification confirmed the difference between ZSD liver and control group. **J** Barcode plot illustrating glycogen metabolism genes expression enrichment in 2-month-old mouse liver. Comparison of ZSD *versus* control unraveled enrichment of glycogen metabolism genes in ZSD mouse liver downregulated genes in line with the lower ZSD mouse liver glycogen content. **K** Absolute glycemia variation after 6 h fasting of 2-month-old mice lead to severe glycemia drop in ZSD mice compared to no variation in control. This confirmed the physiological impact of lower glycogen content in ZSD mice liver. Representative pictures of 6 livers/timepoint/genotype. Scale bar: 200 µm. Two-way ANOVA and n = 6/timepoint/genotype (longitudinal), Spearman's correlation test and n = 18/genotype (correlation) or Mann-Whitney test and n = 6/genotype (2 groups), median ± interquartile range (bars) or best-fit line ± 95% confidence band (scatter-plot), n.s.: not significant, r: correlation coefficient, **: *p*-value < 0.01.

ZSD mice liver expression profile unraveled modulations in multiple pathways among which glucose metabolism was switched to glucose consumption

The principal component analysis performed on estimated transcript abundances derived from RNA-seq data unmasked 3 different gene expression profiles (control males, control females and ZSD mice) suggesting the loss of sexual dimorphism in ZSD liver (**Figure 4A**). 7102 genes were significantly modulated (FDR < 0.05) between control and ZSD mice liver (**Figure 4B**). Over-representation analysis of gene ontology analysis exposed modulations in multiple molecular functions, biological process and cellular components associated with PBD (**Figure 4C**).

The liver glycogen alterations discovered in our ZSD mouse model and the link between carbohydrate metabolism and peroxisome biogenesis, led us to evaluate glucose metabolism gene expression modulation by enrichment analysis[19, 50]. In ZSD liver, glycolysis genes were enriched in the upregulated genes and opposed to

gluconeogenesis gene enrichment in the downregulated genes (**Figure 4D**). A comparison between the modulation levels from Peeters *et al.* gene list and our RNA-seq data uncovered a significant correlation suggesting similar PBD impact on liver gene expression in both mouse models (**Figure 4E**). Liver RNA-seq analysis provided insight into the entire breadth of PBD consequences.

Figure 4 - Zellweger spectrum disorder (ZSD) mouse liver gene expression profile unveiled modulations in multiple pathways among which glucose metabolism was switched to glucose consumption. **A** Scatterplot of the principal component analysis performed on estimated transcript abundances derived from RNA sequencing data collected from 2-month-old control and ZSD mice liver (n = 6/genotype) showed 3 clouds from control males, control females and ZSD mice samples, respectively. This could mean that liver sex phenotype was lost as peroxisome biogenesis disorder consequence. PC1 and PC2 explained 45.7% and 14.3% of the variability, respectively. **B** Volcano plot from RNA sequencing analysis represented > 7000 significantly (false discovery rate (FDR) < 0.05) modulated genes (ZSD *versus* control). Glycogen (black) and glucose (grey) metabolism genes were plotted to highlight their position on the whole analysis. **C** Gene ontology enrichment analysis for molecular functions, biological process and cellular components highlighted significant enrichment in multiple pathways reflecting the vast peroxisome biogenesis disorder consequences on liver gene expression. **D** Barcode plot illustrating glucose metabolism genes expression enrichment in ZSD *versus* control mice liver (n = 6/genotype), no modulation trend was detected. Analysis was further refined to analyze glycolysis and gluconeogenesis independently. This unraveled glycolysis genes enrichment among upregulated genes, in association with gluconeogenesis genes enrichment among downregulated genes. Expression profile in ZSD mouse liver suggested a glucose metabolism switch to glucose consumption. **E** Scatter plot showing significant correlation between gene expression modulation (ZSD *versus* control liver) in our study and reported by Peeters *et al.* in 2011. Spearman's correlation test, r: correlation coefficient, best-fit line ± 95% confidence band.

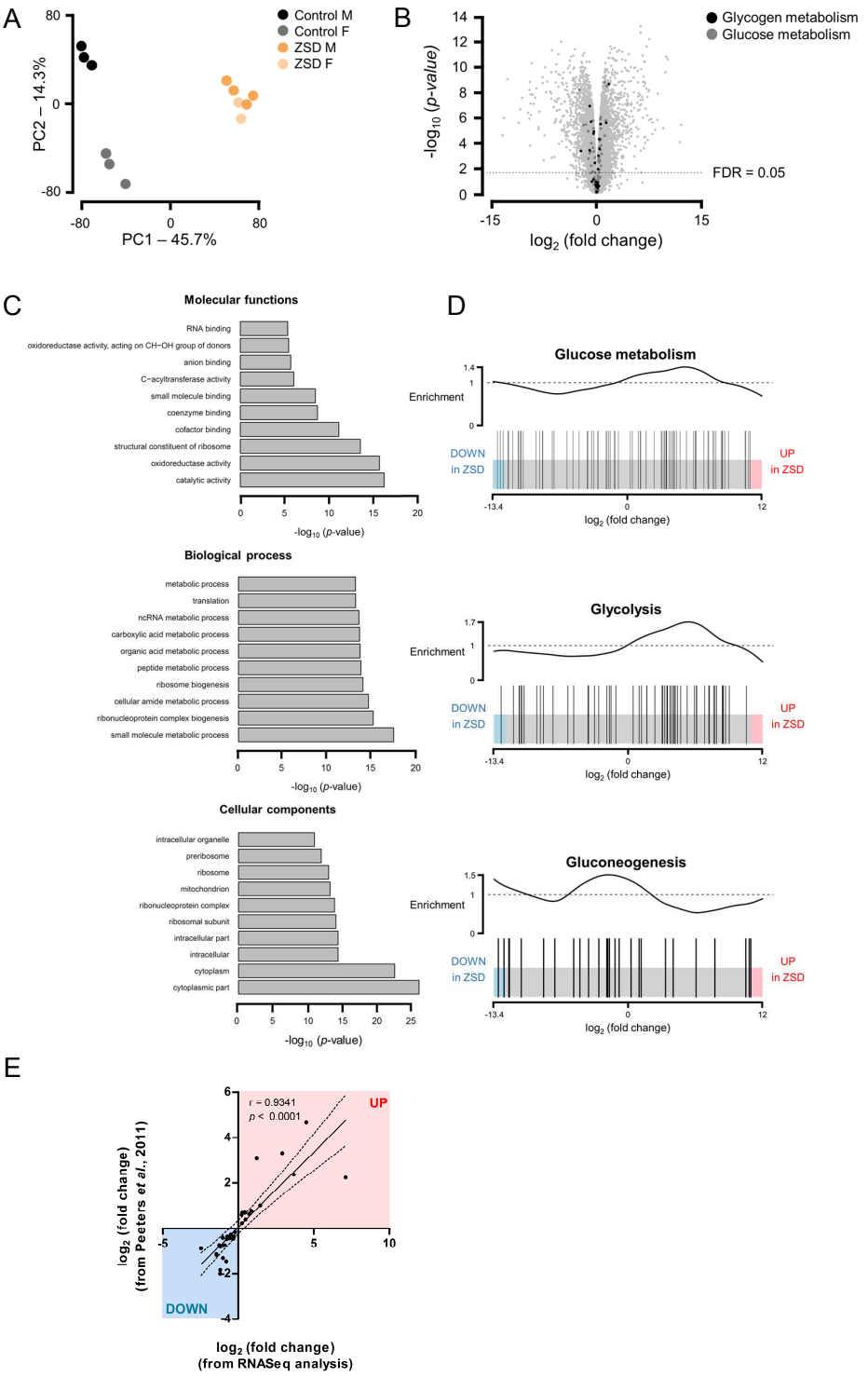
A
Control M
Control F
ZSD M
ZSD F
PC2 – 14.3%
PC1 – 45.7%
B
Glycogen metabolism
Glucose metabolism
-log10 (p-value)
FDR = 0.05
log2 (fold change)
C
Molecular functions
RNA binding
oxidoreductase activity, acting on CH–OH group of donors
anion binding
C-acyltransferase activity
small molecule binding
coenzyme binding
cofactor binding
structural constituent of ribosome
oxidoreductase activity
catalytic activity
-log10 (p-value)
Biological process
metabolic process
translation
ncRNA metabolic process
carboxylic acid metabolic process
organic acid metabolic process
peptide metabolic process
ribosome biogenesis
cellular amide metabolic process
ribonucleoprotein complex biogenesis
small molecule metabolic process
-log10 (p-value)
Cellular components
intracellular organelle
preribosome
ribosome
mitochondrion
ribonucleoprotein complex
ribosomal subunit
intracellular part
intracellular
cytoplasm
cytoplasmic part
-log10 (p-value)
D
Glucose metabolism
Enrichment
DOWN in ZSD
UP in ZSD
log2 (fold change)
Glycolysis
Enrichment
DOWN in ZSD
UP in ZSD
log2 (fold change)
Gluconeogenesis
Enrichment
DOWN in ZSD
UP in ZSD
log2 (fold change)
E
r = 0.9341
p < 0.0001
UP
DOWN
log2 (fold change) (from Peeters et al., 2011)
log2 (fold change) (from RNASeq analysis)

ZSD MEF biochemical and immuno-labelling analysis highlighted PBD

MEF were collected to study *in vitro* peroxisome functionality. MEF VLCFA content was elevated in ZSD donor compared to control, specifically C_{26} and C_{26}/C_{22} and C_{24}/C_{22} ratios were significantly increased (**Figure 5A-E**). Phytanic and pristanic acids were not detected because they are absent from cell medium and they are not synthetized by MEF (data not shown). Peroxisome biogenesis was evaluated by immunofluorescent staining for catalase (peroxisomal matrix enzyme) and PMP70 (peroxisomal membrane protein) which highlighted a decreased catalase import into peroxisomes in ZSD MEF compared to control (**Figure 5F**). Some ZSD MEF exhibited catalase import competent peroxisomes beside cells devoid of this competence. This phenomenon called peroxisomal mosaicism is classically described in cells from milder ZSD patients[2]. eGFP-PTS1, a fluorescent peroxisomal reporter, was expressed in MEF and lead to a more diffuse signal with lighter peroxisome staining in ZSD donor than in control (**Figure 5F**). Together, these data suggest that ZSD MEF is a robust mild ZSD cell model for *in vitro* studies before going for *in vivo* evaluation.

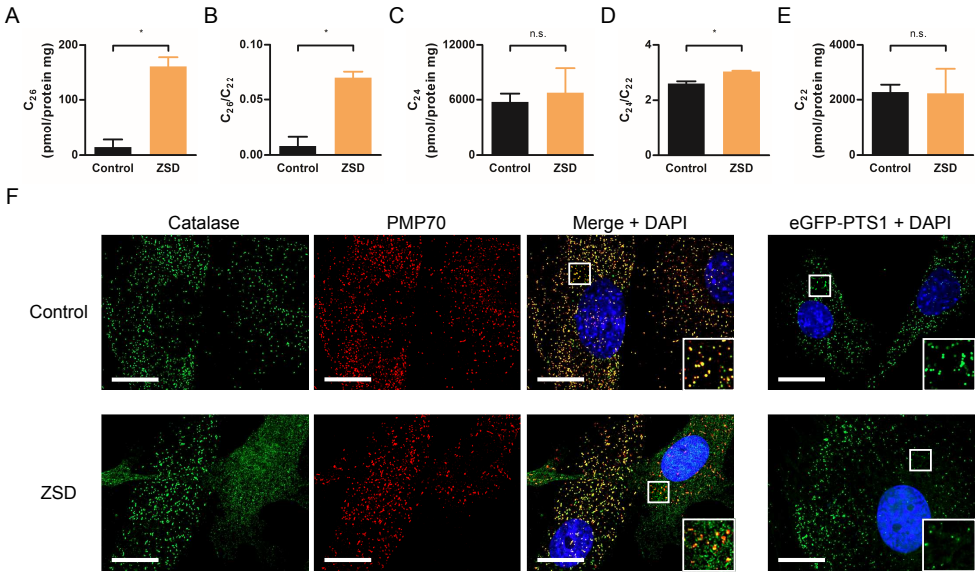

Figure 5 - Zellweger spectrum disorder (ZSD) mouse embryonic fibroblasts (MEF) biochemical evaluation and peroxisome staining highlighted peroxisome biogenesis disorder (PBD) stigma. Very long chain fatty acids **A** C_{26}, **C** C_{24} and **E** C_{22} were quantified in control and ZSD MEF and normalized for protein content. C_{22} was used to calculate **B** C_{26}/C_{22} and **D** C_{24}/C_{22} ratios, both were elevated in ZSD cells. ZSD cells accumulated C_{26} and C_{24} as a consequence of the PBD caused by *Pex1*-G844D homozygous mutation. Mann-Whitney test, n = 4, median ± interquartile range, *: *p*-value < 0.05, n.s.: not significant. **F** Control and ZSD MEF were stained for a peroxisomal matrix protein (catalase), and 70-kDa peroxisomal membrane protein (PMP70) to evaluate peroxisome biogenesis reflected by both markers colocalization. In a second time, MEF were transduced to express green fluorescent protein linked to peroxisome targeting signal 1 (eGFP-PTS1). Nuclei were stained with diamidino-2-phenylindole dihydrochloride (DAPI). Inserts show higher magnification of the boxed area. ZSD MEF harbored PMP70-positive granules without corresponding catalase staining (peroxisome ghosts) confirming PBD. Some ZSD cells contained catalase import competent peroxisomes, a phenomenon known as peroxisomal mosaicism. ZSD MEF exhibited a more diffuse eGFP-PTS1 signal in the cytoplasm than control cells, highlighting PBD. Scale bar: 20 µm.

ZSD mice presented multiple biochemical alterations resulting from PBD

To characterize the biochemical alterations present in our novel ZSD mice strain, we assessed the main biochemical markers found altered in ZSD patients.

Odd-numbered dicarboxylic aciduria was detected in ZSD mice

We collected urine samples from 2-month-old mice to evaluate their organic acids profile. Globally, ZSD mice urine samples contained higher amount of ketone bodies (3-OH butyric acid), dicarboxylic acids (adipic, pimelic, suberic, azelaic and sebacic

acids), 2- and 3-hydoxysebacic acid, Krebs' cycle intermediates (fumaric and succinic acids), glycolic acid and 2-OH-glutaric acid (**Figure 6A**). These urinary data correlates with findings in ZSD patients and reflect PBD consequence on multiple organs[8]. This feature is important as it might serve as global readout for ZSD pre-clinical studies.

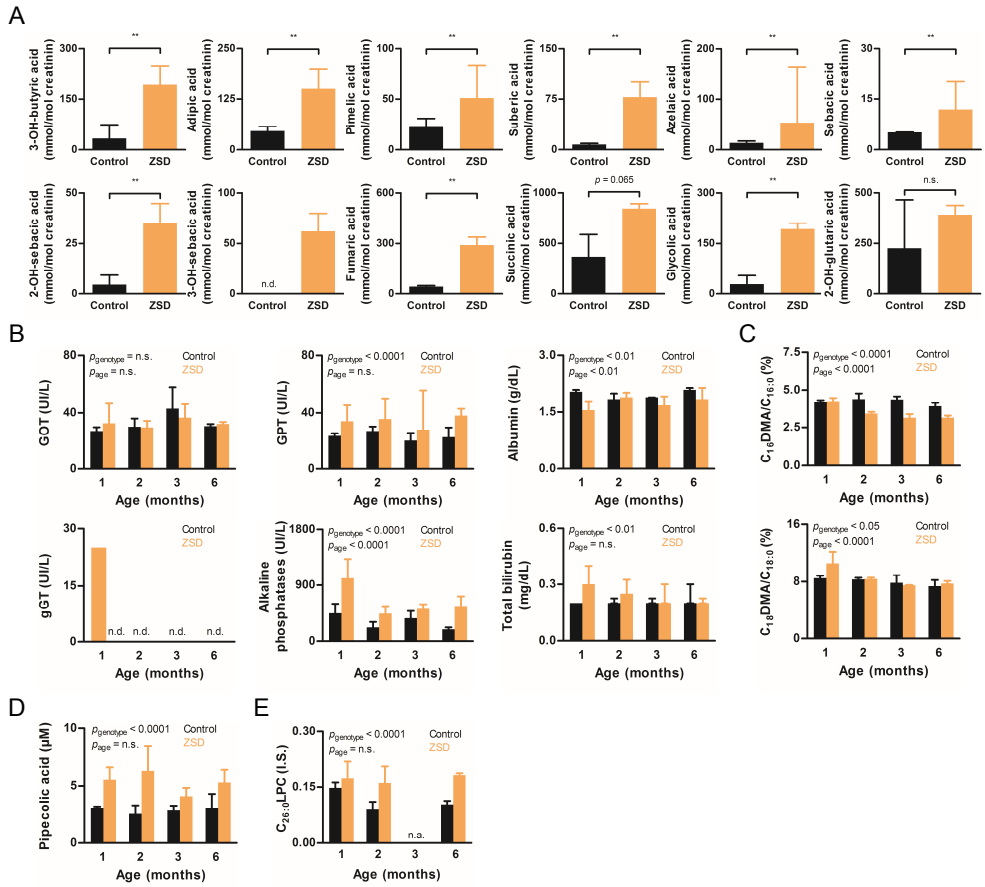

Figure 6 - Zellweger spectrum disorder (ZSD) mice urine organic acid profile, blood peroxisome markers and plasma liver markers fitted with a ZSD. **A** Relevant organic acids detected in 2-month-old mouse urine. In ZSD mouse samples, a broad dicarboxylic aciduria was present from C_6 (adipic acid) to C_{10} (sebacic acid) including odd-numbered acids. As reported for ZSD patients, hydroxylated sebacic acid derivatives and Krebs cycle intermediates (succinic and fumaric acids) were significantly increased in ZSD mice urine. **B** Longitudinal study of plasma liver enzymes and cholestasis markers suggested a chronic liver injury (low albumin level at 1 month and persistent glutamate-pyruvate transaminase (GPT) elevation) associated to progressive improvement of the cholestasis (alkaline phosphatase level decrease and total bilirubin normalization) in ZSD mice. **C** Erythrocyte plasmalogen content was studied longitudinally and was reported as the ratio between $C_{16:0}$ or $C_{18:0}$ dimethyl acetal (DMA) and the

corresponding fatty acid. Plasmalogens are partly synthetized by peroxisomal enzymes thus explaining lower $C_{16:0}$ erythrocytes plasmalogen levels in ZSD mice older than 1 month. Yet, erythrocytes plasmalogen levels can be normal in mild ZSD patients as were $C_{18:0}$ erythrocytes plasmalogen levels in ZSD mice. **D** Plasma pipecolic acid (PA) levels were significantly elevated in ZSD mice as a result of its impaired degradation by the peroxisome. **E** $C_{26:0}$lysophosphatidylcholine (C26LPC) quantified on dried blood spot revealed increased levels in ZSD mice. C26LPC marker is used for newborn screening of X-linked adrenoleukodystrophy, a related peroxisomal disorder, and it is proposed as a sensitive marker for ZSD diagnosis. Data are expressed as a ratio between the signal of the analyte and the signal of its internal standard (I.S.). Mann-Whitney test and n = 6/genotype (2 groups) or two-way ANOVA, n = 6/timepoint/genotype (longitudinal), median ± interquartile range, n.d.: not detected, n.s.: not significant, GOT: glutamate-oxaloacetate transaminase, gGT: gamma-glutamyltransferase, n.a.: not available, **: *p*-value < 0.01.

Plasma liver markers levels depicted chronic liver injury in ZSD mice

Liver disease is present in nearly all ZSD patients. Therefore, we evaluated several hepatic markers in our mouse model[3]. Plasma from ZSD mice showed signs of hepatocyte injury as highlighted by GPT elevation and albumin decrease (**Figure 6B**). In ZSD mice liver, albumin (*Alb*) expression was reduced by nearly 50% and the liver injury/tumor marker *Afp* was upregulated more than 50-fold in line with the suspected hepatocellular insult (**Table 2**). Total bilirubin and alkaline phosphatases activity and, to a lesser extent, gGT elevation suggested cholestasis in ZSD mouse plasma. As for ZSD patients, we found that these markers tended to normalize with age (**Figure 6B**)[4].

Erythrocyte plasmalogen, plasma pipecolic acid, and C26LPC levels were in line with PBD in ZSD mice

Plasmalogen biosynthesis starts inside peroxisomes and their erythrocytes level is used as diagnostic marker for several peroxisomal disorders[51]. $C_{16:0}$ erythrocyte plasmalogen levels were reduced in ZSD mice older than 1 month (**Figure 6C**). Some patients with mild ZSD phenotype may exhibit normal erythrocyte plasmalogens levels as were $C_{18:0}$ erythrocyte plasmalogens in ZSD mice older than 1 months[3]. Pipecolic acid, a metabolite resulting from lysine degradation, accumulated in ZSD mice plasma highlighting a defect during its hepatic peroxisomal

degradation (**Figure 6D**). Quantification of C26LPC is used for the newborn screening of X-linked adrenoleukodystrophy, another peroxisomal disorder, and it was shown that C26LPC is also an effective ZSD marker[52, 53]. In ZSD mice, C26LPC levels were increased and thus confirmed the ZSD phenotype of our mouse model (**Figure 6E**).

BCFA and VLCFA accumulated in ZSD mice plasma and liver

Peroxisomes are responsible for BCFA (phytanic and pristanic acids) and VLCFA metabolism driving us to study them in our mouse model[6]. ZSD mice exhibited BCFA and VLCFA accumulation in both plasma and liver (**Figure 7 A-G**). Plasma and liver phytanic acid and C_{26} levels showed a significant decrease with age in ZSD mice along with significant correlation between plasma and liver levels (**Figure 7A,F**). These correlations suggest that plasma BCFA and VLCFA levels quantification could be used as a proxy for intra-hepatic levels during treatment evaluation in ZSD mice.

Figure 7 - Zellweger spectrum disorder (ZSD) mouse plasma and liver displayed branched-chain and very long-chain fatty acid accumulation. Phytanic acid and C_{26} levels were correlated between the two compartments and tended to normalize with age. Longitudinal study of control (black) and ZSD (orange) mouse **A** phytanic and **B** pristanic acids and **C** C_{22}, **D** C_{24}, **E** C_{24}/C_{22}, **F** C_{26}, **G** C_{26}/C_{22} levels in plasma and liver and their correlation on scatter plot. Two-way ANOVA and n = 6/timepoint/genotype reported as median ± interquartile range (longitudinal), Spearman's correlation test and n = 12/genotype with best-fit line ± 95% confidence band (correlation), r: correlation coefficient, n.s.: not significant.

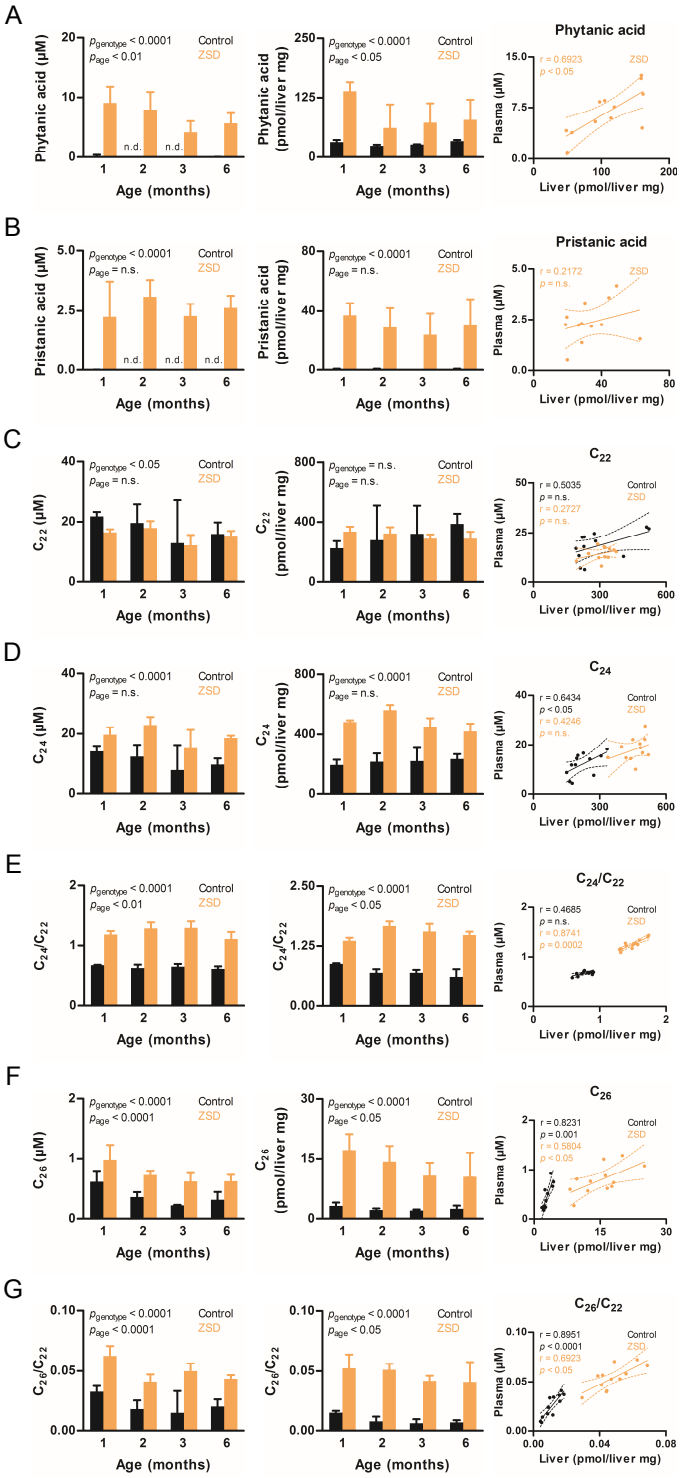
A
Phytanic acid (μM)
$p_{genotype}$ < 0.0001
p_{age} < 0.01
Control
ZSD
n.d.
Age (months)
Phytanic acid (pmol/liver mg)
$p_{genotype}$ < 0.0001
p_{age} < 0.05
Phytanic acid
Plasma (μM)
r = 0.6923
p < 0.05
Liver (pmol/liver mg)
B
Pristanic acid (μM)
$p_{genotype}$ < 0.0001
p_{age} = n.s.
Pristanic acid (pmol/liver mg)
Pristanic acid
r = 0.2172
p = n.s.
C
C_{22} (μM)
$p_{genotype}$ < 0.05
p_{age} = n.s.
C_{22} (pmol/liver mg)
$p_{genotype}$ = n.s.
C_{22}
r = 0.5035
p = n.s.
r = 0.2727
p = n.s.
D
C_{24} (μM)
$p_{genotype}$ < 0.0001
p_{age} = n.s.
C_{24} (pmol/liver mg)
C_{24}
r = 0.6434
p < 0.05
r = 0.4246
p = n.s.
E
C_{24}/C_{22}
$p_{genotype}$ < 0.0001
p_{age} < 0.01
p_{age} < 0.05
C_{24}/C_{22}
r = 0.4685
p = n.s.
r = 0.8741
p = 0.0002
F
C_{26} (μM)
$p_{genotype}$ < 0.0001
p_{age} < 0.0001
p_{age} < 0.05
C_{26} (pmol/liver mg)
C_{26}
r = 0.8231
p = 0.001
r = 0.8804
p < 0.05
G
C_{26}/C_{22}
$p_{genotype}$ < 0.0001
p_{age} < 0.0001
p_{age} < 0.05
C_{26}/C_{22}
r = 0.8951
p < 0.0001
r = 0.6923
p < 0.05

ZSD mice were cholestatic and accumulated oxysterols and C_{27} BA precursors in plasma and liver

PBD are known to induce altered BA metabolism[54]. Therefore, we decided to analyze C_{24} BA and their C_{27} precursors (di- and trihydroxycholestanoic acids) in ZSD mice plasma and liver. Total (un)conjugated C_{24} BA levels were not significantly different in ZSD and control mice plasma (**Figure 8A,B**). Yet, total (un)conjugated C_{24} BA levels were significantly reduced in ZSD mice liver, the organ in which they are produced. The total (un)conjugated C_{24} BA plasma-liver ratio was higher in ZSD mice, highlighting the discrepancy between total (un)conjugated C_{24} BA plasma and liver levels in ZSD mice, compared to control. Moreover, a significant positive correlation was detected between conjugated C_{24} BA plasma and liver levels in ZSD mice, but not in control. Finally, C_{27} BA precursors were only detected in ZSD mice plasma and liver (**Figure 8C**), which confirms that our model induces a relative interruption between C_{27} and C_{24} BA, just as in human PBD. Taken together, these results unraveled a total C_{24} BA accumulation in ZSD mice plasma along with a defect in their plasmatic elimination.

This cholestasis, a well-known phenomenon in ZSD patients, supports our finding of increased plasma cholestasis markers (**Figure 6B**)[11]. From these results, we wanted to go further and investigate the consequences of this C_{27} and C_{24} BA accumulation at the oxysterol level, the early metabolites of cholesterol. We found that both 7-hydroxycholesterol (7-OHC) and 7α-hydroxy-4-cholesten-3-one (7α-OHCnone), formed during initial steps of BA synthesis, were elevated in ZSD mice liver and plasma and showed no evolution with age (**Figure 8D,E**). We also analyzed total cholesterol and found that its levels were decreased in ZSD mice plasma (**Figure**

8F). These results, together with the 3.8-fold *Hmgcr* upregulation in ZSD mice liver (**Table 2**), suggest an increased production rate of oxysterols along with a positive-feedback increased biosynthesis of cholesterol.

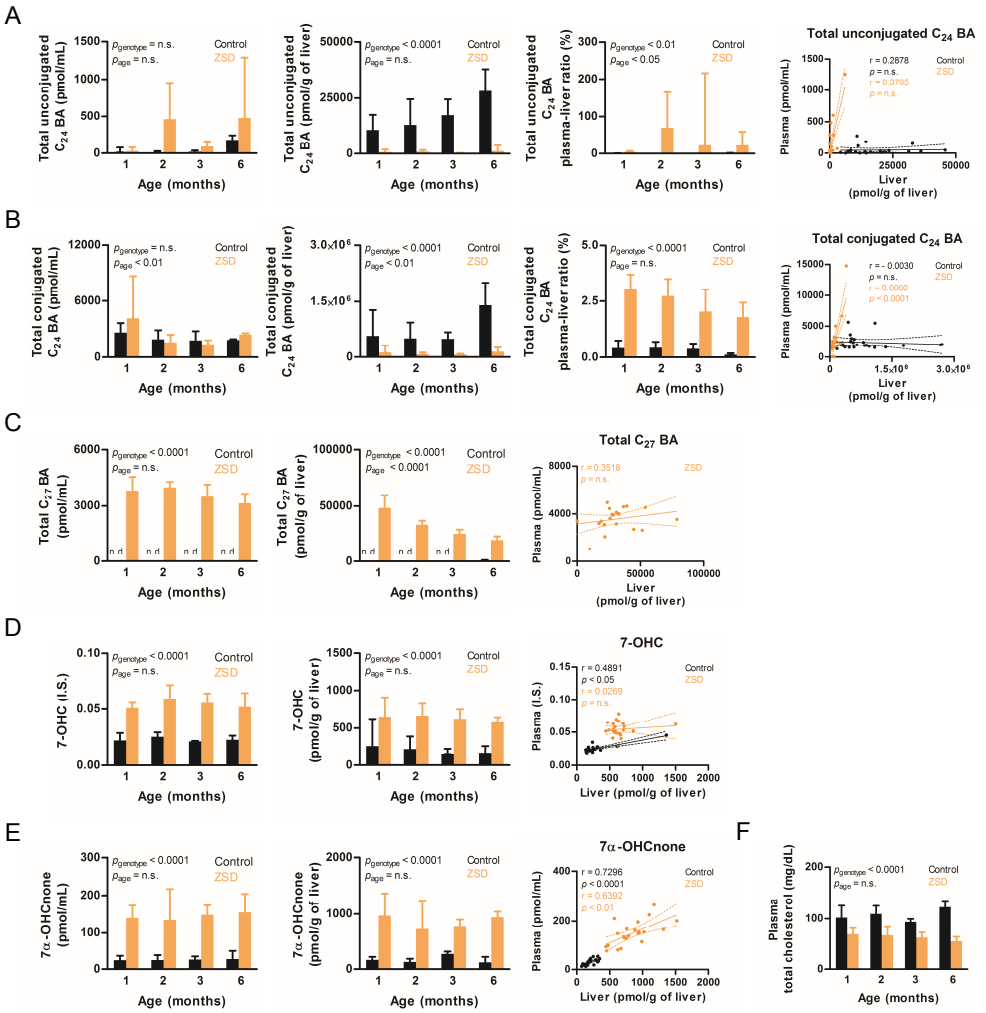

Figure 8 - Zellweger spectrum disorder (ZSD) mouse plasma and liver total C_{24} bile acids (BA) levels underlined cholestasis associated with specific oxysterol species and C_{27} BA accumulation and decreased plasma total cholesterol levels. Longitudinal study of control (black) and ZSD (orange) mouse **A** total unconjugated C_{24} BA, **B** total conjugated C_{24} BA, **C** total C_{27} BA, **D** 7-hydroxycholesterol (7-OHC), **E** 7α-hydroxycholestenone (7α-OHCnone), **F** total cholesterol in plasma and liver and their correlation on scatter plot (excepted for total cholesterol). Un- and conjugated C_{24} BA plasma to liver ratios highlighted cholestasis (i.e., plasma BA accumulation) in ZSD mice. C_{27} BA precursors were only detected in ZSD mice thus confirming the relative interruption between C_{27} and C_{24} BA, just as in human PBD. Both 7-OHC and 7α-OHCnone are formed during initial BA biosynthesis steps and accumulated in ZSD mouse

samples. Plasma total cholesterol levels were lower in ZSD mice. Two-way ANOVA and n = 5-6/timepoint/genotype reported as median ± interquartile range (longitudinal), Spearman's correlation test and n = 21/genotype with best-fit line ± 95% confidence band (correlation), r: correlation coefficient, n.s.: not significant.

Discussion

To overcome ZSD mouse model limitations (i.e., small litters and poor survival rates), the hypomorphic *Pex1*-G844D allele was backcrossed in NMRI background while retaining ZSD mouse phenotype. NMRI ZSD mice exhibited growth retardation, relative hepatomegaly associated to chronic liver injury, hepatocyte hypertrophy and severe liver glycogen metabolism impairment which led to reduced fasting resistance in ZSD mice. Liver RNA-seq underlined the modulation of glycogen metabolism gene expression associated to a switch in glucose metabolism to glucose consumption. We reported multiple peroxisomal biochemical alterations in the ZSD mice, including phytanic acid and C_{26} levels elevation, which tended to normalize with age, along with a specific ZSD urine organic acids profile. Moreover, through correlation between plasma and liver BA levels we could put forth the presence of cholestasis in ZSD mice.

Hepatomegaly is a common finding in ZSD patients, and it was previously described in *Pex1*-G844D C57BL/6N mouse model[3, 11, 21]. In our mouse model, neither fat accumulation, nor sugar (i.e., glycogen) accumulation, nor protein accumulation, nor hepatocyte proliferation could account for the relative hepatomegaly we observed. However, hepatocyte proliferation analysis highlighted an increased hepatocyte density in 1-month-old ZSD mice livers (**Figure 1N**). We postulate that hepatocyte proliferation took place before this age to explain the higher hepatocyte density detected in young ZSD mice liver and that the further progressive hepatocyte hypertrophy (**Figure 1P-R**) accounted for the relative hepatomegaly developing after

this age. The Akt/mTORC1 pathway is a major player in hepatocyte hypertrophy and could be involved in our model (**Table 2**)[55, 56].

Liver injury and fibrosis were less severe in NMRI ZSD mice than in previous *Pex1*-G844D mouse models[21, 22]. Background differences could account for this as it was shown for liver fibrosis response to carbon tetrachloride treatment[57, 58]. Liver disease was responsible for severe lethality in Berendse *et al.* mouse model and we postulate that *Pex1*-G844D backcrossing to NMRI background lead to reduced liver response to PBD insult.

Hiebler *et al.* developed *Pex1*-G844D mouse model in a C57BL/6 × 129 mixed genetic background and bred it with C57BL/6N wild type mice[22]. We bought heterozygous *Pex1*-G844D mice recovered through pure C57BL/6N mouse fertilization with *Pex1*-G844D cryopreserved sperm from Hiebler *et al.* colony. This process relatively increased the C57BL/6N background and larger homozygous regions could explain the strongly reduced C57BL/6N ZSD mice survival in our experience compared to Hiebler *et al*..

ZSD mouse background switch was previously successfully evaluated in *Pex2* KO mouse model[59]. Switch from C57BL/6 × 129Sv to Swiss Webster × 129SvEv background increased survival rate but no data about litters yield is available[17]. Survival rate differences between *Pex1*-G844D knockin mouse models and *Pex2*[17, 59], *Pex5*[16] and *Pex*13[18] KO mouse models are explained by the *Pex1*-G844D protein normal stability and residual functionality compared to lack of protein activity in KO models[21, 23].

Our ZSD mouse model survival rate was increased by 33% to 390% compared to previous *Pex1*-G844D mouse models[21, 22]. Yet, peroxisomal metabolites anomalies

displayed by NMRI ZSD mice were similar to previously published *Pex1*-G844D mouse models. For example, compared to control, ZSD mice C_{26} plasma levels were increased by 1.8-fold and 1.6-fold in our study and in Hiebler *et al*., respectively[22]. Similarly, peroxisomal mosaicism was present in both ZSD MEF from our study and from Berendse *et al.*[21]. Peroxisomal mosaicism is described in cells from milder ZSD patients[2]. Thus, we postulate that there is no difference in PBD severity that could explain the increased survival rate in our study compared to other *Pex1*-G844D mouse models[21, 22].

Pex1-G844D backcrossing in NMRI background exhibit ZSD phenotype similarly to what was published previously regarding (intrauterine) growth retardation[16-18, 21, 22], relative hepatomegaly[21], plasma and liver peroxisomal metabolites accumulation[21], plasma cholesterol levels and endoplasmic reticulum stress[60-62] and liver glycogen metabolism alterations[19, 21] which were also reported in PBD Drosophila model[50]. Liver gene expression modulations were similar to what was reported in a liver-restricted *Pex5* KO mouse model[19].

We went further in deciphering plasma-liver BA and VLCFA correlation to highlight cholestasis and plasma VLCFA level use as a proxy for liver VLCFA content, respectively. Based on our experience with hepatocyte and liver transplantation in ZSD patients, we propose these markers as pre-clinical readout for liver-targeted therapies evaluation in our mouse model[12-14, 63].

To our knowledge, this is the first time ZSD mice urine organic acids profiles were analyzed, and they were similar to ZSD patients[3, 4, 8, 9]. Moreover, longitudinal peroxisomal metabolites study allowed us to underline a trend to normalization for some markers as it was reported for ZSD patients[4]. These data suggest that our

mouse model recapitulate the biochemical history of ZSD patients required for robust pathophysiological studies.

Further studies are needed to evaluate the central nervous system and sensorineural involvement in NMRI ZSD mice. Neither seizures nor severe hypotonia were observed clinically in contrast what was reported for *Pex* KO mouse model[16-18]. Furthermore, studying liver glycogen metabolism alterations in ZSD patients liver biopsy would be of great interest because these anomalies were only deeply characterized in ZSD mouse and Drosophila model[19, 50]. A recent paper evaluated liver histology in 13 ZSD patients but glycogen metabolism impairment was not discussed[64].

Large litters, high survival rate and ZSD bio-clinical phenotype make this NMRI ZSD mouse model highly suitable for the evaluation of liver-targeted therapies. This is very relevant from a translational point of view given the known liver impact on brain development in ZSD[65] and the encouraging bio-clinical results obtained after liver transplantation in ZSD patients[13, 14, 63].

Conclusion

Pex1-G844D NMRI mouse model is a robust mild ZSD mouse model exhibiting classical clinical, biochemical and liver anomalies associated with PBD. This makes *Pex1*-G844D NMRI mouse model a good candidate for liver cell and gene therapies evaluation in ZSD.

Acknowledgments

The authors thank Michele de Beukelaer, Aurélie Daumerie, Tamah Abderrahman, Philippine Debeyne and Anniek Van Landschoot for excellent technical assistance.

We are indebted to P[r] Isabelle Leclercq for numerous pathological comments on liver slides, to Janne Tys for mouse embryonic fibroblasts isolation training, to D[r] Nicolas van Baren for fluorescent scanning expertise and to P[r] Philippe Lysy who provided glucometer & strips.

References

1. Vasiljevic, E., Z. Ye, D.M. Pavelec, B.F. Darst, C.D. Engelman, and M.W. Baker, Carrier frequency estimation of Zellweger spectrum disorder using ExAC database and bioinformatics tools. Genet Med, 2019. 21(9): p. 1969-1976.
2. Waterham, H.R., S. Ferdinandusse, and R.J. Wanders, Human disorders of peroxisome metabolism and biogenesis. Biochim Biophys Acta, 2016. 1863(5): p. 922-33.
3. Klouwer, F.C., K. Berendse, S. Ferdinandusse, R.J. Wanders, M. Engelen, and B.T. Poll-The, Zellweger spectrum disorders: clinical overview and management approach. Orphanet J Rare Dis, 2015. 10: p. 151.
4. Berendse, K., M. Engelen, S. Ferdinandusse, C.B. Majoie, H.R. Waterham, F.M. Vaz, J.H. Koelman, P.G. Barth, R.J. Wanders, and B.T. Poll-The, Zellweger spectrum disorders: clinical manifestations in patients surviving into adulthood. J Inherit Metab Dis, 2016. 39(1): p. 93-106.
5. Vogel, B.H., S.E. Bradley, D.J. Adams, K. D'Aco, R.W. Erbe, C. Fong, A. Iglesias, D. Kronn, P. Levy, M. Morrissey, J. Orsini, P. Parton, J. Pellegrino, C.A. Saavedra-Matiz, N. Shur, M. Wasserstein, G.V. Raymond, and M. Caggana, Newborn screening for X-linked adrenoleukodystrophy in New York State: diagnostic protocol, surveillance protocol and treatment guidelines. Mol Genet Metab, 2015. 114(4): p. 599-603.
6. Wanders, R.J., F.C. Klouwer, S. Ferdinandusse, H.R. Waterham, and B.T. Poll-The, Clinical and Laboratory Diagnosis of Peroxisomal Disorders. Methods Mol Biol, 2017. 1595: p. 329-342.
7. Waterham, H.R. and M.S. Ebberink, Genetics and molecular basis of human peroxisome biogenesis disorders. Biochim Biophys Acta, 2012. 1822(9): p. 1430-41.
8. Korman, S.H., H. Mandel, and A. Gutman, Characteristic urine organic acid profile in peroxisomal biogenesis disorders. J Inherit Metab Dis, 2000. 23(4): p. 425-8.
9. Rocchiccioli, F., P. Aubourg, and P.F. Bougneres, Medium- and long-chain dicarboxylic aciduria in patients with Zellweger syndrome and neonatal adrenoleukodystrophy. Pediatr Res, 1986. 20(1): p. 62-6.
10. De Biase, I., S. Tortorelli, L. Kratz, J.S. S, K. Cusmano-Ozog, and N. Braverman, Laboratory diagnosis of disorders of peroxisomal biogenesis and function: a technical standard of the American College of Medical Genetics and Genomics (ACMG). Genet Med, 2019.
11. Braverman, N.E., G.V. Raymond, W.B. Rizzo, A.B. Moser, M.E. Wilkinson, E.M. Stone, S.J. Steinberg, M.F. Wangler, E.T. Rush, J.G. Hacia, and M. Bose, Peroxisome biogenesis disorders in the Zellweger spectrum: An overview of current diagnosis, clinical manifestations, and treatment guidelines. Mol Genet Metab, 2016. 117(3): p. 313-21.
12. Sokal, E.M., F. Smets, A. Bourgois, L. Van Maldergem, J.P. Buts, R. Reding, J. Bernard Otte, V. Evrard, D. Latinne, M.F. Vincent, A. Moser, and H.E. Soriano, Hepatocyte transplantation in a 4-year-old girl with peroxisomal biogenesis disease: technique, safety, and metabolic follow-up. Transplantation, 2003. 76(4): p. 735-8.
13. Van Maldergem, L., A.B. Moser, M.F. Vincent, D. Roland, R. Reding, J.B. Otte, R.J. Wanders, and E. Sokal, Orthotopic liver transplantation from a living-related donor in an infant with a peroxisome biogenesis defect of the infantile Refsum disease type. J Inherit Metab Dis, 2005. 28(4): p. 593-600.
14. Demaret, T., S. Varma, X. Stephenne, F. Smets, I. Scheers, R. Wanders, L. Van Maldergem, R. Reding, and E. Sokal, Living-donor liver transplantation for mild Zellweger spectrum disorder: Up to 17 years follow-up. Pediatr Transplant, 2018. 22(3): p. e13112.
15. Baes, M. and P.P. Van Veldhoven, Mouse models for peroxisome biogenesis defects and beta-oxidation enzyme deficiencies. Biochim Biophys Acta, 2012. 1822(9): p. 1489-500.

16. Baes, M., P. Gressens, E. Baumgart, P. Carmeliet, M. Casteels, M. Fransen, P. Evrard, D. Fahimi, P.E. Declercq, D. Collen, P.P. van Veldhoven, and G.P. Mannaerts, A mouse model for Zellweger syndrome. Nat Genet, 1997. 17(1): p. 49-57.
17. Faust, P.L. and M.E. Hatten, Targeted deletion of the PEX2 peroxisome assembly gene in mice provides a model for Zellweger syndrome, a human neuronal migration disorder. J Cell Biol, 1997. 139(5): p. 1293-305.
18. Maxwell, M., J. Bjorkman, T. Nguyen, P. Sharp, J. Finnie, C. Paterson, I. Tonks, B.C. Paton, G.F. Kay, and D.I. Crane, Pex13 inactivation in the mouse disrupts peroxisome biogenesis and leads to a Zellweger syndrome phenotype. Mol Cell Biol, 2003. 23(16): p. 5947-57.
19. Peeters, A., P. Fraisl, S. van den Berg, E. Ver Loren van Themaat, A. Van Kampen, M.H. Rider, H. Takemori, K.W. van Dijk, P.P. Van Veldhoven, P. Carmeliet, and M. Baes, Carbohydrate metabolism is perturbed in peroxisome-deficient hepatocytes due to mitochondrial dysfunction, AMP-activated protein kinase (AMPK) activation, and peroxisome proliferator-activated receptor gamma coactivator 1alpha (PGC-1alpha) suppression. J Biol Chem, 2011. 286(49): p. 42162-79.
20. Poll-The, B.T., J. Gootjes, M. Duran, J.B. De Klerk, L.J. Wenniger-Prick, R.J. Admiraal, H.R. Waterham, R.J. Wanders, and P.G. Barth, Peroxisome biogenesis disorders with prolonged survival: phenotypic expression in a cohort of 31 patients. Am J Med Genet A, 2004. 126a(4): p. 333-8.
21. Berendse, K., M. Boek, M. Gijbels, N.N. Van der Wel, F.C. Klouwer, M.A. van den Bergh-Weerman, A.B. Shinde, R. Ofman, B.T. Poll-The, S.M. Houten, M. Baes, R.J.A. Wanders, and H.R. Waterham, Liver disease predominates in a mouse model for mild human Zellweger spectrum disorder. Biochim Biophys Acta Mol Basis Dis, 2019.
22. Hiebler, S., T. Masuda, J.G. Hacia, A.B. Moser, P.L. Faust, A. Liu, N. Chowdhury, N. Huang, A. Lauer, J. Bennett, P.A. Watkins, D.J. Zack, N.E. Braverman, G.V. Raymond, and S.J. Steinberg, The Pex1-G844D mouse: a model for mild human Zellweger spectrum disorder. Mol Genet Metab, 2014. 111(4): p. 522-32.
23. Argyriou, C., A. Polosa, B. Cecyre, M. Hsieh, E. Di Pietro, W. Cui, J.F. Bouchard, P. Lachapelle, and N. Braverman, A longitudinal study of retinopathy in the PEX1-Gly844Asp mouse model for mild Zellweger Spectrum Disorder. Exp Eye Res, 2019: p. 107713.
24. Truett, G.E., P. Heeger, R.L. Mynatt, A.A. Truett, J.A. Walker, and M.L. Warman, Preparation of PCR-quality mouse genomic DNA with hot sodium hydroxide and tris (HotSHOT). Biotechniques, 2000. 29(1): p. 52, 54.
25. Fiebig, T., H. Boll, G. Figueiredo, H.U. Kerl, S. Nittka, C. Groden, M. Kramer, and M.A. Brockmann, Three-dimensional in vivo imaging of the murine liver: a micro-computed tomography-based anatomical study. PLoS One, 2012. 7(2): p. e31179.
26. Sokal, E.M., J. Mostin, and J.P. Buts, Liver metabolic zonation in rat biliary cirrhosis: distribution is reverse of that in toxic cirrhosis. Hepatology, 1992. 15(5): p. 904-8.
27. Orjuela, S., R. Huang, K.M. Hembach, M.D. Robinson, and C. Soneson, ARMOR: An Automated Reproducible MOdular Workflow for Preprocessing and Differential Analysis of RNA-seq Data. G3 (Bethesda), 2019. 9(7): p. 2089-2096.
28. Wingett, S.W. and S. Andrews, FastQ Screen: A tool for multi-genome mapping and quality control. F1000Res, 2018. 7: p. 1338.
29. Ewels, P., M. Magnusson, S. Lundin, and M. Kaller, MultiQC: summarize analysis results for multiple tools and samples in a single report. Bioinformatics, 2016. 32(19): p. 3047-8.
30. Patro, R., G. Duggal, M.I. Love, R.A. Irizarry, and C. Kingsford, Salmon provides fast and bias-aware quantification of transcript expression. Nat Methods, 2017. 14(4): p. 417-419.
31. Cunningham, F., P. Achuthan, W. Akanni, J. Allen, M.R. Amode, I.M. Armean, R. Bennett, J. Bhai, K. Billis, S. Boddu, C. Cummins, C. Davidson, K.J. Dodiya, A. Gall, C.G. Giron, L. Gil, T. Grego, L. Haggerty, E. Haskell, T. Hourlier, O.G. Izuogu, S.H. Janacek, T. Juettemann, M. Kay, M.R. Laird, I. Lavidas, Z. Liu, J.E. Loveland, J.C. Marugan, T. Maurel, A.C. McMahon, B. Moore, J. Morales, J.M. Mudge, M. Nuhn, D. Ogeh, A. Parker, A. Parton, M. Patricio, A.I. Abdul Salam, B.M. Schmitt, H. Schuilenburg, D. Sheppard, H. Sparrow, E. Stapleton, M. Szuba, K. Taylor, G. Threadgold, A. Thormann, A. Vullo, B. Walts, A. Winterbottom, A. Zadissa, M. Chakiachvili, A. Frankish, S.E. Hunt, M. Kostadima, N. Langridge, F.J. Martin, M. Muffato, E. Perry, M. Ruffier, D.M. Staines, S.J. Trevanion, B.L. Aken, A.D. Yates, D.R. Zerbino, and P. Flicek, Ensembl 2019. Nucleic Acids Res, 2019. 47(D1): p. D745-d751.
32. Soneson, C., M.I. Love, and M.D. Robinson, Differential analyses for RNA-seq: transcript-level estimates improve gene-level inferences. F1000Res, 2015. 4: p. 1521.

33. Robinson, M.D., D.J. McCarthy, and G.K. Smyth, edgeR: a Bioconductor package for differential expression analysis of digital gene expression data. Bioinformatics, 2010. 26(1): p. 139-40.
34. Aizarani, N., A. Saviano, Sagar, L. Mailly, S. Durand, J.S. Herman, P. Pessaux, T.F. Baumert, and D. Grun, A human liver cell atlas reveals heterogeneity and epithelial progenitors. Nature, 2019. 572(7768): p. 199-204.
35. MacParland, S.A., J.C. Liu, X.Z. Ma, B.T. Innes, A.M. Bartczak, B.K. Gage, J. Manuel, N. Khuu, J. Echeverri, I. Linares, R. Gupta, M.L. Cheng, L.Y. Liu, D. Camat, S.W. Chung, R.K. Seliga, Z. Shao, E. Lee, S. Ogawa, M. Ogawa, M.D. Wilson, J.E. Fish, M. Selzner, A. Ghanekar, D. Grant, P. Greig, G. Sapisochin, N. Selzner, N. Winegarden, O. Adeyi, G. Keller, G.D. Bader, and I.D. McGilvray, Single cell RNA sequencing of human liver reveals distinct intrahepatic macrophage populations. Nat Commun, 2018. 9(1): p. 4383.
36. Dobie, R., J.R. Wilson-Kanamori, B.E.P. Henderson, J.R. Smith, K.P. Matchett, J.R. Portman, K. Wallenborg, S. Picelli, A. Zagorska, S.V. Pendem, T.E. Hudson, M.M. Wu, G.R. Budas, D.G. Breckenridge, E.M. Harrison, D.J. Mole, S.J. Wigmore, P. Ramachandran, C.P. Ponting, S.A. Teichmann, J.C. Marioni, and N.C. Henderson, Single-Cell Transcriptomics Uncovers Zonation of Function in the Mesenchyme during Liver Fibrosis. Cell Rep, 2019. 29(7): p. 1832-1847.e8.
37. Rakhshandehroo, M., G. Hooiveld, M. Muller, and S. Kersten, Comparative analysis of gene regulation by the transcription factor PPARalpha between mouse and human. PLoS One, 2009. 4(8): p. e6796.
38. Huang, W., K. Ma, J. Zhang, M. Qatanani, J. Cuvillier, J. Liu, B. Dong, X. Huang, and D.D. Moore, Nuclear receptor-dependent bile acid signaling is required for normal liver regeneration. Science, 2006. 312(5771): p. 233-6.
39. Demaret, T., G.E. Courtoy, J. Ravau, P. Van Der Smissen, M. Najimi, and E.M. Sokal, Accurate and live peroxisome biogenesis evaluation achieved by lentiviral expression of a green fluorescent protein fused to a peroxisome targeting signal 1. Histochem Cell Biol, 2020. 153(5): p. 295-306.
40. De Rudder, M., C. Bouzin, M. Nachit, H. Louvegny, G. Vande Velde, Y. Jule, and I.A. Leclercq, Automated computerized image analysis for the user-independent evaluation of disease severity in preclinical models of NAFLD/NASH. Lab Invest, 2019.
41. Passonneau, J.V. and V.R. Lauderdale, A comparison of three methods of glycogen measurement in tissues. Anal Biochem, 1974. 60(2): p. 405-12.
42. Zhang, P., Analysis of Mouse Liver Glycogen Content. Bio-protocol, 2012. 2(10): p. e186.
43. Carroll, N.V., R.W. Longley, and J.H. Roe, The determination of glycogen in liver and muscle by use of anthrone reagent. J Biol Chem, 1956. 220(2): p. 583-93.
44. Sadilkova, K., S.M. Gospe, Jr., and S.H. Hahn, Simultaneous determination of alpha-aminoadipic semialdehyde, piperideine-6-carboxylate and pipecolic acid by LC-MS/MS for pyridoxine-dependent seizures and folinic acid-responsive seizures. J Neurosci Methods, 2009. 184(1): p. 136-41.
45. Mutemberezi, V., J. Masquelier, O. Guillemot-Legris, and G.G. Muccioli, Development and validation of an HPLC-MS method for the simultaneous quantification of key oxysterols, endocannabinoids, and ceramides: variations in metabolic syndrome. Anal Bioanal Chem, 2016. 408(3): p. 733-45.
46. Guillemot-Legris, O., V. Mutemberezi, P.D. Cani, and G.G. Muccioli, Obesity is associated with changes in oxysterol metabolism and levels in mice liver, hypothalamus, adipose tissue and plasma. Sci Rep, 2016. 6: p. 19694.
47. Baes, M. and P.P. Van Veldhoven, Hepatic dysfunction in peroxisomal disorders. Biochim Biophys Acta, 2016. 1863(5): p. 956-70.
48. Goldfischer, S., C.L. Moore, A.B. Johnson, A.J. Spiro, M.P. Valsamis, H.K. Wisniewski, R.H. Ritch, W.T. Norton, I. Rapin, and L.M. Gartner, Peroxisomal and mitochondrial defects in the cerebro-hepato-renal syndrome. Science, 1973. 182(4107): p. 62-4.
49. Scotto, J.M., M. Hadchouel, M. Odievre, M.H. Laudat, J.M. Saudubray, O. Dulac, I. Beucler, and P. Beaune, Infantile phytanic acid storage disease, a possible variant of Refsum's disease: three cases, including ultrastructural studies of the liver. J Inherit Metab Dis, 1982. 5(2): p. 83-90.
50. Wangler, M.F., Y.H. Chao, V. Bayat, N. Giagtzoglou, A.B. Shinde, N. Putluri, C. Coarfa, T. Donti, B.H. Graham, J.E. Faust, J.A. McNew, A. Moser, M. Sardiello, M. Baes, and H.J. Bellen, Peroxisomal biogenesis is genetically and biochemically linked to carbohydrate metabolism in Drosophila and mouse. PLoS Genet, 2017. 13(6): p. e1006825.

51. Braverman, N.E. and A.B. Moser, Functions of plasmalogen lipids in health and disease. Biochim Biophys Acta, 2012. 1822(9): p. 1442-52.
52. Wiens, K., S.A. Berry, H. Choi, A. Gaviglio, A. Gupta, A. Hietala, D. Kenney-Jung, T. Lund, W. Miller, E.I. Pierpont, G. Raymond, H. Winslow, H.A. Zierhut, and P.J. Orchard, A report on state-wide implementation of newborn screening for X-linked Adrenoleukodystrophy. Am J Med Genet A, 2019. 179(7): p. 1205-1213.
53. Klouwer, F.C.C., S. Ferdinandusse, H. van Lenthe, W. Kulik, R.J.A. Wanders, B.T. Poll-The, H.R. Waterham, and F.M. Vaz, Evaluation of C26:0-lysophosphatidylcholine and C26:0-carnitine as diagnostic markers for Zellweger spectrum disorders. J Inherit Metab Dis, 2017. 40(6): p. 875-881.
54. Ferdinandusse, S., S. Denis, P.L. Faust, and R.J. Wanders, Bile acids: the role of peroxisomes. J Lipid Res, 2009. 50(11): p. 2139-47.
55. Gielchinsky, Y., N. Laufer, E. Weitman, R. Abramovitch, Z. Granot, Y. Bergman, and E. Pikarsky, Pregnancy restores the regenerative capacity of the aged liver via activation of an mTORC1-controlled hyperplasia/hypertrophy switch. Genes Dev, 2010. 24(6): p. 543-8.
56. Matot, I., N. Nachmansson, O. Duev, S. Schulz, K. Schroeder-Stein, S. Frede, and R. Abramovitch, Impaired liver regeneration after hepatectomy and bleeding is associated with a shift from hepatocyte proliferation to hypertrophy. Faseb j, 2017. 31(12): p. 5283-5295.
57. Shi, Z., A.E. Wakil, and D.C. Rockey, Strain-specific differences in mouse hepatic wound healing are mediated by divergent T helper cytokine responses. Proc Natl Acad Sci U S A, 1997. 94(20): p. 10663-8.
58. Hillebrandt, S., C. Goos, S. Matern, and F. Lammert, Genome-wide analysis of hepatic fibrosis in inbred mice identifies the susceptibility locus Hfib1 on chromosome 15. Gastroenterology, 2002. 123(6): p. 2041-51.
59. Faust, P.L., Abnormal cerebellar histogenesis in PEX2 Zellweger mice reflects multiple neuronal defects induced by peroxisome deficiency. J Comp Neurol, 2003. 461(3): p. 394-413.
60. Faust, P.L. and W.J. Kovacs, Cholesterol biosynthesis and ER stress in peroxisome deficiency. Biochimie, 2014. 98: p. 75-85.
61. Kovacs, W.J., J.E. Shackelford, K.N. Tape, M.J. Richards, P.L. Faust, S.J. Fliesler, and S.K. Krisans, Disturbed cholesterol homeostasis in a peroxisome-deficient PEX2 knockout mouse model. Mol Cell Biol, 2004. 24(1): p. 1-13.
62. Kovacs, W.J., K.N. Tape, J.E. Shackelford, T.M. Wikander, M.J. Richards, S.J. Fliesler, S.K. Krisans, and P.L. Faust, Peroxisome deficiency causes a complex phenotype because of hepatic SREBP/Insig dysregulation associated with endoplasmic reticulum stress. J Biol Chem, 2009. 284(11): p. 7232-45.
63. Matsunami, M., N. Shimozawa, A. Fukuda, T. Kumagai, M. Kubota, P.F. Chong, and M. Kasahara, Living-Donor Liver Transplantation From a Heterozygous Parent for Infantile Refsum Disease. Pediatrics, 2016. 137(6).
64. Berendse, K., B.G.P. Koot, F.C.C. Klouwer, M. Engelen, F. Roels, M.M. Lacle, P.G.J. Nikkels, J. Verheij, and B.T. Poll-The, Hepatic symptoms and histology in 13 patients with a Zellweger spectrum disorder. J Inherit Metab Dis, 2019. 42(5): p. 955-965.
65. Janssen, A., P. Gressens, M. Grabenbauer, E. Baumgart, A. Schad, I. Vanhorebeek, A. Brouwers, P.E. Declercq, D. Fahimi, P. Evrard, L. Schoonjans, D. Collen, P. Carmeliet, G. Mannaerts, P. Van Veldhoven, and M. Baes, Neuronal migration depends on intact peroxisomal function in brain and in extraneuronal tissues. J Neurosci, 2003. 23(30): p. 9732-41.

Chapter 4.

High dose *versus* low dose syngeneic hepatocyte transplantation in Pex1-G844D NMRI mouse model is safe but does not achieve long term engraftment

Tanguy Demaret[1], Jonathan Evraerts[1], Joachim Ravau[1], Martin Roumain[2], Giulio G Muccioli[2], Mustapha Najimi[1], Etienne M Sokal[1]

[1] Laboratoire d'Hépatologie Pédiatrique et Thérapie Cellulaire, Unité PEDI, Institut de Recherche Expérimentale et Clinique (IREC), Université Catholique de Louvain (UCLouvain), 1200 Brussels, Belgium

[2] Bioanalysis and Pharmacology of Bioactive Lipids Research Group (BPBL), Louvain Drug Research Institute (LDRI), Université Catholique de Louvain (UCLouvain), 1200 Brussels, Belgium

Will be submitted in Cells

Abstract

Genetic alterations in *PEX* genes lead to peroxisome biogenesis disorder in cells, and to Zellweger spectrum disorders (ZSD) in patients. No validated treatment has been shown to modify the dismal natural history associated with ZSD. Living-donor liver transplantation (LT) improved clinical and biochemical outcomes in mild ZSD patients but organ shortage limits its applicability in centers with no access to living donation. Hepatocyte transplantation (HT) was developed to overcome LT limitations. First pediatric HT procedure carried out in Europe was performed in a mild ZSD 4-year-old child with encouraging short term biochemical results. *Pex1*-G844D NMRI mouse model recapitulate mild ZSD phenotype in a robust and easy to breed background. We evaluated low dose (12.5 million hepatocytes/kg) and high dose (50 million hepatocytes/kg) syngeneic male HT via intrasplenic infusion in this ZSD mouse model. HT was feasible and safe in growth retarded ZSD mice. Clinical (weight and food intake) and biochemical parameters (very long-chain fatty acids, abnormal bile acids, etc.) were in accordance with ZSD phenotype but they were not robustly modified by HT. Hepatocyte engraftment was extrapolated from male in female microchimerism quantification by droplet digital PCR. As expected, only one third of the infused cells were detected in the liver 24 h post-HT. No liver nor spleen microchimerism was detected after 7, 14 and 30 days. Future optimizations are required to improve hepatocyte engraftment in ZSD liver. *Pex1*-G844D NMRI mouse model is a robust mild ZSD mouse model suitable for ZSD liver-targeted therapies evaluation.

Introduction

Mild Zellweger spectrum disorder (ZSD) is caused by genetic alterations in *PEX* genes encoding peroxins[1]. Peroxin deficiency lead to peroxisome biogenesis disorder and metabolic imbalance[2]. Metabolites catabolized into peroxisomes (i.e., branched-chain fatty acids (BCFA, phytanic and pristanic acids), very long-chain fatty acids (VLCFA), C_{27} bile acids (BA) precursors, etc.) accumulate into plasma and tissues and compounds synthetized by peroxisomes lack (i.e., plasmalogens, C_{24} BA, etc.)[3]. Most mild ZSD patients survive into childhood and no validated treatment is able to impact their progressive hepatic dysfunction and developmental delay[4]. Living donor liver transplantation (LT) has shown proof of principle that liver-targeted therapies can modify natural history in mild ZSD patients[5-7].

Organ shortage is a major hurdle to pediatric LT. Living donor LT and surgical techniques like split-liver have been developed to increase organ availability[8-10]. Yet, parenchymal function is often preserved in liver-based metabolic diseases making it difficult for these patient to progress on LT waiting list[11]. Hepatocyte transplantation (HT) was developed to overcome LT limitations (i.e., heaviness, cost, organ availability, etc.). HT consists in isolating hepatocytes from liver not suitable for LT and infusing them to a recipient with or without crypreservation[12]. First pediatric HT procedure performed in Europe was in a 4-year-old child affected by mild ZSD[13].

Pex1-G844D NMRI mouse model displays biochemical and hepatic alterations affecting mild ZSD patients[14]. Its easy breeding and robustness make it suitable for preclinical studies and small surgical intervention like HT. In order to strengthen liver-directed therapies in mild ZSD therapeutic approaches, we evaluated two HT protocols in *Pex1*-G844D NMRI mouse model. We followed clinical and biochemical

parameters along with liver hepatocyte engraftment to monitor HT impact on mild ZSD phenotype.

Material and Methods

Mice care, breeding, and genotyping

NMRI mice heterozygous for *Pex1*-G844D allele from in-house colony were bred in a specific-pathogen-free environment in individually ventilated cages with 12h light/12h dark cycle[14]. Wild-type and heterozygous mice exhibited no phenotype and were used as control mice. Mice had unrestricted access to food (Carfil, Mice Breeding diet) and water and were genotyped as described earlier[14]. All animal experiments were performed in compliance with the Practice Guidelines for Laboratory Animals of Belgium and approved by the local ethical review board.

Hepatocyte transplantation

Male mouse hepatocytes were freshly isolated from control littermate by collagenase P (Roche, 11213873001) as described here[15]. Cells were suspended at 1.25 or 5 million hepatocytes/mL in N-acetylcysteine 4% (NAC, Lysomucyl, Zambon) in phosphate buffered saline (PBS, Lonza, 15-512F). Two HT protocols were evaluated based 10 µL/g of body weight infusion leading to 12.5 or 50 million cells/kg, further referred as low dose HT and high dose HT, respectively. HT was performed in the morning based on a modified protocol from[16]. Briefly, under isoflurane anesthesia, cells were infused by intrasplenic injection through 25G needle at 50 µL/minute with a syringe press (CMA 400, microdialysis) (**Figure 1A,B**). Control mice received 100 µL PBS-NAC. All mice received 20 mL/kg warmed NaCl 0.9% (Mini-Plasco NaCl 0.9%, B.Braun) subcutaneously along with buprenorphine (Temgesic, Schering-

Plough) 0.1 mg/kg subcutaneously once before procedure and then twice a day for 2 days. Mice groups and follow-up are presented (**Table 1**, **Figure 1C**). Two ZSD mice infused with high dose HT were sacrificed earlier to evaluate microchimerism longitudinally (**Figure 1C**). These mice were excluded from HT outcomes analysis.

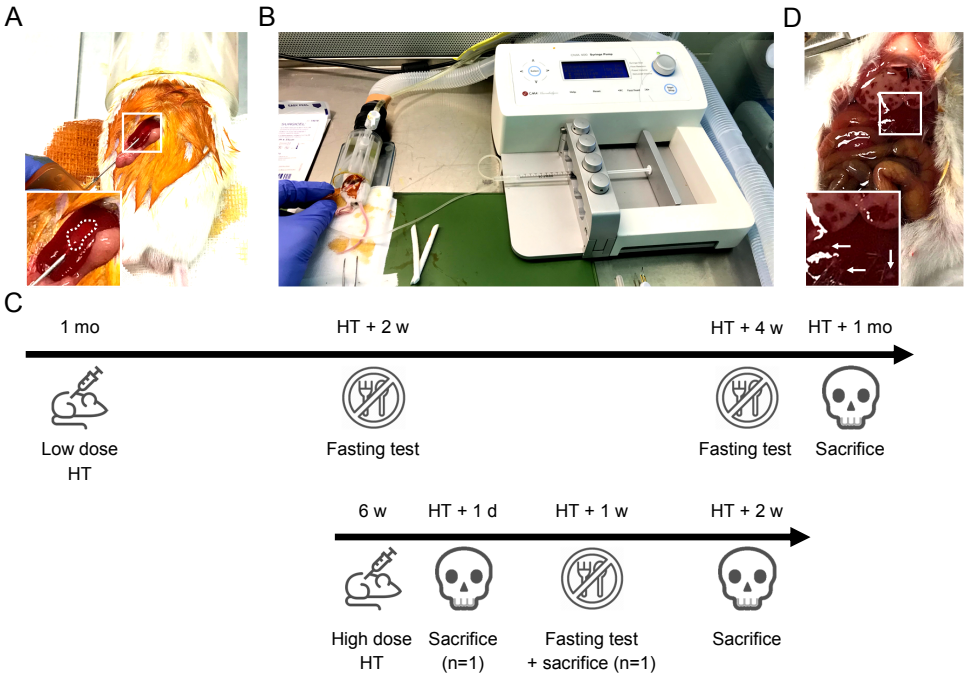

Figure 1 - **A** Mouse in right lateral decubitus with intra-splenic 25G needle insertion. Note the discolored spleen area inside the dotted line confirming the correct intra-splenic infusion flushing erythrocytes. **B** Device setup used for HT: syringe press on the right, heating pad (green) and anesthesia tunnel delivering isoflurane mixed with oxygen and collecting exhaled gases. **C** Schematic description of the two HT protocols including fasting tests, sacrifices for microchimerism evaluation and samples collection at the end of the study. **D** Macroscopic liver evaluation 24 h after high dose HT highlighting large necrosis areas in right and left median lobes. Left lateral lobe displayed smaller necrosis areas (white arrows). Inserts show magnification of the boxed areas.

Table 1. Hepatocyte transplantation protocol details.

HT protocol	Dose	Age at HT	Euthanasia post-HT	Control mice + PBS-NAC	ZSD mice + HT	ZSD mice + PBS-NAC
Low dose	12.5 millions/kg	1 month	1 month	6	3	2
High dose	50 millions/kg	6 weeks	2 weeks	6	10[a]	6

[a] 2 of the mice were sacrificed after 1 day (n = 1) and 7 days (n = 1) for longitudinal microchimerism evaluation, and were excluded from HT outcomes analysis.
HT: hepatocyte transplantation, PBS: phosphate buffered saline, NAC: N-acetylcysteine, n.a.: not applicable.

Clinical evaluation and glycemia

Food and mice weight were checked once a week. Blood drop was collected from the tail vein and morning glycemia was measured using glucometer (FreeStyle Precision Neo, Abbott). Mice were placed in a clean cage without food access during 6h after what glycemia was controlled to evaluate glycemic response to fast (**Table 1**, **Figure 1C**).

Blood and liver collection

One month or 2 weeks post-HT (**Table 1**), mice were anesthetized by intraperitoneal injection with the anesthetical solution containing ketamine and xylazine at final concentration of 100 mg/kg and 10 mg/kg, respectively. Plasma and liver lobes were collected as described previously[14]. Briefly, plasma was aliquoted and snap frozen in liquid nitrogen. Left lateral lobe was fixed in formaldehyde 4% (VWR, 11699408) overnight and embedded in paraffin. Left medial lobe (LML) was snap frozen in liquid nitrogen and stored at -80°C.

Peroxisomal markers quantification

BCFA, VLCFA, oxysterols, BA and pipecolic acid were quantified as described earlier[14].

Histological analyses

Formalin-fixed paraffin-embedded left lateral liver lobes were cut into 5 µm thick sections and processed for hematoxylin and eosin (H&E), Periodic-acid Schiff (PAS) and Sirius red (SR) staining. Slides processed for digitalization and quantification as already described[14].

Microchimerism evaluation

Theoretical microchimerism at infusion was estimated by dividing infused hepatocytes number by NMRI mouse hepatocellularity equivalent to (mean ± standard deviation (SD)) 109 ± 8 million hepatocytes/g liver individually adjusted for current liver weight extrapolated from relative liver weight at sacrifice. NMRI mouse hepatocellularity was calculated as described elsewhere[17], based on protein quantification of 9 NMRI mice livers and 2 NMRI mice hepatocyte suspensions. Mice LML and spleen were screened for microchimerism (male hepatocytes in female organ) based on predesigned droplet digital polymerase chain reaction (ddPCR) *Sry* (Mm.PT.58.28492124.g, Integrated DNA Technologies) and *Rpp30* (qMmuCEP0054985, Bio-Rad) assays performed in multiplex on genomic DNA as described here[18]. *Sry* and *Rpp30* are located on chromosomes Y and 19, respectively. *Sry/Rpp30* copy number ratio is expected to be equal to 0.5 and 0 in male and female, respectively. Male microchimerism in female is estimated from the *Sry/Rpp30* copy number ratio multiplied by two because *Sry* is present in one copy (on the Y chromosome) for each two *Rpp30* copies (on chromosomes 19).

General statistical analysis and artwork

Kruskal-Wallis test with Dunns post-test with 95% confidence intervals were performed using GraphPad Prism v. 5.02 for Windows (GraphPad Software). *P*-values < 0.05 were considered significant. When considered significant, Dunns post-test was reported on graph. Publisher (Office 365, Microsoft) was used to draw figures.

Results

HT was well tolerated in ZSD mice

In the next hours following HT, mice cleaned the surgical wound as detected by decreased Betadine staining on post-operative day (POD) 1. To avoid suture traction, food kibbles were disposed on the litter during 24 h and mice started to eat them during POD1. Macroscopic liver evaluation at POD1 showed large necrosis area (**Figure 1D**). During the post-HT period, none of the mice lost more than > 5% body weight and none of the mice died (**Figure 2A, 3A**). Food intake was not modified by HT (see below).

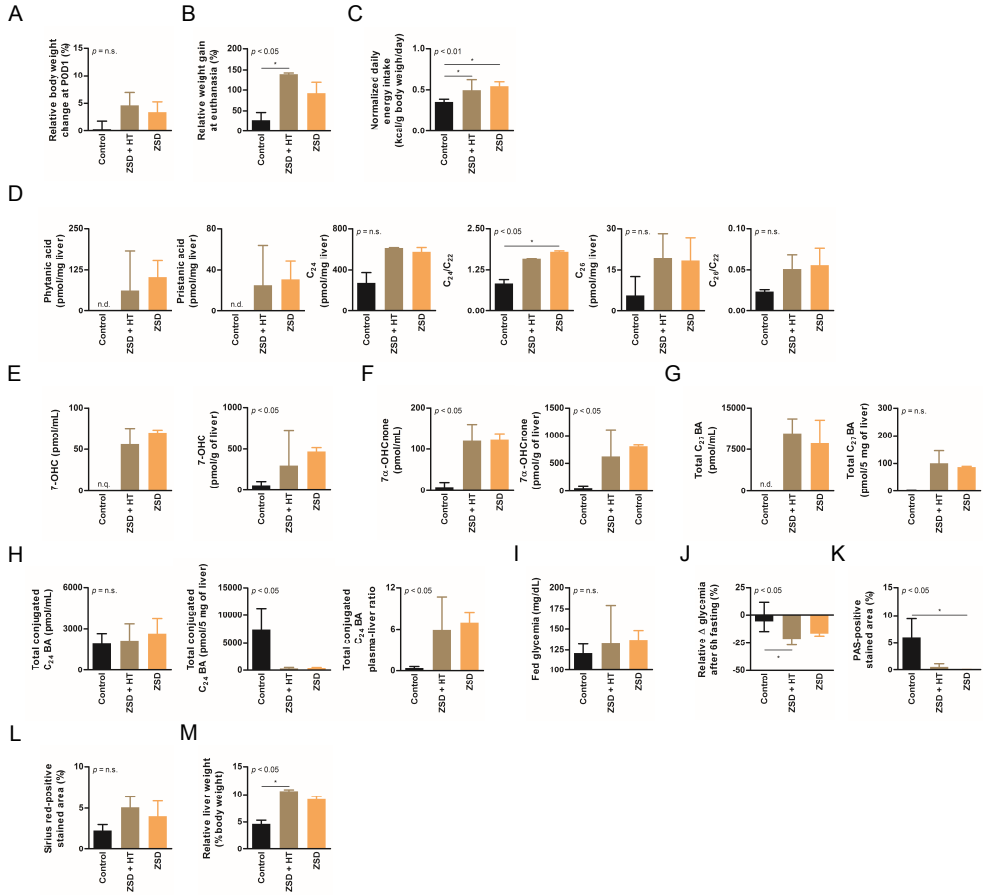

Figure 2 - HT outcome measures highlighted disease phenotype in ZSD mice but failed to detect low dose HT impact in treated mice. **A** Relative body weight change at post-operative day (POD) 1, **B** relative weight gain at final follow-up, **C** normalized daily energy intake, **D** liver branched-chain and very long-chain fatty acids levels and ratio on C_{22}, **E** plasma and liver oxysterols 7-hydroxycholesterol (7-OHC) and **F** 7α-hydroxycholestenone (7α-OHCnone) levels, **G** plasma and liver total C_{27} bile acids (BA) precursors levels, **H** plasma, liver and plasma-liver ratio of total conjugated C_{24} BA levels, **I** fed glycemia, **J** relative fasting glycemia drop (both fasting tests gave similar results and were merged on the graph, an outlier control mice was excluded from both tests), **K** relative liver Periodic-acid Schiff (PAS)-positive stained area (proxy for glycogen content), **L** relative liver Sirius red-positive stained area (proxy for collagen content) and **M** relative liver weight at sacrifice in control (n = 6), Zellweger spectrum disorder (ZSD) mice infused with low dose HT (n = 3) and ZSD mice sham operated (n = 2). Kruskal-Wallis test, n = 6-3-2 (except for D: n = 3-3-2 and J: n = 10-6-4), median ± interquartile range, *: *p*-value < 0.05, n.s.: not significant.

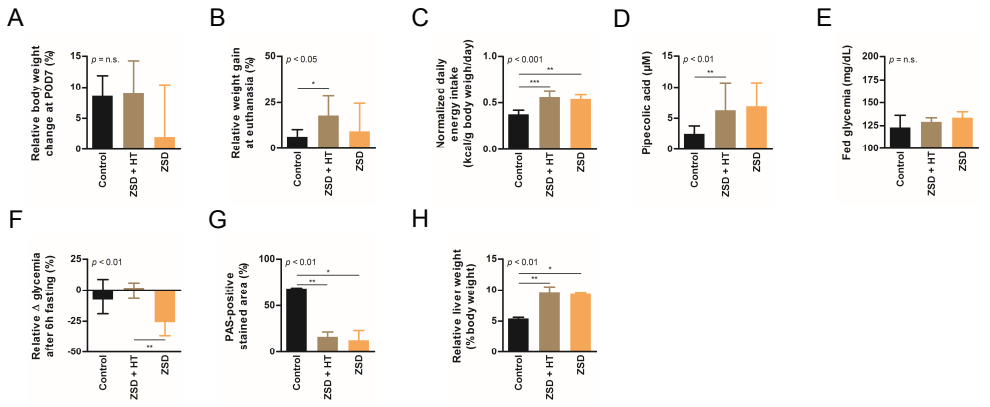

Figure 3 - High dose HT protocol confirmed ZSD phenotype in affected mice and corrected fasting glycemia drop in ZSD mice, but this was not correlated to increased liver PAS-positive stained area. Relative body weight change at **A** post-operative day (POD) 7 or **B** sacrifice, **C** normalized daily energy intake, **D** plasma pipecolic acid levels, **E** fed glycemia, **F** relative fasting glycemia drop, **G** relative liver Periodic-acid Schiff (PAS)-positive stained area (proxy for glycogen content) and **H** relative liver weight in control (n = 6), Zellweger spectrum disorder (ZSD) mice treated with high dose HT (n = 8) and ZSD mice sham operated (n = 6). Kruskal-Wallis test, n = 6-8-6, median ± interquartile range, *: *p*-value < 0.05, n.s.: not significant.

Growth and normalized daily energy intake were not affected by HT

ZSD mice exhibit growth retardation despite higher normalized daily energy intake[14]. These anomalies were confirmed in this study and they were not modified by low nor high dose HT (**Figure 2B,C&3B,C**).

HT did not modify plasma nor liver peroxisomal marker anomalies

ZSD mice present classical liver and plasma peroxisomal markers alterations[14]. Liver BCFA were not detected in control mice and they did not seem affected by low dose HT in ZSD mice (**Figure 2D**). Liver VLCFA levels quantification did not highlighted significant accumulation in ZSD mice because of low sample size (**Figure 2D**). Plasma and liver oxysterols and BA levels were in accordance with our previous report and were not modified by low dose HT (**Figure 2E-H**). ZSD mice cholestasis was confirmed by total conjugated C_{24} BA plasma-liver ratio elevation, as previously reported[14], and it was not influenced by HT (**Figure 2H**).

Based on our experience of dramatic plasma pipcolic acid levels decrease shortly after LT and HT in ZSD patients[7, 13], it was the only biochemical marker quantified in high dose HT protocol. Plasma pipecolic acid levels were increased in ZSD mice but high dose HT did not modify this parameter (**Figure 3D**).

Fasting glycemia in ZSD mice was improved after high dose HT but this was not correlated to liver glycogen content

ZSD mice present glycemic alterations related to liver glycogen metabolism anomalies[14]. Fed glycemia was not significantly different between control and ZSD mice (**Figure 2I, 3E**). Fasting glycemia was significantly lower in ZSD mice and this was rescued by high dose HT (**Figure 2J, 3F**). Unfortunately, this was not correlated to liver PAS-positive stained area (a proxy for liver glycogen content[14]) which remained strongly lowered in ZSD mice liver compared to control (**Figure 2K, 3G**).

HT did not reverse relative hepatomegaly in ZSD mice

ZSD mice liver present a slight elevation in collagen deposition as measured by SR staining. This was not statistically evident in low dose HT ZSD mice partly because of the reduced sample size (**Figure 2L**). Another striking ZSD mice feature is their relative hepatomegaly[14]. This was confirmed in both HT protocols, but they failed to modify this hallmark of the disease (**Figure 2M, 3H**).

Male liver microchimerism was detected in female ZSD mice after 24 h and was lost during follow-up

Theoretical liver microchimerism at infusion was (mean ± SD) 0.110 ± 0.003% (n = 3) and 0.461 ± 0.038% (n = 10) for low dose and high dose HT, respectively. *Sry/Rpp30* copy number ratio was measured in by ddPCR on more than 35.000 droplets for each sample (**Table 2**). No liver microchimerism could be detected on

low dose HT protocol samples (n = 2 females). At high dose HT POD1, liver microchimerism was measured at 0,15% (n = 1 female), equivalent to one third of the theoretical liver microchimerism at infusion. After POD1, no significant liver microchimerism was detected (n = 5 females). Among both protocols, no significant spleen microchimerism was detected by ddPCR (data not shown).

Table 2. Microchimerism evaluation on mice liver in low dose and high dose HT protocols

Sample	Total droplet count	Mean *Sry* concentration (copy/µL)	Mean *Rpp30* concentration (copy/µL)	Mean *Sry*/*Rpp30* ratio	Calculated microchimerism
Male hepatocytes	52789	465	897	0.518467	n.a.
No gDNA control	55916	0	0	n.a.	n.a.
Low dose HT					
Male + PBS-NAC	36195	507	1020	0.499494	n.a.
Female + PBS-NAC	48151	0	946	0	0%
Female + HT	48029	0	957	0	0%
Female + HT	38277	0	1306	0	0%
High dose HT					
Male + PBS-NAC	51464	514	1005	0.511389	n.a.
Female + PBS-NAC	52453	0	1100	0	0%
Female + HT (POD1)	55802	0.7	944	0.000748	0.150%
Female + HT (POD7)	54368	0	914	0	0%
Female + HT	57503	0	1002	0	0%
Female + HT	59883	0.020[a]	1043	0.000018	0.004%
Female + HT	55344	0	940	0	0%
Female + HT	58628	0	992	0	0%

Microchimerism was evaluated by droplet digital polymerase chain reaction (ddPCR) on genomic DNA (gDNA) extracted from female mouse liver and adequate controls (male hepatocytes, male liver and female liver sham infused). ddPCR was used to detect gDNA *Sry* (Y chromosome) and *Rpp30* (chromosome 19) copies in female mice infused with male mouse hepatocytes.
[a] based on one positive droplet.
HT: hepatocyte transplantation, n.a.: not applicable, gDNA: genomic DNA, PBS-NAC: phosphate buffered saline and N-acetylcysteine (= sham), POD: post-operative day.

Discussion

No validated treatment has been shown to modify the natural history in ZSD patients. We evaluated low dose *versus* high dose HT as therapeutic approach in mild ZSD mouse model. We confirmed robustness and ZSD phenotype in *Pex1*$^{G844D/\ G844D}$ mice. Both HT doses were safe even in these growth retarded mice. No long term hepatocyte engraftment could be detected. In consequence, no clinically relevant therapeutic effect was convincingly evidenced.

Two third of the infused hepatocytes were lost after 24 h as published in rat and mouse HT model[19, 20]. In ZSD, toxic peroxisomal metabolites could potentially alter hepatocytes viability in the circulation before they reach sinusoids[21]. In addition, Kupfer cells seems to be a major player in exogenous cell clearance and altering their phagocytic properties is a way to improve engraftment in rat model[22]. Mouse hepatocytes and sinusoids size could account for lower cell engraftment observed compared to rat HT models[23, 24]. A study about syngeneic male HT in female mice lead to 0.13-0.25% microchimersim 3-7 days after HT but no longitudinal data are reported and HT protocol is lacking (i.e., mouse background, drug used to improve engraftment, etc.)[19].

A 4-year-old mild ZSD patient received 2 billion hepatocytes (10^8 cells/kg of body weight, 2.5% theoretical microchimerism[25]) during a total of 5 days[13]. Male in female microchimerism measured on liver biopsy performed on the day of the last infusion reported 0.1-0.25% male cells[19]. In this child, hepatocyte loss during HT was equal to 90-95% as measured on last day of infusion. No long term hepatocyte engraftment was reported but biochemical parameters improved suggesting cell persistence[13]. Yet, after short term effect resulting probably from circulating cells (up to day 5) spontaneous trend to biochemical normalization cannot be excluded as it has been reported in some mild ZSD patients[26]. Compared to LT, HT biochemical impact is reduced in ZSD patients[7].

Poor hepatocyte engraftment in ZSD mice could be explained by the absence of selective advantage of the infused wild-type hepatocytes over ZSD hepatocytes. Hepatocyte proliferation was reported in ZSD mice liver but no necrosis was detected[14]. Absence of space for hepatocyte engraftment could be a major factor

impairing HT in ZSD mouse liver. Moreover engraftment could be partly impaired in ZSD mice liver due to *Cxcl12* and *Hgf* downregulation (GSE145524), chemokines implicated in mesenchymal stromal cells recruitment and hepatocyte proliferation, respectively[27]. Several strategies have been developed to improve hepatocyte engraftment such as hepatotoxic drugs[22], preparative hepatic irradiation[28] combined or not with partial hepatectomy[29] and (repeated) reversible portal vein embolization[30]. The vast majority were evaluated in rat HT models. In mice, uPA$^{+/+}$-SCID mouse model combines liver insult leading to regenerative stimulus and immunosuppression for xenogenic liver cell therapy, but combining uPA$^{+/+}$-SCID background to *Pex1*-G844D NMRI mouse would potentially modify the robustness of the model[31]. Globally, only a fraction of these approaches is translatable into clinical practice and most of them are not devoid of risks[32].

Our study strengthened the ZSD phenotype of *Pex1*-G844D NMRI mouse model and demonstrated its suitability for therapeutic interventions like liver cell therapy on young light ZSD mice. Small sample size in low dose HT protocol limited the statistical significance of the results. High dose HT protocol allowed us to conclude that hepatocyte engraftment was a barrier to therapeutic efficacy. In the future, techniques to improve liver cell engraftment (see above) or liver *Pex1* gene therapy could be evaluated in this mild ZSD mouse model to restore liver peroxisome biogenesis. Proof of concept was already evaluated by HT and LT in mild ZSD patients[7, 13].

Conclusion

HT in *Pex1*-G844D NMRI mice was safe and confirmed robustness and ZSD phenotype. Both, low dose and high dose HT failed to achieve long term hepatocyte engraftment. In consequence, no impact on disease markers was evidenced.

Acknowledgments

The authors thank Michele De Beukelaer, Tamah Abderrahman and Philippine Debeyne for excellent technical assistance. Pr Philippe Lysy provided glucometer & strips.

References

1. Steinberg, S., L. Chen, L. Wei, A. Moser, H. Moser, G. Cutting, and N. Braverman, The PEX Gene Screen: molecular diagnosis of peroxisome biogenesis disorders in the Zellweger syndrome spectrum. Mol Genet Metab, 2004. 83(3): p. 252-63.
2. Portsteffen, H., A. Beyer, E. Becker, C. Epplen, A. Pawlak, W.H. Kunau, and G. Dodt, Human PEX1 is mutated in complementation group 1 of the peroxisome biogenesis disorders. Nat Genet, 1997. 17(4): p. 449-52.
3. Wanders, R.J., F.C. Klouwer, S. Ferdinandusse, H.R. Waterham, and B.T. Poll-The, Clinical and Laboratory Diagnosis of Peroxisomal Disorders. Methods Mol Biol, 2017. 1595: p. 329-342.
4. Klouwer, F.C., K. Berendse, S. Ferdinandusse, R.J. Wanders, M. Engelen, and B.T. Poll-The, Zellweger spectrum disorders: clinical overview and management approach. Orphanet J Rare Dis, 2015. 10: p. 151.
5. Van Maldergem, L., A.B. Moser, M.F. Vincent, D. Roland, R. Reding, J.B. Otte, R.J. Wanders, and E. Sokal, Orthotopic liver transplantation from a living-related donor in an infant with a peroxisome biogenesis defect of the infantile Refsum disease type. J Inherit Metab Dis, 2005. 28(4): p. 593-600.
6. Matsunami, M., N. Shimozawa, A. Fukuda, T. Kumagai, M. Kubota, P.F. Chong, and M. Kasahara, Living-Donor Liver Transplantation From a Heterozygous Parent for Infantile Refsum Disease. Pediatrics, 2016. 137(6).
7. Demaret, T., S. Varma, X. Stephenne, F. Smets, I. Scheers, R. Wanders, L. Van Maldergem, R. Reding, and E. Sokal, Living-donor liver transplantation for mild Zellweger spectrum disorder: Up to 17 years follow-up. Pediatr Transplant, 2018. 22(3): p. e13112.
8. Otte, J.B., J. de Ville de Goyet, R. Reding, L. Van Obbergh, F. Veyckemans, M.A. Carlier, M. De Kock, S. Clement de Clety, P. Clapuyt, E. Sokal, J. Lerut, I. Delbeke, V. Dierick, M. Janssen, R. Rosati, and F. Libert, Pediatric liver transplantation: from the full-size liver graft to reduced, split, and living related liver transplantation. Pediatr Surg Int, 1998. 13(5-6): p. 308-18.
9. Gurevich, M., V. Guy-Viterbo, M. Janssen, X. Stephenne, F. Smets, E. Sokal, C. Lefebvre, J.L. Balligand, T. Pirotte, F. Veyckemans, P. Clapuyt, R. Menten, D. Dumitriu, E. Danse, L. Annet, S.C. Clety, T. Detaille, D. Latinne, C. Sempoux, P.F. Laterre, C. de Magnee, J. Lerut, and R. Reding, Living Donor Liver Transplantation in Children: Surgical and Immunological Results in 250 Recipients at Universite Catholique de Louvain. Ann Surg, 2015. 262(6): p. 1141-9.
10. Otte, J.B., Pediatric liver transplantation: Personal perspectives on historical achievements and future challenges. Liver Transpl, 2016. 22(9): p. 1284-94.

11. Khan, Z. and S.C. Strom, Hepatocyte Transplantation in Special Populations: Clinical Use in Children. Methods Mol Biol, 2017. 1506: p. 3-16.
12. Coppin, L., E. Sokal, and X. Stephenne, Hepatocyte Transplantation in Children. Methods Mol Biol, 2017. 1506: p. 295-315.
13. Sokal, E.M., F. Smets, A. Bourgois, L. Van Maldergem, J.P. Buts, R. Reding, J. Bernard Otte, V. Evrard, D. Latinne, M.F. Vincent, A. Moser, and H.E. Soriano, Hepatocyte transplantation in a 4-year-old girl with peroxisomal biogenesis disease: technique, safety, and metabolic follow-up. Transplantation, 2003. 76(4): p. 735-8.
14. Demaret, T., M. Roumain, J. Ambroise, J. Evraerts, J. Ravau, C. Bouzin, B. Bearzatto, J.L. Gala, H. Stepman, S. Marie, M.-F. Vincent, G.G. Muccioli, M. Najimi, and E. Sokal, Longitudinal study of Pex1-G844D NMRI mouse model: A robust pre-clinical model for mild Zellweger spectrum disorder. Biochim Biophys Acta Mol Basis Dis, 2020.
15. Stephenne, X., M. Najimi, D.K. Ngoc, F. Smets, L. Hue, B. Guigas, and E.M. Sokal, Cryopreservation of human hepatocytes alters the mitochondrial respiratory chain complex 1. Cell Transplant, 2007. 16(4): p. 409-19.
16. Angarita, S.A.K., B. Truong, S. Khoja, M. Nitzahn, A.K. Rajbhandari, I. Zhuravka, S. Duarte, M.G. Lin, A.K. Lam, S.D. Cederbaum, and G.S. Lipshutz, Human hepatocyte transplantation corrects the inherited metabolic liver disorder arginase deficiency in mice. Mol Genet Metab, 2018. 124(2): p. 114-123.
17. Sohlenius-Sternbeck, A.K., Determination of the hepatocellularity number for human, dog, rabbit, rat and mouse livers from protein concentration measurements. Toxicol In Vitro, 2006. 20(8): p. 1582-6.
18. Lombard, C.A., A. Fabre, J. Ambroise, J. Ravau, F. Andre, N. Jazouli, M. Najimi, X. Stephenne, F. Smets, J.L. Vaerman, and E.M. Sokal, Detection of Human Microchimerism following Allogeneic Cell Transplantation Using Droplet Digital PCR. Stem Cells Int, 2019. 2019: p. 8129797.
19. Wang, L.J., Y.M. Chen, D. George, F. Smets, E.M. Sokal, E.G. Bremer, and H.E. Soriano, Engraftment assessment in human and mouse liver tissue after sex-mismatched liver cell transplantation by real-time quantitative PCR for Y chromosome sequences. Liver Transpl, 2002. 8(9): p. 822-8.
20. Gupta, S., P. Rajvanshi, R. Sokhi, S. Slehria, A. Yam, A. Kerr, and P.M. Novikoff, Entry and integration of transplanted hepatocytes in rat liver plates occur by disruption of hepatic sinusoidal endothelium. Hepatology, 1999. 29(2): p. 509-19.
21. Ferdinandusse, S., S. Denis, P.L. Faust, and R.J. Wanders, Bile acids: the role of peroxisomes. J Lipid Res, 2009. 50(11): p. 2139-47.
22. Joseph, B., H. Malhi, K.K. Bhargava, C.J. Palestro, R.S. McCuskey, and S. Gupta, Kupffer cells participate in early clearance of syngeneic hepatocytes transplanted in the rat liver. Gastroenterology, 2002. 123(5): p. 1677-85.
23. Rajvanshi, P., A. Kerr, K.K. Bhargava, R.D. Burk, and S. Gupta, Studies of liver repopulation using the dipeptidyl peptidase IV-deficient rat and other rodent recipients: cell size and structure relationships regulate capacity for increased transplanted hepatocyte mass in the liver lobule. Hepatology, 1996. 23(3): p. 482-96.
24. Gupta, S., P. Rajvanshi, and C.D. Lee, Integration of transplanted hepatocytes into host liver plates demonstrated with dipeptidyl peptidase IV-deficient rats. Proc Natl Acad Sci U S A, 1995. 92(13): p. 5860-4.
25. Fox, I.J., J.R. Chowdhury, S.S. Kaufman, T.C. Goertzen, N.R. Chowdhury, P.I. Warkentin, K. Dorko, B.V. Sauter, and S.C. Strom, Treatment of the Crigler-Najjar syndrome type I with hepatocyte transplantation. N Engl J Med, 1998. 338(20): p. 1422-6.
26. Berendse, K., M. Engelen, S. Ferdinandusse, C.B. Majoie, H.R. Waterham, F.M. Vaz, J.H. Koelman, P.G. Barth, R.J. Wanders, and B.T. Poll-The, Zellweger spectrum disorders: clinical manifestations in patients surviving into adulthood. J Inherit Metab Dis, 2016. 39(1): p. 93-106.
27. Dollet, P.E., J. Ravau, F. Andre, M. Najimi, E. Sokal, and C. Lombard, Comprehensive Screening of Cell Surface Markers Expressed by Adult-Derived Human Liver Stem/Progenitor Cells Harvested at Passage 5: Potential Implications for Engraftment. Stem Cells Int, 2016. 2016: p. 9302537.
28. Yamanouchi, K., H. Zhou, N. Roy-Chowdhury, F. Macaluso, L. Liu, T. Yamamoto, G.R. Yannam, C. Enke, T.D. Solberg, A.B. Adelson, J.L. Platt, I.J. Fox, J. Roy-Chowdhury, and C. Guha, Hepatic irradiation augments engraftment of donor cells following hepatocyte transplantation. Hepatology, 2009. 49(1): p. 258-67.

29. Guha, C., B. Parashar, N.J. Deb, M. Garg, G.R. Gorla, A. Singh, N. Roy-Chowdhury, B. Vikram, and J. Roy-Chowdhury, Normal hepatocytes correct serum bilirubin after repopulation of Gunn rat liver subjected to irradiation/partial resection. Hepatology, 2002. 36(2): p. 354-62.
30. Gaillard, M., H. Tranchart, P. Lainas, O. Trassard, S. Remy, A. Dubart-Kupperschmitt, and I. Dagher, Improving Hepatocyte Engraftment Following Hepatocyte Transplantation Using Repeated Reversible Portal Vein Embolization in Rats. Liver Transpl, 2019. 25(1): p. 98-110.
31. Najimi, M., D.N. Khuu, P.A. Lysy, N. Jazouli, J. Abarca, C. Sempoux, and E.M. Sokal, Adult-derived human liver mesenchymal-like cells as a potential progenitor reservoir of hepatocytes? Cell Transplant, 2007. 16(7): p. 717-28.
32. Barahman, M., P. Asp, N. Roy-Chowdhury, M. Kinkhabwala, J. Roy-Chowdhury, R. Kabarriti, and C. Guha, Hepatocyte Transplantation: Quo Vadis? Int J Radiat Oncol Biol Phys, 2019. 103(4): p. 922-934.

Chapter 5.

Living-donor liver transplantation for mild Zellweger spectrum disorder: Up to 17 years follow-up

Tanguy Demaret[1,*], Sharat Varma[1,*], Xavier Stephenne[1], Françoise Smets[1], Isabelle Scheers[1], Ronald Wanders[2], Lionel Van Maldergem[3], Raymond Reding[4], Etienne M Sokal[1]

[1] Service de Gastro-Entérologie et Hépatologie Pédiatrique, Cliniques universitaires Saint-Luc, Université Catholique de Louvain (UCLouvain), 1200 Brussels, Belgium

[2] Laboratory Genetic Metabolic Diseases, Department of Clinical Chemistry, Academic Medical Center, Amsterdam, The Netherlands

[3] Centre de Génétique Humaine, Centre Hospitalier Régional Universitaire de Besançon, Université de Franche-Comté, Besançon, France

[4] Unité de Chirurgie Pédiatrique, Cliniques universitaires Saint-Luc, Université Catholique de Louvain (UCLouvain), 1200 Brussels, Belgium

* Both authors contributed equally to this work

Pediatric Transplantation (2018)

Abstract

Mild Zellweger spectrum disorder, also described as Infantile Refsum disease, is attributable to mutations in *PEX* genes. Its clinical course is characterized by progressive hearing and vision loss, and neurodevelopmental regression. Supportive management is currently considered the standard of care, since no treatment has shown clinical benefits. Liver transplantation (LT) was shown to correct levels of circulating toxic metabolites, partly responsible for chronic neurological impairment. Of three patients having undergone LT for mild ZSD, one died after LT, while the other two displayed significant neurodevelopmental improvement on both the long- (17 years post-LT) and short-term (9 months post-LT) follow-up. We documented a sustained improvement of biochemical functions, with a complete normalization of plasma phytanic, pristanic and pipecolic acid levels. This was associated with stabilization of hearing and visual functions, and improved neurodevelopmental status, which has enabled the older patient to lead a relatively autonomous lifestyle on the long-term. The psychomotor acquisitions have been markedly improved as compared to their affected siblings who did not undergo LT and exhibited a poor neurological outcome with severe disabilities. We speculate that LT performed before the onset of severe sensorineural defects in mild ZSD, enables partial metabolic remission and improved long-term clinical outcomes.

Introduction

Zellweger spectrum disorders (ZSD) is a clinical spectrum of diseases due to abnormal formation and function of peroxisomes, attributable to defective peroxins that are encoded by the *PEX* genes[1].The manifestations of these inborn errors metabolism, are seen as a continuum between the severe Zellweger Syndrome (OMIM #214100) and the milder Heimler syndrome (OMIM #234580, #616617). Clinical presentation varies from death in infancy to neurodevelopmental delays among those who survive beyond the first decade of life[2, 3]. Among the long-term survivors, the lack of independent living skills is the most noticeable and handicapping. Characteristically elevated levels of phytanic, pristanic, pipecolic, and very-long-chain fatty acids (VLCFA), and bile acid intermediates are observed in the plasma of affected children. Additionally, the plasmalogen concentration in red blood cell (RBC) membranes is decreased. The current standard of care consists of avoiding exposure to phytanic acid[4], which is suggested to exert a direct toxic effect on neurological tissues[5]. We previously demonstrated the short-term benefit of liver transplantation (LT)[6] and liver cell transplantation (LCT)[7] on biochemical and clinical outcome, as reported for other organelle disease[8, 9]. We have herein reported our broadened experience, describing the long-term outcome of the same individual who received an LT 17 years ago, while including other LT-recipients for the same indication.

Patients description

The demographic description, clinical features at initial presentation, diagnostic characteristics, and LT details are given in **Table 1**. Patient 1 (P#1) was diagnosed

with mild ZSD at an early age before severe neurological handicap developed. Her older affected sibling was already severely handicapped and exhibited advanced sensorineural impairment. P#1 underwent an LT after approval by the institutional ethics committee and following receipt of informed consent from the family concerning the theoretical basis of the treatment. Following LT, significant improvement was seen in quality of life and other aspects, as previously reported by our team at 2 years post-LT[6]. P#3's parents approached us to perform an LT for their child, since available treatments did not prove clinically beneficial. When he underwent LT, their 2-year-old son was unable to stay in a sitting position, and his older affected sibling was severely handicapped.

A third patient (P#2) received an LT for the same indication, but died suddenly 18 days afterwards due to an acute hypotension episode with hyperkalemia (8.51 mmol/L) and hyponatremia (127.5 mmol/L). The follow-up in this patient was too short for the assessment of any clinical or neurodevelopmental improvement, and has therefore not been described below; the patient characteristics and biochemical evolution are however mentioned in **Table 1** and **Table 2**. In the following study, we have shared our long-term data pertaining to biochemical, clinical, and neurodevelopmental responses in P#1 and P#3.

Table 1. Demographic description, clinical features at initial presentation, diagnostic characteristics, and LT details of the patients.

Characteristics	Patient 1	Patient 2	Patient 3
Demographics			
Age at initial presentation	1 month	2 months	2 months
Gender	Female	Female	Male
Ethnicity	Caucasian	Caucasian	Syrian-Chinese
Clinical features			
Family history	Elder sibling diagnosed with a mild ZSD	First child of the couple	Elder sibling diagnosed with a mild ZSD
Antenatal and natal history	Small for gestational age (birth weight <P3)	Chronic fetal distress, dilated colon	Nothing significant

Table 1. Demographic description, clinical features at initial presentation, diagnostic characteristics, and LT details of the patients.

Characteristics	Patient 1	Patient 2	Patient 3
At presentation	Facial dysmorphism, feeding disturbances, nystagmus, axial hypotonia and hepatomegaly	Facial dysmorphism, steatorrhea	Facial dysmorphism, nystagmus, axial hypotonia, peripheral hypertonia, hepatomegaly
Brain MRI	Normal, no leukodystrophy	Normal, no leukodystrophy	Polymicrogyria
Diagnostic characteristics			
Plasma VLCFA			
C_{26} (0.45-1.32 µmol/L)	8.93 (6.8x ULN)	6.11 (4.6x ULN)	2.26 (1.7x ULN)
C_{24}/C_{22} (0.32-1.11)	2.08 (1.9x ULN)	1.48 (1.3x ULN)	1.36 (1.2x ULN)
C_{26}/C_{22} (0-0.02)	0.55 (27.5x ULN)	0.25 (12.5x ULN)	0.15 (7.5x ULN)
Plasma phytanic acid (0-9 µmol/L)	0.3 (within normal range)	18.58 (2.1x ULN)	30.47 (3.4x ULN)
Plasma pristanic acid (0-3 µmol/L)	Not available	6.38 (2.1x ULN)	7.22 (2.4x ULN)
Plasma pipecolic acid (0.6-4.1 µmol/L)	34 (8.3x ULN)	Not done	450 (109.8x ULN)
RBC membrane plasmalogens			
C16 DMA : C16 FA (0.046-0.082)	0.044 (0.96x LLN)	0.122 (1.49x ULN)	0.047 (within normal range)
C18 DMA : C18 FA (0.115-0.265)	0.105 (0.91x LLN)	0.165 (within normal range)	0.019 (0.17x LLN)
Genetic evaluation	PEX1 heterozygote c.3710A>C ; unknown p.Ala1237Glu ; unknown	PEX12 compound heterozygote c.126+1G>T ; c.1047_1049delACA splicing defect ; p.Gln349del	PEX1 compound heterozygote c.547G>A ; c.1099del p.Arg183Ter ; p.Gln367LysfsTer20
Pre-LT treatment	Low phytanic acid diet and DHA	Vitamin D & K and calcium	DHA
LT details			
Donor	Living-related	Living-related	Living-related
Age of donor	30 years	45 years	34 years
Age of recipient at LT	7 months	24 months	25 months
IS post LT			
Induction	Tacrolimus + corticosteroids	Tacrolimus + basiliximab	Tacrolimus + basiliximab
Maintenance	Tacrolimus + mycophenolate mofetil	Tacrolimus monotherapy	Tacrolimus monotherapy
Number of ACR	2	1	0
Complications	CMV colitis, cholangitis, biliary stenosis, C.difficile infection, intrahepatic abscess	Deceased of unrelated causes 18 days post-LT	CMV infection, C.difficile infection

The values are shown as number of times of the upper/lower limit of the normal between parenthesis. LT: liver transplantation, ZSD: Zellweger spectrum disorder, MRI: magnetic resonance imaging, VLCFA: very long chain fatty acids, ULN: upper limit of the normal, LLN: lower limit of the normal, RBC: red blood cell, DMA: dimethylacetals, FA: fatty acids, wt: wild-type, DHA: docosahexaenoic acid, IS: immunosuppression, ACR: acute and chronic rejections, CMV: cytomegalovirus.

Biochemical response after LT in mild ZSD

A significant and sustained improvement in both children's biochemical profile was noticed. These children exhibited increased VLCFA, phytanic, pristanic, and pipecolic acid levels, and decreased RBC membrane plasmalogen concentration at diagnosis (**Table 1**). Pre-LT C_{26}/C_{22} ratio in P#1 and P#3 were 27xULN and 7xULN, respectively, showing a dramatic decrease soon after LT. Both children maintained C_{26}/C_{22} ratios under 4xULN at last biochemical follow-up (i.e., at 17 years and 9 months post-LT, respectively). Plasma pipecolic levels normalized in P#1 until 15 years post-LT, after which a gradual increase was observed whereas P#3 displayed normal levels until last follow-up (**Figure 1**, **Table 2**). Plasma phytanic and pristanic acid levels after LT remained normal in both children. Post-LT, C_{27} bile acid intermediates (dihydroxycholestanoic acid and trihydroxycholestanoic acid) were undetectable in P #1 and plasmalogen content in RBC showed fluctuating levels in all children.

Table 2. Biochemical parameters pre-LT and post-LT

Time of measure	Plasma VLCFA			Plasma phytanic acid (0-9 µmol/L)	Plasma pristanic acid (0-3 µmol/L)	Plasma pipecolic acid (0.6-4.1 µmol/L)	RBC membrane plasmalogens	
	C_{26} (0.45-1.32 µmol/L)	C_{24}/C_{22} (0.32-1.11)	C_{26}/C_{22} (0-0.02)				C_{16} DMA:C_{16} FA (0.046-0.082)	C_{18} DMA:C_{18} FA (0.115-0.265)
Patient 1								
5 mo pre-LT	8.93	2.076	0.547	0.3[a]		34	0.044	0.105
3 mo pre-LT	7.06	1.56	0.303	1.6[a]				
1 d post-LT	1.9	1.162	0.152	1.34		2.19		
1 mo post-LT	2.87	1.139	0.178	1.2	5.39			
2 mo post-LT	1.84	1.246	0.046	0.43				
3 mo post-LT	1.16	1.322	0.074	0		2.06	0.064	0.134
4 mo post-LT	2.23	1.375	0.062	0			0.038	0.101
5 mo post-LT	2.6	1.389	0.081	0			0.046	0.108
6 mo post-LT	2.22	1.197	0.058	0	0	1	0.045	0.11
9 mo post-LT	1.96	1.266	0.063	0.81				
11 mo post-LT	3.06	1.373	0.102	1.3				
12 mo post-LT	3.02	1.191	0.073	6.4				
13 mo post-LT	3.4	1.187	0.1	6.4			0.06	0.14
2 y post-LT	0.49	1.393	0.094	0.35	0.77	1	0.035	0.121
3 y post-LT	0.51	0.842	0.012	2.11	0.07	1.8		
15 y post-LT	5.64	1.212	0.112	1.32	0.23	1.7		
16 y post-LT	4.96	1.226	0.077	3.26	0.1	6.5	0.058	0.055
17 y post-LT	5.14	1.056	0.074	1.92	0.27	11.7		
Patient 2								
13 mo pre-LT	5.76	1.428	0.245	15.77	6.37			
11 mo pre-LT	6.11	1.478	0.246	18.58	6.38		0.122	0.165
12 d post-LT	2.32	1.097	0.058	0.95	0.14			
Patient 3								
2 mo pre-LT	2.26	1.043	0.081	30.47	7.22	254		
1 mo pre-LT	1.75	1.362	0.151	16.54	3.9	450	0.047	0.019
2 d post-LT	1.05	1.064	0.045	5.33	0.83			
1 mo post-LT	2.51	1.085	0.069	3.91	0.4	2.5		
4 mo post-LT	2.28	1.407	0.08	6.87	0.86	2.3	0.052	0.055
9 mo post-LT	1.86	1.249	0.059	3.14	0.21	2.3		

[a] Normal value attributable to young age (inadequate duration for accumulation of phytanic acid).
The normal values are shown between parenthesis. LT: liver transplantation, VLCFA: very long chain fatty acids, RBC: red blood cells, DMA: dimethylacetals, FA: fatty acids.

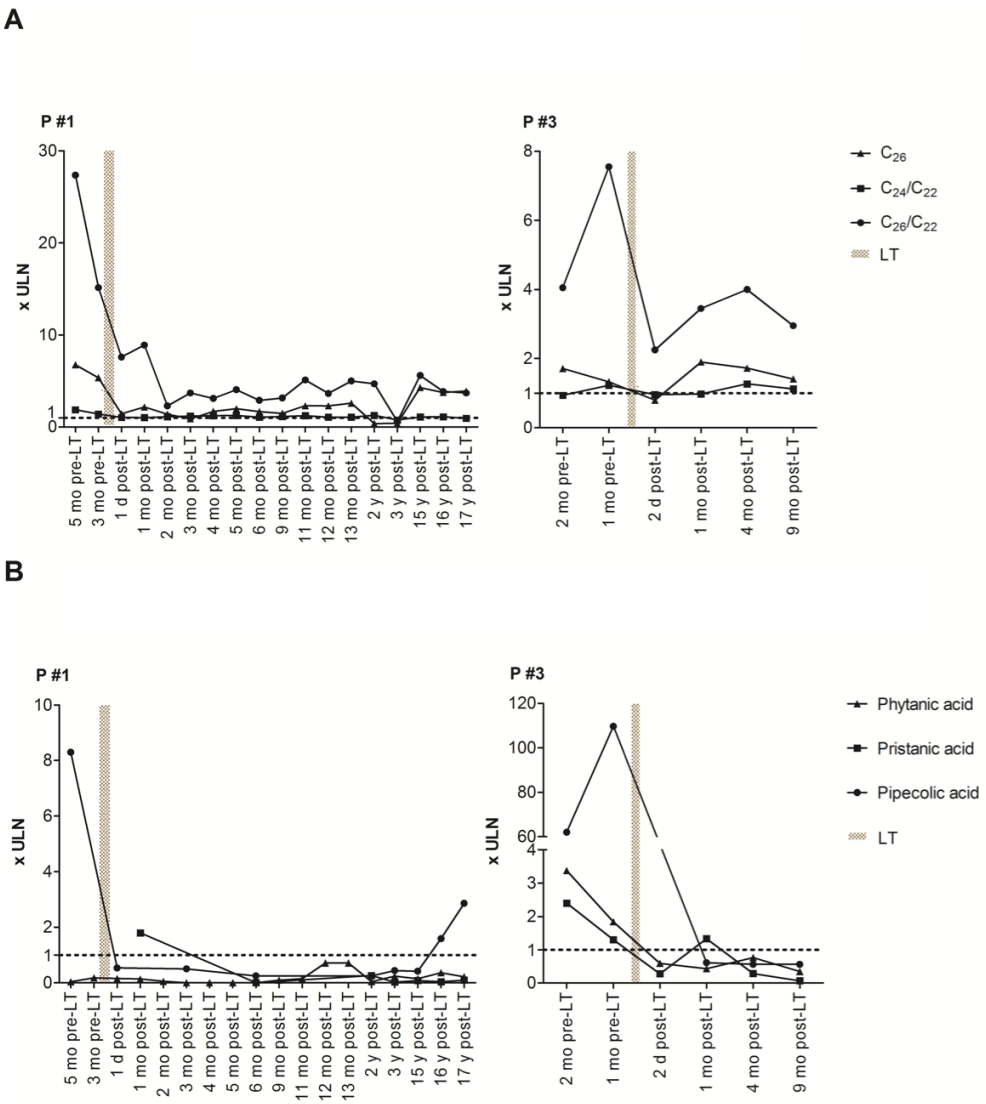

Figure 1 - Patient 1 and 3's biochemical trend. Plasma **A** VLCFA, **B** BCFA, and pipecolic acid levels (expressed as number of times of the upper limit of the normal); in patient 1 and 3. xULN: number of times of the upper limit of the normal, LT: liver transplantation, VLCFA: very-long-chain fatty acids, BCFA: branched-chain fatty acids.

Sensorineural response after LT in mild ZSD

For both children, sensorineural responses including vision and hearing improved in certain aspects, while there was no further worsening, i.e., stabilization of function,

for others (**Figure 2**). As these are slowly evolving changes, they could be better observed in P#1 with a significantly longer follow-up duration.

P#1's auditory acuity assessed by brainstem-evoked response audiometry (BERA) remained nearly stable post-LT (60dB pre-LT and 80dB at 7 years post-LT). At the age of 13 years, i.e., 12 years post-LT, she successfully underwent a cochlear implant insertion in the left ear because of chronic suppurative otitis media. For P#3, serial BERA has not been performed yet, and he continues to utilize the same hearing aids as before.

Significant improvement in nystagmus was observed post-LT in P#1. Deterioration arrest was noticed in P#1, in which visually evoked potentials remained normal, without any cataract formation. The electroretinogram pre-LT displayed reduced scototopic amplitude (70 and 50 µV for left and right eyes, respectively), combined with a tigroid retinitis pigmentosa in the eye fundus. Her visual acuity is 1/10 and showed no evolution after LT.

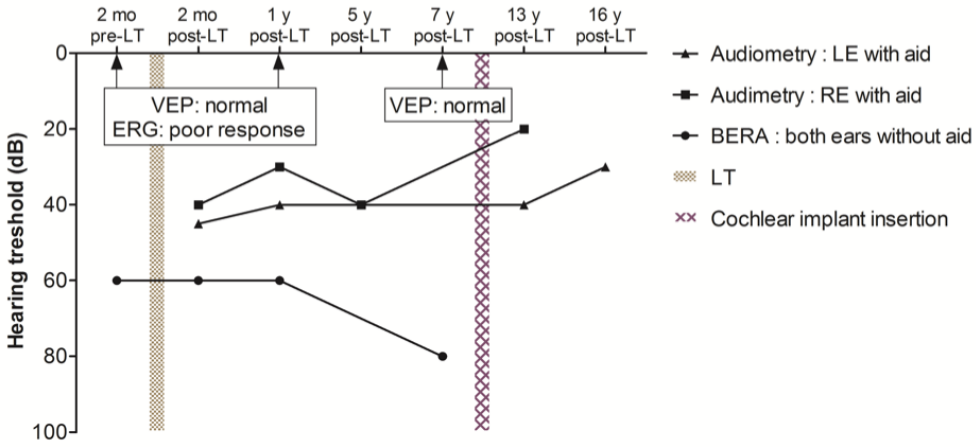

Figure 2 - Patient 1 hearing thresholds measured by BERA (without aid) or audiometry (with aid). LT: liver transplantation, VEP: visual evoked potentials, ERG: electroretinogram, BERA: brainstem-evoked response audiometry, LE: left ear, RE: right ear.

Growth and development response after LT in mild ZSD

The long-term follow-up of P#1 indicated that she consistently developed according to her growth curve concerning height (- 3.7 standard deviation (SD) at last follow-up), weight (- 4.3 SD at last follow-up) and head circumference (- 2 SD at last follow-up) from the age of 6 months, i.e., since LT. Her pubertal growth spurt was remarkably well sustained, and she attained menarche at the age of 15 years. For P#3, a similar analysis would need a longer follow-up duration, which is not available. To assess developmental progress, we calculated developmental quotient (DQ = normal age of milestone acquisition divided by chronological age) across motor and language spheres sequentially after LT. DQ was based on the Denver Developmental Screening Test when available[10], and otherwise on the Milestone Checklists[11] (**Figure 3**).

After transplantation, P#1 acquired several milestones, though with delay. She is currently autonomous after having acquired independent living skills, is being educated in a school for the visually impaired, and has social interactions. There is a strong contrast in comparison to her elder sister with the same disease, as she is totally dependent on care for her daily activities. P#3 experienced a dramatic improvement in his social interaction skills in his 9 months of post-LT life, since he has become more responsive to verbal and non-verbal communication. He has additionally acquired the sitting position without support and is able to stand with support at 9 months post-LT, which he had never been able to do before.

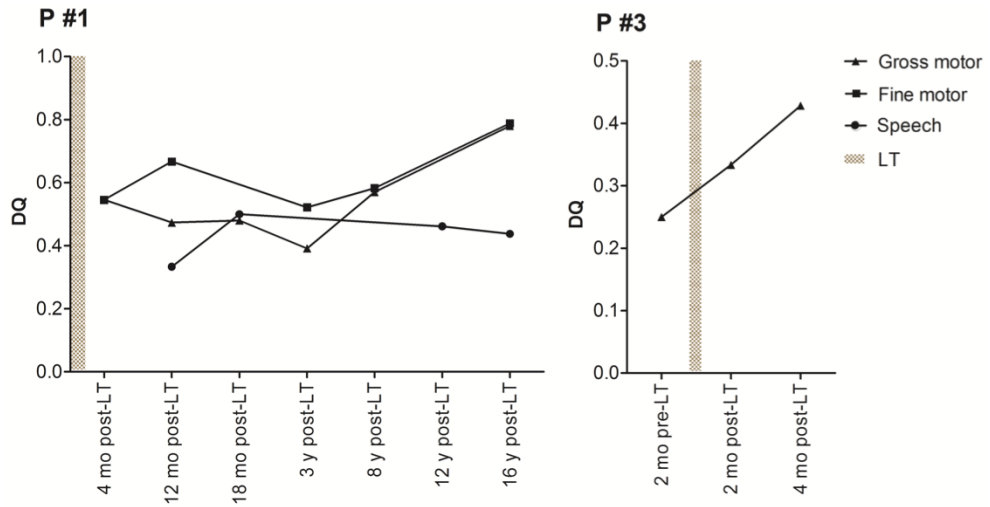

Figure 3 - Patient 1 and 3 developmental milestone acquisition measured by the developmental quotient. DQ: developmental quotient, LT: liver transplantation.

Allograft function

Allograft outcome in terms of liver function, rejection episodes, fibrosis evolution, immune-suppression requirement, post-LT hospital stay, metabolic control, and other surgical complications has not been any different from LT performed for other indications. P#1 experienced two episodes of rejection and suffered from biliary stenosis requiring surgical intervention, while the last protocol biopsy conducted at 15 years post-LT showed mild-moderate fibrosis (Metavir 2, Liver Allograft Fibrosis Score 3/9-P2S1C0) without significant inflammation. P#3 neither experienced any rejection episodes nor any other complications. Both are currently managed with tacrolimus-based immune-suppression regimen.

Discussion

This report on the long-term evolution of the first LT for mild ZSD was expected by the metabolic community[12]. We included one additional patient, whose outcome

corroborated the benefit of LT on circulating metabolites, clinical outcome and autonomy acquisition. Both children had received a transplant relatively early in life and before they developed a profound neurological handicap. Consequently, their neurodevelopmental outcomes were better than their older affected siblings who had not been transplanted.

In our experience of having performed 3 LT for mild ZSD, P#2 died 18 days post-LT after an acute hypotension episode with electrolyte imbalance, which could be compatible with acute adrenal insufficiency. Primary adrenal insufficiency is an underdiagnosed complication in ZSD[13] and cortisone supplementation should be prescribed to patients with an altered Synacthen® test[12]. This further highlights the need for experienced centers to perform LT in mild ZSD and to manage the affected patients.

Pre-LT phytanic acid level was elevated except in P#1 which can be attributable to a low-phytanic acid diet and his young age (inadequate duration for accumulation of phytanic acid)[14, 15]. Phytanic acid was shown to be a toxic metabolite[5] prompting the adoption of low-phytanic acid diet as a treatment modality[16]. This approach did not result in symptom stabilization or improvement in our patient, as it has also been previously reported[14]. Following LT, the phytanic acid levels normalized in all patients as the new allografted liver cleared the toxic metabolite (**Figure 1, Table 2**). Similar observation was made by the Japanese team that has also recently performed LT for mild ZSD[17]. On the long term, P#1's low phytanic acid diet became more liberal (i. e. she eats now green vegetables, fish and red meat).

In ZSD, characteristically elevated pristanic and pipecolic acid levels are seen. *In vitro* pristanic and pipecolic acids were shown to induce oxidative stress in

cerebellum and cerebral cortex of young rats[18-20], which implicates these metabolites to have a neurotoxic effect in ZSD. Remarkably both normalized after LT and also LCT[7]. The normalization of these metabolite levels could account for the neurodevelopmental benefit that was observed in our patients.

In ZSD, the VLCFA levels are raised due to their inadequate metabolism in the peroxisomes and have a vast range of toxic effects[21]. C_{26}/C_{22}, C_{24}/C_{22} ratios showed a decrease post-LT in both our patients, as was also seen by Matsunami et al. In isolation the C_{26} levels decreased until 15 years post-LT, C_{24} levels decreased and the C_{22} increased, which resulted in improvement of the C_{26}/C_{22} and C_{24}/C_{22} ratios. The new allografted liver is thought to correct the VLCFA metabolism, this would have resulted in a decrease of C_{26}, C_{24} and also of C_{22}. This is in contrast to our observation, wherein C_{26}, C_{24} decreased but unexpectedly C_{22} increased. As post-LT Tacrolimus is administered, it could possibly affect the VLCFA (C_{22}) explaining the above finding; but this aspect is a mere speculation as it has never been evaluated and needs further studies.

C_{27} bile acid intermediates classically accumulate in ZSD. They were previously shown to be undetectable 2 years post-LT[6] and at last follow-up in P#1. They were not measured in P#2 and P#3. In a recent trial cholic acid therapy in ZSD without severe liver disease was shown to decrease bile acid intermediates but failed to demonstrate a benefit on the other implicated toxic metabolites. Unfortunately, clinical improvement wasn't evaluated in this study, given the short duration of follow-up[22].

Post-LT RBC plasmalogens levels don't draw any clear trend of evolution. They are manufactured in the peroxisomes of bone marrow precursor cells[23], thus no effect

would be expected after LT. Thirty years ago, oral plasmalogen supplementation was tried in a few patients with mild ZSD[24, 25]. They showed some benefit, but no further study was performed since then.

Limited language and verbal skills are observed in half of the patients surviving into adulthood[3, 26]. P#1 verbal skills were acquired in early post-LT period and subsequently stabilized (**Figure 3**). 17 years post-LT, P#1 achieved relative social autonomy, and can dress herself, eat and travel by herself to school. Her hearing ability stabilized after receiving the cochlear implant and the improvement of nystagmus was remarkable.

There was a clear contrast between the post-LT evolution of P#1 and P#3 in comparison to their older siblings who followed the natural disease outcome. The 19-year-old elder sister of P#1 exhibited a complete lack of independent living skills to the extent of an inability to walk, along with a total lack of interest and interaction with her surroundings. P#3's elder 7-year-old brother displayed a similar evolution; he is completely bedridden, with a total lack of interest in his surroundings. Nonetheless intra-familial phenotypic variability was published previously[27] and this could partially account for the contrast seen in our patients. No geno-phenotype correlation could be drawn in our patients since the mutations they carry were previously reported in other patients without any clinical information[28, 29]. A study on patients with mild-*est* ZSD surviving until adulthood (i.e., excluding patients who died before) showed a late normalization of certain metabolites levels in a subset of patients. By extrapolation it could be proposed that our patients would also have shown biochemical improvement later in life. Given our current limitations of understanding ZSD, wherein we cannot predict the clinical evolution; the above

proposition would be the “best case scenario” that can be imagined for any child having ZSD. Unfortunately, by when it would become explicit whether neurological involvement is going to be severe or not, the window of opportunity to perform a LT would have been shut. Furthermore, our patients showed a decrease in toxic metabolites levels just after LT which cannot be the natural history of the disease, consequently protecting them from the toxicity during the key neurodevelopmental period of childhood. Hence, we speculate that if LT is to be considered it should be early and, definitely, before the onset of profound neurocognitive impairment.

Moreover, ZSD diagnosis before neurological deficit appears is rendered possible since $C_{26:0}$lysophosphatidylcholine level assessment has recently been added to the newborn screening in the United States for the early detection of X-linked adrenoleukodystrophy, a related peroxisomal disorder[12]. Though we and others[17] have achieved significant improvements in this disease usually associated with dismal outcomes, further evaluation is required to strengthen the place of LT as a therapy to modify the natural history of ZSD and to identify children who would most likely benefit from this approach. Among the promising future therapies, adult derived liver stem/progenitor cells hold significant promise[30] as demonstrated by initial *in vitro* data[31].

Conclusion

In two patients affected by a mild ZSD, LT induced short- (9 months of follow-up) and long-term (>17 years of follow-up) metabolic improvement and neurodevelopmental benefits in comparison to their respective affected non-transplanted sibling.

References

1. Waterham, H.R. and M.S. Ebberink, Genetics and molecular basis of human peroxisome biogenesis disorders. Biochim Biophys Acta, 2012. 1822(9): p. 1430-41.
2. Waterham, H.R., S. Ferdinandusse, and R.J. Wanders, Human disorders of peroxisome metabolism and biogenesis. Biochim Biophys Acta, 2016. 1863(5): p. 922-33.
3. Berendse, K., M. Engelen, S. Ferdinandusse, C.B. Majoie, H.R. Waterham, F.M. Vaz, J.H. Koelman, P.G. Barth, R.J. Wanders, and B.T. Poll-The, Zellweger spectrum disorders: clinical manifestations in patients surviving into adulthood. J Inherit Metab Dis, 2016. 39(1): p. 93-106.
4. Braverman, N.E., G.V. Raymond, W.B. Rizzo, A.B. Moser, M.E. Wilkinson, E.M. Stone, S.J. Steinberg, M.F. Wangler, E.T. Rush, J.G. Hacia, and M. Bose, Peroxisome biogenesis disorders in the Zellweger spectrum: An overview of current diagnosis, clinical manifestations, and treatment guidelines. Mol Genet Metab, 2016. 117(3): p. 313-21.
5. Leipnitz, G., A.U. Amaral, A. Zanatta, B. Seminotti, C.G. Fernandes, L.A. Knebel, C.R. Vargas, and M. Wajner, Neurochemical evidence that phytanic acid induces oxidative damage and reduces the antioxidant defenses in cerebellum and cerebral cortex of rats. Life Sci, 2010. 87(9-10): p. 275-80.
6. Van Maldergem, L., A.B. Moser, M.F. Vincent, D. Roland, R. Reding, J.B. Otte, R.J. Wanders, and E. Sokal, Orthotopic liver transplantation from a living-related donor in an infant with a peroxisome biogenesis defect of the infantile Refsum disease type. J Inherit Metab Dis, 2005. 28(4): p. 593-600.
7. Sokal, E.M., F. Smets, A. Bourgois, L. Van Maldergem, J.P. Buts, R. Reding, J. Bernard Otte, V. Evrard, D. Latinne, M.F. Vincent, A. Moser, and H.E. Soriano, Hepatocyte transplantation in a 4-year-old girl with peroxisomal biogenesis disease: technique, safety, and metabolic follow-up. Transplantation, 2003. 76(4): p. 735-8.
8. Sokal, E.M., R. Sokol, V. Cormier, F. Lacaille, P. McKiernan, F.J. Van Spronsen, O. Bernard, and J.M. Saudubray, Liver transplantation in mitochondrial respiratory chain disorders. Eur J Pediatr, 1999. 158 Suppl 2: p. S81-4.
9. Najimi, M., F. Defresne, and E.M. Sokal, Concise Review: Updated Advances and Current Challenges in Cell Therapy for Inborn Liver Metabolic Defects. Stem Cells Transl Med, 2016. 5(8): p. 1117-25.
10. Frankenburg, W.K. and J.B. Dodds, The Denver developmental screening test. J Pediatr, 1967. 71(2): p. 181-91.
11. The milestone checklist. February 23, 2015 August 18, 2016 January 10, 2017]; Available from: https://www.cdc.gov/ncbddd/actearly/milestones/.
12. Klouwer, F.C., K. Berendse, S. Ferdinandusse, R.J. Wanders, M. Engelen, and B.T. Poll-The, Zellweger spectrum disorders: clinical overview and management approach. Orphanet J Rare Dis, 2015. 10: p. 151.
13. Berendse, K., M. Engelen, G.E. Linthorst, A.S. van Trotsenburg, and B.T. Poll-The, High prevalence of primary adrenal insufficiency in Zellweger spectrum disorders. Orphanet J Rare Dis, 2014. 9: p. 133.
14. Sa, M.J., J.C. Rocha, M.F. Almeida, C. Carmona, E. Martins, V. Miranda, M. Coutinho, R. Ferreira, S. Pacheco, F. Laranjeira, I. Ribeiro, A.M. Fortuna, and L. Lacerda, Infantile Refsum Disease: Influence of Dietary Treatment on Plasma Phytanic Acid Levels. JIMD Rep, 2016. 26: p. 53-60.
15. Wanders, R.J., J. Komen, and S. Ferdinandusse, Phytanic acid metabolism in health and disease. Biochim Biophys Acta, 2011. 1811(9): p. 498-507.
16. Baldwin, E.J., F.B. Gibberd, C. Harley, M.C. Sidey, M.D. Feher, and A.S. Wierzbicki, The effectiveness of long-term dietary therapy in the treatment of adult Refsum disease. J Neurol Neurosurg Psychiatry, 2010. 81(9): p. 954-7.
17. Matsunami, M., N. Shimozawa, A. Fukuda, T. Kumagai, M. Kubota, P.F. Chong, and M. Kasahara, Living-Donor Liver Transplantation From a Heterozygous Parent for Infantile Refsum Disease. Pediatrics, 2016. 137(6).
18. Dalazen, G.R., M. Terra, C.E. Jacques, J.G. Coelho, R. Freitas, P.N. Mazzola, and C.S. Dutra-Filho, Pipecolic acid induces oxidative stress in vitro in cerebral cortex of young rats and the protective role of lipoic acid. Metab Brain Dis, 2014. 29(1): p. 175-83.
19. Busanello, E.N., V.G. Lobato, A. Zanatta, C.G. Borges, A.M. Tonin, C.M. Viegas, V. Manfredini, C.A. Ribeiro, C.R. Vargas, D.O. de Souza, and M. Wajner, Pristanic acid provokes lipid, protein,

and DNA oxidative damage and reduces the antioxidant defenses in cerebellum of young rats. Cerebellum, 2014. 13(6): p. 751-9.
20. Leipnitz, G., A.U. Amaral, C.G. Fernandes, B. Seminotti, A. Zanatta, L.A. Knebel, C.R. Vargas, and M. Wajner, Pristanic acid promotes oxidative stress in brain cortex of young rats: a possible pathophysiological mechanism for brain damage in peroxisomal disorders. Brain Res, 2011. 1382: p. 259-65.
21. Wanders, R.J., S. Ferdinandusse, P. Brites, and S. Kemp, Peroxisomes, lipid metabolism and lipotoxicity. Biochim Biophys Acta, 2010. 1801(3): p. 272-80.
22. Berendse, K., F.C. Klouwer, B.G. Koot, E.M. Kemper, S. Ferdinandusse, K.V. Koelfat, M. Lenicek, F.G. Schaap, H.R. Waterham, F.M. Vaz, M. Engelen, P.L. Jansen, R.J. Wanders, and B.T. Poll-The, Cholic acid therapy in Zellweger spectrum disorders. J Inherit Metab Dis, 2016.
23. Braverman, N.E. and A.B. Moser, Functions of plasmalogen lipids in health and disease. Biochim Biophys Acta, 2012. 1822(9): p. 1442-52.
24. Greenberg, C.R., A.K. Hajra, and A.B. Moser, Triple therapy of a patient with a generalized peroxisomal disorder. Am J Hum Genet, 1987. 41(Suppl): p. A64.
25. Holmes, R.D., G.N. Wilson, and A. Hajra, Oral ether lipid therapy in patients with peroxisomal disorder. Inherited Metab Dis, 1987. 10(Suppl.): p. 239-241.
26. Vandana, V.P., P.S. Bindu, M. Nagappa, S. Sinha, and A.B. Taly, Audiological findings in Infantile Refsum disease. Int J Pediatr Otorhinolaryngol, 2015. 79(8): p. 1366-9.
27. Simons, J. and M. Nowaczyk, Phenotypic Variability in Fraternal Twins with PEX1 Mutations: Zellweger Syndrome with Discordant Clinical Phenotype. MJM, 2013. S5(001): p. 1-3.
28. Yik, W.Y., S.J. Steinberg, A.B. Moser, H.W. Moser, and J.G. Hacia, Identification of novel mutations and sequence variation in the Zellweger syndrome spectrum of peroxisome biogenesis disorders. Hum Mutat, 2009. 30(3): p. E467-80.
29. Steinberg, S., L. Chen, L. Wei, A. Moser, H. Moser, G. Cutting, and N. Braverman, The PEX Gene Screen: molecular diagnosis of peroxisome biogenesis disorders in the Zellweger syndrome spectrum. Mol Genet Metab, 2004. 83(3): p. 252-63.
30. Sokal, E.M., X. Stephenne, C. Ottolenghi, N. Jazouli, P. Clapuyt, F. Lacaille, M. Najimi, P. de Lonlay, and F. Smets, Liver engraftment and repopulation by in vitro expanded adult derived human liver stem cells in a child with ornithine carbamoyltransferase deficiency. JIMD Rep, 2014. 13: p. 65-72.
31. Tondreau, T., M. Tulé, M. Najimi, M.-F. Vincent, and E. Sokal, Human adult liver progenitor cells (HALPCS) is a promising tool to restore peroxisomal dysfunction as infantile Refusm's disease. J Pediatr Gastroenterol Nutr, 2013. 56 Suppl 2: p. 92.

Chapter 6.
General discussion and conclusions

General discussion and implications

In vitro PBD evaluation in skin fibroblasts isolated from ZSD patients has been used for two decades to find molecules that could restore PB and potentially modify the dismal natural history of ZSD[1]. In the meantime, several molecules with such features have discovered[2-5]. Some of them were or are currently evaluated in clinical trials (NCT01838941, NCT03856866) but, to the best of our knowledge, none have shown to dramatically impact the morbidity related to ZSD. Moreover, some lead compounds detected by such methods may not be translatable into clinical outcomes because of their toxicity[6]. In addition, it should not be forgotten that one of the major organs involved in ZSD is located beyond the blood-brain barrier and that cells in a dish do not reproduce that feature. Nonetheless, *in vitro* drug screening in ZSD might be the first step (before *in vivo* evaluation, see below) to find a treatment for these dreadful diseases and we postulate that our eGFP-PTS1 lentiviral vector could ease this process[7].

Relevant readouts are required before setting up any therapeutic interventions in both mouse models and human clinical trials. Validated biological readouts are lacking for ZSD. In ZSD patients, C_{26} plasma levels and two peroxisomal enzyme activity levels (C_{26} beta-oxidation and DHAPAT) were correlated with a clinical severity score and survival, respectively[8, 9]. Yet, correlation does not mean that by decreasing C_{26} plasma levels we could reduce ZSD severity, as it was regrettably shown in X-ALD[10]. In addition, C_{26} plasma level decrease was reported in ZSD patients reaching adulthood without any alleviation of the morbidity associated with ZSD[11]. Clues might come from unbiased lipidomic study of ZSD patient skin fibroblasts that unveiled several phospholipid species ratios which are associated

with disease severity[12]. In our mild ZSD mouse model, beside classical biochemical peroxisomal markers, we evaluated fasting test tolerance and urine organic acid profile. Fasting test reflects liver glycogen metabolism impairment but since this feature has never been described in ZSD patients, its clinical relevance is unknown. ZSD mouse urine organic acid profile is similar to ZSD patients and might reflect the peroxisomal and mitochondrial metabolism status of the whole organism[13, 14]. The scientific community is urgently looking for reliable, specific and relevant biomarkers of treatment response in ZSD as it was discovered for others IEM[15]. We hope that by optimizing a mild ZSD mouse model we could help find a cure and robust treatment response markers for ZSD.

Liver-targeted therapeutic approaches in ZSD begun by cholic acid evaluation in case reports[16-18] followed by a rigorous mouse model study[19] and finally a well-designed clinical trial[20] and its extension[21]. Cholic acid suppresses endogenous bile acid synthesis and thus, avoids C_{27} BA intermediates accumulation and their toxic effects[22]. Post-LT, we also reported complete disappearance of toxic C_{27} BA intermediates from ZSD patients' plasma[23, 24]. In addition, the liver graft evolution did not seem to be different from LT performed for other indications. Nonetheless, organ availability is a barrier to pediatric LT, especially in IEM patients because they usually do not meet the classical criteria for LT (e.g., decompensated cirrhosis)[25]. Living-donor LT was the solution used to overcome this barrier for all LT in ZSD patients[23, 24, 26]. As for other IEM, the use of a heterozygous donor did not impede the procedure[27]. HT is a second, experimental, option as an alternative to living-donor LT[28-31]. Eighteen months post-HT, plasma abnormal bile acids and VLCFA levels decreased in our ZSD patient[29]. The dynamic evolution, with an early but transient

effect of the hepatocyte mass, followed by a more sustained, progressive, increased effect on abnormal bile acids and VLCFA levels, supports the direct effect of the HT instead of a natural evolution, as reported for surviving ZSD patients[11]. This effect was indeed similar, although less pronounced, than the effect of full liver transplantation. To elucidate HT impact on ZSD, we performed HT on our mild ZSD mouse model. Unfortunately, we were not able to demonstrate cell engraftment and no biochemical nor clinical improvement was detectable. In the future, we think that efforts should be focused on improving hepatocyte engraftment and promoting living-donor LT for patients with IEM including ZSD patients[32, 33].

Perspectives

A *Pex1* adeno-associated virus (AAV) vector was developed to evaluate *Pex1* gene retinal augmentation therapy for the retina in Pex1-G844D mouse model[34]. It would be interesting to adapt the AAV vector for hepatic gene delivery and hepatocytic gene expression. Many readouts, including clinical ones, were characterized in our mouse model. Measuring how much liver PB recovery can impact these readouts could intensify liver-targeted therapy research in ZSD. Moreover, given the fact that liver *Pex* gene rescue in a *Pex* knockout mouse model impacted brain development[35], evaluating the effect of this treatment on extra-hepatic tissue could support further the LT indication for ZSD patients.

Clustered regularly interspaced short palindromic repeats (CRISPR)/CRISPR-associated protein 9 (Cas9) technology has brought the possibility to edit a precise region of the genome[36]. A dual AAV CRIPSR/Cas9 delivery system was used to correct up to 29% of the mutated alleles in a humanized ornithine transcarbamylase-

deficient liver mouse model[37]. Since nearly 17% of the ZSD patients carry the PEX1 p.G843D allele[38], the CRISPR/Cas9 correction of the genetic alteration could be a potential therapeutic approach.

LT or gene therapy for ZSD ?

Organ shortage is one of the major hurdle to LT. In ZSD, LT is performed to provide metabolic support (i.e. not because of liver failure) and it does not cure the disease. Thus, we can postulate that no organ allocation system would ever favor this indication compared to biliary atresia, for example. Yet, hope is provided by the proof-of-principle that heterozygous carriers are suitable to perform living-donor liver transplantation for ZSD patients[23, 24, 26]. AAV-based gene therapy, like LT, also faces material shortage. Producing high titers of viral vectors is challenging and requires scalable process[39]. In conclusion, both therapeutic approaches require scarce material.

Wild-type AAV are responsible for common cold and exposure to them leads to immunization directed against the AAV capsid. Depending on the serotype and the age of the patients, up to 60% of the subjects harbor anti-AAV antibodies[40]. This so-called *pre-existing immunity* impedes AAV-based gene therapy application in seropositive patients and precludes any vector readministration. Several strategies are under evaluation to overcome this major obstacle to *in vivo* gene therapy. Mingozzi's team recently reported that preadministration of imlifidase, an IgG-cleaving endopeptidase, in non-human primates, allowed enhanced liver transduction and vector readministration[41]. In the LT world, pre-existing immunity is a reality in the rare cases of retransplantation and more frequently during ABO-

incompatible living-donation[42]. Since specific preconditioning regimen have been developed, ABO-incompatible living-donation is safe and feasible[43]. In brief, both LT and gene therapy can be exposed to *pre-existing immunity* which can be by-passed by specific protocols.

AAV-based gene therapy elicits immune response towards the viral capsid (*vide supra*) but also towards the transgene product. Hopefully, the liver is able to induce tolerance, making liver gene therapy a convenient approach to express foreign antigens[44]. Since peroxins are intracellular proteins, we do not expect that they could be functionally targeted by anti-peroxins circulating antibodies in case of PEX gene therapy or LT; contrary to what was reported in 2 patients transplanted because of bile salt export pump deficiency (BSEP), also known as progressive familial intrahepatic cholestasis type 2. Post-LT, the 2 patients developed recurrence of the disease that was related to neutralizing antibodies directed against the newly exposed BSEP protein at the plasma membrane[45]. To conclude about *de novo* expression of a specific PEX protein in a ZSD patient, we do not expect that a specific immune response could inhibit the PEX protein functionality, no matter which therapeutic approach is chosen.

Post-LT, the liver graft continues to grow following the recipient growth. The patient survival at 10-year post-LT is above 90% [46]. On the opposite, AAV-based liver gene therapy in children is limited by the risk of transgene expression loss due to liver growth. This occurs because transgenes delivered by AAV vectors are mainly episomal and do not integrate into the host genome. Liver cell divisions occurring during liver growth lead to dilution of the episomes and loss of transgene

expression[44]. In the future, this could be overcome by transgene genomic integration achieved by CRISPR/Cas9 technology or lentiviral vectors[36, 47, 48].

Both LT and liver gene therapy face limitations. Nonetheless, LT is readily available in clinical practice. In ZSD, as for several other IEM[49], LT gave the proof of principle that liver-targeted therapy is able to modify the natural history of the disease paving the way for future liver gene therapy developments in this indication.

Conclusions

We improved an *in vitro* method and an *in vivo* mouse model to study PBD, and we reported the results of two therapeutic approaches in ZSD. Even if the road is still long until we find a cure for ZSD patients[50], we are convinced that the data gathered and shared will support the future therapeutic developments in ZSD.

Acknowledgments

I thank Emilie Van Leemput for language editing.

References

1. Wei, H., S. Kemp, M.C. McGuinness, A.B. Moser, and K.D. Smith, Pharmacological induction of peroxisomes in peroxisome biogenesis disorders. Ann Neurol, 2000. 47(3): p. 286-96.
2. Berendse, K., M.S. Ebberink, L. Ijlst, B.T. Poll-The, R.J. Wanders, and H.R. Waterham, Arginine improves peroxisome functioning in cells from patients with a mild peroxisome biogenesis disorder. Orphanet J Rare Dis, 2013. 8: p. 138.
3. MacLean, G.E., C. Argyriou, E. Di Pietro, X. Sun, S. Birjandian, P. Saberian, J.G. Hacia, and N.E. Braverman, Zellweger spectrum disorder patient-derived fibroblasts with the PEX1-Gly843Asp allele recover peroxisome functions in response to flavonoids. J Cell Biochem, 2019. 120(3): p. 3243-3258.
4. Dranchak, P.K., E. Di Pietro, A. Snowden, N. Oesch, N.E. Braverman, S.J. Steinberg, and J.G. Hacia, Nonsense suppressor therapies rescue peroxisome lipid metabolism and assembly in cells from patients with specific PEX gene mutations. J Cell Biochem, 2011. 112(5): p. 1250-8.
5. Zhang, R., L. Chen, S. Jiralerspong, A. Snowden, S. Steinberg, and N. Braverman, Recovery of PEX1-Gly843Asp peroxisome dysfunction by small-molecule compounds. Proc Natl Acad Sci U S A, 2010. 107(12): p. 5569-74.
6. Heier, C.R. and C.J. DiDonato, Translational readthrough by the aminoglycoside geneticin (G418) modulates SMN stability in vitro and improves motor function in SMA mice in vivo. Hum Mol Genet, 2009. 18(7): p. 1310-22.
7. Demaret, T., G.E. Courtoy, J. Ravau, P. Van Der Smissen, M. Najimi, and E.M. Sokal, Accurate and live peroxisome biogenesis evaluation achieved by lentiviral expression of a green

fluorescent protein fused to a peroxisome targeting signal 1. Histochem Cell Biol, 2020. 153(5): p. 295-306.
8. Klouwer, F.C.C., A. Meester-Delver, F.M. Vaz, H.R. Waterham, R.C.M. Hennekam, and B.T. Poll-The, Development and validation of a severity scoring system for Zellweger spectrum disorders. Clin Genet, 2017.
9. Gootjes, J., P.A. Mooijer, C. Dekker, P.G. Barth, B.T. Poll-The, H.R. Waterham, and R.J. Wanders, Biochemical markers predicting survival in peroxisome biogenesis disorders. Neurology, 2002. 59(11): p. 1746-9.
10. Aubourg, P., C. Adamsbaum, M.C. Lavallard-Rousseau, F. Rocchiccioli, N. Cartier, I. Jambaque, C. Jakobezak, A. Lemaitre, F. Boureau, C. Wolf, and et al., A two-year trial of oleic and erucic acids ("Lorenzo's oil") as treatment for adrenomyeloneuropathy. N Engl J Med, 1993. 329(11): p. 745-52.
11. Berendse, K., M. Engelen, S. Ferdinandusse, C.B. Majoie, H.R. Waterham, F.M. Vaz, J.H. Koelman, P.G. Barth, R.J. Wanders, and B.T. Poll-The, Zellweger spectrum disorders: clinical manifestations in patients surviving into adulthood. J Inherit Metab Dis, 2016. 39(1): p. 93-106.
12. Herzog, K., M.L. Pras-Raves, M.A. Vervaart, A.C. Luyf, A.H. van Kampen, R.J. Wanders, H.R. Waterham, and F.M. Vaz, Lipidomic analysis of fibroblasts from Zellweger spectrum disorder patients identifies disease-specific phospholipid ratios. J Lipid Res, 2016. 57(8): p. 1447-54.
13. Rocchiccioli, F., P. Aubourg, and P.F. Bougneres, Medium- and long-chain dicarboxylic aciduria in patients with Zellweger syndrome and neonatal adrenoleukodystrophy. Pediatr Res, 1986. 20(1): p. 62-6.
14. Korman, S.H., H. Mandel, and A. Gutman, Characteristic urine organic acid profile in peroxisomal biogenesis disorders. J Inherit Metab Dis, 2000. 23(4): p. 425-8.
15. Arkadir, D., T. Dinur, S. Revel-Vilk, M. Becker Cohen, C. Cozma, M. Hovakimyan, S. Eichler, A. Rolfs, and A. Zimran, Glucosylsphingosine is a reliable response biomarker in Gaucher disease. Am J Hematol, 2018. 93(6): p. E140-e142.
16. Setchell, K.D., P. Bragetti, L. Zimmer-Nechemias, C. Daugherty, M.A. Pelli, R. Vaccaro, G. Gentili, E. Distrutti, G. Dozzini, A. Morelli, and et al., Oral bile acid treatment and the patient with Zellweger syndrome. Hepatology, 1992. 15(2): p. 198-207.
17. Heubi, J.E., K.D.R. Setchell, and K.E. Bove, Long-Term Cholic Acid Therapy in Zellweger Spectrum Disorders. Case Rep Gastroenterol, 2018. 12(2): p. 360-372.
18. Heubi, J.E. and W.P. Bishop, Long-Term Cholic Acid Treatment in a Patient with Zellweger Spectrum Disorder. Case Rep Gastroenterol, 2018. 12(3): p. 661-670.
19. Keane, M.H., H. Overmars, T.M. Wikander, S. Ferdinandusse, M. Duran, R.J. Wanders, and P.L. Faust, Bile acid treatment alters hepatic disease and bile acid transport in peroxisome-deficient PEX2 Zellweger mice. Hepatology, 2007. 45(4): p. 982-97.
20. Berendse, K., F.C. Klouwer, B.G. Koot, E.M. Kemper, S. Ferdinandusse, K.V. Koelfat, M. Lenicek, F.G. Schaap, H.R. Waterham, F.M. Vaz, M. Engelen, P.L. Jansen, R.J. Wanders, and B.T. Poll-The, Cholic acid therapy in Zellweger spectrum disorders. J Inherit Metab Dis, 2016.
21. Klouwer, F.C.C., B.G.P. Koot, K. Berendse, E.M. Kemper, S. Ferdinandusse, K.V.K. Koelfat, M. Lenicek, F.M. Vaz, M. Engelen, P.L.M. Jansen, R.J.A. Wanders, H.R. Waterham, F.G. Schaap, and B.T. Poll-The, The cholic acid extension study in Zellweger spectrum disorders: results and implications for therapy. J Inherit Metab Dis, 2018.
22. Ferdinandusse, S., S. Denis, G. Dacremont, and R.J. Wanders, Toxicity of peroxisomal C27-bile acid intermediates. Mol Genet Metab, 2009. 96(3): p. 121-8.
23. Demaret, T., S. Varma, X. Stephenne, F. Smets, I. Scheers, R. Wanders, L. Van Maldergem, R. Reding, and E. Sokal, Living-donor liver transplantation for mild Zellweger spectrum disorder: Up to 17 years follow-up. Pediatr Transplant, 2018. 22(3): p. e13112.
24. Van Maldergem, L., A.B. Moser, M.F. Vincent, D. Roland, R. Reding, J.B. Otte, R.J. Wanders, and E. Sokal, Orthotopic liver transplantation from a living-related donor in an infant with a peroxisome biogenesis defect of the infantile Refsum disease type. J Inherit Metab Dis, 2005. 28(4): p. 593-600.
25. Darwish, A.A., P. McKiernan, and C. Chardot, Paediatric liver transplantation for metabolic disorders. Part 1: Liver-based metabolic disorders without liver lesions. Clin Res Hepatol Gastroenterol, 2011. 35(3): p. 194-203.
26. Matsunami, M., N. Shimozawa, A. Fukuda, T. Kumagai, M. Kubota, P.F. Chong, and M. Kasahara, Living-Donor Liver Transplantation From a Heterozygous Parent for Infantile Refsum Disease. Pediatrics, 2016. 137(6).

27. Morioka, D., Y. Takada, M. Kasahara, T. Ito, K. Uryuhara, K. Ogawa, H. Egawa, and K. Tanaka, Living donor liver transplantation for noncirrhotic inheritable metabolic liver diseases: impact of the use of heterozygous donors. Transplantation, 2005. 80(5): p. 623-8.
28. Coppin, L., E. Sokal, and X. Stephenne, Hepatocyte Transplantation in Children. Methods Mol Biol, 2017. 1506: p. 295-315.
29. Sokal, E.M., F. Smets, A. Bourgois, L. Van Maldergem, J.P. Buts, R. Reding, J. Bernard Otte, V. Evrard, D. Latinne, M.F. Vincent, A. Moser, and H.E. Soriano, Hepatocyte transplantation in a 4-year-old girl with peroxisomal biogenesis disease: technique, safety, and metabolic follow-up. Transplantation, 2003. 76(4): p. 735-8.
30. Sokal, E.M., Liver transplantation for inborn errors of liver metabolism. J Inherit Metab Dis, 2006. 29(2-3): p. 426-30.
31. Smets, F., M. Najimi, and E.M. Sokal, Cell transplantation in the treatment of liver diseases. Pediatr Transplant, 2008. 12(1): p. 6-13.
32. Pham, T.A., G.M. Enns, and C.O. Esquivel, Living donor liver transplantation for inborn errors of metabolism - An underutilized resource in the United States. Pediatr Transplant, 2016. 20(6): p. 770-3.
33. Mogul, D.B., J. Lee, T.S. Purnell, A.B. Massie, T. Ishaque, D.L. Segev, and J.F.P. Bridges, Barriers to access in pediatric living-donor liver transplantation. Pediatr Transplant, 2019. 23(6): p. e13513.
34. Argyriou, C., J.Y. Song, A. Polosa, B. Cecyre, J.-F. Bouchard, P. Lachapelle, J. Bennett, and N. Braverman, AB037. rAAV mediated PEX1 gene augmentation improves visual function in a mouse model for Zellweger spectrum disorder. Annals of Eye Science, 2018. 3(3): p. AB037.
35. Janssen, A., P. Gressens, M. Grabenbauer, E. Baumgart, A. Schad, I. Vanhorebeek, A. Brouwers, P.E. Declercq, D. Fahimi, P. Evrard, L. Schoonjans, D. Collen, P. Carmeliet, G. Mannaerts, P. Van Veldhoven, and M. Baes, Neuronal migration depends on intact peroxisomal function in brain and in extraneuronal tissues. J Neurosci, 2003. 23(30): p. 9732-41.
36. Cicek, Y.A., D.C. Luther, J.A. Kretzmann, and V.M. Rotello, Advances in CRISPR/Cas9 Technology for in Vivo Translation. Biol Pharm Bull, 2019. 42(3): p. 304-311.
37. Ginn, S.L., A.K. Amaya, S.H.Y. Liao, E. Zhu, S.C. Cunningham, M. Lee, C.V. Hallwirth, G.J. Logan, S.S. Tay, A.J. Cesare, H.A. Pickett, M. Grompe, K. Dilworth, L. Lisowski, and I.E. Alexander, Efficient in vivo editing of OTC-deficient patient-derived primary human hepatocytes. JHEP Rep, 2020. 2(1): p. 100065.
38. Ebberink, M.S., P.A. Mooijer, J. Gootjes, J. Koster, R.J. Wanders, and H.R. Waterham, Genetic classification and mutational spectrum of more than 600 patients with a Zellweger syndrome spectrum disorder. Hum Mutat, 2011. 32(1): p. 59-69.
39. Tomono, T., Y. Hirai, H. Okada, Y. Miyagawa, K. Adachi, S. Sakamoto, Y. Kawano, H. Chono, J. Mineno, A. Ishii, T. Shimada, M. Onodera, A. Tamaoka, and T. Okada, Highly Efficient Ultracentrifugation-free Chromatographic Purification of Recombinant AAV Serotype 9. Mol Ther Methods Clin Dev, 2018. 11: p. 180-190.
40. Fitzpatrick, Z., C. Leborgne, E. Barbon, E. Masat, G. Ronzitti, L. van Wittenberghe, A. Vignaud, F. Collaud, S. Charles, M. Simon Sola, F. Jouen, O. Boyer, and F. Mingozzi, Influence of Pre-existing Anti-capsid Neutralizing and Binding Antibodies on AAV Vector Transduction. Mol Ther Methods Clin Dev, 2018. 9: p. 119-129.
41. Leborgne, C., E. Barbon, J.M. Alexander, H. Hanby, S. Delignat, D.M. Cohen, F. Collaud, S. Muraleetharan, D. Lupo, J. Silverberg, K. Huang, L. van Wittengerghe, B. Marolleau, A. Miranda, A. Fabiano, V. Daventure, H. Beck, X.M. Anguela, G. Ronzitti, S.M. Armour, S. Lacroix-Desmazes, and F. Mingozzi, IgG-cleaving endopeptidase enables in vivo gene therapy in the presence of anti-AAV neutralizing antibodies. Nat Med, 2020.
42. Evrard, V., J.B. Otte, E. Sokal, J.S. Rochet, F. Haccourt, F. Gennari, D. Latinne, J. Jamart, and R. Reding, Impact of surgical and immunological parameters in pediatric liver transplantation: a multivariate analysis in 500 consecutive recipients of primary grafts. Ann Surg, 2004. 239(2): p. 272-80.
43. Gurevich, M., V. Guy-Viterbo, M. Janssen, X. Stephenne, F. Smets, E. Sokal, C. Lefebvre, J.L. Balligand, T. Pirotte, F. Veyckemans, P. Clapuyt, R. Menten, D. Dumitriu, E. Danse, L. Annet, S.C. Clety, T. Detaille, D. Latinne, C. Sempoux, P.F. Laterre, C. de Magnee, J. Lerut, and R. Reding, Living Donor Liver Transplantation in Children: Surgical and Immunological Results in 250 Recipients at Universite Catholique de Louvain. Ann Surg, 2015. 262(6): p. 1141-9.
44. Ginocchio, V.M., R. Ferla, A. Auricchio, and N. Brunetti-Pierri, Current Status on Clinical Development of Adeno-Associated Virus-Mediated Liver-Directed Gene Therapy for Inborn Errors of Metabolism. Hum Gene Ther, 2019. 30(10): p. 1204-1210.

45. Maggiore, G., E. Gonzales, M. Sciveres, M.J. Redon, B. Grosse, B. Stieger, A. Davit-Spraul, M. Fabre, and E. Jacquemin, Relapsing features of bile salt export pump deficiency after liver transplantation in two patients with progressive familial intrahepatic cholestasis type 2. J Hepatol, 2010. 53(5): p. 981-6.
46. Darius, T., J. Rivera, F. Fusaro, Q. Lai, C. de Magnee, C. Bourdeaux, M. Janssen, P. Clapuyt, and R. Reding, Risk factors and surgical management of anastomotic biliary complications after pediatric liver transplantation. Liver Transpl, 2014. 20(8): p. 893-903.
47. Naldini, L., Gene therapy returns to centre stage. Nature, 2015. 526(7573): p. 351-60.
48. Follenzi, A., M. Battaglia, A. Lombardo, A. Annoni, M.G. Roncarolo, and L. Naldini, Targeting lentiviral vector expression to hepatocytes limits transgene-specific immune response and establishes long-term expression of human antihemophilic factor IX in mice. Blood, 2004. 103(10): p. 3700-9.
49. Sokal, E.M., A. Lopez-Silvarrey, J.P. Buts, and J.B. Otte, Orthotopic liver transplantation for type I glycogenosis unresponsive to medical therapy. J Pediatr Gastroenterol Nutr, 1993. 16(4): p. 465-7.
50. Wanders, R.J.A., Peroxisomal disorders: Improved laboratory diagnosis, new defects and the complicated route to treatment. Mol Cell Probes, 2018. 40: p. 60-69.

Chapter 7.
Collaborations and awards

Congress abstracts

Liver transplantation does not impact the renal function outcome in Alagille syndrome (European Association for the Study of the Liver – International Liver Congress, Amsterdam, 2017)

Tanguy Demaret, Sharat Varma, Yelena Vainilovich, Ugur Halac, Diana El Bizri, Jérôme Ambroise, Isabelle Scheers, Xavier Stephenne, Françoise Smets, Etienne Sokal

Background and aims

Alagille syndrome (AS) is an autosomal dominant multi-systemic disorder caused by pathogenic variants in *JAG1* and *NOTCH2*. Characteristic findings include hepatic involvement with bile duct paucity and 20-50% eventually need a liver transplantation (LT). Post-LT Tacrolimus induced nephropathy is well recognized and 40% of AS patients have an underlying renal anomaly. In the current study we analyzed the impact of LT and Tacrolimus on the evolution of renal function (RF) in children with AS.

Methods

Retrospective study including 50 children that satisfied 3 of 5 major Alagille syndrome criteria and under regular follow-up at our center between 1984 and 2016. Clinical, biochemical and radiological data were collected at similar time points of follow-up among the transplanted and non-transplanted children. The timepoints were at diagnosis or at LT and after 1-2 years, 2-3 years, 3-5 years, 5-7 years and 7-10 years of follow-up. The RF was estimated by glomerular filtration rate (eGFR) using the updated Schwartz formula. The RF outcomes of children with AS having undergone LT were compared with those without LT and also with children having undergone LT for non-AS related indication but without associated nephropathy.

Results

28 of 50 (56%) included AS children underwent LT and were compared with 77 children transplanted for non-AS indications. Mean eGFR post-LT in AS patients and non-AS patients were 93.8 mL/min and 143.2 mL/min, respectively (difference: 49.4 mL/min, $p < 0.0001$). Among children with AS mean eGFR observed in those who did not receive LT was 87.9 mL/min, -5.9 mL/min compared to those who received LT though this was statistically insignificant ($p = 0.32$). Presence of renal ultrasound abnormalities was correlated to RF impairment in AS patients, with or without LT: -14.6 mL/min (98.5 mL/min vs 83.9 mL/min, $p = 0.03$) and -40.9 mL/min (97.8 mL/min vs 56.9 mL/min, $p < 0.0001$), respectively.

Conclusion

Post-LT renal function outcomes are significantly worse in children with AS being the primary disease. Among the children with AS, the RF outcome is not worse after LT.

Chapter 7

Clinical features and natural history of 1154 Alagille syndrome patients: results from the International Multicenter GALA Study Group (European Association for the Study of the Liver – International Liver Congress, London, 2020)

Shannon Vandriel, Jian-She Wang, Li Liting, Huiyu She, Piotr Czubkowski, Irena Jankowska, Dorota Gliwicz, David Piccoli, Kathleen Loomes, Nancy Spinner, Etienne Sokal, Tanguy Demaret, Emanuele Nicastro, Lorenzo D'Antiga, Rima Fawaz, Silvia Nastasio, Susan Siew, Michael Stormon, Henrik Arnell, Björn Fischler, Kyung Mo Kim, Woo Yim Baek, Saul Karpen, Rene Romero, Winita Hardikar, Sahana Shankar, Amin Roberts, Helen Evans, Maria Camila Sanchez, Maria Lorena Cavalieri, Palaniswamy Karthikeyan, Suzanne Davison, M.K. Jensen, Marianne Kavan, Henkjan Verkade, Way Seah Lee, James Squires, Chatmanee Lertudomphonwanit, Ryan Fischer, Henry Lin, Wikrom Karnsakul, Deirdre Kelly, Ruben Quiros-Tejeira, Cristina Targa Ferreira, Elisa Carvalho, Seema Alam, Jesus Banales, Giuseppe Indolfi, Catherine Larson-Nath, Pinar Bulut, Pier Luigi Calvo, Pamela Valentino, Cigdem Arıkan, Kathleen Schwarz, Ino Kanavaki, Antal Dezsőfi, Raquel Borges-Pinto, Sabina Wiecek, Quais Mujawar, Jernej Brecelj, Nanda Kerkar, Ermelinda Santos-Silva, Carolina Jimenez-Rivera, Orith Waisbourd-Zinman, Gabriella Nebbia, Emmanuel Gonzalez, Richard Thompson, Bettina Hansen, Binita Kamath and The GALA Study Group.

Background and aims

Alagille Syndrome (ALGS) is a rare multisystem disorder and one of the most frequent inherited causes of neonatal cholestasis. Prior cohort studies in ALGS largely come from tertiary liver centers and therefore select for the most severely affected cholestatic patients. As a result, the full spectrum of ALGS liver involvement remains unclear. Furthermore, a comprehensive assessment of extrahepatic manifestations in a large cohort of patients is missing. In 2017, the Global ALagille Alliance (GALA) Study Group was established to overcome these limitations.

Methods

Multicenter retrospective analysis of children with a clinically and/or genetically confirmed diagnosis of ALGS, born between Jan-1997 and Aug-2019. Histopathological features in liver biopsies were compared using the Kruskal-Wallis

test. Cox proportional hazards models were constructed to determine transplant-free survival (TFS) in ALGS patients who underwent a Kasai or biliary diversion (BD). TFS and overall survival were estimated using the Kaplan-Meier method.

Results

1154 ALGS (58% male) patients from 25 countries were included (median follow-up 5.6 years, IQR 2.3 – 11.3). Of the 77% genetically confirmed patients, 93% have a *JAG1* mutation and 4% a *NOTCH2* mutation (69% de novo). Any cardiac anomaly was the most common clinical manifestation (89%), followed by characteristic facies (88%), posterior embryotoxon (49%), butterfly vertebrae (44%), and renal anomalies (35%). Available MRI and CT reports revealed cerebral and intra-abdominal vascular anomalies in 34% and 31% of patients, respectively. 82% of ALGS patients presented with neonatal cholestasis. 494 baseline liver biopsy reports were reviewed (**Table 1**) and revealed an increasing frequency of bile duct paucity with age ($p = 0.01$) and notably, bile duct plugs in 6% and proliferation in 20% of biopsies < 6 months. 10- and 18-year TFS rates in 911 ALGS patients presenting with neonatal cholestasis were 57% and 41%, respectively. ALGS patients who underwent a Kasai (HR 3.3, 95% CI 2.4 - 4.5; $p < 0.001$) or BD (HR 2.0, 95% CI 1.4 - 3.7; $p = 0.004$) had significantly lower rates of TFS. Overall survival rates were 90.9% and 88.6%, respectively.

Conclusion

Here we describe the largest global cohort of ALGS to date representing a broad range of institutions. Almost 60% of ALGS children with neonatal cholestasis will undergo liver transplantation by the age of 18 years. This dataset provides a global view of ALGS and a foundation for future natural history studies.

Table 1. Histopathological features in 494 baseline native liver biopsies.

	Biopsy <6 months	Biopsy ≥6 and <24 months	Biopsy ≥24 months	*P*-value
Histopathologic Findings, % (*n*)	307	84	106	
Bile duct paucity	61% (233)	63% (53)	77% (82)	0.01*
Giant cell transformation	40% (124)	11% (9)	4% (4)	0.001*
Bile duct proliferation	20% (62)	18% (15)	7% (7)	0.005*
Duct/ductular bile plugs	6% (19)	5% (4)	2% (2)	0.21

Characterization of the NOTCH2-associated Alagille syndrome phenotype: Results from the international multicenter GALA study group (World Congress of Pediatric Gastroenterology, Hepatology and Nutrition, Copenhagen, 2020)

Shannon Vandriel, Jian-She Wang, Li Liting, Huiyu She, Piotr Czubkowski, Irena Jankowska, Dorota Gliwicz, David Piccoli, Kathleen Loomes, Nancy Spinner, Etienne Sokal, Tanguy Demaret, Emanuele Nicastro, Lorenzo D'Antiga, Rima Fawaz, Silvia Nastasio, Susan Siew, Michael Stormon, Henrik Arnell, Björn Fischler, Kyung Mo Kim, Woo Yim Baek, Saul Karpen, Rene Romero, Winita Hardikar, Sahana Shankar, Amin Roberts, Helen Evans, Maria Camila Sanchez, Maria Lorena Cavalieri, Palaniswamy Karthikeyan, Suzanne Davison, M.K. Jensen, Marianne Kavan, Henkjan Verkade, Way Seah Lee, James Squires, Chatmanee Lertudomphonwanit, Ryan Fischer, Henry Lin, Wikrom Karnsakul, Deirdre Kelly, Ruben Quiros-Tejeira, Cristina Targa Ferreira, Elisa Carvalho, Seema Alam, Jesus Banales, Giuseppe Indolfi, Catherine Larson-Nath, Pinar Bulut, Pier Luigi Calvo, Pamela Valentino, Cigdem Arıkan, Kathleen Schwarz, Ino Kanavaki, Antal Dezsőfi, Raquel Borges-Pinto, Sabina Wiecek, Quais Mujawar, Jernej Brecelj, Nanda Kerkar, Ermelinda Santos-Silva, Carolina Jimenez-Rivera, Orith Waisbourd-Zinman, Gabriella Nebbia, Emmanuel Gonzalez, Richard Thompson, Bettina Hansen, Binita Kamath.

Background and aims

Alagille Syndrome (ALGS) is a rare autosomal dominant disorder caused by heterozygous mutations in one of two genes, *JAGGED1* (*JAG1*) or *NOTCH2*. *JAG1* mutations have been identified in 94.3% of individuals with a clinically confirmed diagnosis of ALGS, while *NOTCH2* mutations have been reported in 2.5%. Due to its rarity, the phenotype of *NOTCH2*-associated ALGS has only been reported in a handful of individuals. The Global Alagille Alliance (GALA) Study Group has ascertained the largest international cohort of ALGS to date, allowing characterization of the phenotypic characteristics associated with *NOTCH2* mutations in comparison to those with *JAG1* mutations in an international cohort ALGS patients.

Methods

This was a retrospective, multicenter study collecting clinical, histopathological, and genetic data on children and young adults with ALGS, born between Jan-1997 and Aug-2019. ALGS patients with a pathogenic mutation in *JAG1* or *NOTCH2* were included in this analysis. Clinical and histopathological features between ALGS patients with *JAG1* or *NOTCH2* mutations were compared using chi-square test or Fisher's exact test, as appropriate. Transplant-free survival (TFS) and overall survival rates were compared between groups using the Kaplan-Meier method.

Results

We compared 32 ALGS (66% male) patients with a *NOTCH2* mutation to 818 (57% male) ALGS patients with a *JAG1* mutation (**Table 1**). Missense mutations were the most common NOTCH2 variants, 59%, followed by splice site, 21%, frameshift, 13%, and nonsense mutations, 7%. A lower fraction of *NOTCH2*-ALGS patients presented with neonatal cholestasis in comparison to *JAG1*-ALGS patients (66% vs. 82%, $p = 0.02$). Review of baseline liver biopsies demonstrated that bile duct paucity was similarly present in *NOTCH2* (55%) and *JAG1* (60%, $p = 0.26$) patients. *NOTCH2*-ALGS patients were significantly less likely to have characteristic facies (41% vs. 88%, $p < 0.001$), a cardiac anomaly (46% vs. 91%, $p < 0.001$), posterior embryotoxon (12% vs. 51%, $p < 0.001$), or butterfly vertebra (4% vs. 44%, $p < 0.001$). Renal anomalies did not differ significantly between the two groups (32% vs. 35%, $p = 0.79$). Baseline head MRI reports were available in 11 *NOTCH2*-ALGS patients and revealed anomalies of the internal carotid arteries in 36%. Only 31% of patients with a *NOTCH2* mutation fulfilled the classic diagnostic criteria (≥3 of 6 classic features). 10- year TFS in patients presenting with neonatal cholestasis was comparable between *NOTCH2* and *JAG1* patients, (68% and 61%, respectively;

NS), as were 18-year TFS (51%, and 48%, respectively; NS). Overall survival rates at 10- and 18-year were also similar for *NOTCH2* and *JAG1* ALGS patients and consistently above 90%.

Conclusion

This is the largest cohort of ALGS patients with NOTCH2 mutations described. Missense mutations predominate in *NOTCH2*-ALGS, in comparison to the well reported predominance of protein-truncating mutations in *JAG1*-ALGS. *NOTCH2*-ALGS patients exhibit significantly reduced penetrance of extrahepatic features of ALGS. Since all of these patients were ascertained from liver clinics there is a bias in favor of liver involvement, however these data suggest that reliance on classical clinical phenotypic definitions of ALGS may miss patients with *NOTCH2*-related disease and that genetic testing is crucial for diagnosis. Further investigation will be necessary to determine if additional clinical features are present in *NOTCH2*-associated ALGS patients. Despite the phenotypic differences, the natural history with respect to survival and TFS did not differ between the *JAG1* and *NOTCH2* groups.

Table 1. Comparison of clinical features in ALGS patients with a *JAG1* or *NOTCH2* mutation.

	JAG1	***NOTCH2***	***P*-value**
n	818	32	
Male, % (n)	57% (463)	66% (21)	0.45
Family history, % (n)	31% (n=186/424)	38% (n=9/24)	0.75
Characteristic features, % (n)			
Bile duct paucity	60% (n=208/334)	55% (n=11/20)	0.26
Neonatal cholestasis	82% (n=653/796)	66% (n=21/32)	0.02
Characteristic facies	88% (n=649/738)	41% (n=13/28)	<0.001
Any cardiac anomalies	91% (n=659/722)	46% (n=13/28)	<0.001
Posterior embryotoxon	51% (n=334/657)	12% (n=3/25)	<0.001
Butterfly vertebrae	44% (n=313/710)	4% (n=1/25)	<0.001
Renal anomalies	35% (n=245/466)	32% (n=9/28)	0.79

Chapter 7

Guidelines

Minimal information for studies of extracellular vesicles 2018 (MISEV2018): a position statement of the International Society for Extracellular Vesicles and update of the MISEV2014 guidelines (Journal of Extracellular Vesicles, 8(1), 2019)

Clotilde Théry, Kenneth W Witwer, (…) , Tanguy Demaret, (…) , Catherine A Lombard, (…), Davide Zocco & Ewa K Zuba-Surma

Abstract

The last decade has seen a sharp increase in the number of scientific publications describing physiological and pathological functions of extracellular vesicles (EV), a collective term covering various subtypes of cell-released, membranous structures, called exosomes, microvesicles, microparticles, ectosomes, oncosomes, apoptotic bodies, and many other names. However, specific issues arise when working with these entities, whose size and amount often make them difficult to obtain as relatively pure preparations, and to characterize properly. The International Society for Extracellular Vesicles (ISEV) proposed Minimal Information for Studies of Extracellular Vesicles ("MISEV") guidelines for the field in 2014. We now update these "MISEV2014" guidelines based on evolution of the collective knowledge in the last four years. An important point to consider is that ascribing a specific function to EV in general, or to subtypes of EV, requires reporting of specific information beyond mere description of function in a crude, potentially contaminated, and heterogeneous preparation. For example, claims that exosomes are endowed with exquisite and specific activities remain difficult to support experimentally, given our still limited knowledge of their specific molecular machineries of biogenesis and release, as compared with other biophysically similar EV. The MISEV2018 guidelines include

tables and outlines of suggested protocols and steps to follow to document specific EV-associated functional activities. Finally, a checklist is provided with summaries of key points.

Original articles

Intracranial Hypertension and Papilledema in a Large Cohort of Pediatric Patients with Alagille syndrome (Journal of Pediatric Gastroenterology and Nutrition, 2020)

Nathalie Rock, Tanguy Demaret, Xavier Stephenne, Isabelle Scheers, Francoise Smets, Valérie A McLin, Antonella Boschi, Etienne M Sokal.

Background and aims

Ophthalmic abnormalities are amongst the five major criteria required for a diagnosis of Alagille syndrome (ALGS), of which embryotoxon, pseudo-papilledema, and hypopigmented retinopathy are the most common. Papilledema with or without intracranial hypertension (ICHT) is rarely described. We report nine pediatric cases of ALGS with bilateral papilledema, five of which were diagnosed with ICHT.

Methods

The ophthalmic data from 125 patients were reviewed including 85 patients with clinically and/or genetically (n = 37) proven ALGS and 40 patients liver transplanted for other indications. The study inclusion criteria were positive diagnosis of ALGS and availability of ophthalmic follow-up data.

Results

Nine (13%) of the 69 patients meeting the inclusion criteria had papilledema. The neurological and neuroimaging results in all nine patients were normal. These nine patients were categorized into four groups: (1) a non-transplant group (n = 1), (2) a group with pretransplant papilledema persistent after liver transplantation (LT)

(n = 2), (3) a group with papilledema occurring after LT with spontaneous resolution (n=2), and (4) a group with papilledema and signs of ICHT after LT (n=5). The patients with ICHT were treated with steroids alone (n = 1) or with acetazolamide (n = 4). A ventriculoperitoneal shunt was placed in two of the five cases because of progressive visual loss. Pseudopapilledema was present in 10 additional patients (14.5%, 10/69). One (2.5%) of the 40 patients without ALGS developed papilledema after LT.

Conclusion

True ICHT may be underdiagnosed in patients with ALGS. Our findings underscore the need for close ophthalmic follow-up before and after LT in these patients.

Awards, grants and invited lectures

2016

Metabolic liver disease workshop: travel award (500€)

2017

Belgian Week of Gastroenterology research grant (2.500€)

Astellas research grant (1.000€)

European Association for the Study of the Liver: senior-junior invited lecture

European Association for the Study of the Liver: travel award (800€)

European Society for Paediatric Gastroenterology Hepatology and Nutrition: young investigator award (750€)

Global foundation for Peroxisomal Disorders: travel award (1.000$)

Academic Medical Center: invited lecture

2018

Administration board of Cliniques universitaires Saint-Luc: invited lecture

2019

European Leukodystrophies Association: invited lecture

Best oral presentation award from the jury of the IREC PhD Day 2019

2020

Laboratory of analytical biochemistry of Cliniques universitaires Saint-Luc: invited lecture

Histochemistry and Cell Biology: cover figure